



NASA SP-201

CASE FILE COPY

ANALYSIS OF
APOLLO 8
PHOTOGRAPHY AND VISUAL OBSERVATIONS



NATIONAL AERONAUTICS AND SPACE ADMINISTRATION

ANALYSIS OF
APOLLO 8
PHOTOGRAPHY AND VISUAL OBSERVATIONS

COMPILED BY
NASA MANNED SPACECRAFT CENTER



Scientific and Technical Information Division
OFFICE OF TECHNOLOGY UTILIZATION
NATIONAL AERONAUTICS AND SPACE ADMINISTRATION
Washington, D.C.

1969

For Sale by the Superintendent of Documents,
U.S. Government Printing Office, Washington, D.C. 20402
Price \$4.25
Library of Congress Catalog Card Number 71-601481

Contents

	Page
INTRODUCTION.....	vii
<i>Richard J. Allenby</i>	
ACKNOWLEDGMENTS.....	ix
CHAPTER 1. VISUAL OBSERVATIONS.....	1
<i>William A. Anders, James A. Lovell, and Frank Borman</i>	
Introduction.....	1
Color.....	1
Surface Textures.....	1
Mare Areas.....	1
Highland Areas.....	2
Slopes.....	2
Ray Patterns.....	2
Probable Impact Features.....	3
Small Bright Halo Craters.....	3
Large Impact Craters.....	3
Probable Volcanic Features.....	3
Regional Features.....	3
Dark Craters.....	3
Possible Lava Tubes.....	3
Regional Faulting.....	3
General Lunar Visibility.....	4
Terminator.....	4
Zero-Phase Angle.....	4
Subsolar Area.....	4
Earthshine.....	4
Astronomical Observations.....	4
Solar Corona.....	4
Dim-Light Phenomena.....	4
Terrestrial Observations.....	4
CHAPTER 2. INITIAL PHOTOGRAPHIC ANALYSIS.....	9
Areal Coverage.....	9
<i>James H. Sasser and F. El-Baz</i>	
Comparison With Luna III Photographs.....	9
<i>E. A. Whitaker</i>	
Discussion of Named Features.....	11
<i>E. A. Whitaker</i>	
Provisionally Approved Nomenclature.....	11
Proposed Nomenclature.....	12
Geology.....	12
Preliminary Comparison of Apollo 8 and Lunar Orbiter Photography.....	12
<i>Robert G. Strom</i>	
Introduction.....	12
Resolution.....	12
High-Illumination Photography.....	13
Terminator Photography.....	15
Summary.....	16
Preliminary Interpretations of Lunar Geology.....	16
<i>D. E. Wilhelms, D. E. Stuart-Alexander, and K. A. Howard</i>	
Lunar Far Side.....	16
Lunar Near Side.....	18

	Page
Craters.....	21
Crater Characteristics.....	21
<i>F. El-Baz</i>	
Introduction.....	21
Crater Interiors.....	22
Crater Rays.....	23
Blocks.....	23
Crater Chains.....	25
Rayed Craters and Bright-Halo Craters.....	29
<i>Newell J. Trask and Gordon A. Swann</i>	
Hypersonic Gas Flow.....	30
<i>J. A. O'Keefe, W. S. Cameron, and Harold Masursky</i>	
Possible Volcanic Features.....	32
Landforms.....	32
<i>F. El-Baz and H. G. Wilshire</i>	
Sublimates.....	34
<i>E. A. Whitaker</i>	
Colorimetry.....	35
General Statement—The Color of the Moon.....	35
<i>E. A. Whitaker and A. F. H. Goetz</i>	
Apollo 8 Color Experiment.....	36
<i>A. F. H. Goetz</i>	
Introduction.....	36
The Experiment.....	36
Data Return.....	36
Image Processing.....	36
Photometry.....	38
An Investigation of the Lunar Heiligenschein.....	38
<i>E. A. Whitaker</i>	
Theoretical Photometry.....	40
<i>H. A. Pohn, R. L. Wildey, and H. W. Radin</i>	
Introduction.....	40
Significance of Photography.....	40
Advantages of Apollo 8 Photographs Over Earlier Data.....	40
Preliminary Results.....	41
Photometric Function Reductions.....	41
<i>James L. Dragg and Harold L. Prior</i>	
Visibility and Apollo 8 Photographic Results.....	44
<i>K. Ziedman</i>	
Introduction.....	44
Summary of Results.....	44
Discussion.....	48
Comparison of Orbital and LM-Descent Viewing Conditions.....	48
Shadow Visibility and Visual Dynamic Range.....	49
Lunar Surface Simulation.....	51
Evaluation of Photoclinometric Profile Derivation.....	51
<i>B. K. Lucchitta and N. A. Gambell</i>	
Origin of the Study.....	51
Procedure.....	52
Geometric and Film Parameters.....	52
Format and Microdensitometer Parameters.....	52
Selection of Photograph.....	52
Obtaining Parameters.....	52
Scanning of the Area and Computer Program Modification.....	53
Results.....	53
Comparison With Photogrammetric Profiles Obtained From the AP/C Plotter.....	53
Comparison of Slopes From Lunar Orbiter Frame H-33, Framelet 739, With Slopes From Apollo 8 Frame 2082-D.....	55

CONTENTS

V

	Page
Evaluation	55
Vertical Resolution of Slope Profiles	59
Applications of Photoclinometry	59
Advantages of Apollo 8 Photography	59
Selenodesy and Cartography	59
Evaluation of the Photography	59
<i>D. W. G. Arthur</i>	
Apollo 8 Control Points	59
<i>Richard L. Nance</i>	
The Figure of the Moon	63
<i>W. H. Michael, Jr.</i>	
Photogrammetry	64
Photogrammetric Data Reduction	64
<i>Paul E. Norman, Merritt J. Bender, and R. D. Esten</i>	
Introduction	64
Photogrammetric Evaluation of Photography	64
Camera Calibration Data	65
Analytical Aerial Triangulation	65
Topographic Mapping	67
Photogrammetry of Apollo 8 Photography	68
<i>Sherman S. C. Wu</i>	
Introduction	68
Preliminary Photogrammetric Evaluation	69
Model of Vertical Photography (Magazine D)	69
Model of Convergent Photography (Magazine C)	73
Comparison Between Photogrammetric and Photoclinometric Profiles	75
Discussion	77
Camera Calibration	77
Establishment of Control Points	77
Absolute Orientation of a Model of Vertical Photography With the Tracking Data (Speed and Time Interval)	78
Simulation of Lunar Module Photography and Lunar Module Landing Conditions	78
<i>D. D. Lloyd</i>	
Experiment Operation	78
Hardware and Image Motion Compensation Considerations	79
Hardware Limitations of Light-Collecting Capability	79
Derivation of IMC: Requirements	79
Techniques for Providing the Required Geometric Instructions	80
Measurement of Residual Smear	81
Method	81
Measurement Data Obtained	81
Results	81
Summary	81
References	82
CHAPTER 3. ASTRONOMICAL AND EARTH OBSERVATIONS	85
Astronomical Observations	85
<i>L. Dunkelmann and Robert O. Hill</i>	
Astronomical Moonwatch During Apollo 8	85
<i>William B. Chapman</i>	
Preliminary Results of Apollo 8 Optical Tracking Experiment	86
<i>Harold B. Liemohn</i>	
Introduction	86
Participants	86
Sightings	86
Unconfirmed Interpretation	88
Discussion of Photographs	88
Conclusions	91
Smithsonian Observations of Apollo 8 Near Earth	92
<i>Staff, Smithsonian Astrophysical Observatory, and Otha H. Vaughan, Jr.</i>	

	Page
Introduction.....	92
The Baker-Nunn Camera.....	92
The Observations.....	93
Mission Events Related to Mount Haleakala Photography.....	93
Mission Events Related to the San Fernando, Spain, Photographs.....	95
Data.....	96
Discussion.....	101
References.....	102
CHAPTER 4. BACKGROUND.....	103
Introduction.....	103
<i>Richard J. Allenby</i>	
Photographic Objectives.....	104
<i>Robert O. Hill and Lewis C. Wade</i>	
Notes on Film Selection and Use.....	106
<i>James L. Dragg and Robert O. Hill</i>	
Use of Type 2485 Film.....	107
<i>L. Dunkelman and Robert O. Hill</i>	
Calibration Information.....	107
<i>James L. Dragg and Alan Wells</i>	
Introduction.....	107
Specifications and Tolerances.....	107
Measurements From a Typical Lens.....	108
Spectral Transmittance of the Lens/Window Combination.....	111
Film Sensitometric Calibration.....	112
<i>James L. Dragg</i>	
Camera Exposure Calculations.....	114
<i>George R. Blackman</i>	
Exposure Evaluations.....	118
<i>James L. Dragg and Harold L. Prior</i>	
Magazine C.....	118
Magazine D.....	119
Magazine E.....	120
Apollo Camera Resolution Tests.....	120
<i>A. F. H. Goetz</i>	
Processing of Apollo 8 Onboard Film.....	122
<i>Richard W. Underwood</i>	
Introduction.....	122
SO-368 Processing.....	123
SO-168 Processing.....	123
SO-121 Processing.....	124
Type 3400 Processing.....	125
Type 2485 Processing.....	125
Stereoscopic Strip Photography.....	126
<i>Paul E. Norman, Robert O. Hill, and Lewis C. Wade</i>	
Photographic Targets of Opportunity.....	127
<i>Lewis C. Wade</i>	
APPENDIX A—DATA AVAILABILITY.....	129
APPENDIX B—GLOSSARY OF TERMS.....	335
APPENDIX C—AUTHOR AFFILIATION.....	337

Introduction

RICHARD J. ALLENBY

Apollo 8 was launched from Cape Kennedy, Fla., at 7:50 a.m., e.s.t., on December 21, 1968. Two hours 50 minutes later, translunar injection was performed; and astronauts Col. Frank Borman, the commander; Capt. James A. Lovell, Jr., the command module pilot; and Maj. (now Lt. Col.) William A. Anders, the lunar module pilot, were on their way to the Moon. The spacecraft was placed in an elliptical lunar orbit at 69 hours 8 minutes after liftoff. After flying two elliptical orbits of 168.5 by 60 nautical miles with an inclination of 12° to the Equator, the spacecraft was placed in a nearly circular orbit of 59.7 by 60.7 nautical miles, in which it remained for eight orbits. At 89 hours 19 minutes, transearth injection was performed from behind the Moon. A nearly flawless mission was completed on the morning of December 27 when splashdown occurred in the Pacific Ocean after a total elapsed time of 147 hours.

Lt. Gen. Sam C. Phillips, the Director of the Apollo Program, announced that such a mission was being considered at a press conference on August 19, 1968. Formal announcement that NASA was preparing Apollo 8 for an orbital flight around the Moon was released to the press on November 12, 1968.

The primary purpose of this mission was to further progress toward the goal of landing men on the Moon by gaining operational experience and testing the Apollo systems. However, a great effort was also made to accomplish worthwhile scientific tasks with photography and visual observations by the astronauts.

In planning the scientific tasks to be attempted on this mission, it was obvious that one of the prime tasks should be photography of the lunar surface. Such photography would furnish valuable information on the following:

1. Approach topography and landmarks for the early Apollo landings
2. The scientific merit and the roughness of areas for possible follow-on Apollo landings
3. The broad structure and characteristics of the lunar surface

During the orbital part of the mission, a major portion of the lunar far side would be in sunlight. Although almost all of the far side of the Moon has been photographed by the automated Lunar Orbiter spacecraft, the photography generally was made with the spacecraft relatively far from the Moon, limiting the Lunar Orbiter photographs to an average resolution of approximately 100 meters. Thus, Apollo photographs of the far side would have much better resolution than existing pictures.

Finally, it was recognized that contamination, both as it relates to window fogging (which did occur) and to contamination clouds around the spacecraft, should be studied for both scientific and operational interests.

In summary, Apollo 8 was a highly technical and operationally difficult mission with a very tight schedule for science mission planning. That a worthwhile scientific plan was generated is a tribute to the scientists associated with the mission. Accomplishment of so many of these tasks was possible only through the close cooperation of all the center and program offices, and an outstanding effort by the flight crew. The scientific groundwork laid during the Apollo 8 mission will contribute substantially to the more extensive scientific missions that will follow.

Acknowledgments

Many professional and amateur astronomers throughout the world observed the Apollo 8 spacecraft in flight, and photographed and reported these observations. Meanwhile, other astronomers observed the Moon and watched for lunar transient events—those infrequently observed changes in appearance of lunar features that indicate possible fluorescence of surface material or gases escaping from the Moon. Special thanks are extended to the following persons: Larry Bornhorst, Wallace Calkins, Bruce Campbell, Martin Green, Bill Hendrickson, Jean Pierrette Jean, D. G. King-Hele, C. W. Kohlenberger, Ronald Rogerio de Freitas Mourao, Alex Oanowita, and Roger Tuthill.

The authors would also like to express their appreciation to all those who provided valuable data and assisted in carrying out experiments and evaluations presented in this report. The following persons contributed specific data that were used in specific sections of the report: F. C. Billingsley, F. Collen, Sol Giles, Raymond Jordan, Noel T. Lamar, Charles Manry, T. B. McCord, Bruce Murray, Gary Nakata, Samuel Priebe, D. H. Refoy, Raymond Sabata, Julio Salinas, Francis Schafer, Fred Southard, Bill Straight, Richard Thompson, Jurrie van der Woude, and Wilbur R. Wollenhaupt.

The crew of Apollo 8 acknowledges the assistance of Dr. Harrison H. Schmitt in the preparation of chapter 1.

1

Visual Observations

WILLIAM A. ANDERS, JAMES A. LOVELL, AND FRANK BORMAN

INTRODUCTION

The unique scientific aspect of the flight of Apollo 8 was the exposure of man and his accumulated training and experience to an environment previously examined only through the programmed systems of unmanned spacecraft. This was an opportunity for the observation of another planetary surface in a situation that combined continuously varying viewing geometry and lighting with the exceptional dynamic range and color discrimination of the human eye. Add to this the potential of the experienced human mind for both objective and interpretive selection of data to be recorded.

These thoughts prompted the authors to schedule as much refresher and supplemental training in lunar geology as the test-flight nature of the Apollo 8 mission would allow. Much of the training was keyed to the application of a critical item checklist (table 1-I, p. 5) to existing Lunar Orbiter photographs. In addition to this training, we had use of an average eye resolution of about 100 feet from a 60-n.-mi. altitude and a 10 × monocular telescope. Limitations on our observations consisted primarily of partially fogged or smeared side and hatch windows, operational constraints on spacecraft attitudes, and required changes in the planned timelines.

COLOR

Subtle color variations in the materials of the lunar surface have been previously noted by special spectrometric photographic techniques uti-

lizing terrestrial telescopes. Thus, the observation and spatial context of any color variations observable from 60 n. mi. were of particular interest. There is general agreement among the authors that regional variations in lunar surface color are in shades of gray, possibly with faint brownish hues similar to the color of dirty beach sand. Our photographs on black-and-white film illustrate observed general lunar color more closely than do the initial printings of the color films. Neither were specific colors observed associated with any particular lunar features.

These observations do not seem surprising, in retrospect, because the terrestrial colors with which we are familiar can be attributed largely to the effects of oxidation, the biosphere, and water.

SURFACE TEXTURES

Mare Areas

Both the far-side and near-side terminators were across dark mare or marelike areas during most of the 10 Apollo 8 lunar orbits. The surfaces of the marelike materials in the far-side basin XV resembled those of mare materials on the front side in their detailed characteristics—that is, relatively smooth, with numerous small craters and crater clusters superimposed on them. On the other hand, the variety of the number and moderate scale features such as depressions, domes, benches, and cones was much greater than was observed on near-side mare areas.

The near-side mare materials of the Sea of Fertility, illuminated at low-to-moderate phase

angles, appeared very much like mare materials we had studied on moderate-resolution, moderate-Sun-angle Orbiter photographs, except for the greater number of small bright halo craters observable at zero phase. The surface of the mare materials in the southern part of the Sea of Tranquility on the approach to landing site 1 and the terminator resembled the surface of a frozen sea with a broad, but irregular, swell. Although not as concentrated as in the far-side basin XV, the domes, cones, filled craters, depressions, and overlapping benches on the mare materials near landing site 1 gave the area an appearance similar to a subdued version of the Pinacate volcanic region of Sonora, Mexico, as seen from aircraft at about 40 000 feet altitude.

The marelike materials of the far-side crater Tsiolkovsky were the darkest appearing materials we observed. Our flightpath took us about 200 n. mi. north of Tsiolkovsky, and our visibility to the south was limited by window fogging; however, this mare did appear to be very smooth, again with the exception of the ubiquitous small craters. Through the monocular telescope, and then barely with the unaided eye, we were able to discern several large boulders on this surface next to the base of the central peak. To be observable from over 200 n. mi., these boulders must be several hundred meters in diameter. One of the boulders appeared to have a track leading away from it, indicating it had rolled off the central peak. Other than these boulders in Tsiolkovsky, no boulders were observed on mare materials, even during use of the spacecraft sextant for landmark tracking.

Highland Areas

Most of the far-side highland terrain was illuminated at relatively high Sun angles with a corresponding loss in visible textural detail. Under this lighting the surface materials appeared to be essentially homogeneous. At moderate Sun angles, in the region near longitude 160° W, there was a subtle but widespread fine lineation of shallow, locally irregular troughs and ridges running across craters and intercrater materials alike. This texture resembled, on a less massive scale, the textures radiating from the Orientale basin, and also that which would be left by a grass rake on ir-

regular ground. In some places the texture was similar to sets of linear sand dunes. Locally, the trend of this texture was roughly parallel to irregular chains of craters set in an irregular herringbone pattern. This was particularly pronounced near the western rim of the far-side basin XV.

At high phase angles near the subsolar point, the visible surface texture of the far-side highlands was dominated by a peppering of small bright halo craters. There were many times more such craters than we had expected to see based on our premission studies of Orbiter photographs.

Slopes

We found that we could see considerable detail on slopes, both those in shadow and those under high illumination. Under high-Sun-angle illumination (low phase angle), the slopes of crater walls, particularly the steep walls of new craters, showed a wide spectrum of albedo variation. The albedo texture of these walls was one of downslope streaking of the lower two-thirds to three-quarters, and a tendency toward roughly horizontal banding in the remaining upper portion of the walls. The texture strongly suggests that talus slopes have formed downslope from layered materials in the upper crater walls. The fact that small craters are very rare on these steep slopes relative to the nearby flat areas indicates relatively continuous and recent downslope movement of material.

The inner walls of large craters are characterized by terraces and/or lobes of material that strongly suggest slump and landslide activity. These processes are probably the dominant processes in the gradual subduing of the raised portions of the rims of large craters.

Ray Patterns

Some of the most distinctive surface textures we observed were ray patterns radiating from many of the most sharply defined craters. The most extensive of these patterns were visible in the highlands only near the subsolar point or somewhat farther from this point after our trans-earth insertion burn. On the mare surfaces, some ray patterns, such as the two distinctive rays from Messier A, were markedly visible. There was no detectable thickness to any observed rays.

PROBABLE IMPACT FEATURES

Small Bright Halo Craters

One of the most striking features of the lunar far side is the number of small (less than 1000 meters in diameter) rayed and bright halo craters that are visible near the subsolar point. There were several times more of these bright craters than we had expected from our premission study of Orbiter photographs. At progressively lower Sun angles on the surface, these presumably fresh craters become visually less obvious; but we should expect that they are also more abundant in the landing areas than previously indicated.

Large Impact Craters

Our limited observation of large craters having the irregularly surfaced rims and apparent ejecta blankets characteristic of impact craters did not disclose much new information except for the observations on slope surface textures reported in the preceding paragraphs. Some large craters have single large spiral patterns on their floors which are difficult to explain except by some form of differential slumping. We were, however, impressed by the relatively subdued features of most large far-side craters compared to most craters visible in the mare regions of the near side.

The crater Taruntius, although it has a well-defined central peak and surrounding array of secondary craters, is unusual in appearance as compared to other large impact craters. Its single rim is sharper in cross section, and there is a prominent, roughly circular crack pattern in its floor materials.

PROBABLE VOLCANIC FEATURES

Regional Features

The region known as Smyth's Sea contains several examples of large craters with concentric double rims. The material of the floors of these craters and that between the double rims appeared identical in texture, albedo, and color to the surrounding mare. These observations support previous proposals we have heard that mare materials were once relatively fluid and were implaced largely by volcanic processes originating essentially directly below their present location.

The very dark marelike areas in the crater Humboldt were visible to us after the transearth insertion burn. These irregular lobate areas form a discontinuous ring between the brighter floor and walls of the crater, and in shape and detailed outlines they strongly resemble the young dark lava flows of the western United States. In addition to these marelike areas between the floor and wall, there were several very bright polygonal cracks visible in Humboldt's floor materials at our particular lighting angle.

The volcanic appearance of the surface textures of materials in the far-side basin XV and in the vicinity of landing site 1 have been mentioned in a preceding section of this chapter.

Dark Craters

Two distinct examples of sharply defined, fresh-looking dark craters several miles in diameter were observed. These craters have very dark interior walls in contrast to the bright walls of most other fresh-looking craters. One such crater was somewhere southeast of the Sea of Crises and north of our orbital path; and the other was south of our path at about 110° E longitude. These craters must be classified as of uncertain origin and certainly are not as clearly of impact origin as many of the fresh craters we observed.

Possible Lava Tubes

The western rim and inner walls and bench of the far-side basin are crossed by a branching pattern of irregular troughs. The pattern strongly resembles that of lava tubes such as those in flows on the slopes of Maunaloa, Hawaii. This resemblance recommends caution when interpreting similar features on the Moon as trains of secondary impact craters.

Regional Faulting

Craters and crater-related features dominate the portion of the Moon we viewed from Apollo 8; however, several well-developed examples of graben-type regional faulting were visible. Although we were specifically interested in observations related to the question of regional strikeslip faulting, no evidence of such faulting was observed. Local enechelon offsets in grabens indicate that shearing stresses have been present but were

released by graben development rather than strike-slip faulting as is common on Earth. This difference between terrestrial and lunar regional faulting suggests the possibility of a major difference in tectonic processes and/or crustal mechanical properties.

The most striking grabens observed were the Cauchy rilles northeast of landing site 1 in the Sea of Tranquility. The southernmost graben grades without interruption into a set of two irregular fault scarps which are stepped down to the south.

GENERAL LUNAR VISIBILITY

Terminator

Our training had indicated that the observation of fine topographic details would be best at and near the terminators. This fact was even more pronounced in flight than we had anticipated. Also confirmed was the ability to see detail in the shadowed side of craters due to backscattered light from the brightly illuminated opposite wall of the crater. Detail was also visible in the bright wall areas.

Zero-Phase Angle

Visibility was poor in areas viewed at low phase angle, but was better than had been expected. Topographic detail could be picked out in areas within about 5° of zero phase, particularly at low Sun angles; that is, when we looked at the lunar surface along the Sun line. Part of the explanation of our ability to see detail at or near zero phase may be tied to the fact that this point is always moving along the surface. This allows the integration and extrapolation of detail observed first under favorable lighting to be carried into the zero-phase area.

Subsolar Area

The visibility in the subsolar area was similar to that near zero phase close to the terminators, except that topographic detail was difficult to observe due to the complete lack of shadows in the surrounding terrain. Albedo differences were, of course, clearly visible within this area and were

the clues to major topographic variations insofar as these variations were related to different surface properties. The lack of clear-cut topographic patterns made recognition and tracking of navigational landmarks very difficult in this area.

EARTHSHINE

Our major surprise with respect to visibility was the clarity with which features could be viewed in earthshine, particularly after a few minutes of light adaptation. At one point we were able to distinguish the floor, benches, and walls of the crater Copernicus with surprisingly good definition. Landmark tracking would probably be feasible in earthshine, but difficult. There does not generally appear to be sufficient light to attempt landings under these conditions; however, this possibility should not be eliminated without further study.

ASTRONOMICAL OBSERVATIONS

Solar Corona

The solar corona was observed once through the scanning telescope just before spacecraft sunrise. It appeared as a very bright glow just above the sunrise point at the horizon with dimmer streamers fanning out above and away from this point.

Dim-Light Phenomena

No specific dim-light phenomena were observed, although areas proposed to contain them were examined visually. The Magellanic clouds appear to have been observed, however, during the night pass of one of the late lunar orbits.

Terrestrial Observations

Very little time was devoted to observations of the Earth on Apollo 8. One interesting high-altitude cloud, however, was seen shortly after spacecraft sunrise during the two orbits prior to translunar injection. This was a long, thin, brownish-gray cloud that appeared to be slightly north of our track and below our orbital altitude of about 100 n. mi. This cloud may be related to our S-IVB effluents.

TABLE 1-I.—*Critical Item Checklist*

<i>Observation Targets Index</i>	
Apollo sites (A)	Dark halo (DC)
Boulder fields (BF)	Elongate (EC)
Color (C)	Grabens/faults (G/F)
Contacts (C3)	High relief surfaces (HR)
Crater fill:	Impact craters (large, fresh)
Concentric (CF)	(IC)
Domed (DCF)	Low relief surfaces (LR)
Turtle back (TBF)	Outcrops (OTC)
Darkness (spacecraft):	Ridges (R)
Atmosphere	Rilles (RL)
Gegenschein	Slopes (terra) (ST)
Star field	Strain diagram
Zodiacal light	Sunrise (spacecraft)
Delta-rimmed craters (DR)	Surveyors (S)
Domes (D)	Terminators
Earthshine	Transients
Eruptive craters:	Translunar/transearth
Chain (CC)	Uncratered surfaces (US)
	Zero-phase (Z)

NOTE.—Abbreviations of key features to typical examples spotted on the Target of Opportunity Chart.

An asterisk indicates an item for which visual observation may be particularly fruitful.

(A) *Apollo Sites*

- Note contacts other than those now known (see Apollo Site Landmark Chart)
- Subjective judgments on lighting limits for LM landing
- Note albedo contrasts at zero phase

Regional contacts, color variations, *landmarks

(S) *Surveyors*

- Observe and plot location of white spacecraft, the spacecraft shadow, or specular flashes

*Location: Flashes, shadow, white spot
Position—Surveyor V

(C3) *Contacts*

- Note other contrasts besides albedo and/or topography

Contrast: Color, relief, patterns, cratering, boulders
Geometry: *Sharpness, shape, elevation change

(IC) *Impact Craters (Large, Rayed)*

- Determine overlapping relationships between ponds and other rim materials
- Identify flow structures in rim materials
- Identify any layers, color differences, or caves on crater wall scarps
- Identify any eruptive cones, flows, or domes at base of crater-wall scarps

Type: Rayed, bright-halo, sharp-rimmed, low-rimmed, subdued

Shape: Circular, asymmetric, polygonal, terraced
Secondaries: Fields, loops, branchings, clusters
Rim: Radial patterns, concentric patterns, boulder fields, dune fields, *flow patterns, *colors
*Ponds: Size limit, surface texture, flow patterns, boulders, superposition, sources
Walls: Textures, patterns, *layers, contacts, flows, channels, *caves, *colors
Benches: Rim relation, *pond relation, *wall contact, channels, *eruptive features
Floor: Textures, flow patterns, fracture patterns, boulder fields, *eruptive features, colors
Central peak: *Layers, *layer orientation, contacts, colors

(HR) *High Relief Surfaces*

- Determine any local variations in albedo or color

Type: *Knobby terra, *domed terra, cratered terra, hummocky terra, parallel ridges, arcuate ridges
Associations: *Eruptive features, patterns, boulder fields, crater fields, superposition, elongate craters
Color: Variation, change sharpness, associations, shape
*Source: Point, line, multiple, covered, direction

(LR) *Low Relief Surfaces*

- Identify source of any observed flows

Type: Mare basin, mare region, very dark region, light basin, smooth terra, very light region
Relief: Low domes, low ridges, rimless depressions, patterns, boulders, halo craters
Color: Variation, change sharpness, associations, shape
*Source: Point, line, multiple, covered, direction
*Benches: Type, color contrast, pattern contrast, crater contrast, front slope relations, superposition

(DF/TBF/CF) *Domed/Turtle Back/Concentric Crater Fill*

- Identify any associated eruptive features

Type: Concentric, domed, polygonal, knobby, combination
Association: Crater type, *eruptive features, age relations
Characteristics: Relief, patterns, color, boulders, filling level

(ST) *Slopes (Terra)*

- Note any indications of layers or other structure

*Layers, *contacts, *outcrop, boulders, patterns, color

(BF) *Boulder Fields*

- Note minimum and maximum sizes observed 10° to 25° from the terminator
- Subjective judgments on SCT tracking of landed LM
- Note association and direction of boulder tracks

Association: Isolated, crater rim, crater wall, slope, dark halo, talus, slide

TABLE 1-I.—*Critical Item Checklist*—Continued

<p>Geometry: Size, shape, pattern, *boulder sizes *Tracks: Direction, length, starting position Source: Erosion, impact, eruption, *outerop</p> <p>(US) <i>Uncratered Surfaces</i></p> <ul style="list-style-type: none"> Note position and describe characteristics *Characteristics: Relief, color, albedo, reflections, patterns, boulders, fractures 	<p>Type: Mare, terra Shape: Rounded, flat-topped, elongate branching, *lobate Characteristics: Size, *slopes, *lobes, colors, *age relations Central crater: Size, shape, rim, wall texture, *caves, channels, bottom, colors *Superimposed cone (see Dark Halo Crater Checklist) *Associations: Surface, eruptive features, dikes</p>
<p>(OTC) <i>Outerops</i></p> <ul style="list-style-type: none"> Note location and associations of any observed outerops *Association: Crater wall, central peak, rille wall, terra slope, eruptive feature *Characteristics: Size, shape, color, reflections, accessibility 	<p>(DR) <i>Delta-Rimmed Craters</i></p> <ul style="list-style-type: none"> Determine if rim is a composite of cones, domes, and/or flows
<p>(DC/EC/CC) <i>Dark Halo/Elongate/Chain Craters</i></p> <ul style="list-style-type: none"> Identify any shallow impact crater fields near base of cone Identify any associated flows, channels, or color Identify any layers or caves in crater wall <p>Shape: Circular, elliptical, arcuate, linear Halo: Shape, limits, relief, patterns, rays, *boulders, small craters, colors, superposition Cone: Shape, breaching, *channels, patterns, boulders, *colors Crater: Shape, wall texture, caves, channels, bottom, *colors *Associations: Alinements, domes, flows, faults, contacts, geologic units, age relations</p>	<p>(RL) <i>Rilles</i></p> <ul style="list-style-type: none"> Observe <i>tails of sinuous rilles</i> for evidence of alluvial deposits Observe <i>heads of sinuous rilles</i> for evidence of exact source of any erosion agents Note any interruptions in continuity of small sinuous rilles, such as ridges or bridges Determine any interruptions in continuity of small sinuous rilles, such as ridges or bridges Determine strain relationships near angular and arcuate rilles
<p>(G/F) <i>Grabens/Faults</i></p> <ul style="list-style-type: none"> Note nature, age, and direction of offsets Determine associated strain relationships <p>Shape: Linear, enechelon, angular Associations: Eruptive features, rilles, parallelism, constant angles, age relations *Offsets: Contacts, ridges, craters, patterns Ends: Shape, termination point</p>	<p>(C) <i>Color</i></p> <ul style="list-style-type: none"> If visible color is observed, note associated features in as much detail as possible Note any color contrasts on cliffs or steep slopes <p>*Association: Mare bench, halo crater, dome, cliff, boulder field, rille, very dark or very light/fresh areas *Color chart: Best match, range, phase variation Contacts: Change, sharpness, associated variations</p>
<p>(R) <i>Ridges</i></p> <ul style="list-style-type: none"> Identify any attached or superimposed flows, cones, or dikes Determine associated strain relationships <p>Type: Mare, terra Shape: Rounded, flat-topped, wrinkle, branching, composite Characteristics: Colors, age relation *Association: Cones, domes, dikes, local flows, rilles, fractures</p>	<p>(Z) <i>Zero-Phase</i></p> <ul style="list-style-type: none"> At zero-phase point on mare approximately 16° from terminator, note horizontal and vertical limits of effective washout Judge lighting limits for LM landing
<p>(D) <i>Domes</i></p> <ul style="list-style-type: none"> Identify any attached or superimposed flows, cones, or dikes 	

TABLE 1-I.—*Critical Item Checklist*—Continued

- Note any albedo contrasts on cliffs and steep slopes
Albedo: *Contacts, features, detailed associations
*Washout: Horizontal limits, vertical limits, range function, terrain function, relief definition limit

Terminator

- Identify any flow fronts on low relief surfaces
- Identify any alluvial and/or braided fans at the tails of sinuous rilles
- Note any glows or obscurations at lunar sunrise (near side) terminator
*Subtle relief: Benches, flows, patterns, roughness, boulder fields
*Lunar sunrise: Glows, obscurations

Earthshine

- Evaluate landing and landmark tracking feasibility
Washout: Horizontal limits, vertical limits, range function, terrain function, relief definition limit
Visibility: Dark adaptation, features visible, minimum crater size, Earth angle function
*Features: Known detail, relief contrast
Zero phase: Albedo contrast, washout, *spotmeter
*Landmarks: Smallest crater, initial points

Transients

- Note associated features and temporal variations
Position: Declination/direction, *association
Characteristics: Brightness, color, type, size, shape, obscuration, flash
*Variation: Temporal, movement, terminator, position
*Source: Feature, area

Darkness (Spacecraft)

- Note celestial position and coverage of any observed dim-light phenomena such as:
Star field: General density, identification
Gegenschein: Antisolar (Gemini), intensity, shape
Zodiacal light: 90° from Sun to corona
Atmosphere: Star halo, glow after sunset or prior to sunrise
Libration points: Central Gemini, begin observation at LOS

Sunrise (Spacecraft)

- Note celestial limits of solar corona
- Note beginning and extent of limb brightening prior to sunrise
- Note first observation of contamination cloud and change in visibility immediately after sunrise
Limb brightening: Start GET, start position, max GET, max position, colors, diffuse light GET, diffuse light position
Solar corona: First light GET, boundary GET, streamer direction, bead GET, bead position, colors
Exterior contamination: Cloud GET, visibility change
star recognition, S/C shadow

Translunar / Transearth

- Note celestial position and coverage of any dim-light phenomena
Aurora: Shape, color, limits
Exterior contamination: Star field degradation, temporal changes
Libration points: 21.5 hours GET, Pisces (♊), Aries (♈), Pleiades

2

Initial Photographic Analysis

AREAL COVERAGE

JAMES H. SASSER AND F. EL-BAZ

The combined Apollo 8 photographic coverage of the lunar surface is summarized in figure 2-1. Much of this area was photographed by Luna III and Lunar Orbiters I to V. However, the Apollo 8 photography was taken with different lighting conditions and at different viewing angles. In addition, the resolution of Apollo 8 photography is in most cases significantly better.

Detailed index charts of the areal coverage of the different film magazine types can be found in

the pocket of the inside back cover. Coverage by the film magazines is indicated by different colors, and frame numbers are given within the footprints of the frames. Data pertaining to the 70-mm film are also tabulated in appendix A, together with reproductions of the recovered film.

COMPARISON WITH LUNA III PHOTOGRAPHS

E. A. WHITAKER

The Soviet spacecraft Luna III photographed the lunar eastern limb and adjacent far-side areas in October 1959, under essentially full-Moon

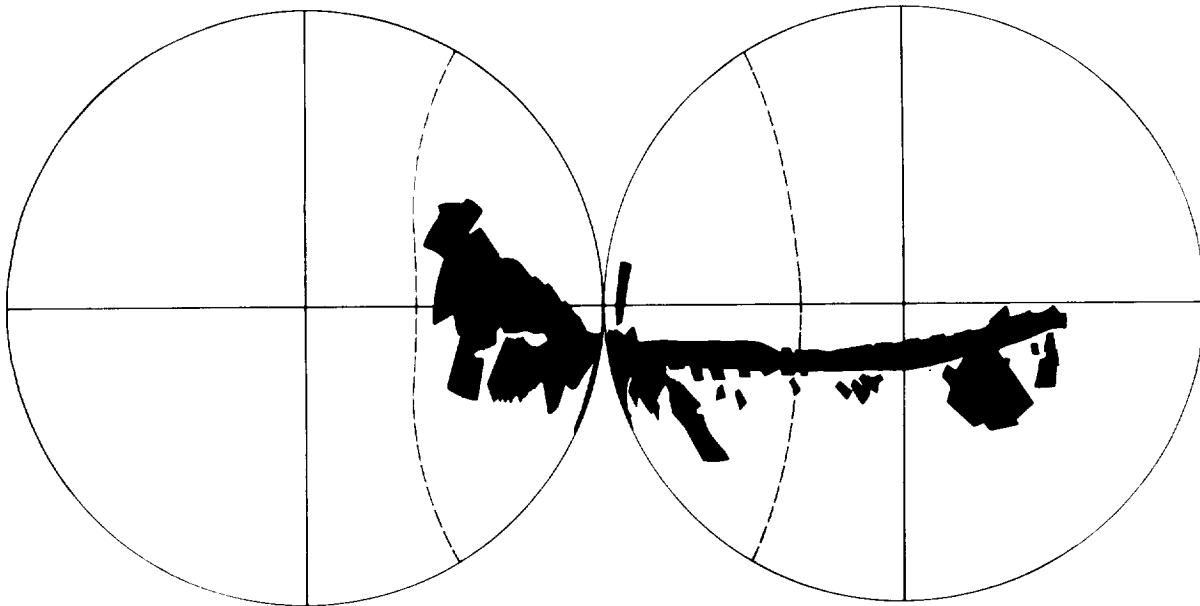


FIGURE 2-1.—Lunar-surface coverage of Apollo 8 photography.

illumination. Although analysis of the material by two Soviet groups (Leningrad and Moscow) produced somewhat different results, the Moscow group added 18 new names to the more prominent features. The most definitive discussion of the Luna III material is probably that given in references 2-1 and 2-2.

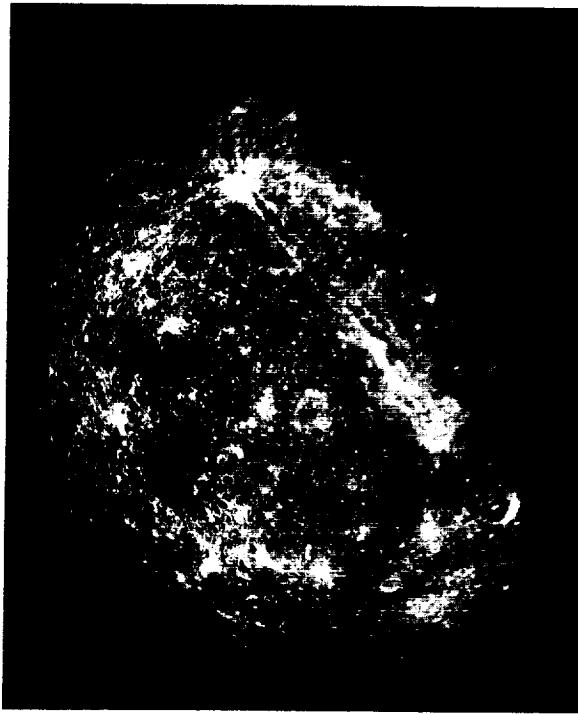


FIGURE 2-2.—Apollo 8 frame 2506-B recentered on Luna III subspacecraft point.

Although the five Lunar Orbiters photographed the entire area included in the Luna III material, the totally different illumination and viewing-angle conditions have largely rendered comparative studies impossible. However, these difficulties have now been almost entirely removed by the Apollo 8 acquisition of a number of photographs of the Moon after transearth injection (TEI). Illumination conditions closely matched those for Luna III (less than 7° difference), and viewing directions were not grossly different during this phase of photography.

For Luna III, the subspacecraft point was

17° N, 117° E. For Apollo 8 frame 2506-B, the corresponding coordinates were 8° S, 67° E, a difference of 25° latitude and 50° longitude. To facilitate comparison of the photographs, an image of frame 2506 was projected onto a precision 36-inch-diameter matte-white hemisphere using a $10\frac{1}{2}$ -inch-focus lens for nearly correct restoration of the geometry. The direction from which this image was then photographed was approximately the same as that of the Luna III photograph, although the correct scale distance could not be duplicated. Figure 2-2 is a reproduction of this recentered view. Figure 2-3 is a somewhat

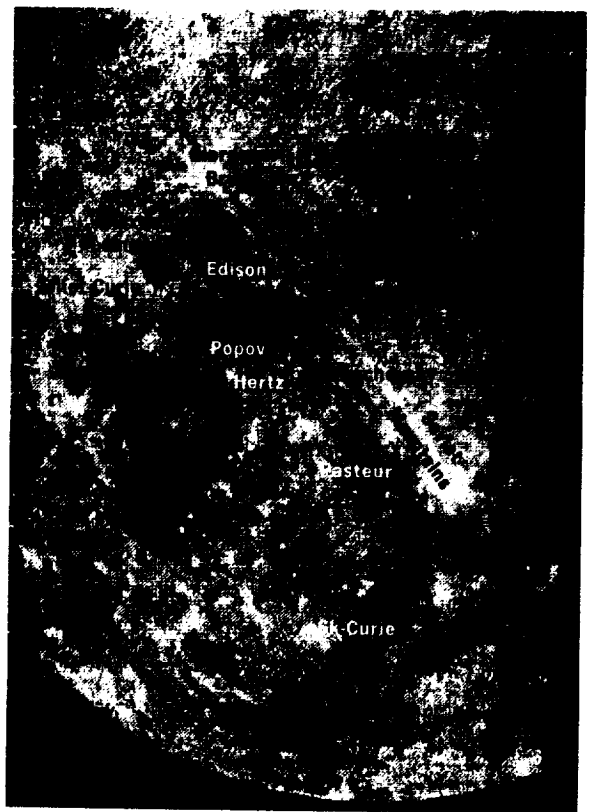


FIGURE 2-3.—Best Luna III frame with Soviet nomenclature added.

cleaned-up version of the best high-resolution Luna III frame, originally published in references 2-1 and 2-2. A considerable degree of correspondence exists between the two figures, particularly when viewed with a stereoscope.

DISCUSSION OF NAMED FEATURES

E. A. WHITAKER

PROVISIONALLY APPROVED NOMENCLATURE

The 18 new names given to far-side features by the Moscow group were submitted to and provisionally approved by the International Astronomical Union (IAU) in 1961 (ref. 2-3). Of these, 12 are covered by the Apollo 8 photography. It is, therefore, comparatively simple to ascertain the topographical nature and charted coordinates of these features via the sequence: Luna III map to Luna III photograph to recentered Apollo 8 photograph to appropriate Lunar Orbiter photographs to Aeronautical Chart and Information Center (ACIC), USAF, Lunar Farside Chart LFC-1. The latter records only 3 of the 12 names in question, namely Joliot-Curie, Lomonosov, and Tsiolkovsky. The remainder are discussed briefly.

1. *Giordano Bruno*.—Although at the center of a major ray system (fig. 2-4) which extends onto the earthward hemisphere as far as Mare Crisium, this sharp crater is only about 25 km in diameter.

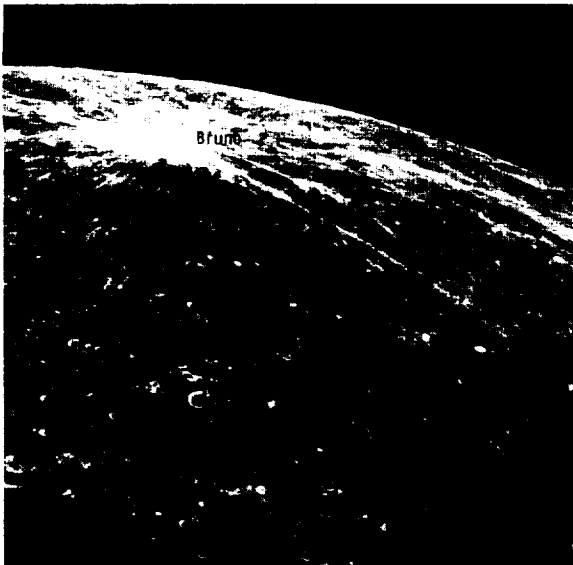


FIGURE 2-4.—Apollo 8 frame 2209-D showing Giordano Bruno ray system and other named features.

It is best seen on Lunar Orbiter V M-181 and is charted at 37.7° N, 102.5° E, on LFC-1.

2. *Maxwell*.—This is a 100-km-diameter formation with a dark, flat floor, overlapped by Lomonosov (fig. 2-4). It is best seen on Lunar Orbiter V M-181 and is charted at 31° N, 99° E, on LFC-1.

3. *Edison*.—Edison is a 60-km-diameter, dark-floored formation contiguous with Lomonosov (fig. 2-4). It is best seen on Lunar Orbiter V M-181 and is charted at 26.2° N, 100° E, on LFC-1.

4. *Popov*.—A 6-km-diameter crater situated in an ill-defined bright area (fig. 2-4), Popov is best seen on Lunar Orbiter IV M-146. It is not charted on LFC-1 but would be situated at 15.5° N, 97.5° E.

5. *Hertz*.—A 10-km-diameter crater with a small nimbus, Hertz is situated on the floor of a larger crater (fig. 2-4). It is best seen on Lunar Orbiter II M-196 and is charted at 11.5° N, 98.7° E, on LFC-1.

6. *Lobachevsky*.—This feature is a vague, darkish area that does not correlate with a crater. The area is best seen on Lunar Orbiter II M-196 and is centered at 8° N, 110° E, on LFC-1.

7. *Pasteur*.—A sharp-edged crater some 30 km in diameter with moderately bright walls, Pasteur is surrounded by a vague nimbus. It is best seen on Lunar Orbiter II M-196 and is charted at 9° S, 109° E, on LFC-1.

8. *Skłodowska-Curie*.—The central crater of this small but conspicuous nimbus is only 5 km in diameter. Best seen on Lunar Orbiter II M-196, it is charted at 21.2° S, 99.5° E, on LFC-1.

9. *Soviet Range (Montes Sovietici)*.—This elongated bright area was misinterpreted as a mountain range by the Moscow group (ref. 2-4). The author previously interpreted the marking as two distinct overlapping ray systems (refs. 2-1 and 2-2), a conclusion confirmed by Apollo 8 photographs. The center of the southernmost ray system is a sharp-featured crater 35 km in diameter, best seen on Lunar Orbiter III M-121 and charted at 5.7° S, 121.5° E, on LFC-1. The center of the more northerly system is a 90-km-diameter crater with sharp features and a large central peak. It is poorly depicted on Lunar Orbiter I M-136 (overexposed) and Lunar Orbiter IV M-122 (low resolution). It is charted at 4° N, 120° E, on LFC-1.

PROPOSED NOMENCLATURE

At the 1967 General Assembly of the IAU, it was agreed that the new names for lunar far-side features suggested by the Soviets on the basis of their Luna III and Zond III missions should be held in abeyance until a specially appointed subcommittee could examine the whole question taking the far-side Lunar Orbiter photography into account. As a guideline, it was decided that about 500 new names be used; that is approximately the number of craters 50 km in diameter or larger that are present on the far side.

The following recommendations will be forwarded to Commission 17 (The Moon) of the IAU by the author for action by the Subcommittee on Lunar Nomenclature:

1. The natures and coordinate positions of the following features are confirmed: Giordano Bruno, Maxwell, Lomonosov, Edison, Joliot-Curie, and Tsiolkovsky.

2. The following names should be reassigned: Popov, Hertz, Lobachevsky, Pasteur, and Sklodowska-Curie.

3. Montes Sovietici (Soviet Range) is incorrectly classified.

4. The source craters of the bright ray system, which was misinterpreted as a mountain range by the Soviets, should receive names. The northern crater will receive a name automatically because of its diameter, but the diameter of the southern crater is less than 50 km. Giordano Bruno is also less than 50 km, but the retention of its name is indicated because of its extensive ray system.

GEOLOGY

PRELIMINARY COMPARISON OF APOLLO 8 AND LUNAR ORBITER PHOTOGRAPHY

ROBERT G. STROM

Introduction

Both the Apollo 8 and Lunar Orbiter photography are good sources of information for geologic and terrain studies of the lunar surface. The Lunar Orbiter photography provides high-resolution coverage of practically the entire surface of the Moon. However, the Apollo 8 photography has several important advantages over the Lunar

Orbiter data, and although it does not replace the Lunar Orbiter data, the Apollo 8 photography does supplement the records.

The Apollo 8 photography has provided good stereoscopic coverage unhampered by the slightly offset strips characteristic of the Lunar Orbiter photographs. It is now possible to obtain accurate quantitative measurements of the elevations and slope angles of relatively large areas of the lunar surface by standard photogrammetric techniques. Accurate contour maps and accurate positioning of features on the back side should now become a reality.

Relatively distortion-free, full-disk lunar photographs were obtained from Apollo 8. These will enable the selenodesist to make accurate position measurements and better determine the figure of the Moon.

Because the Apollo 8 film was returned to Earth, it was possible to process it under controlled conditions. Therefore, the Apollo 8 photographic prints have a greater dynamic range than the Lunar Orbiter prints; one result is that the Sun-exposed slopes show considerably more detail than comparable Sun-exposed slopes on the Lunar Orbiter prints.

One of the most valuable aspects of the Apollo 8 photography is that extensive photographs under high-illumination conditions (Sun angle greater than or equal to 50° from the horizontal) were obtained for large areas of the lunar far side. This achievement has resulted in much new information that has an important bearing on geologic interpretation and terrain studies, and which should be of significance to future lunar ground operations.

Also new with Apollo 8 is vertical high-resolution terminator photography (Sun angle less than or equal to 7° from the horizontal), which shows very small elevation differences and emphasizes fine structural detail. The Lunar Orbiter records contain only several medium-resolution photographs with Sun angles less than 7° , and even these are not well exposed near the terminator.

Resolution

A preliminary evaluation of the resolution of the Apollo 8 photography indicates that the vertical 80-mm lens records have a resolution slightly better than the best Lunar Orbiter photographs

of the far side taken with the 610-mm lens. This greater resolution is due to the fact that the Apollo 8 spacecraft was at an altitude of 110 km above the lunar surface, whereas the Lunar Orbiter spacecraft was at an altitude of approximately 1300 to 1400 km over the far side. It is possible to resolve craters of approximately 60 meters in diameter on the high-resolution Lunar Orbiter photographs and of approximately 50 meters on the Apollo 8 photographs of the far side. However, the Apollo 8 prints used in making the comparison are sixth generation and, therefore, may be subject to an approximate 10- to 15-percent loss in resolution over the original film.

The Apollo 8 250-mm lens vertical photography taken from lunar orbit was recorded on color film SO-368. The resolution is approximately three times better than the 80-mm lens photography, recording craters as small as 17 meters in diameter. However, the prints made from the color transparencies and used in making the comparison are fifth generation and are, therefore, subject to an approximate 10-percent loss in resolution over the original film.

In summary, the Apollo 8 vertical photography has a resolution approximately 1.2 to 4.2 times higher than the best Lunar Orbiter photography of the lunar far side. A more accurate determination of the Apollo 8 photographic resolution must await examination of the original film.

High-Illumination Photography

One of the most important aspects of the Apollo 8 photography is the acquisition of high-resolution photographs under high-illumination conditions. For the first time, it is possible to compare topographic features photographed by Lunar Orbiter under relatively low lighting conditions (phase angle of approximately 20°) with the same features photographed by Apollo 8 under high lighting conditions (phase angles greater than or equal to 50°) and with approximately the same resolution.

Figures 2-5 to 2-8 are pairs of Lunar Orbiter and Apollo 8 photographs of the same areas taken under different lighting conditions. The Lunar Orbiter photographs were all taken at a relatively constant Sun angle of approximately 20° from the horizontal, while the Apollo 8 frames record Sun angles varying from 34° to 77° . As the Sun angle becomes greater, differences in albedo become

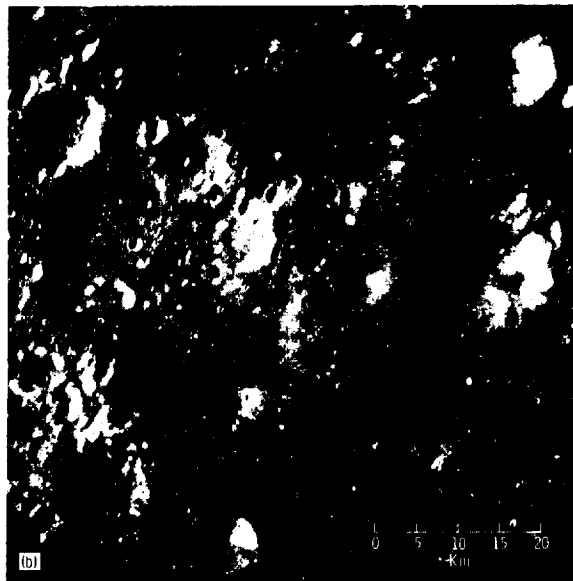
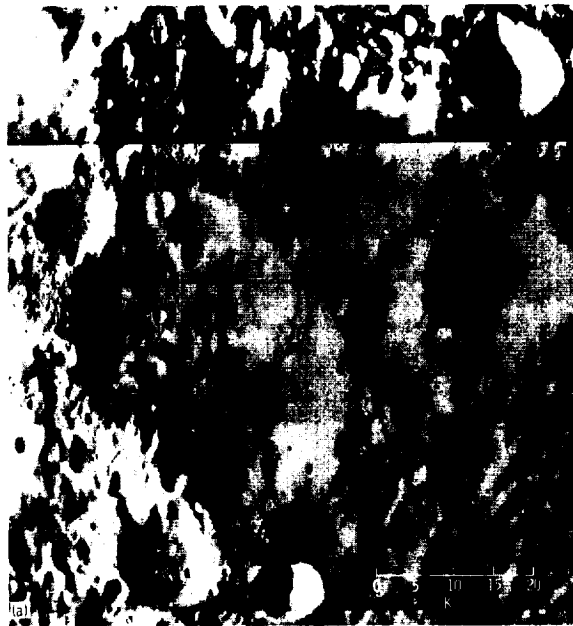


FIGURE 2-5.—Comparison of photography of same area (11° S, 174° E) on the lunar far side. (a) Portion of Lunar Orbiter II frame H-33 (Sun angle 20°); (b) Apollo 8 frame 2081-D (Sun angle 34°).

more apparent. On the Apollo 8 photograph in figure 2-5(b), albedo differences are just beginning to appear at a phase angle of 34° , and it is still easy to recognize topographic features by their shadows. At the higher phase angles (51° , 62° ,

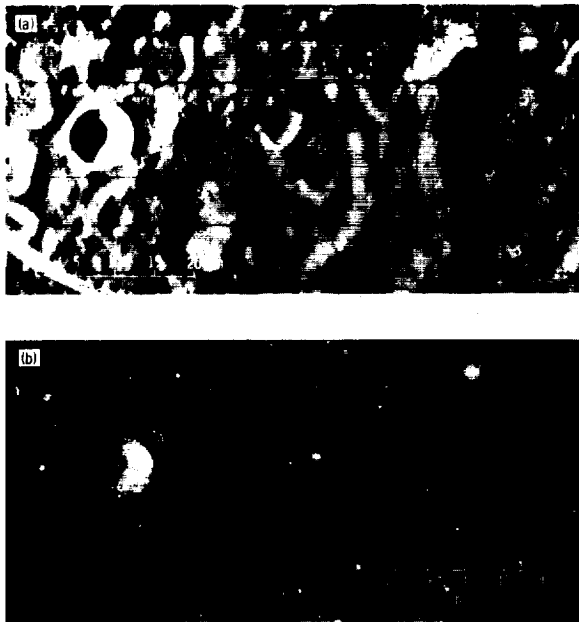


FIGURE 2-6.—Comparison of photography of same area (13° S, 157° E) on the lunar far side. (a) Portion of Lunar Orbiter II frame H-75 (Sun angle 19°); (b) Apollo 8 frame 2100-D (Sun angle 51.5°).

and 77°), shown respectively in figures 2-6(b), 2-7(b), and 2-8(b), the albedo differences are readily apparent; but it becomes considerably more difficult to recognize elevation differences because of the lack of shadows.

The surface of the Moon at high phase angles is covered by thousands of small bright spots and streaks which were observed visually and described by the Apollo 8 astronauts. These bright spots and streaks represent either the relatively steep slopes found on the interiors of craters and sides of hills, or rays and nimbi surrounding small, sharp craters. Examples of bright interior crater slopes are indicated at A in figures 2-6(b) and 2-7(b). These craters are sharp rimmed and bowl shaped, as seen on the matching low-Sun-angle Lunar Orbiter photographs (A in figs. 2-6(a) and 2-7(a)). The crater in figure 2-6 is about 8 km in diameter and 1.5 km deep, while that in figure 2-7 is about 10 km in diameter and 2 km deep. Judging by the extinction of shadows in craters of similar size and shape on other Apollo 8 photographs, the interior slopes are between 30° and 40° , the most likely angle being roughly 35° . On the interior slopes near the rim crest, the material



FIGURE 2-7.—Comparison of photography of same area (14° S, 146° E) on the lunar far side. (a) Portion of Lunar Orbiter I frame H-115 (Sun angle 20°); (b) Apollo 8 frame 2112-D (Sun angle 62°).

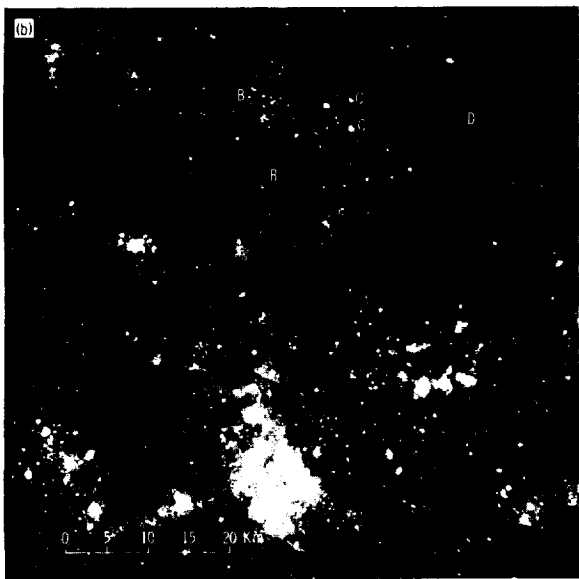


FIGURE 2-8.—Comparison of photography of same area (12° S, 127° E) on the lunar far side. (a) Portion of Lunar Orbiter I frame H-136 (Sun angle 21°); (b) Apollo 8 frame 2129-D (Sun angle 77°).

has a mottled appearance, which grades downslope into alternating dark and light streaks, the bright streaks being dominant over the dark. These bright streaks and patches probably represent newly exposed surfaces resulting from the downslope movement of the material.

Terminator Photography

The Apollo 8 mission succeeded in obtaining well-exposed vertical terminator photography at phase angles less than 7° . The Lunar Orbiter records contain only a few medium-resolution photographs with Sun angles less than 7° , and even these are not well exposed near the terminator. This type of photography is important, because it shows very small elevation differences and emphasizes fine structural detail that is not apparent on photographs taken at higher Sun angles. Analysis of terminator photography is not only important to the geologic interpretation of surface features but it is also helpful to mobility studies for roving vehicles.

Figure 2-9 is an Apollo 8 photograph taken at 5° S, 153° W, near the sunset terminator at a Sun angle of 2° . This photograph shows numerous shallow depressions and swales that are not visible at higher Sun angles. Unfortunately, all well-exposed Apollo 8 vertical high-resolution terminator photography was taken of the highlands on the far side of the Moon. The astronauts described the mare surface very near the sunrise terminator as having undulations similar to the surface of the sea. It is important to determine if these slight undulations are no more than features similar to the shallow depressions and swales seen in

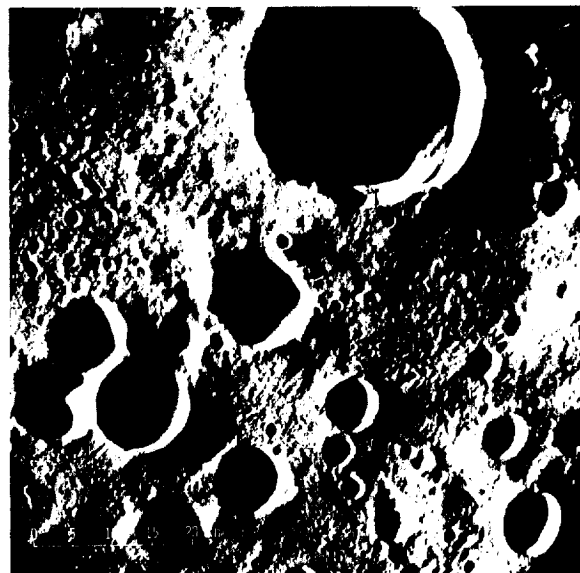


FIGURE 2-9.—Apollo 8 frame 2048-D of lunar far side.

figure 2-9, or if there is some fundamental difference between the very gentle topography of the maria and highlands.

Summary

The Apollo 8 photography is an important source of new information for geologic and terrain studies of the lunar surface. Several of the new aspects of this photography include:

1. Undistorted stereoscopic coverage along a continuous strip of terrain of more than 4800 km.
2. Relatively distortion-free, full-disk lunar photographs.
3. High-resolution photography exhibiting a continuous variation of Sun angles from 0° to 80°.

The resolution of the Apollo 8 vertical photography is roughly 1.2 to 4.2 times higher than the best far-side Lunar Orbiter records, and thus provides the highest resolution of the lunar far side acquired to date.

Conclusions from a comparison of the Lunar Orbiter low-illumination and Apollo 8 high-illumination photography include:

1. The degree of brightness is directly related to the inclination of the slope; the steeper the slope the brighter it is at high Sun angles.
2. The bright interior slopes of craters result from the downslope movement of material, exposing fresh surfaces.
3. All small craters with bright rays and nimbi on the high-illumination Apollo 8 photography correspond to sharp, fresh-appearing craters on the low-illumination Lunar Orbiter records. However, not all small sharp-appearing craters on the Lunar Orbiter records are bright on the high-illumination Apollo 8 photographs. Since the bright-halo craters are apparently the freshest craters, it appears that the examination of high-illumination photography is the best method of determining the degree of freshness of craters.
4. For safety reasons, bright, blocky crater halos and bright, possibly unstable, slopes should be initially avoided in ground operations. However, bright craters may be ideal for gathering fresh rocks that have been excavated from the solid subsurface layer.

PRELIMINARY INTERPRETATIONS OF LUNAR GEOLOGY

D. E. WILHELMS, D. E. STUART-ALEXANDER,
AND K. A. HOWARD

Lunar Far Side

The Apollo 8 photography augments the Lunar Orbiter photography of the far side. For the first time, good high-illumination photographs were taken from a spacecraft so that areas of different reflectivity could be delineated; in particular, rayed craters and mare areas. Reflectivity as seen on near-full-Moon photographs has been an essential tool in small-scale (1:1 000 000 and 1:5 000 000) lunar geologic mapping, and the lack of high-resolution reflectivity data has reduced the effectiveness of large-scale mapping. Such data are useful in estimating relative crater ages, locating rough terrain (bright), and identifying young volcanic deposits (dark). The Apollo 8 far-side photography also includes the best terminator photography obtained from a spacecraft. Both the high-Sun and low-Sun vertical photographs show good detail of the area directly under the orbital track, and the oblique photographs reveal a mountain range that had not been previously identified.

Two extensive ray systems that just overlap are shown in high-illumination Apollo photographs. A discussion of these ray systems, forming the so-called Soviet Mountains, and the source craters is given in the section of this chapter entitled "Discussion of Named Features." These two relatively small craters must be among the youngest on the Moon. Other such brightly rayed craters will probably be found from future high-illumination photography of the rest of the lunar far side.

Albedo variations are quite distinct in most high-Sun photographs (fig. 2-10). The abundance and wide distribution of fresh, rayed craters, down to the smallest resolvable sizes, are particularly impressive. Most of the ray patterns are symmetrical; however, several bright-rayed craters display ray-excluded zones. A discussion of this fact and of possible causes is given in the section of this chapter entitled "Craters."

Albedo differences are also distinct on mare surfaces. For example, Mare Smythii, whose circular form shows up with exceptional clarity,

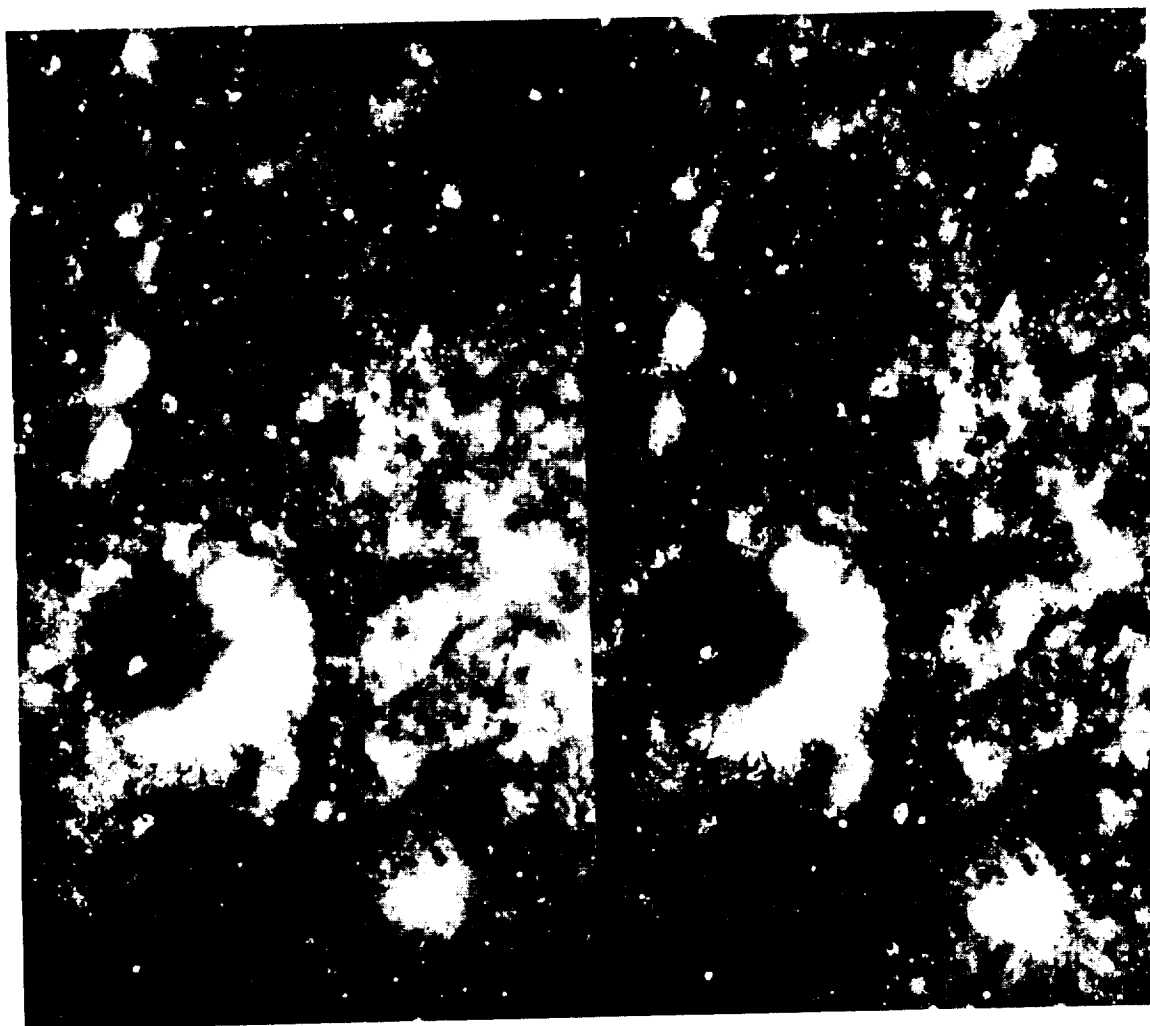


FIGURE 2-10.—Stereoscopic pair (Apollo 8 frames 2103-D and 2104-D). These photographs were taken at high Sun illumination and show various geologic features such as stripes in mass-wasting debris on crater walls; horizontal structure high on crater walls; numerous small, bright craters; and topographic features barely visible monoscopically.

appears in one high-illumination picture to have a partial dark border around a lighter interior (fig. 2-2). This is reminiscent of the wider dark border of Mare Humorum. Apparently, some of the youngest and darkest volcanic products are emplaced at the margins of circular basins.

Light and dark stripes running down crater walls much like stone stripes in talus are common (fig. 2-10). A zone of irregular, but generally horizontal, stripes is characteristically observed higher on the walls. The horizontal separation probably represents two kinds of mass wasting above and below a break in the slope along crater walls. Some horizontal stripes appear to be con-

tinuous around a number of craters and almost certainly represent a layer or a rock ledge.

The oblique shots from Apollo 8 are also useful because they cover a wide field of view and because relief features are seen more clearly. One interesting discovery from the oblique photography is a mountain range 200 km long located at 20° S, 160° W (fig. 2-11). This mountain range does not seem to be associated with any crater or basin. The range is also discernible in the upper center portion of Lunar Orbiter I frame M-38.

The strip of continuous photographic coverage makes conspicuous any variations in normal terrain patterns. For example, oddly patterned terra



FIGURE 2-11.—Mountain range on lunar far side (Apollo 8 frame 2319-E).

consisting of numerous subdued hummocks and swales, but containing few fresh craters, was identified at latitude 10° S, longitude 180° E. The topography is similar to the probable-volcanic units of the lunar near side in the vicinity of the craters Zupus and Descartes, and is crossed by an unusual round scarp or flow front similar to a mare ridge. (See the section of this chapter entitled "Possible Volcanic Features.") These features had been overlooked until they were seen in Apollo 8 photographs, but reexamination of Lunar Orbiter photographs showed that the unusual texture extends over a broad region to the south. A second area of interest is a field of secondary craters selected from Lunar Orbiter photography as Apollo Target of Opportunity (ATO) 12 at 9° S, 164° W. Although the intricate pattern of secondary craters, gouges, and lineaments in this area is displayed in detail by Apollo 8 photographs, the wide views of the Lunar Orbiter pictures are necessary to see the relation of the secondaries to their source craters and to the surrounding terrain. The Apollo 8 and Lunar Orbiter pictures are clearly complementary.

Lunar Near Side

It was hoped that additional photography could be obtained of large areas of the eastern front side and east limb where Lunar Orbiter photography is inadequate for reliable regional geologic studies. This section of the report describes the

extent to which knowledge of this region has been increased by Apollo 8 photography or can be improved by future lunar photography.

The south and east parts of the Crisium basin and the adjacent so-called lake country of small irregular maria were photographed poorly by Lunar Orbiter, and one location along the east Crisium basin margin was missed completely because of light-struck film. The same area was covered by Apollo 8 photography, but all of the photographs have relatively poor resolution. However, many of the photographs are useful for positioning of features, because they give a perspective that is different from Earth-based and Lunar Orbiter photographs. The color pictures of magazine B taken during TEI of large parts of the lunar disk centered near the eastern limb (fig. 2-2) fill in the previous coverage, provide an excellent perspective, and have better resolution than the Earth-based photographs. However, their resolution is less than that of the Lunar Orbiter photographs. The complex maria in this east-limb region can be mapped from these color photographs. Other coverage is on black-and-white film. Numerous photographs of magazine G (the high-speed film) cover this area and much of the rest of the eastern part of the Moon. These pictures have resolutions typical of Earth-based photographs, although again with a different perspective. Frames 2863 to 2866 are the best photographs taken of this entire area during the Apollo 8 mission and, therefore, for the area along the east Crisium basin margin missed by Lunar Orbiter, the best of all photographs. It is unfortunate that the Apollo 8 photographs were not taken with finer-grained film and a longer focal lens, or both. (The writer is not sure whether these photographs were taken with the 80-mm or 250-mm lens.) Photographs on magazine D (frames 2203 to 2206), taken with the 250-mm lens during TEI (before the color photographs were taken), also give useful regional views of the Mare Crisium/lakes region, although they show smaller areas than the other magazines and have poor resolution (film-grain limited); frame 2206 covers the totally missed spot. Other frames taken with the 250-mm lens on this magazine give similar regional views of the area farther east, at and beyond 90° E. Frames 2181 to 2184, which include part of the lake country, were

taken obliquely with the 80-mm lens; therefore, their resolution is also quite low, even though they were taken in lunar orbit.

Mare Fecunditatis, the Secchi peninsula (target of opportunity (T/O) 78a), and Mare Tranquillitatis were photographed most often by forward-looking obliques. A large block of photographs of this area is on magazine E. One sequence (frames 2339 to 2345)—in addition to some rather dark, poorly detailed pictures of Messier and Messier A (T/O 75), Mare Fecunditatis, and the Secchi peninsula—includes two excellent, well-exposed, and well-illuminated scenes in Mare Tranquillitatis taken with the 250-mm lens. One of these (fig. 2-12), which includes the Cauchy rilles and Cauchy domes (T/O 87, frame 2344), shows the area better than does any Lunar Orbiter photograph and is useful in spite of the extreme obliquity and low resolution. The same description applies to the other frame (2345, fig. 2-13) in the vicinity of landing site 1 where, unfortunately, the window cuts off the landing site 1 from view. The so-called training sequence (frames 2271 to 2309) is an improvement over Lunar Orbiter IV photography in approximately the first two frames, where the near scene is within the poor Lunar Orbiter IV frame H-61. The next frames, however, within



FIGURE 2-12.—Cauchy domes and rilles (Apollo 8 frame 2344-E).



FIGURE 2-13.—The crater Maskelyne F and the area north of landing site 1 (Apollo 8 frame 2345-E).

the area covered by Lunar Orbiter I frame M-41 and Lunar Orbiter IV frames H-66 and H-73, are not particularly useful. The western, near-terminator pictures in the vicinity of landing site 1 are underexposed and are north of landing site 1 proper. The only good frames in this sequence are frames 2300 to 2309 (fig. 2-14), which were taken when the camera was pointed back. The film sensitivity had also improved greatly, possibly through prefogging. Crater densities, fine textures in several geologic units (including one probably like that in landing site 1, unit *tm* in fig. 2-14), and relations among mare ridges (showing overlap of a subdued ridge by a sharp one) are all brought out in the low-Sun illumination (fig. 2-14).

The part of the continuous strip of magazine C that falls within the Fecunditatis-Secchi-Tranquillitatis area has too low a resolution to be any more useful than even the poorest Lunar Orbiter photographs, because it was taken at an extreme oblique angle and with the 80-mm lens. The only useful parts of the latter strip on the front side are those near the subspaceship point; namely, those in the eastern parts of frames to approximately 2798 covering the terra east of Langrenus. These frames have better resolution than the Lunar Orbiter photographs of the same area. Ages of craters are easier to determine from the Apollo 8 photographs than from the Lunar Orbiter photographs, because the details of mass wasting seen on Apollo photographs are more diagnostic of age than the details of topography seen on the Lunar Orbiter photographs taken at a lower Sun angle. Forward-looking obliques taken with the



- c Crater material
- cci Irregular crater material, clusters (volcanic)
- ci Irregular crater material, single
- d Dome material (volcanic?)
- m Mare material
- mh Hilly mare material (small volcanic constructs?)
- mr Undivided mare ridge material
- mr₁ Older mare ridge material
- mr₂ Younger mare ridge material
- th Hilly terra material
- tm Terra-mantling material (similar to that in site 2 P-2?)
- ts Smooth terra material
- Contact
- - - Inferred contact
- ||||| Depression
- ▼ Scarp

FIGURE 2-14.—Area northeast of landing site 1.

80-mm lens are best out to approximately 5° from the subspacecraft point and are useful out to 10°.

Frames 2779 to 2788, magazine C, are in the vicinity of Mare Smythii and include some of the ring craters (possible calderas) characteristic of this region. The photographs have a much higher resolution and a very different illumination than the best Lunar Orbiter picture, IV H-27. A comparison of Lunar Orbiter and Apollo pictures taken at different illuminations was one of the main objectives of Apollo 8 photography, and the vicinity of Mare Smythii is the only place it can be done with near-vertical pictures taken on the near side. (For the results of this comparison, see

the subsection "Rayed Craters and Bright-Halo Craters" in the section of this chapter entitled "Craters.")

The obliques taken with the 250-mm lens near the terminator of the Goelenius-Capella area (magazine E) (for example, fig. 2-15) are a considerable improvement over Lunar Orbiter IV H-65. The type of terrain can be identified; the age of craters and other units can be estimated by their freshness; and craters on plains surfaces can be counted. The photographs are also an improvement over Lunar Orbiter IV H-72, but less so, because the latter are fairly good. The main objective achieved by the sequence was to fill in the Colombo area (T/O 73). A large number of the targets of opportunity selected to be taken on this mission are nearby, but most of them are either not within the strip taken or they are shadowed by higher peaks. The only ones seen are the McClure cluster (T/O 72) and the hilly, probably volcanic materials (T/O 84). These illustrate the potential value of target preselection. However, the other Apollo 8 pictures add information on the fine textures of craters and relatively flat-lying materials that permits their classification. It is concluded that pictures taken with the 250-mm lens out to 12° to 14° from the groundtrack are useful for geologic purposes.

Extreme obliques taken near the terminator south of the track after the Goelenius-Capella



FIGURE 2-15.—Part of Mare Fecunditatis and the craters Goelenius, Magelhaens, Magelhaens A, and Colombo A (Apollo 8 frame 2225-E).

pass (also magazine E) show the crater Daguerre (T/O 94) and much of Mare Nectaris. The copies of these which were available for study are too dark to be useful, but copies viewed earlier at the NASA Manned Spacecraft Center were good and potentially useful. However, these extremely oblique photographs should be used in conjunction with vertical photographs from Lunar Orbiter, which show shapes in plain view better than Apollo 8. Southwest of Daguerre is a cracked, low, circular, domelike area about 30 km in diameter that is cut by fresh cracks and split into blocks standing at various levels. This feature was observed on Lunar Orbiter photographs (H-72), but its raised, domelike character was not recognized until the Apollo 8 picture, which was taken at a lower Sun illumination. It is one of several probable volcanic features in this margin of Mare Nectaris.

There are two sequences in magazine E taken at an extreme oblique angle of the Sinas-Jansen-Vitruvius area (including T/O 106 and T/O 107) near the terminator north of the track. One sequence (frames 2846 to 2850) has the proper exposure to bring out useful detail at the very low Sun angle and gives by far the best pictures of this area. Details of mare ridges and a variety of domes are brought out by shadows. The other sequence (frames 2334 to 2338) is too dark to be useful. (At least, the copies available to the writers are too dark.) The good pictures among these demonstrate that near-terminator photography is always desirable even at extreme oblique angles, provided it is properly exposed.

Targets of opportunity taken obliquely in the east-limb region, where the Sun angle was intermediate (39° to 63°), yielded approximately the amount of information hoped for when taken with the 250-mm lens. The photographs (taken on magazine E) are an improvement in resolution over Lunar Orbiter photographs of the same region, and neither the lack of strong shadows nor high albedo contrast prevents information from being extracted. The best of these T/O photographs is that of T/O 65, the crater Kapteyn (frame 2270). Its angle of obliquity (6° from the groundtrack) is quite satisfactory for good perspective and resolution, and details of the mass-wasting process of its slopes can be seen. Other pictures, though good, yield few new geologic results. Target of opportunity 58, thought to be

a fairly fresh crater with secondaries (frames 2262 to 2264), turned out to be not so fresh and was partly missed; the pictures are of little interest except as fill-in. Crater Behaim (T/O 63), with a domical central peak (frames 2268 and 2269), was well photographed, although the angle was at approximately the extreme of usefulness (10° from the groundtrack); however, the peak lacks detail, and nothing was learned about its origin. The crater Ansgarius was also included with these targets and provides a view of older, large craters.

CRATERS

Crater Characteristics

F. EL-BAZ

Introduction

Apollo 8 photography will be of value in the study of the cratering process in general and probable impact craters in particular, because areas on the far side of the Moon that are heavily populated with probable impact craters received good photographic coverage with favorable lighting and viewing conditions. Some craters of probable volcanic origin, however, were also photographed.

Some of the more imposing impact features were photographed following TEI, where near-full-Moon photographs (frames 2462 to 2506, magazine B) display a number of bright-rayed craters. Several of the familiar probable impact craters on the Earth side are clearly visible (fig. 2-2). The crater Humboldt is in the lower part of the photograph, and the mare-filled crater Tsiolkovsky is near the lower right edge. Two bright ray systems forming the so-called Soviet Mountains dominate the area in the middle portion of the photograph (figs. 2-2 and 2-4).

At high-Sun angles, details of impact craters are well recorded. This is particularly true in the case of fresh or relatively young craters, where the usually bright ejecta surrounding the crater contrast strongly in albedo with their surroundings. For this reason, most of the vertical as well as the oblique high-Sun photographs taken by the Apollo 8 crew appear "peppered" with small, bright spots, many of which are surrounded by radial ray systems (fig. 2-10). The Apollo 8 astro-

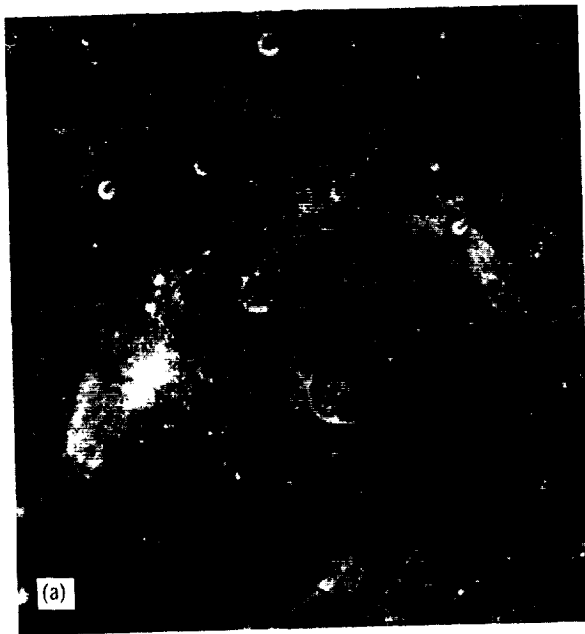


FIGURE 2-18.—Crater rays. (a) Ray-excluded zones around probable impact craters (Apollo 8 frame 2869-G); (b) oblique view of craters Messier and Messier A. Note the zero-phase point directly below the craters. The Sun angle is 17° (Apollo 8 frame 2341-E).

at 11° S, 165° W. The interior walls of the crater are terraced, and the terraces display layering. The crater has an irregular but fresh-appearing central peak, and the floor is strewn with large mounds of rock. The outer rim of the crater shows characteristics of impact-produced ejecta, including a number of secondary crater chains. Lunar Orbiter I photograph M-28 shows that the crater has a well-developed bright-ray system.

Figure 2-20 is a set of Apollo 8 photographs depicting large blocks of lunar rocks. One segment of the crater is enlarged in figure 2-20(a). The layering is brought out by the effect of shadows (Sun angle 17°). In this 250-mm lens view, block fields are quite evident on the floor, along the terraced walls, and on the crater rim. Two large blocks, larger than 100 meters in diameter, are circled; one is on the rim and the other on the

crater wall. Many other blocks are visible, especially near the upper edge of the photograph.

In figure 2-20(b), large blocks are clearly seen on the shadowed crater wall in the middle of the photograph. The area illustrated in figure 2-20(c) is within 5° on the lunar surface from the crater in figures 2-19 and 2-20(a). In the center of the photograph, a small trough cuts through an old, subdued crater. Near the southern end of the trough, a large north-south-trending ridge or block can be seen clearly. This ridge resembles a half-buried disk standing on edge. A block near the northern end of the trough displays a similar form. (The block circled on the outer rim of the impact crater in fig. 2-20(a) bears similarity to this form.)

Other blocks were observed visually by the Apollo 8 crew on the central peak of Tsiolkovsky.



FIGURE 2-19.—Impact crater with well-developed field of secondaries (Apollo 8 frame 2245-E).

In agreement with studies relating block size to crater size, the large blocks observed by Apollo 8 occur in and around large craters. No doubt many small blocks are present in association with smaller craters on the far side, but they were not resolved by the lenses used.

Crater Chains

Continuous and/or discontinuous chains of craters and crater clusters are common on the lunar surface. Many of these are similar to volcanic crater chains on the Earth and may be the product of lunar volcanism. Others appear to be

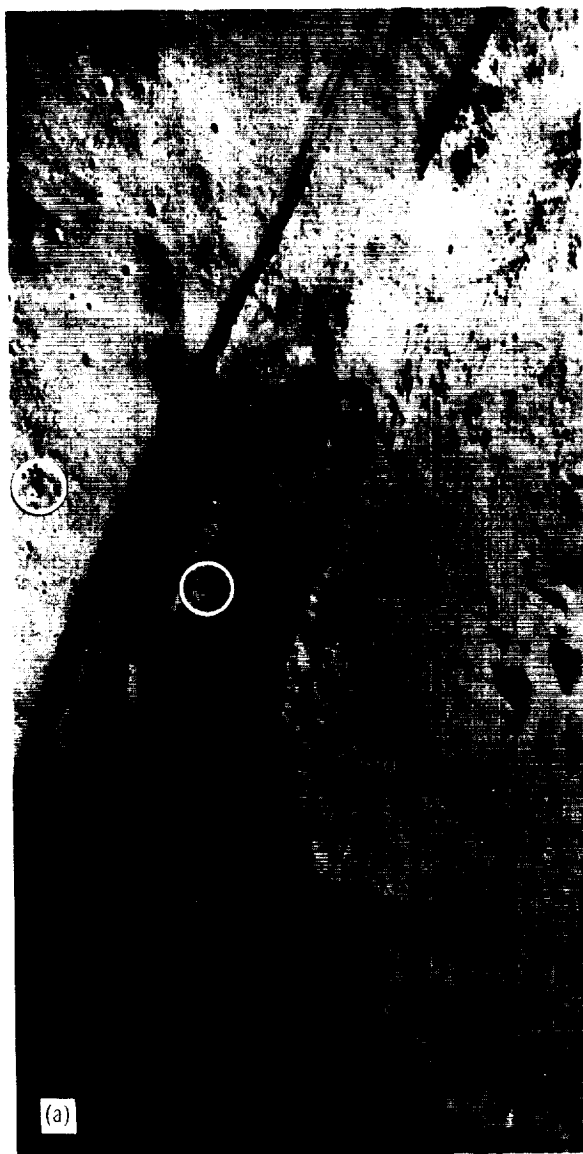


FIGURE 2-20.—Apollo 8 photographs depicting large blocks of lunar rock. (a) Frame 2328-E, (b) frame 2266-E, (c) frame 2060-D.

the product of ejected material from impact craters and are described as secondary crater chains.

Apollo 8 photography includes several examples of crater chains (figs. 2-21 and 2-22). In figure 2-21, a crater chain is made of several round-to-elongated craters alined in one direction. The

chain is discontinuous; the crater in the lower right corner of the photograph is separated from the rest of the chain. Between this crater and the next one in the chain is a trough which is probably a graben. The four craters in the middle are of approximately equal size but of varying depth.

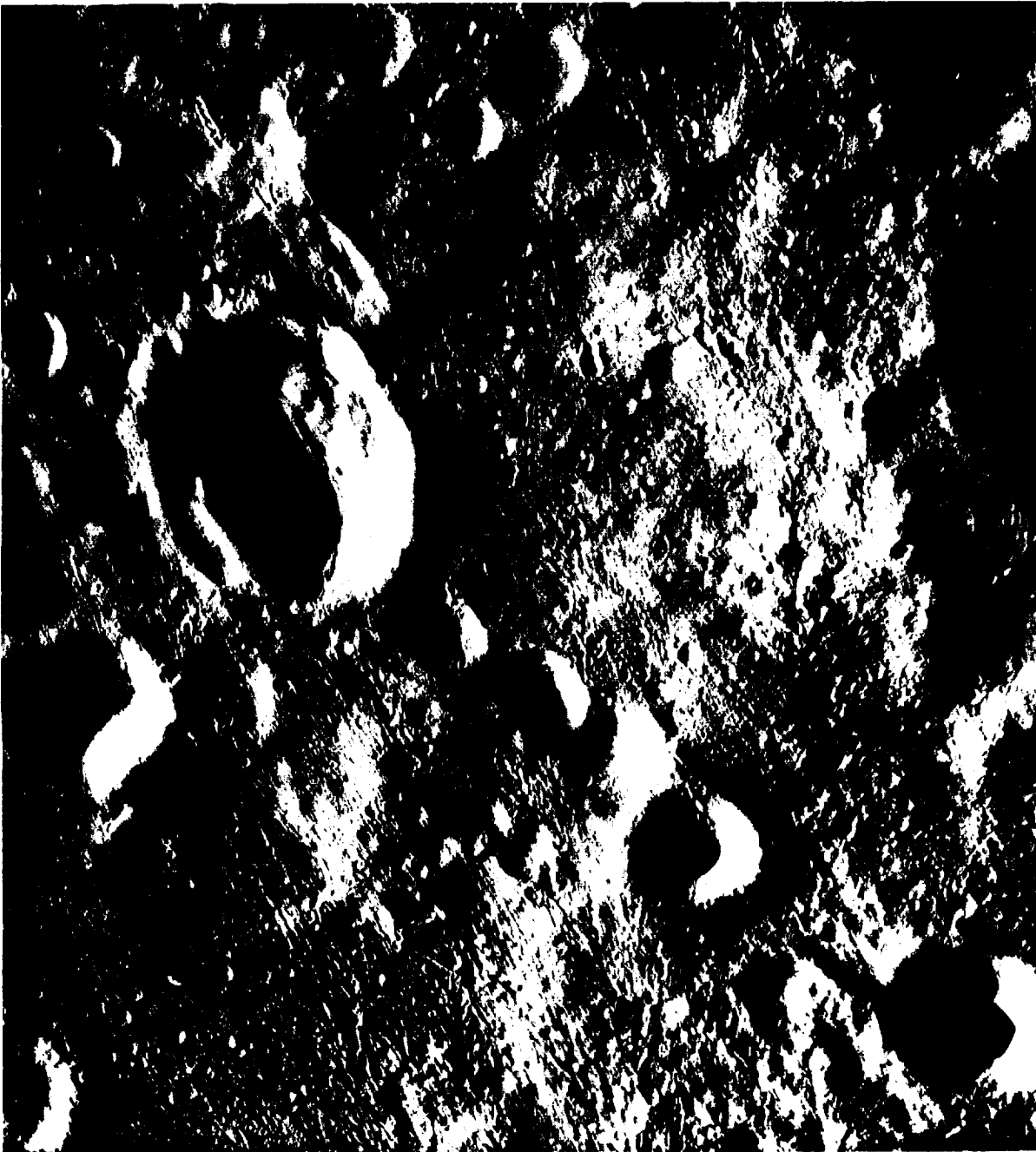


FIGURE 2-21.—A probable volcanic crater chain (Apollo 8 frame 2673-C).

The largest depression, on the upper left end of the chain, has an elongated form, a raised-but-not-very-sharp rim, and an irregular interior. This interior is suggestive of a crater pair rather than of a single crater. These characteristics suggest

that the chain is of internal origin; that is, that it is a volcanic crater chain.

The photograph in figure 2-22 was taken at low-Sun angle, about 7° . Although shadows cover part of the crater interiors, much detail is clearly



FIGURE 2-22.—A probable secondary crater chain (Apollo 8 frame 2053-D).

visible. The crater chain running from the lower right to the upper left parts of the photograph is different from the crater chain described previously. In this case, a large, elongated depression abuts against a crater with a polygonal form. Following a break in the chain, a crater cluster made of craters similar in shape is seen. The craters of the cluster are of different sizes, but their depths are proportional to their sizes.

Both parts of the crater chain are surrounded by lineaments, which form an irregular V-shape pointing toward the lower right end of the chain. Such features have been called "herringbone" structures and are thought to be the product of deposition of material from ejecta streams that are secondary to a larger impact crater. (See the section of this chapter entitled "Hypersonic Gas Flow.") This array is located at about 5° S,

157° W. It bears similarity to other chains of craters and crater clusters previously photographed by Lunar Orbiter IV. The array is believed to be, and probably is, secondary to the craterlike Mare Orientale.

Small craters also form continuous and/or discontinuous chains. Apollo 8 near-terminator photography of the lunar far side includes several examples.

Rayed Craters and Bright-Halo Craters

NEWELL J. TRASK AND GORDON A. SWANN

It has long been known that contrasts in the albedo of lunar surface materials show up most clearly under high angles of Sun illumination. Spacecraft photographs have indicated clearly that this effect extends to small features, especially craters with rays and bright halos. Very few rayed and bright-halo craters are seen on photographs taken with low angles of Sun illumination in contrast to numerous such features on higher-Sun-angle photographs. The photographs taken by the Apollo 8 crew include many with angles of Sun illumination higher than those of any previous spacecraft photography. As expected, these high-Sun-angle photographs show a myriad of bright spots at the positions of craters with rays, bright halos, and walls. These craters are of interest because they are the youngest features on the Moon and may be surrounded by fresh ejecta of lunar bedrock. Also, they may pose hazards to landing spacecraft.

Direct comparison of several of the Apollo 8 frames can be made with Lunar Orbiter photographs of comparable scale taken with much lower Sun angles. Seventy-five craters on part of Apollo 8 frame 2787-C on the east limb appear to have rays or bright halos, compared to 18 craters in the same area covered by Lunar Orbiter IV H-27. Corresponding numbers on Apollo 8 frame 2112-D on the far side and Lunar Orbiter I H-115 are 65 and 12, respectively. Thus, many craters in the Apollo landing sites may have rays or bright halos that are presently unrecognized. Figure 2-23 shows a typical cumulative count of bright-halo and rayed craters from Apollo 8 photography. Only craters having a clearly defined bright halo or set of rays were included; bright spots which

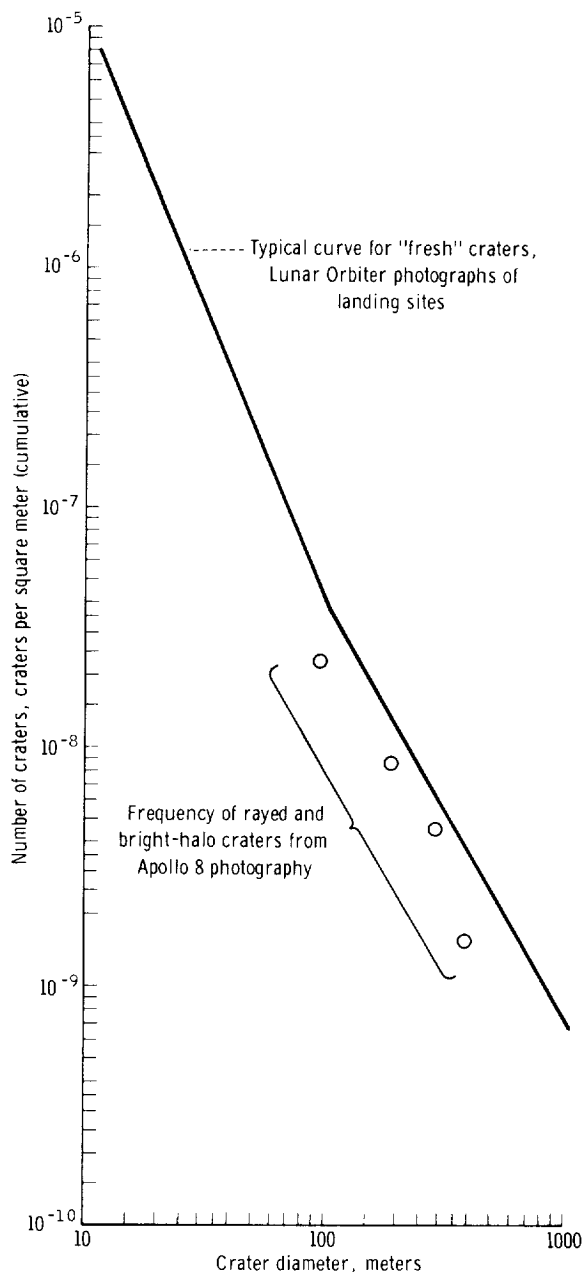


FIGURE 2-23.—Frequency of rayed and bright-halo craters on Apollo 8 photography compared with frequency of "fresh" or eumorphic craters on low-Sun-illumination photographs.

might be only the bright walls of craters were not included, although many are probably small, bright-halo craters. Also shown is a typical count of so-called eumorphic or "sharp" craters in Apollo landing sites made from low-Sun-angle

photographs. Allowing for differences in judgment as to what constitutes a sharp crater, the two curves are in essential agreement for crater diameters of 100 meters. Accurate counts of rayed and bright-halo craters for diameters less than this cannot be made on the Apollo 8 photographs presently available to us; and whether the two curves continue to agree to smaller sizes is not known. High-Sun-angle photography with higher resolution could answer this question. Nor is it known if the points for the bright-halo and rayed craters apply equally to the areas studied and to the Apollo landing sites, but it seems likely that they do. Visual comparison also shows clearly that some large, sharp craters (up to several kilometers in diameter) do not have bright halos, although they do have bright walls. Apparently, the rays and bright halos are of such a thickness that they have been destroyed on some large craters, although this degradation has not appreciably changed the apparent sharpness of the rim crest.

An important observation made during the comparison of the Apollo 8 and Lunar Orbiter photographs is that several craters on sunward-facing slopes are not especially sharp and yet have distinct bright halos. These craters have somewhat fuzzy, indistinct halos on the Lunar Orbiter photography, and it was not clear if these were genuine bright halos or were some sort of optical effect developed on the bright, sunward-facing slope. The first interpretation now appears to be correct. In annotating large-scale photographs of the Apollo landing sites for use in the onboard data package, all mappers noticed similar questionable bright-halo craters without sharp rim crests on sunward-facing slopes. Some of these were shown as bright-halo craters, but many were not. It now appears that the number of bright-halo craters in the landing sites should be increased at least by these examples which earlier were in question. The bright-halo craters without sharp rim crests probably are morphologically subdued from the time of their formation because of the instability of loose debris on the slopes.

Assessment of the hazards posed by the probable increase in the number of rayed and bright-halo craters in the Apollo landing sites depends on the interpretation placed on these features. The usual interpretation is that the rays and bright halos

around small craters (10 to 100 meters in diameter) consist of blocks quarried from lunar bedrock beneath the lunar regolith that have not been exposed to the darkening effects of space radiation (ref. 2-5). Thus, the number of subresolution blocks around small craters in the Apollo landing sites may be higher than currently anticipated. If this interpretation is correct, however, there should be a limiting diameter below which craters do not have bright halos or rays; the limiting diameter at any point would depend on the local thickness of the regolith. Estimates of the thickness of the regolith in the landing sites range from 1 to 10 meters (ref. 2-6); new craters up to 40 meters in diameter might lack ejected blocks if they formed in an area of the thickest regolith development. Other origins for rays and bright halos should not be ruled out at present. The importance of pulverization, grain size, and grain shape in producing rays has been emphasized (ref. 2-7); and an origin as sublimates resulting from the impact of cometary debris has been suggested by some. Determination of whether or not there is a cutoff in bright-halo craters below a certain diameter that correlates roughly with the thickness of the regolith would have an important bearing on the validity of these theories.

Hypersonic Gas Flow

J. A. O'KEEFE, W. S. CAMERON, AND
HAROLD MASURSKY

High-resolution lunar photography, especially that of Apollo 8 and Lunar Orbiters IV and V, shows a curious set of markings, denoted "grass raking" by the Apollo 8 astronauts, around most of the large impact craters. Near Tycho, Copernicus, Aristarchus, Mösting C, and the unnamed far-side crater at 11° S, 165° W, a pattern is visible, the predominant element of which is a kind of braid. Figure 2-19, from Apollo 8 photographs, shows a sharp, new, far-side impact crater. Figure 2-21, centered near 7° S, 167° W, shows part of the pattern near the same crater. Figure 2-24 from Lunar Orbiter V shows part of the pattern near Copernicus with its "bird's-foot" pattern. Lineations are seen which form approximately equal angles with the radius from the center of the crater. In some regions, these line-

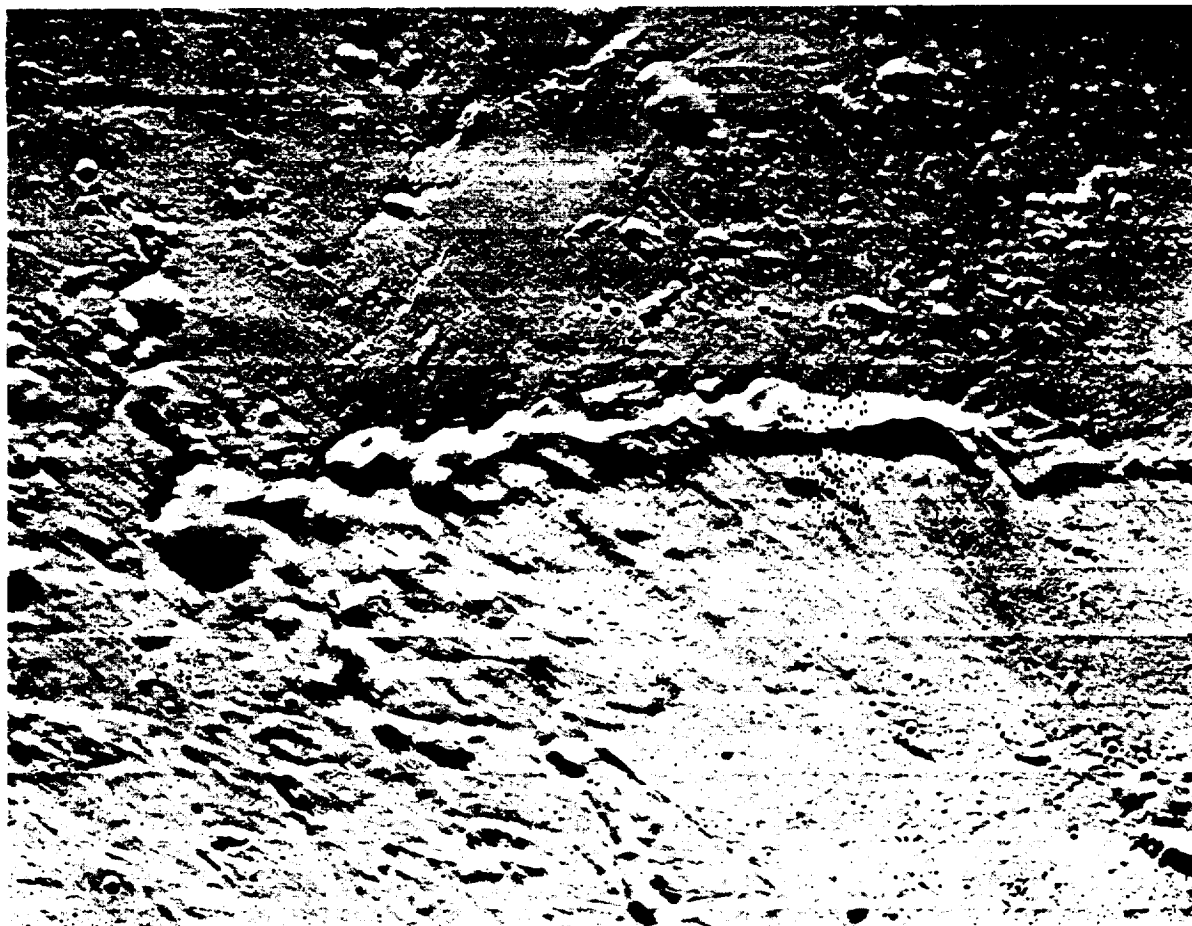


FIGURE 2-24.—Chain of secondary craters of Copernicus, showing bird's-foot pattern (Lunar Orbiter V frame M-144).

ations are visible as appendages to craters, especially when these craters occur in lines. In other areas, the lineations are not obviously associated with craters but simply extend across the surface. The characteristic thing about the lineations is that, wherever they are observed, they make, in any given region, a definite angle with the radius from the center of the associated crater.

The markings may be caused by splashing of ejecta from secondary craters. Similar markings have been experimentally produced (ref. 2-8) by hypersonic turbulent flow in wind tunnels (fig. 2-25). These markings are also found on reentry heat shields.

It has been shown that the Ries suevite produced by shock metamorphism accompanying the impact event has lost most of its water (ref. 2-9). Similar results are known for the other impact

glass (ref. 2-10). Even if the amount of water contained in the lunar rocks is small, the strong heating of many cubic miles of rock by a large impact event will produce large volumes of gas.

Great impact events are thought to produce a base surge similar to those produced by atomic blasts (ref. 2-11). The base surge is a particulate-material-laden mass of gas that pours out over the surrounding region with high velocity after the event. Perhaps deposits formed by this mechanism surround young lunar craters like Censorinus, Mösting C, Aristarchus, and the Mare Orientale basin.

On the lunar surface, the base surge would expand into a vacuum and reach very high velocities. At a temperature of 2000° C, the velocity of sound in the gas is probably near 1 km/sec, and the Mach angle from the patterns appears

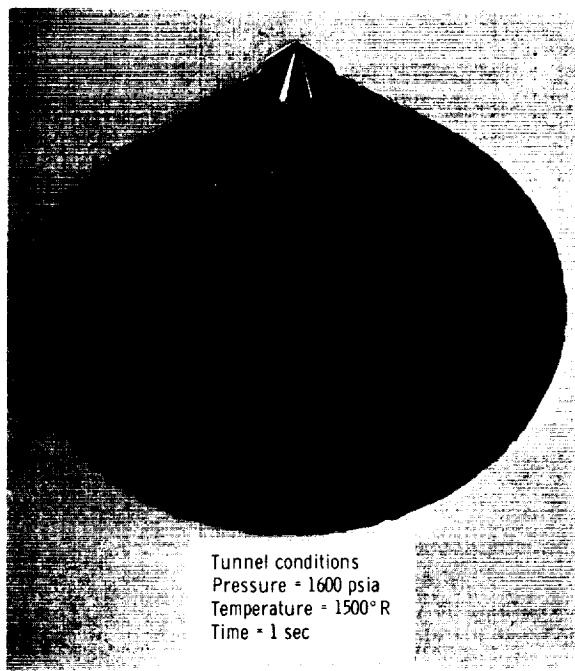


FIGURE 2-25.—Pattern produced by hypersonic turbulent flow in a wind tunnel.

to be at 10° . The Mach number is then 6 or more, and the velocity of flow is 4 km/sec. Since the velocity of escape from the Moon is 2.5 km/sec, this mechanism seems to offer the possibility of removal of material (refs. 2-12 and 2-13) from the lunar surface by ablation of this kind. That is, the deposits surrounding impact craters, the peculiar marking around secondary crater chains, the "grass raking," and the ejection of fragments from the lunar surface may be caused in part by the hypersonic gas flow.

POSSIBLE VOLCANIC FEATURES

Landforms

F. EL-BAZ AND H. G. WILSHIRE

Only a few probable volcanic landforms were photographed by Apollo 8. The section of this chapter entitled "Preliminary Interpretations of Lunar Geology" includes descriptions of several areas where regional volcanism appears to have been responsible for some surface units and structures. In the section of this chapter entitled "Craters," probable volcanic craters and crater

chains (fig. 2-21) were described. The following is a brief description of the constructional landforms which may be the products of volcanism.

A few steep-sided cones with elongated and breached summit pits were photographed by Apollo 8. One such positive feature is illustrated in figure 2-26, where the hill (18 km in diameter) is surrounded by an apron of lower relief. Although the Lunar Orbiter photograph H-36 of this site suggests that the feature may possibly be the result of impact, the feature probably constitutes a volcanic cone and associated flows. A similar example is seen in Apollo 8 frame 2686-C. In this case, a steep-sided cone with a breached summit crater (approximately 10 km in diameter) occurs near the center of a large flat-floored crater. Here again, this feature may be an impact crater on a small hill.

The only probable volcanic domes observed in the photography are the Cauchy domes, which are clearly visible in frame 2344 (fig. 2-12). The Sun angle and viewing direction of this photograph were suitable for the delineation of the difference in appearance of the smooth-surfaced, broad, low domes with distinct summit craters from that of the rugged domes.

A number of flows and flow fronts of probable volcanic origin were detected in the Apollo 8 photographs. At least two examples are pictured in figure 2-27. A crater, which is cut by the upper right edge of the photograph, displays a raised rim and an extremely irregular floor. The floor is strewn with irregular, positive features and a number of small craters. The rim crest of the crater appears to have been the starting point of a number of flows. One flow trends in a southeasterly direction and ends in a pool of dark material. The floor of a large crater southeast of the pool also displays a flow front reminiscent in gross morphology of those on the northeastern floor of the crater Copernicus (which may be debris flows).

Scarps which may be flow fronts of volcanic material or debris are seen in the left portion of figure 2-27. One of these is very sharp and clearly delineates at least one generation of dark mantling material. The scarp cuts across several craters, which suggests, alternatively, that it may be a fault scarp or at any rate tectonically controlled. A crater located near the lower end of the pictured

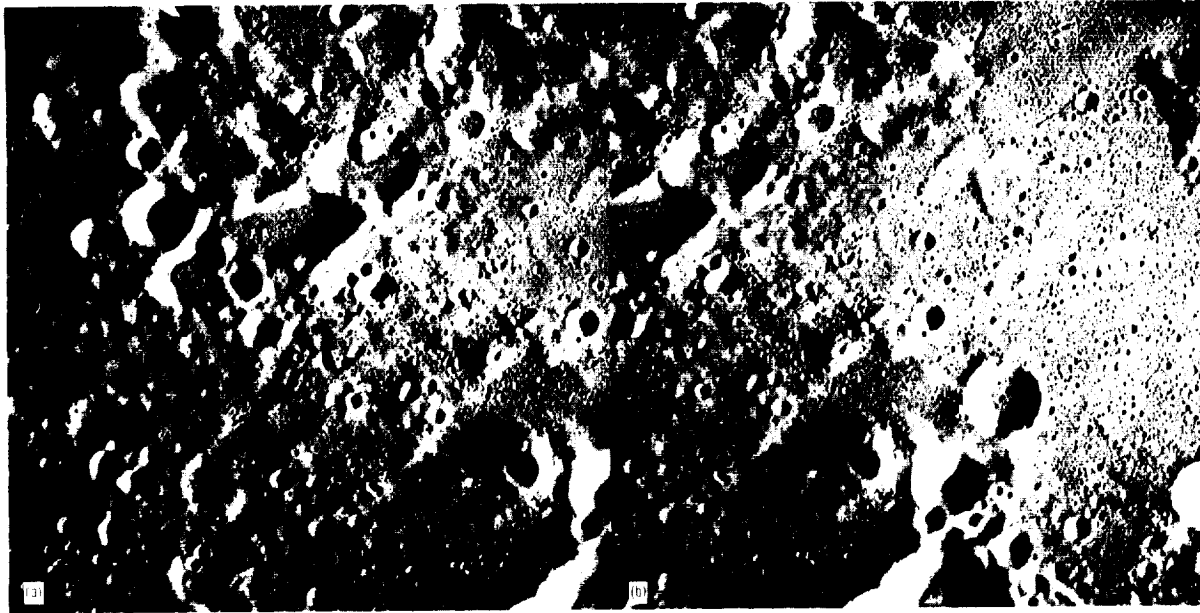


FIGURE 2-26.—Stereogram of area on lunar far side depicting a probable volcanic cone (Apollo 8 frames 2055-D and 2056-D). (a) Frame 2055-D, (b) frame 2056-D.

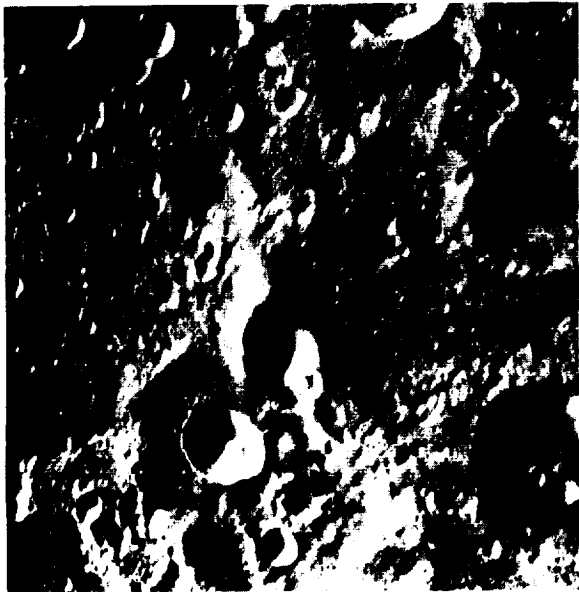


FIGURE 2-27.—Probable volcanic or debris flows (Apollo 8 frame 2687-C).

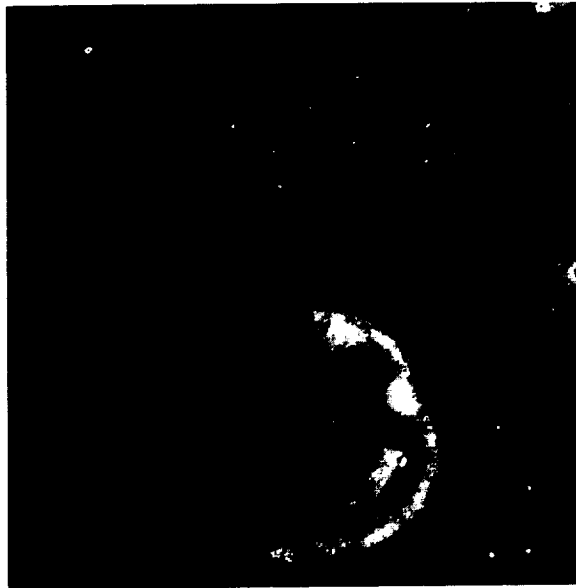


FIGURE 2-28.—Apollo 8 frame 2709-C, showing debris flow lobe.

part of the scarp is about 18 km in diameter. This crater displays a subdued rim and a dark apron of mantling material in a subradial texture.

Other flow lobes are more likely to have origi-

nated as debris flows rather than volcanic flows. An example, which may be seen in Apollo 8 frame 2709-C (fig. 2-28), is a conspicuous narrow lobe which extends from the inner wall of a large crater toward its center.

Sublimates

E. A. WHITAKER

The possibility has recently been discussed (ref. 2-15) that some of the bright markings observed on the lunar surface at small phase angles might be caused by deposits of certain materials which have sublimed during internal lunar heating. Since that time, Lunar Orbiter photographs have revealed other features which may tentatively be ascribed to sublimated substances, because their appearance is not easily ascribed to any of the normally accepted lunar surface processes.

These markings may be divided into two classes. The first is exemplified by a number of white-topped hills in the general area north of Mare

Vaporum (which could, however, be bedrock exhumed from burial by dark mantling materials). The second class is exemplified by the well-known marking, Reiner γ , and, more particularly, by the chain of bright patches extending both north and south of this feature. Lunar Orbiter IV frames H-157 and H-162 show that these markings do not correlate with surface topography.

Lunar Orbiter photography has revealed the presence of two more regions displaying such markings. One region is centered at 35° S, 165° E, and is best seen on Lunar Orbiter II frame M-75; the other is situated immediately north of Mare Marginis and is partially visible on Lunar Orbiter II frame M-196.

Some Apollo 8 photographs display this region

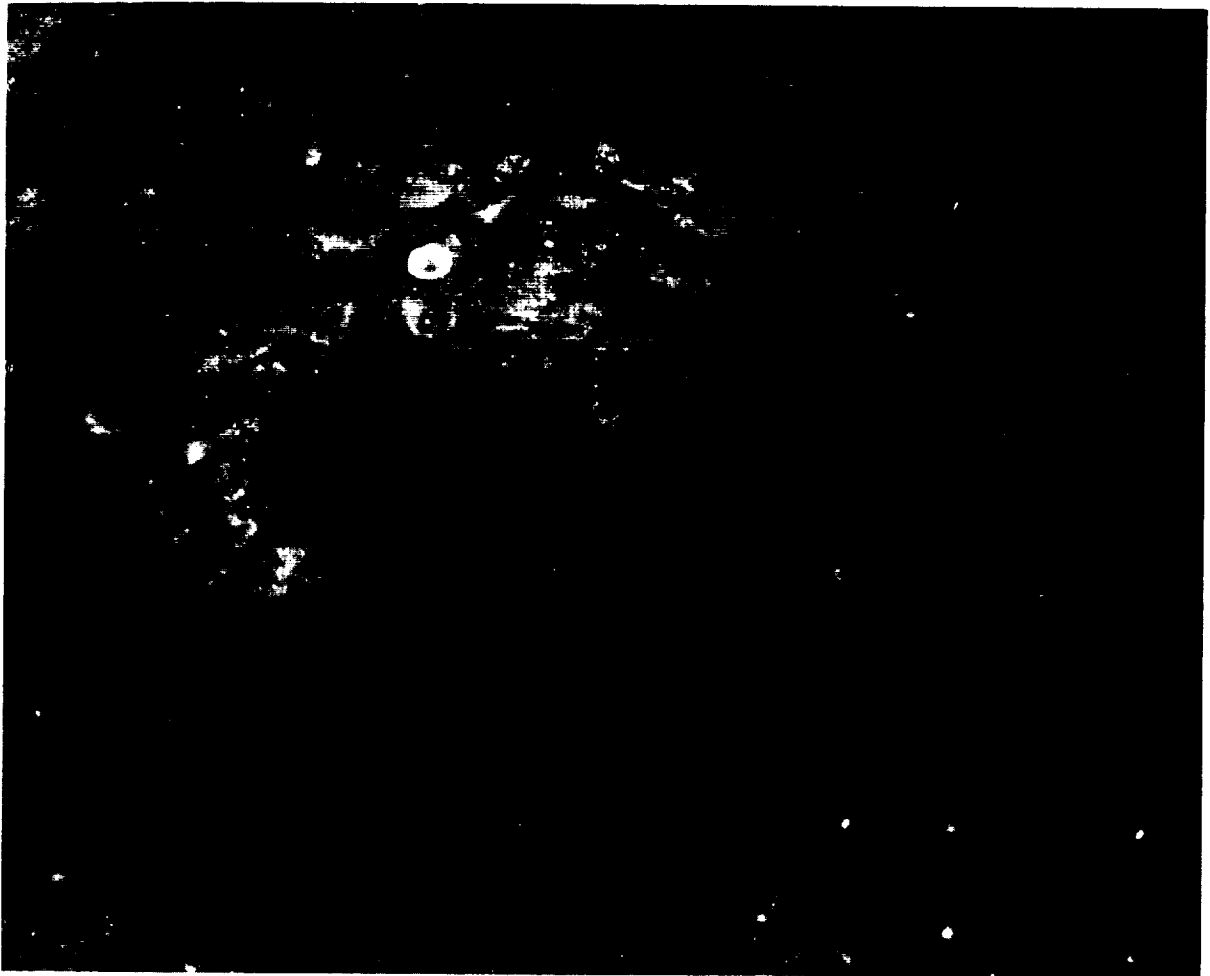


FIGURE 2-29.—Unusual surface markings in region of northern Mare Marginis and crater Goddard (from Apollo 8 frame 2208-D).

under high illumination. In these photographs, the full extent of this unusual group of markings can be appreciated. Figure 2-29 illustrates the brightest region of these markings, which surround the large dark-floored crater Goddard, and should be compared with figures 10, 11, and 12 of reference 2-15. Clearly, more work needs to be done on these features before any firm conclusions can be drawn.

COLORIMETRY

GENERAL STATEMENT—THE COLOR OF THE MOON

E. A. WHITAKER AND A. F. H. GOETZ

Confusion has arisen over apparently conflicting estimates of the color of the surface of the Moon. The astronauts' most frequent lunar descriptions, such as "gray" and "whitish-gray," agree with measurements made by Surveyor III (ref. 2-16). However, precision measurements made from the Earth definitely show that the color is not pure gray but, as the astronauts also suggested, rather a brownish gray. Correctly exposed color films, taken either from lunar orbit or from the Earth, invariably display a warm rather than a cool tint.

It has long been recognized that the color of the lunar surface is not entirely monotonous, but that small differences of tint are displayed by the maria (ref. 2-17). More recently, it has been found that the color also changes with phase, a phenomenon caused by differential polarization at different wavelengths. The mean relative reflectivity of the lunar surface compared with a completely nonselective reflector is illustrated in figure 2-30 and is based on data given in reference 2-18, which also gives the transmission data for the filters used. Any substance which reflects a continuous spectrum in the manner exemplified by figure 2-30 will appear browner, or warmer, to the eye than the illuminating light.

Comparisons of measurements of the color of the Moon and of the color of a distinctly brown Hawaiian lava showed the lava to be the browner (ref. 2-19). A comprehensive study of lunar surface colors has shown that even the "bluest" areas (for example, Aristarchus) are somewhat brownish, a result obtained earlier (ref. 2-20).

A number of investigators have attempted to interpret color differences measured from the

Earth as caused by differences in particle size (refs. 2-21 and 2-22), age (refs. 2-23 and 2-24), or composition (ref. 2-25). A strong argument has been made in favor of compositional differences being the cause of color differences, based on the results of an extensive series of differential photometric measurements.

If subsequent evidence proves the correlation between spectral reflectivity and composition, and sufficient "ground truth" can be obtained, accurate high-resolution color measurement will be a useful tool in geologic mapping of the lunar surface.

Photoelectric photometry is the most accurate means for making spectral reflectivity measurements. Accuracies of 0.1 percent were obtained (ref. 2-25). However, at the present time, photometry is a slow, point-for-point method, not suitable for large-area coverage or convenient data display. With some sacrifice in accuracy, photographic methods can be used. By using microdensitometry, photographic plates can be analyzed for quantitative color differences; but, again, data display is difficult, and the method is time consuming. Telescopic color-difference pictures that give qualitative color information in image form have been produced (ref. 2-26). In this method, a print is produced from a sandwich of a blue negative and a red positive plate. Color boundaries, particularly in mare regions, are easily detected. Errors are introduced, however, because

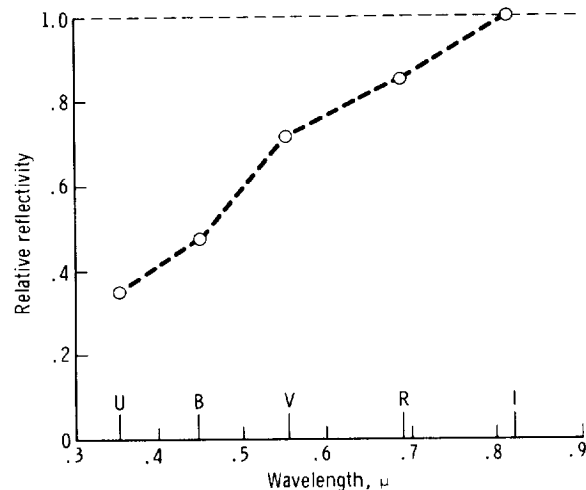


FIGURE 2-30.—Reflectivity of lunar surface compared with that of nonselective reflector.

of the difficulty of accurately controlling the photographic development and reproduction processes over a wide dynamic range.

An image-processing method has been developed to utilize the high information content and good display characteristics of photography and to circumvent the difficulties of standard microdensitometry in order to obtain quantitative color information. Details of this method will be discussed in the following section.

A study of differential color photometry (ref. 2-25) reveals that a large number of spectral curves, particularly in the mare regions, exhibit a nearly linear behavior in the wavelength region of 4000 to 7000 Å. Therefore, the greater the wavelength separation of the points in the spectrum observed, the greater the difference signal obtained. Typical differences obtained across color boundaries in the maria, after albedo normalization, are 4 to 7 percent. Such color differences are not detectable by the eye or on color film without special enhancement techniques.

APOLLO 8 COLOR EXPERIMENT

A. F. H. GOETZ

Introduction

Apollo 8 presented a unique platform from which to perform high-resolution lunar colorimetric photography. All previous spectral reflectivity or color measurements, with the exception of those made by Surveyor (ref. 2-16), have been made from the Earth where even good atmospheric seeing limits resolution to approximately 1 km at the lunar subearth point. Furthermore, no far-side color measurements had been undertaken prior to Apollo 8.

The Experiment

The design of the Apollo 8 two-color experiment was largely dictated by hardware and mission constraints. Color-separation photography on black-and-white film was the only feasible method for obtaining quantitative color information from orbit. Two filters were chosen to give the greatest wavelength separation commensurate with spacecraft-window transmission and film-sensitivity constraints. The filters, 47B (center wavelength

4350 Å) and 29+0.6ND (center wavelength 6600 Å), were mounted in a slide device, which attached to the lens in lieu of a filter. Exposures were made alternately through each filter. The time between exposures was less than 5 seconds. Using the Hasselblad camera and 80-mm lens, lunar-surface resolution from orbit was expected to be 50 meters, approximately 20 times greater than the best Earth-based telescope photography.

Data Return

For operational reasons, no scheduled T/O photography, including red-blue filter photography, was carried out in the ninth orbit. At this time, the filter holder was used to reduce the light level in the television camera. Following TEI, a number of red-blue photographs were taken with the 250-mm lens. Accidentally, 33 exposures were made on SO-368 (color) film and were, therefore, not usable for analysis. Unfortunately, these were the best exposures made, as the images filled almost the entire frame. Shortly after TEI, eight pairs of red-blue photographs were exposed on type 2485 high-speed film. This film had been intended for dim-light photography, but was exposed according to the plan for type 3400 film. Thirteen exposures were also made using the polarizing filters. No exposure calibration was made before processing the 2485 film (magazine G). Therefore, no quantitative color data can be retrieved from these images. Magazine E (type 3400 film) contains 10 pairs of red-blue exposures. However, the full-Moon, quarter-phase images measure only 8 mm or less in diameter, making them unsuitable for analysis.

Image Processing

The requirement for reducing a large number of color-separation photographs to obtain high-resolution, quantitative color data precluded the use of standard microdensitometry methods.

The Jet Propulsion Laboratory (JPL) Image Processing Laboratory offered to assist in the analysis of Apollo 8 two-color photography. The process is a variation of routines used in the analysis of other types of photography (refs. 2-27 and 2-28).

To develop and test the method, telescope photographs of several lunar areas were taken through a spacecraft window and through the

appropriate filters. The film and processing were identical to that used for the Apollo 8 flight. Sensitometric calibration strips were preexposed through the same filters.

Both the film and the calibration strips were digitized with a scanning spot size of 25μ . A 10 000-picture-element (pixel) sample of each calibration step was scanned. Plots of the digital number (DN) versus density (D) of the initially exposed wedges produced overall system calibration curves, DN versus the logarithm of the exposure ($\log E$) for each of the filters.

Each picture was scanned several times, and the multiple scans were averaged to minimize noise, after which a geometric correction program was used to register the red and blue pictures to each other. These became the master input pictures for the processing.

Each picture was then converted to the $\log E$ domain through application of the appropriate calibration curve to each pixel. The relative exposure between pictures was then adjusted to give an equal DN in each picture in an area defined by observation to be gray. Subtraction of one picture from the other is the equivalent of taking the ratio of the exposures, which results

in a "picture" that is independent of overall albedo differences, the negative values of which represent varying shades of one color, while zero represents gray, and positive values represent the other color. The colors are progressively more intense as the DN departs from zero.

Figures 2-31 and 2-32 are the original, scanned photographs, taken with 47B and 92+0.6ND (center wavelength 6600 \AA) filters, respectively. Plato, Sinus Iridum, and a portion of Mare Imbrium are visible. Figure 2-33 is the difference



FIGURE 2-31.—Mare Imbrium, including Plato and Sinus Iridum, taken at Mount Wilson Observatory. This photograph was taken through Mount Wilson's 24-inch telescope through an Apollo spacecraft heat-shield window using 35-mm 3400 film and a 47B (blue) filter. The original negative was scanned with a 25μ spot size and the tape replayed to produce this photograph.



FIGURE 2-32.—Same as figure 2-31, but taken through a 92+0.6ND (red) filter.



FIGURE 2-33.—Blue-minus-red difference picture. In this photograph, boundaries exhibiting uniform color in spite of albedo contrasts, such as the eastern rim of Sinus Iridum, demonstrate the dynamic range and good resolution achieved by this method.

picture in which the light areas are blue and the dark areas are red. The differences have been expanded to nearly fill the dynamic range of the processor. A point known as Mare Imbrium 2 (ref. 2-25), located southeast of Heraclides Promontory, was chosen to be gray.

The major color boundary in Mare Imbrium has been measured photoelectrically (ref. 2-25). A color difference of 5.5 ± 0.5 percent was measured across the boundary at the points Mare Imbrium 3 and 4. The corresponding difference found by image processing is 5 ± 2.5 percent.

PHOTOMETRY

AN INVESTIGATION OF THE LUNAR HEILIGENSCHN

E. A. WHITAKER

The occurrence of the heiligenschein as a terrestrial phenomenon has undoubtedly been known since ancient times. More recently, it has been described and its production attributed to two distinct phenomena (refs. 2-29 and 2-30):

1. Internal reflections within transparent beads (as in beaded projection screens, reflective tape, and paint) or drops (as in dew on a lawn).

2. A shadowing phenomenon in structures such as vegetation, whereby all shadows are hidden at very small phase angles.

Recent work (ref. 2-7) has shown that a number of terrestrial substances display a distinct heiligenschein effect; but, from this work, it not possible to decide whether or not other phenomena may also be effective.

Photometric work (ref. 2-31) has established the fact that the brightness of all illuminated portions of the Moon increases rapidly near full Moon. A similar effect was noted and measured (refs. 2-32 and 2-33) in the case of the asteroids. It was found that, for phase angles greater than approximately 5° , brightness increased linearly (on a logarithmic scale) with decreasing phase; but, for angles less than 5° , the brightness increased much more rapidly. This nonlinear surge was termed the "opposition effect." Later, a similar phenomenon on the Moon was noted and measured (ref. 2-20), the brightness at 1° phase being almost 50 percent greater than at 5° . Prior

lunar photometry (refs. 2-34 and 2-35) is not sufficiently precise to separate this opposition effect from the general linear phase effect.

From the work reported in reference 2-20, it was predicted that the surface of the Moon should display a strong heiligenschein. This prediction was first confirmed by photographs transmitted by Surveyor I (ref. 2-36) in which the shadow of the camera is seen to be surrounded by a bright halo several degrees in diameter. Although a few photographs transmitted by Lunar Orbiter V include the zero-phase point, those Apollo 8 photographs that include this point afford the first opportunity to make detailed measurements of the lunar heiligenschein. For accurate work, a recording microphotometer should be used and allowances should be made for vignetting and other geometrical effects. However, as an interim procedure, two frames (frames 2126 and 2148) which showed minimum albedo differences in the area of the heiligenschein were chosen. A transparent millimeter scale was attached, in turn, to each of these frames (which were in the form of positive film transparencies), and measurements of density were taken at eight 1-mm intervals in each direction outward from the brightest point using a simple visual spot densitometer. Two of the sensitometric step wedges at the tail of the film were also measured.

Once the density differences of the original wedge steps and the scale of the photograph were known, the actual relative reflectivity of the lunar surface at various angular distances from the zero-phase point was easily determined. The results are presented in table 2-I.

To determine the brightness/phase-angle curve for larger phase angles, it is advantageous to make use of the integrated brightness measurements of Rougier (in ref. 2-37). The lunar photometric function has been correctly shown (ref. 2-38) to be the product of the following three phase functions:

1. The phase function of the particles forming the "fairy castle" layer.

2. The Lommel-Seeliger term $\cos i / (\cos i + \cos \epsilon)$ for the visible shadowing within that layer, where i is the angle of incidence and ϵ is the angle of emergence.

3. A retrodirective function which corrects the

TABLE 2-I.—*Measurements of the Heiligenschein*[Film gamma at density of heiligenschein = 3.2; image scale for 80-mm focus lens = $0.72^\circ/\text{mm}$]

Distance from zero phase, mm	Equivalent degrees	Mean film density	Equivalent brightness
0.....	0	1.15	1.00
1.....	.7	1.30	.90
2.....	1.4	1.40	.84
3.....	2.2	1.49	.78
4.....	2.9	1.56	.75
5.....	3.6	1.61	.72
6.....	4.3	1.655	.70
7.....	5.0	1.69	.68
8.....	5.8	1.73	.66

last term by allowing for the hiding of those shadows at small phase angles.

The expression used in reference 2-38 for this last term is not correct, however, and a more accurate expression has now been obtained. The author of this section has also shown that an excellent fit between Rougier's results and theory (in ref. 2-37) can be obtained by assuming a bulk density of about 40 percent (60 percent porosity) for the fairy-castle layer and a Lambert function for the individual particles (in the small-phase-angle range used here). By adapting the function to the conditions of the measured frames (phase angle = angle of emergence; angle of incidence = constant at about 0°), the solid line in figure 2-34 is obtained. The vertical bars indicate Rougier's measurements of the waxing and waning Moon also adapted to the preceding conditions. The heiligenschein measurements have been plotted so that the value for 5° phase angle agrees with the Rougier value.

As noted in reference 2-38, the steepness of the retrodirective function depends solely upon the bulk density of the reflecting layer. A retrodirective function can be fitted to the heiligenschein peak, but it is then impossible to fit the Rougier results except by using a very peculiar and unknown phase function for the particles.

In summary, the lunar heiligenschein is the result of two distinct phenomena. Shadow-hiding in the fairy-castle layer causes a brightening of about 2.2 percent per degree for phase angles

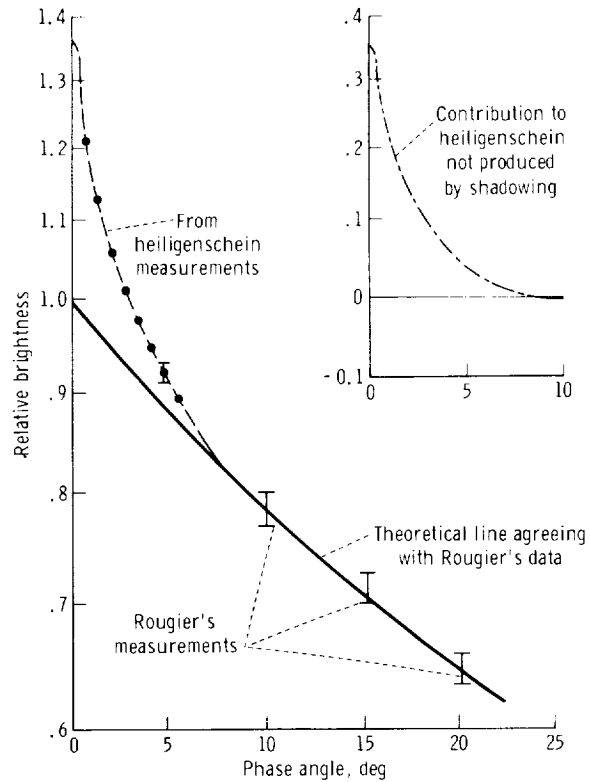


FIGURE 2-34.—Relative brightness of lunar surface at various angular distances from zero-phase point.

between 20° and 0° . In the range of 5° through 0° , however, an additional nonlinear brightening occurs that boosts the reflectivity by an extra 35 percent beyond the extrapolated zero-phase value. This brightening is presumably similar to the phenomenon observed and reported in reference 2-7, and may be caused by an internal reflection effect and/or some other effect (for example, diffraction) not yet investigated. Regarding the possible translucency of the particles, the Lambert phase function for the particles requires an additional factor of $0.08(1 - \cos g)^2$, where g is phase angle. This may be partly an indication of translucency. Even more interesting are the recent polarimetric studies carried out, at various wavelengths, at the Lunar and Planetary Laboratory of the University of Arizona. In these studies, the lunar results can be duplicated only by particles which display some degree of translucency.

THEORETICAL PHOTOMETRY

H. A. POHN, R. L. WILDEY, AND H. W. RADIN

Introduction

The Apollo 8 photographs have provided a wealth of data for studies of the lunar photometric function:

1. The first calibrated lunar photograph at less than about 1.5° phase angle and the first observations of the heiligenschein.

2. The first zero-phase photograph of the lunar far side.

3. The best-calibrated high-resolution lunar photography to date.

4. The first high-resolution photometric data on original film.

The Apollo 8 pictures provide the first opportunity to determine the lunar photometric function in the vicinity of zero phase without extrapolation. The pictures also provide the first opportunity for an accurate determination of the photometric function, in a single terrain unit, over a fairly wide range of photometric angles.

Significance of Photography

Since the Earth subtends an angle of about 2° (diameter) at the Moon, and the Sun subtends about 0.5° , the closest possible approach to zero phase for telescopic observations is about 1.5° at the center of the disk. (The range is from 1.25° at the limb nearest eclipse to 1.75° at the far limb, for no penumbral shadowing.) The photometric function rises sharply with decreasing phase angle in this region; therefore, the extrapolation to zero phase is subject to error. Apollo 8 photographs are the first ones taken from lunar orbit to contain the zero-phase point within the range of calibration.

Advantages of Apollo 8 Photographs Over Earlier Data

Most earlier photometric analysis has been done from Earth-based telescopic photography. (Limited photoelectric observations have been carried out.) Apollo 8 photographs have much higher resolution, a much wider range of photometric angles in a single terrain unit, and freedom from atmospheric "seeing" effects. In comparison to earlier lunar missions, the paramount photo-

graphic accomplishment of Apollo 8, from the standpoint of photometry, is the return of the film. (The imaging system also has a higher degree of basic internal photometric integrity.) The return of the film to Earth permits better calibration, more uniform processing, and a wider dynamic range than has been achieved in the past. The inherent errors of indirect picture transmission are also avoided.

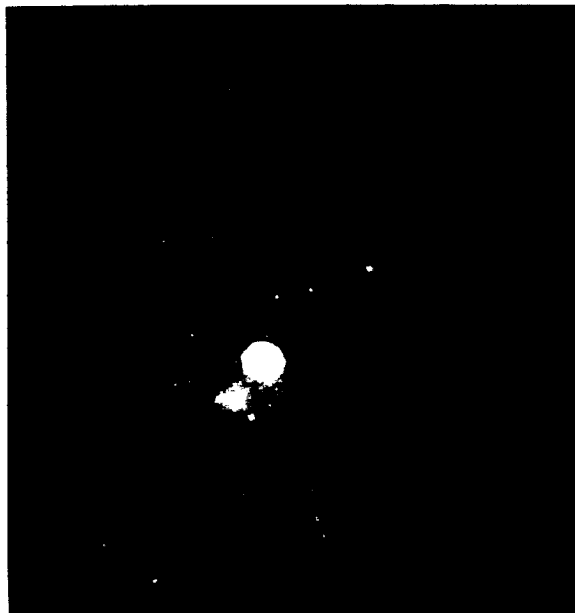


FIGURE 2-35.—Apollo 8 frame 2148, showing zero-phase point.

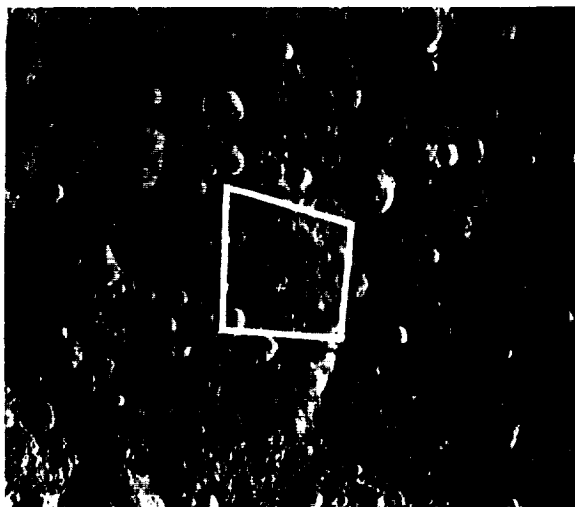


FIGURE 2-36.—Portion of Lunar Orbiter II frame M-196, showing location of Apollo 8 frame 2148.

Preliminary Results

An isodensity trace of the zero-phase region of Apollo 8 frame 2148 (figs. 2-35 to 2-37) shows that the photometric function increases much

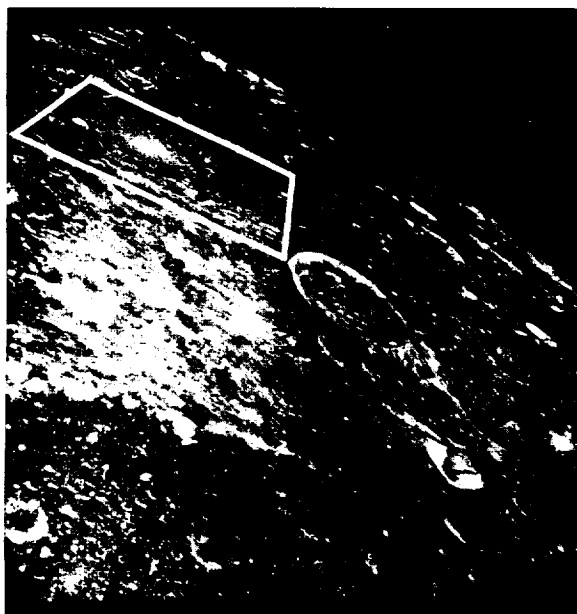


FIGURE 2-37.—Apollo 8 oblique frame 2751, showing location of Apollo 8 frame 2148.

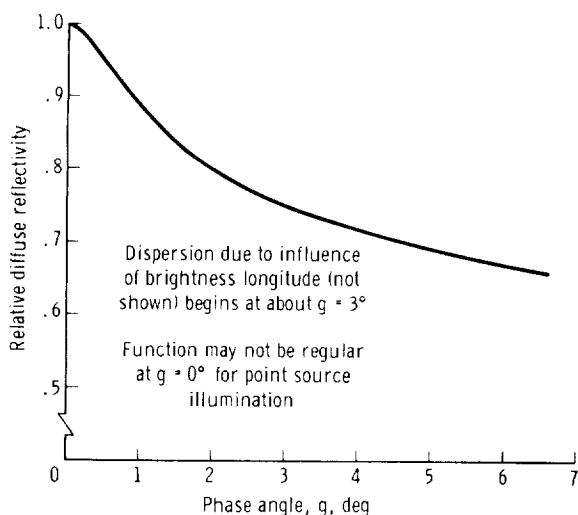


FIGURE 2-38.—Lunar photometric function near zero phase.

more sharply with decreasing phase angle than was previously believed. Lunar reflectivity is about 20 percent higher at zero phase than at a 1.5° phase angle. An approximate curve is shown in figure 2-38; these results are subject to later refinement.

PHOTOMETRIC FUNCTION REDUCTIONS

JAMES L. DRAGG AND HAROLD L. PRIOR

The Apollo 8 photography offered the first opportunity to perform detailed photometric reduction at zero phase. (At this condition, Surveyor and Lunar Orbiter photographs reached saturation, and telescopic observations are occulted.) Approximately 60 frames including the zero-phase point were recorded on Apollo 8 magazines C and D, type 3400 black-and-white film. Six of these frames, all from magazine D, were selected for a quick-look analysis: 2124, 2134, 2138, 2145, 2147, and 2149. Selection of these particular frames was based on the following:

1. They were taken at a camera aperture of $f/11$ where camera lens calibration was available for relative transmission off-axis. All magazine C frames were taken at $f/5.6$.

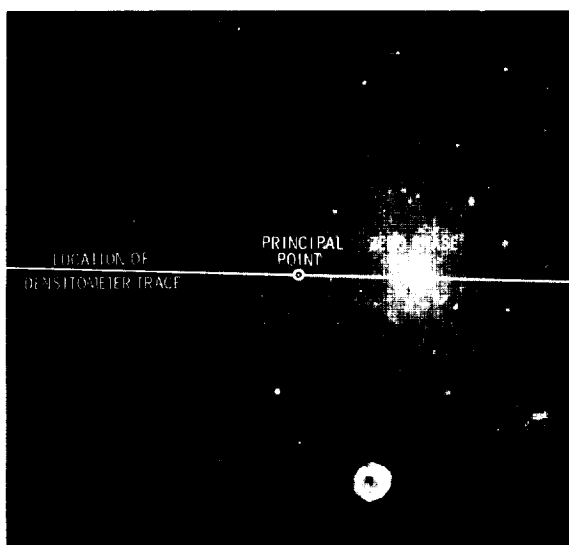


FIGURE 2-39.—Apollo 8 frame 2147-D, showing densitometer trace, principal point, and zero-phase point.

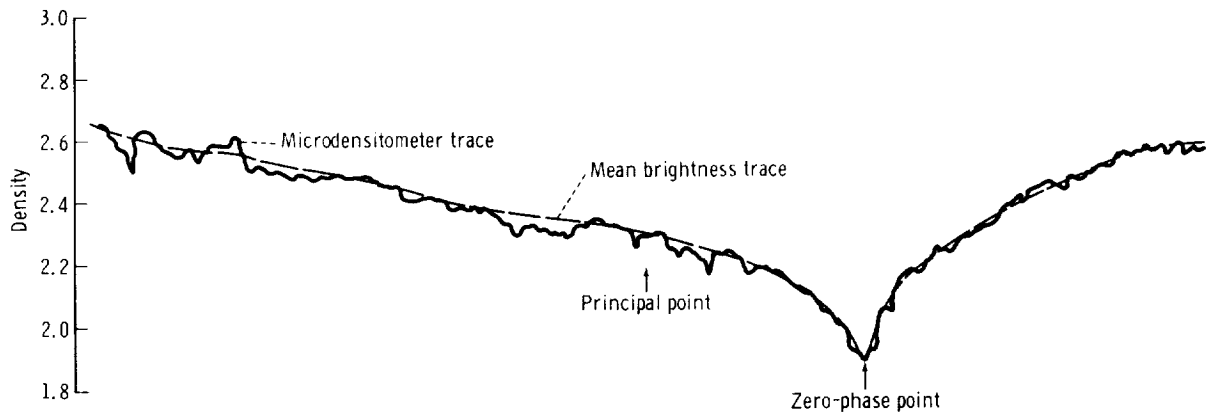


FIGURE 2-40.—Apollo 8 frame 2147-D master positive traces and points.

2. All frames were taken approximately vertically, allowing simplified geometrical calculations based on single densitometric scans through the principal point and zero-phase point. Magazine C frames were taken with a 12° camera pitch angle.

The principal point and zero-phase point were located on each frame, and densitometric traces (figs. 2-39 and 2-40) were extracted from frame edge to frame edge through these points. A second-generation master positive was used for all scanning. A mean brightness trace was fitted to each microdensitometer trace. The assumption was made that variations of the microdensitometer trace from the mean brightness trace were caused by local variations in albedo and slope, and that the mean trace corresponded to a uniform sphere and albedo. Eighty-two data points were extracted, and the phase angle g and luminance longitude α computed for each data point. Conversion of the microdensitometer data to exposures was performed through the use of sensitometric strip 4B (fig. 2-41) preexposed onto the head end of the flight film. The exposures were corrected for lens transmission characteristics, but have not been corrected for potential spacecraft-window-transmission effects. The values for each frame were then normalized to zero phase.

Data points within each frame were limited to approximately 20° or less, both in phase angle

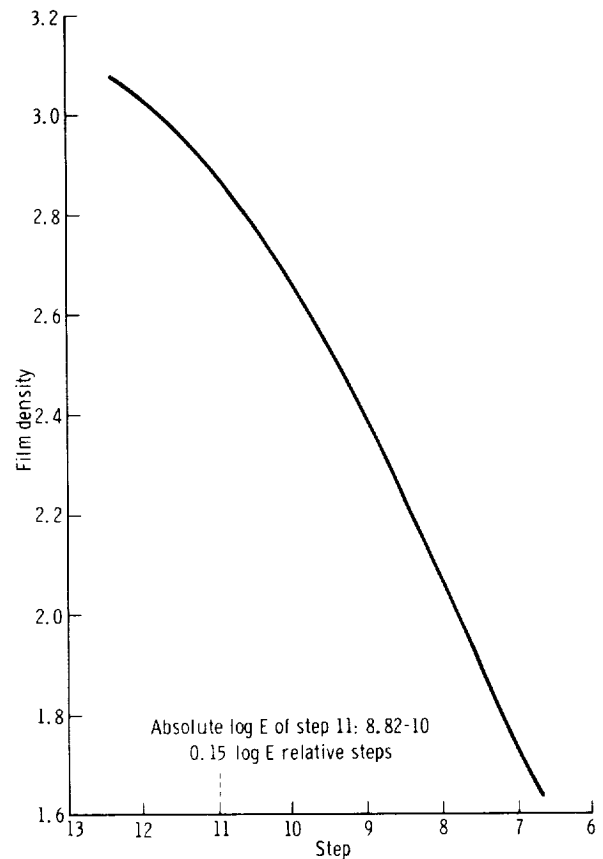


FIGURE 2-41.— $D \log E$ curve for strip 4B, Apollo 8 magazine D.

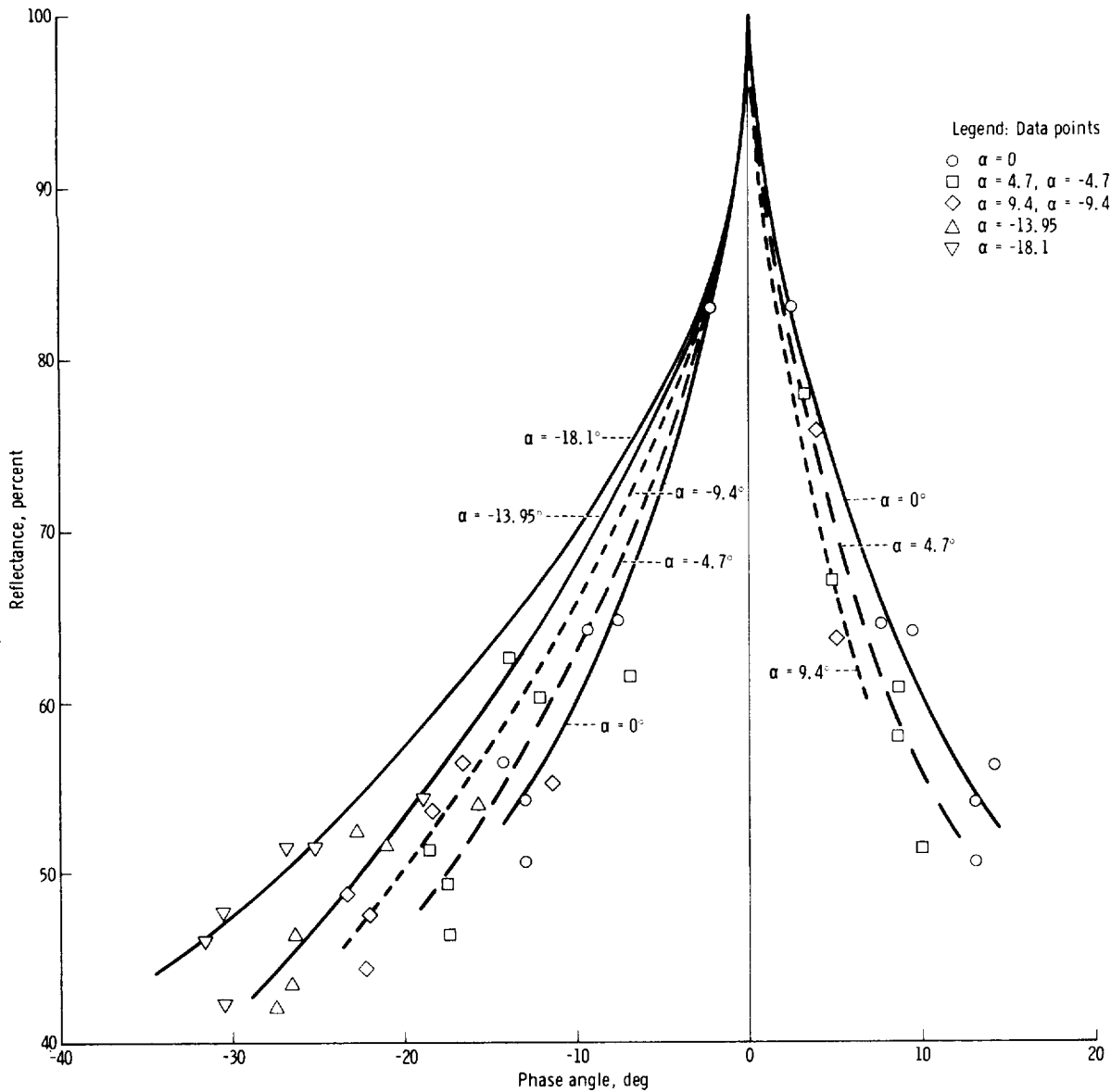


FIGURE 2-42.—Data points for various luminance longitudes (α).

and luminance longitude. Data points and fitted curves are plotted (fig. 2-42) for $\alpha = 0^\circ, 4.7^\circ, 9.4^\circ, -4.7^\circ, -9.4^\circ, -13.95^\circ$, and -18.1° . The curve for zero α is also plotted against the JPL fits (ref. 2-39) to data of Fedorets and Sytinskaya, with all curves normalized to zero phase. The results show (fig. 2-43) a better fit to the Sytins-

kaya data, with a slightly sharper falloff from zero phase. This sharper falloff may be an improvement in the function, or it may be indicative of an adjusted function for the highlands of the lunar far side. The data scatter does indicate that additional and more detailed reduction of this type is warranted from the Apollo 8 photography.

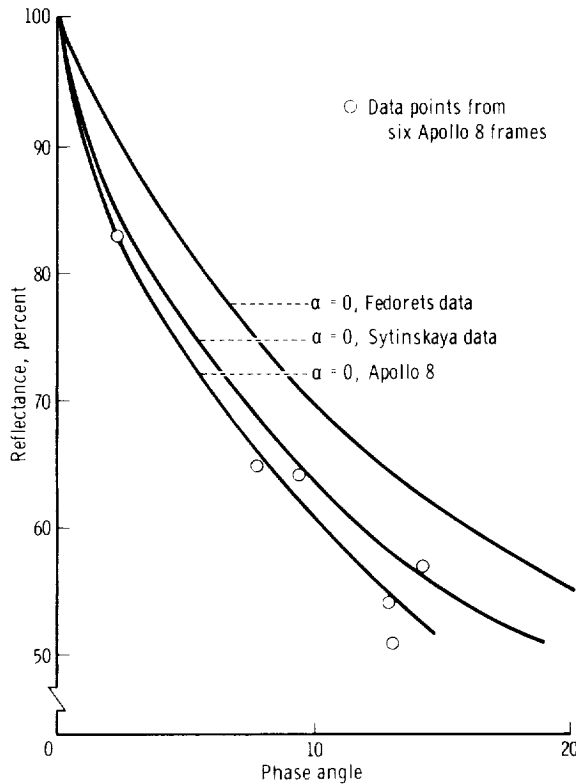


FIGURE 2-43.—Curve for zero luminance longitude plotted against Jet Propulsion Laboratory fits to Fedorets and Sytinskaya data.

VISIBILITY AND APOLLO 8 PHOTOGRAPHIC RESULTS

K. ZIEDMAN

Introduction

Visual observations by the Apollo 8 crew have increased the knowledge of lunar-feature visibility. The photographic records document some of these observations and are an additional source of data for studying lunar photometric functions and visibility problems. The purpose of this section is to summarize the observational and photographic results as they pertain to visibility and to compare the results with previous studies and simulations. In particular, the question of Sun-elevation-angle constraints during LM landing is reviewed.

Summary of Results

The terminology for the viewing conditions of interest is illustrated in figure 2-44. For simplicity, only the in-plane case is diagrammed. Critical viewing conditions for lunar operations are those for looking near and at the zero-phase point, for viewing at high-Sun angles, and when the observer-line-of-sight (OLOS) elevation angle θ_A is less than the Sun-line-of-sight (SLOS) elevation angle θ_S . The washout that occurs at the zero-phase point and the loss of contrast that occurs when θ_A is less than θ_S have been thought to present a serious problem for lunar module (LM) landing. In addition, substantial differences in surface appearance occur between the relatively flat and homogeneous smooth maria and the rougher highlands. The former, of course, are of interest for the first three or four landing missions, whereas the latter are of interest for the later exploration-oriented missions.

The most important of the Apollo 8 observations are the following:

1. The zero-phase washout is less severe and more limited in size than anticipated.
2. Albedo differences, especially in the highlands, assist visibility to a greater extent than anticipated.
3. Detail could be seen in shadows.
4. Surface features could be seen under earth-shine.

The general decrease in topographic information at higher Sun angles, especially relative height information, was much as expected. The latter is illustrated in figure 2-45, which shows two frames from the fourth-revolution stereoscopic strip of roughly comparable terrain for low- and high-Sun-angle conditions. The overall flattening and loss of terrain-height information in the high-Sun-angle frame is apparent; however, substantial detail can still be seen because of albedo differences.

A washout, or zero-phase region, can be seen in figure 2-45(b). The overprinted ellipses are constant phase-angle contours and indicate that the washout, under the conditions of high-Sun and nearly vertical viewing, subtends about 3° . An obvious feature of figure 2-45(b) is the many small, bright craters. A result of importance for visibility is the somewhat contradictory situation in which these steep craters (which should be avoided by the LM) are best seen at high Sun

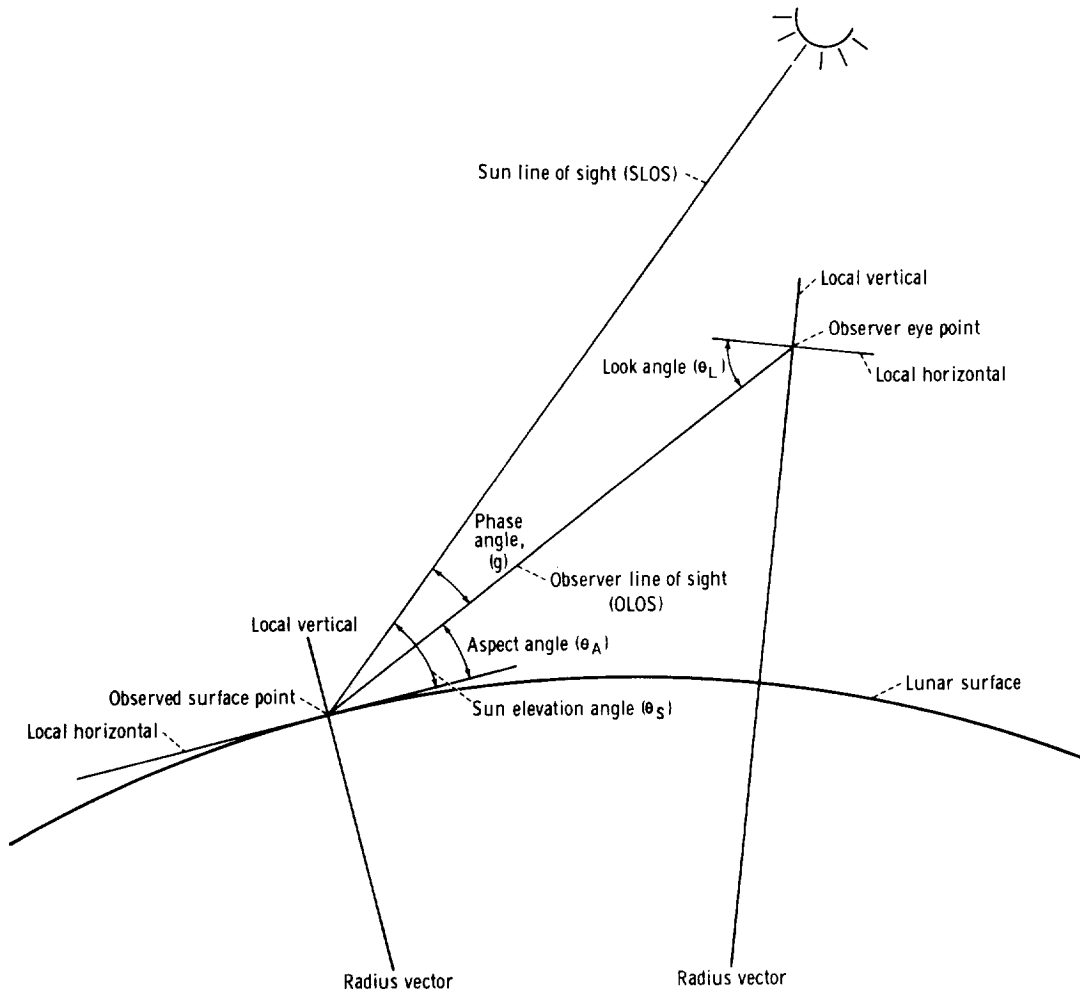


FIGURE 2-44.—Definition of viewing situation.

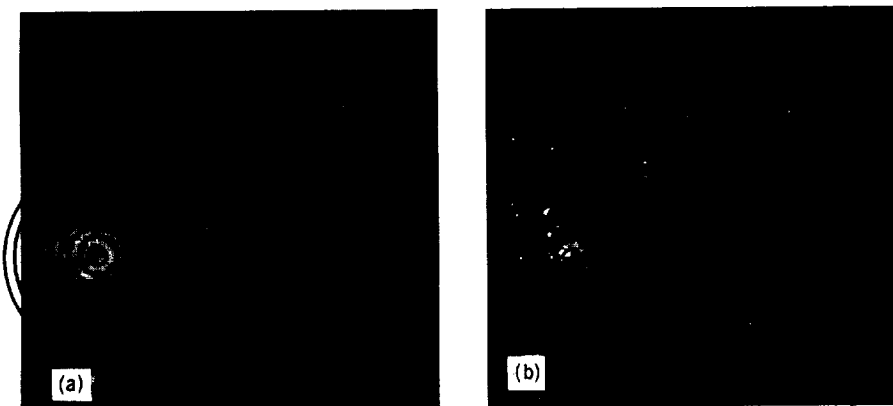
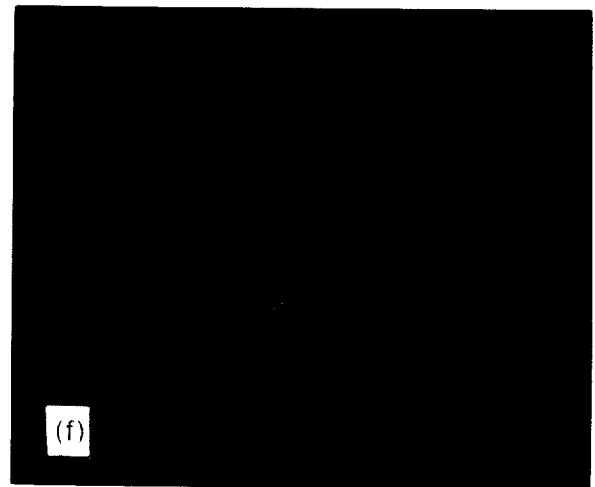
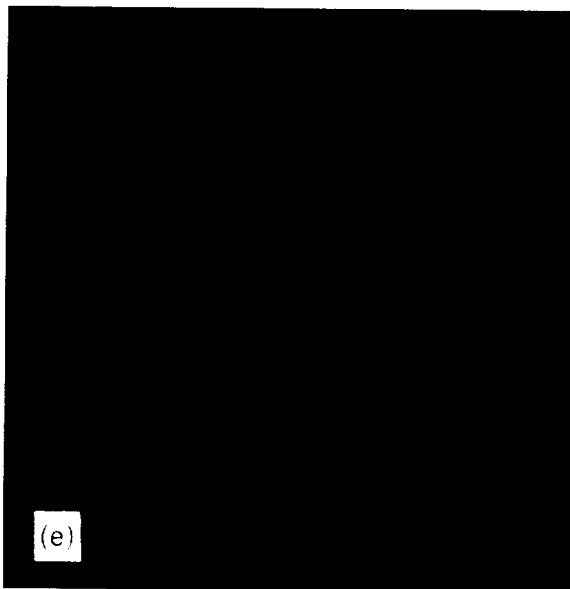
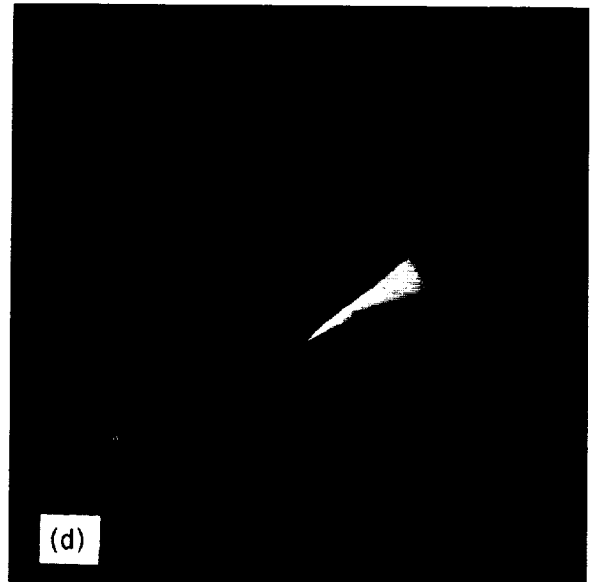
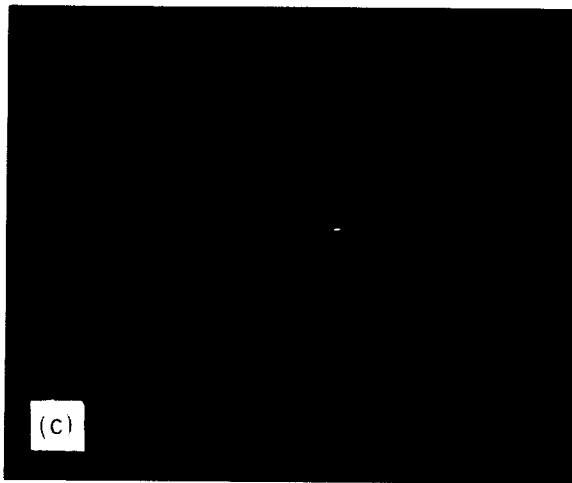
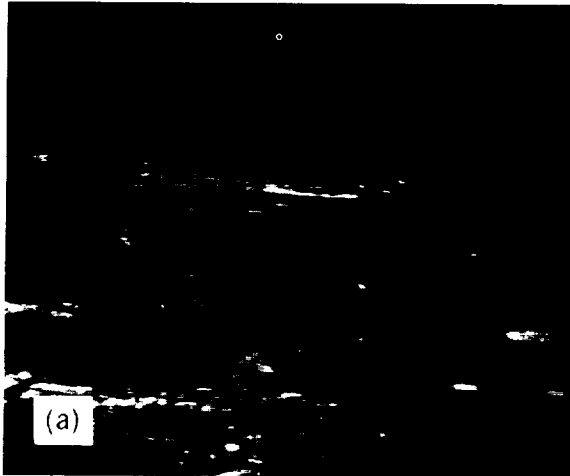


FIGURE 2-45.—Equal phase angle contours from 1° to 10° for Apollo 8 frames 2124 and 2125. (a) Frame 2125, (b) frame 2124.



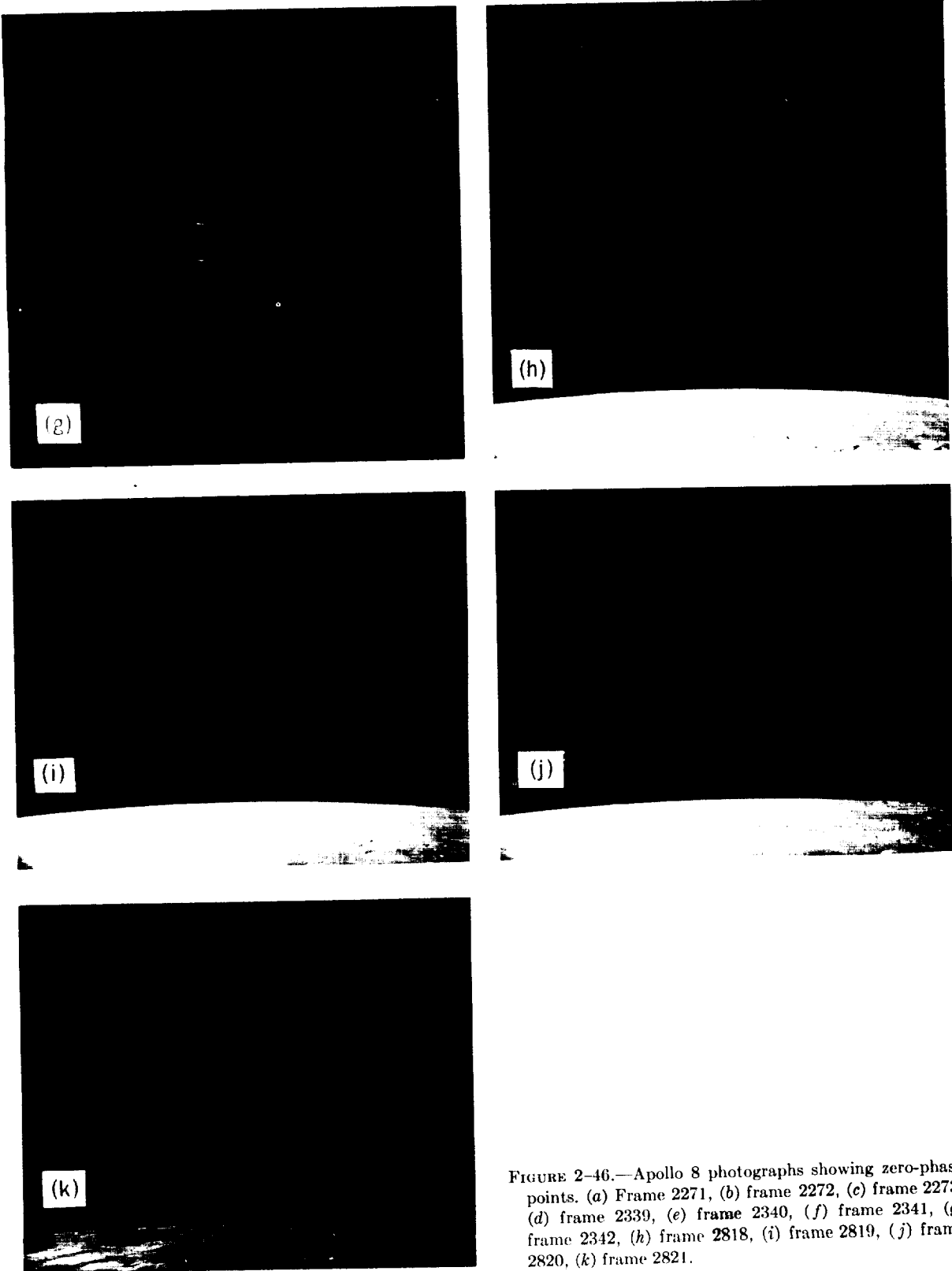


FIGURE 2-46.—Apollo 8 photographs showing zero-phase points. (a) Frame 2271, (b) frame 2272, (c) frame 2273, (d) frame 2339, (e) frame 2340, (f) frame 2341, (g) frame 2342, (h) frame 2818, (i) frame 2819, (j) frame 2820, (k) frame 2821.

angles, whereas relative terrain heights and slopes are best seen at low Sun angles.

Zero-phase points, or what appears to be near-zero phase, were obtained on a few frames covering maria regions and under conditions similar to those of LM descent. These are frames 2271, 2272, and 2273 (magazine E) of the training sequence near landing site 1 (250-mm lens); 2339 to 2342 (magazine E), taken near Mare Fecunditatis (80-mm lens); and 2818, 2819, 2820, and 2821 (magazine C), with a near-zero-phase point in Mare Tranquillitatis (80-mm lens). This set of photographs is shown in figure 2-46 and is discussed further in the section of this chapter entitled "Simulation of Lunar Module Photography and Lunar Module Landing Conditions."

Discussion

Comparison of Orbital and LM-Descent Viewing Conditions

The nominal landing point during LM descent is seen at a 16° aspect angle θ_A measured from the local horizontal at the landing point to the line of sight to the LM. Thus, it is appropriate to examine the Apollo 8 visual observations and photographs for conditions which include surface regions viewed at aspect angles in the neighborhood of 16° , particularly for the cases when the scene includes the zero-phase or near-zero-phase points. Referring to figure 2-44, the look angle θ_L is defined as the deviation of the OLOS from the spacecraft local horizontal. This angle is the quantity which an observer would use to describe the angular size or direction of surface features. To compare the LM-descent and orbital viewing conditions, the manner in which two angles, the phase and aspect angles, vary as a function of θ_L at the two altitudes is compared. The aspect angle is a measure of foreshortening, an important degradation factor for high-oblique viewing. The phase angle g is also related to visibility. The question posed is whether the region enclosed by a given g or a given θ_A would subtend a substantially different θ_L between orbital and high-gate altitudes. If these cases are indeed different, a washout region defined in terms of θ_L from 60 n. mi. will be a different size compared to a washout region also defined in terms of θ_L , but from an altitude of 1 or 2 n. mi.

Aspect angle and g for four altitudes are shown as a function of θ_L in figures 2-47 and 2-48. Phase angle was calculated by assuming zero phase at the surface point corresponding to θ_A of

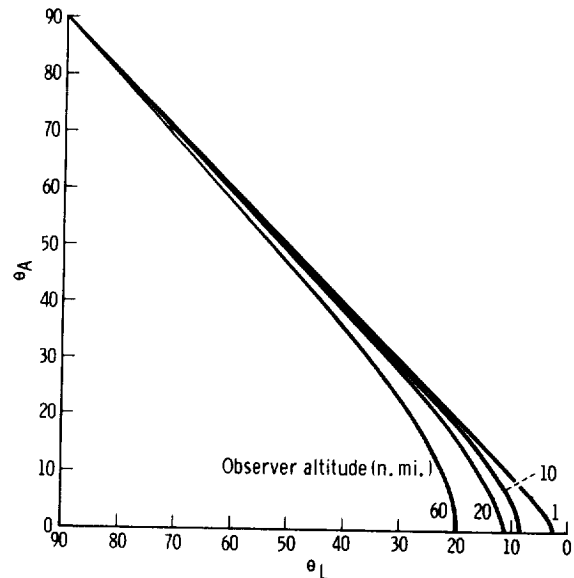


FIGURE 2-47.—Aspect angle versus look angle for four altitudes (in-plane geometry).

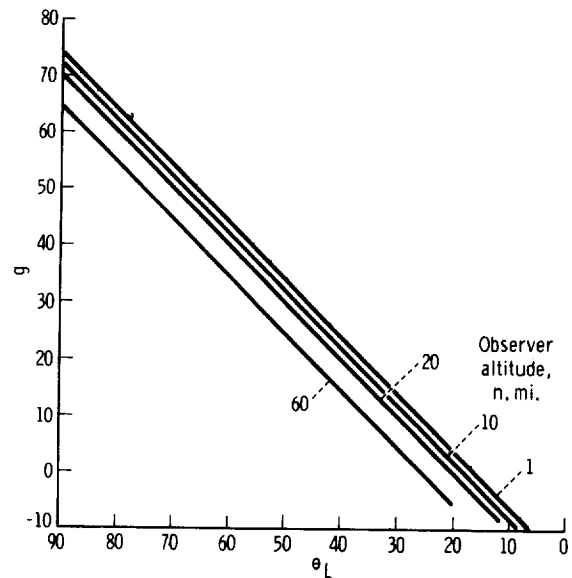


FIGURE 2-48.—Phase angle versus look angle for four altitudes (in-plane geometry).

16°; that is, for $\theta_A = 16^\circ$, $\theta_S = 16^\circ$. To compare the effect of altitude, examine the change that occurs in θ_A as θ_L is varied around the θ_L value corresponding to $\theta_A = 16^\circ$. (At 1 n. mi., $\theta_L = 15^\circ$; at 60 n. mi., $\theta_L = 25^\circ$.) It is clear that the θ_A change corresponding to, for example, a $\pm 5^\circ$ θ_L variation is quite different between altitudes of 1 and 60 n. mi. The difference is greatest downrange of the 16° θ_A point; substantial foreshortening of surface features occurs beyond this point for the higher altitude. In fact, the horizon is reached at $\theta_L = 20^\circ$ at 60 n. mi. This results in poorer visibility of features at 60 n. mi. compared to 1 n. mi., relative to their visibility at $\theta_A = 16^\circ$ when viewing down range of that point. Note also that the absolute value of θ_L to the $\theta_A = 16^\circ$ point increases about 10° between 60 and 1 n. mi.

A plot of g versus θ_L corresponding to the preceding conditions (zero phase set at $\theta_A = 16^\circ$ for all altitudes) is shown in figure 2-48. For this case, the variation of g about the zero-phase point is the same at each altitude for a given θ_L variation. The only change is a displacement of the function along the θ_L axis of an amount equal to the central angle between the zero-phase points for the various altitudes.

The importance of these comments is in the fact that observing the lunar surface at a θ_A of 16° from 60 n. mi. does not effectively simulate the LM landing situation, due to the foreshortening effect. At this altitude, a series of photographs that include the zero-phase point for Sun elevation angles from about 10° to 30° is required to cover the range of conditions during LM landing.

Shadow Visibility and Visual Dynamic Range

The demonstration of visibility in shadow regions has implications for lunar surface operations and for future lunar photography. Shadow regions have been considered a potential hazard for surface extravehicular activity and for LM and flier operations, because holes in shadows or protuberances covered by shadows might not be detected. The luminance in the shadow observed from Apollo 8 is presumably caused by backscatter from adjacent illuminated areas. This effect is especially evident in shadows within craters. An estimate can be made of the amount of illumina-

tion based on the fact that the crew was able to observe detail; that is, the surface luminance must have been greater than the visual threshold for visibility in a dark area surrounded by a larger, brighter area.

Related to this question is the problem of comparing the dynamic range of film and of the eye. A number of comments have been made concerning the Apollo 8 results to the effect that the eye has a greater dynamic range than film. Such comments are misleading unless the actual conditions of measurement are specified, such as type of film, granularity, $D \log E$ curve, and type of criteria (such as discriminable gray steps or resolvable detail) by which the film and visual dynamic ranges are measured. Visual dynamic range is often described by the total operating range of the visual system for the lowest threshold for seeing to the point at which light intensity will cause pain or damage. This description is inappropriate as a basis for comparison to film sensitivity. Although the eye can operate over a range of 10^{10} , it cannot do so at any one time. At a given time, the eye has a single operating point, and the variation in light level around the operating point to which it responds is substantially smaller than the total range of 10^{10} . The operating point itself is determined by the adaptation luminance to which the eye is exposed. The adaptation level is a weighted function of the luminance distribution in the visual field, and can roughly be taken as the average luminance. Depending on the adaptation level, the eye may have a dynamic range greater or smaller than a given film-development combination. In the case of seeing in shadows, the eye has an advantage over film in that it can adapt to the dark and, therefore, become more sensitive if the shadow region is observed over a time period.

The amount of light in a shadow region needed for visibility was bounded by examination of two criteria:

1. What luminance level is necessary to raise the brightness of a small dark spot just above complete black when it is seen against a larger, bright surround? This is the minimum luminance necessary to perceive anything in a shadow and can be considered a noise level.
2. What luminance level is necessary to see

detail inside a dark spot bounded by a larger, bright surround? This criterion will require a greater luminance than the first and can be used as an upper estimate.

As is usually the case, such threshold values will depend on many parameters: the angular size and luminance of the surround; the angular size of the dark area; the angular size and contrast of the critical detail for the second criterion; and the specific judgment required of the observer. To correlate with Apollo 8 observations, a surround should be used that subtends at least 20° to 30° at the eye and a dark area should be used that simulates a shadow that subtends 2° to 5°. The size of features visible to the crew in the shadow is not known to this author.

Data from reference 2-40 approximate the conditions necessary for estimating the first criterion. From a 180° surround with a 1.5° dark area, the just-visible luminance in the 1.5° area was determined as a function of surround luminance. The results are shown in figure 2-49. Also plotted are the results obtained in reference 2-41 for a somewhat different type of experiment, although these results agree well with the reference 2-40 data in the region of interest. At a 10° θ_s, the average luminance of the lunar surface is 325 ft-L for viewing vertically, assuming an overall reflectance factor of 0.1, a reflectance of 0.25 along the line of sight, and solar illumination of 13 000

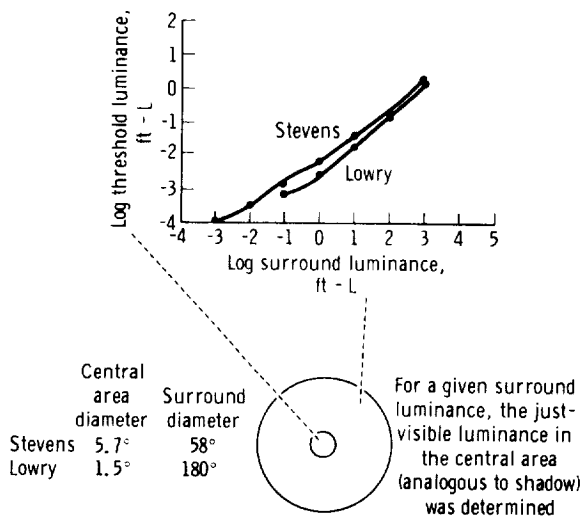


FIGURE 2-49.—Just-visible luminance as a function of surround luminance.

lumens/ft². Entering this value on the ordinate of figure 2-48, a just-visible luminance of 0.3 to 0.56 ft-L is obtained, or about 0.001 to 0.002 of the surround luminance.

To estimate the luminance required for detailed visibility, the size and contrast of the detail should be specified. Unfortunately, this cannot be done without additional information from the crew as to visible feature size. However, an experiment described in reference 2-42 can serve to set an upper luminance level for small detail. Subjects in that experiment estimated orientation of Landolt "C" ring of the following dimensions: outside diameter = 9.65 minutes of arc, stroke and gap width = 1.93 minutes of arc. Contrast ratios were determined for various background and surround luminances and sizes using the following equation:

$$\text{Contrast ratio } C = \frac{L_T - L_B}{L_B}$$

where L_T = target luminance for 50 percent correct judgments and L_B = background luminance.

For a background (or shadow) size of 5° and a surround luminance of 176 ft-L, the following contrast thresholds were found for 50 percent correct judgments: at a shadow luminance of 18.73 ft-L, $C = 0.25$; at a shadow luminance of 1.57 ft-L, $C = 1.5$. Because lunar-feature contrasts in shadows are likely to be on the order of a few tenths or less, it is concluded that shadow luminance would have to be on the order of 10 ft-L for detection of small detail. This detail size is probably unrealistic; critical feature size was more likely in the region of 10 to 20 minutes of arc, in which case a tenfold reduction in threshold to about 1 ft-L is reasonable.

It is concluded that shadow luminance was greater than 0.6 ft-L and less than 1 to 10 ft-L for 325-ft-L average lunar surface luminance. Be-

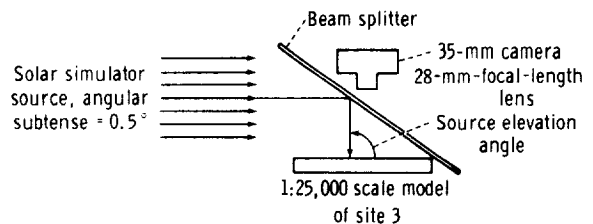


FIGURE 2-50.—Viewing conditions for zero-phase photographs of lunar-surface model.

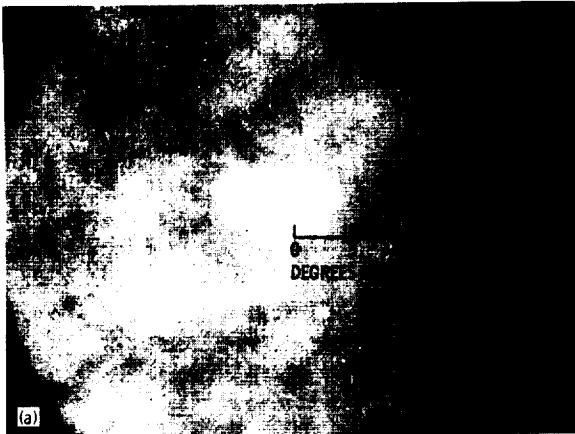


FIGURE 2-51.—Lunar surface model dusted with copper oxide (landing site 3). (a) Sun elevation 90° , (b) Sun elevation 80° , (c) Sun elevation 70° .

cause visual threshold contrast ratios are nearly constant in the range from 10- to 1000-ft-L surround luminance, the ratios of $0.6/325 = 0.002$ and $10/325 = 0.031$ can be used to estimate shadow luminances for other surround values.

It must be emphasized that the threshold values are greatly affected by target contrast and size, which are unknown. However, these estimates are believed sufficiently accurate to establish film exposure conditions for photographing in the shadows. A further conclusion is that the standard lunar photometric functions, measured with an essentially collimated source subtending a small angle, may be inappropriate for determining shadow luminance and contrasts in shadows, because the shadow area is illuminated diffusely.

Lunar Surface Simulation

Simulations of the lunar surface for visibility studies have been of two types:

1. Analytical, using a lunar photometric model.
2. Physical, using a model dusted with copper oxide or portland cement.

An attempt was made to compare the appearance of a copper-oxide-dusted model with Apollo 8 photographs under high Sun illumination. Photographs of a 1:25 000-scale model (8 by 12 in.) of landing site 3 were taken under the conditions shown in figure 2-50. The results are shown in figure 2-51 for 90° , 80° , and 70° Sun angles and a vertical view angle. In this figure, the camera line of sight is normal to the model center. Also shown are Apollo 8 frames with corresponding Sun angles. It can be seen that the model appearance and washout extent are similar for the two cases, allowing for the uniform albedo and relative smoothness of the model.

EVALUATION OF PHOTOCINOMETRIC PROFILE DERIVATION

B. K. LUCCHITTA AND N. A. GAMBELL

Origin of the Study

The availability of Apollo 8 vertical stereoscopic-pair photography (magazine D, type 3400 film) of the Moon led to an opportunity to compare slopes derived by photometric methods with slopes derived by photogrammetric methods.

Procedure

Geometric and Film Parameters

Because of the short time available for the photometric analysis, the computer program (ref. 2-43) for slope derivation from Lunar Orbiter pictures (on 35-mm GRIE film) was modified and used. Using vertical photography (0° tilt),¹ the following parameters are necessary for the computations:

1. Longitude and latitude of the center of the frame (70-mm film).
2. Altitude of the camera lens above the surface.
3. Deviation from north (angle between ground north and picture-frame coordinate system).
4. Sun angle (solar elevation).
5. Longitude and latitude of the subsolar point.
6. *X*- and *Y*-coordinates (picture-frame coordinate system) of the zero-phase point.
7. Focal length of the lens.
8. Location of the initial point of the area to be scanned in picture-frame coordinates.
9. Scan angle (angle between the trace of the phase plane and the *X*-axis of the picture-frame coordinate system).
10. Exposure values for the calibration gray scale (Apollo 8 type 3400 film).
11. Density values for the gray scale of the fourth-generation, 70-mm, type 3400 film.
12. Shutter speed of camera for the picture used.

Format and Microdensitometer Parameters

The following format is required in the program from reference 2-43:

1. Chit area of approximately 20 mm by 8 mm (20 mm along the phase line).
2. Fifteen parallel scans along traces of the phase planes (scans 0.6 mm apart).
3. Up to 500 points per scan.
4. Phase angle between 40° and 110° .
5. Machine parameters as given in table 2-II.
6. A minitape, onto which the density levels are coded in 168 steps (binary coded decimal).

¹ In the case of camera-axis tilt, additional parameters are necessary for the computations.

Selection of Photograph

The vertical stereoscopic-pair photographic coverage of the Moon extended approximately from 80° E to 150° W along the back side. The photographs near the terminator (approximately 150° W) were unsuitable for clinometry because of large shadow areas; those near the limb (90° E) were unsuitable because of small phase angles. Frame 2082 (magazine D, Kodak Panatomic X aerial, type 3400 film) at a scale of 1:1 375 000 was selected as showing sufficient detail for photometric analysis. The scanning was done on a fourth-generation positive.

Obtaining Parameters

The focal length (80 mm), Sun angle (35°), altitude of the spacecraft (110 km), and exposure values for the calibration gray scale were obtained from the support data books. (Reference app. A of this document for further information.) The approximate latitude and longitude of the nadir point were available in the chart of footprints of the photography.

Additional parameters were obtained or approximated in the following manner:

More precise latitude and longitude were derived from Lunar Orbiter photography by image matching, using Lunar Orbiter II frame H-33. The north deviation angle was obtained by the same method. Thus, the values used were (1) 174.3° E, (2) 9.9° S, and (3) 183° N deviation angle (as defined in ref. 2-44).

The latitude and longitude of the subsolar point are necessary for calculating the coordinates of the zero-phase point. To obtain these quantities, the exact time at which the photograph was taken has to be known. The time was approximated to within an hour (1) by knowing the orbit number, the position at which the picture was taken, and

TABLE 2-II.—*Joyce-Loebl MK CS Microdensitometer Parameters*

Condenser, mm.....	32
Optical magnification factor.....	20
Mechanical magnification factor.....	10
Vertical aperture, mm.....	1.5
Horizontal aperture, mm.....	1.5
Spot size, mm.....	0.075 by 0.075
Wedge, density units.....	F-140, 0 to 2.4
Encoder levels.....	1-168

TABLE 2-III.—*Gray Scale Calibration Values (Magazine D Positive)*

Step	Exposure values	Relative density values	Brightness values
1.....	0.083	2.1967	263.291
2.....	.105	2.1605	332.278
3.....	.121	2.0760	382.911
4.....	.152	1.9312	481.013
5.....	.182	1.6898	575.949
6.....	.219	1.3036	693.038
7.....	.276	.7846	886.076
8.....	.324	.3138	1025.316
9.....	.408	.0121	1291.139

the time required for one orbit; and (2) from the orbit number, position, and time of a television transmission to Earth. Knowing the time, the coordinates of the subsolar point were interpolated from ephemeris data for 1968. A supporting computer program established the picture-frame coordinates of the zero-phase point and the scan angle. Because of a Lunar Orbiter scale conversion in the computer program, the scan angle was erroneously established as 4° (measured clockwise from the X -axis). Although it was not used, the correct scan angle was later established as being 10° . The coordinates of the initial point were measured with the Mann comparator on the 70-mm film. The density values of the calibration gray scale were calculated from microdensitometer scans. It was found convenient to use a density of 0.3 as a base for the measurements. Nine steps of the gray scale were used for the density-to-brightness conversion (table 2-III).

Scanning of the Area and Computer Program Modification

The chit area was scanned on the microdensitometer, and the coded data were put on tape, which was processed in the 360/65 computer as specified in the reference 2-43 program. The following modifications had to be made on the procedure and the computer program in order to meet the specifications of the 70-mm spacecraft film as opposed to the normally used 35-mm GRE Lunar Orbiter film:

1. A correction scan across the orbiter framelet width (correcting errors introduced through television lines) had to be omitted.

2. The correct exposure values for the Apollo 8 film (type 3400) gray scale had to be substituted.

3. A scale conversion from 70-mm to 35-mm film had to be eliminated.

Results

Comparison With Photogrammetric Profiles Obtained From the AP/C Plotter

Figure 2-52 shows an outline of the area scanned. The initial point is at the northeast



FIGURE 2-52.—Apollo 8 frame 2082, area of comparison of photoclinometric profiles with photogrammetric profiles.

corner of the outlined area. The scanning direction is toward the northwest. Topographic profiles of the 15 scans (figs. 2-53 and 2-54) were plotted on the XYZ plotter at a scale of 1:100 000. The first few scans at the north side of the photograph show a relatively flat crater bottom with a slight rise (approximately 600 meters) over the crater rim, and a marked dropoff (approximately -300 meters) at the end. The intermediate scans are

relatively flat, with gentle ups and downs (on the order of 400 meters) and some dropoff toward the end. The last scans (south side of picture) show a definite rise over the rim of the crater (1200 meters). Photogrammetric profiles along the same plane along scan 1, approximately scan 8, and scan 15 (fig. 2-55) were provided by the AP/C plotter. In a comparison between the methods, scan 15 (fig. 2-56) shows good agreement

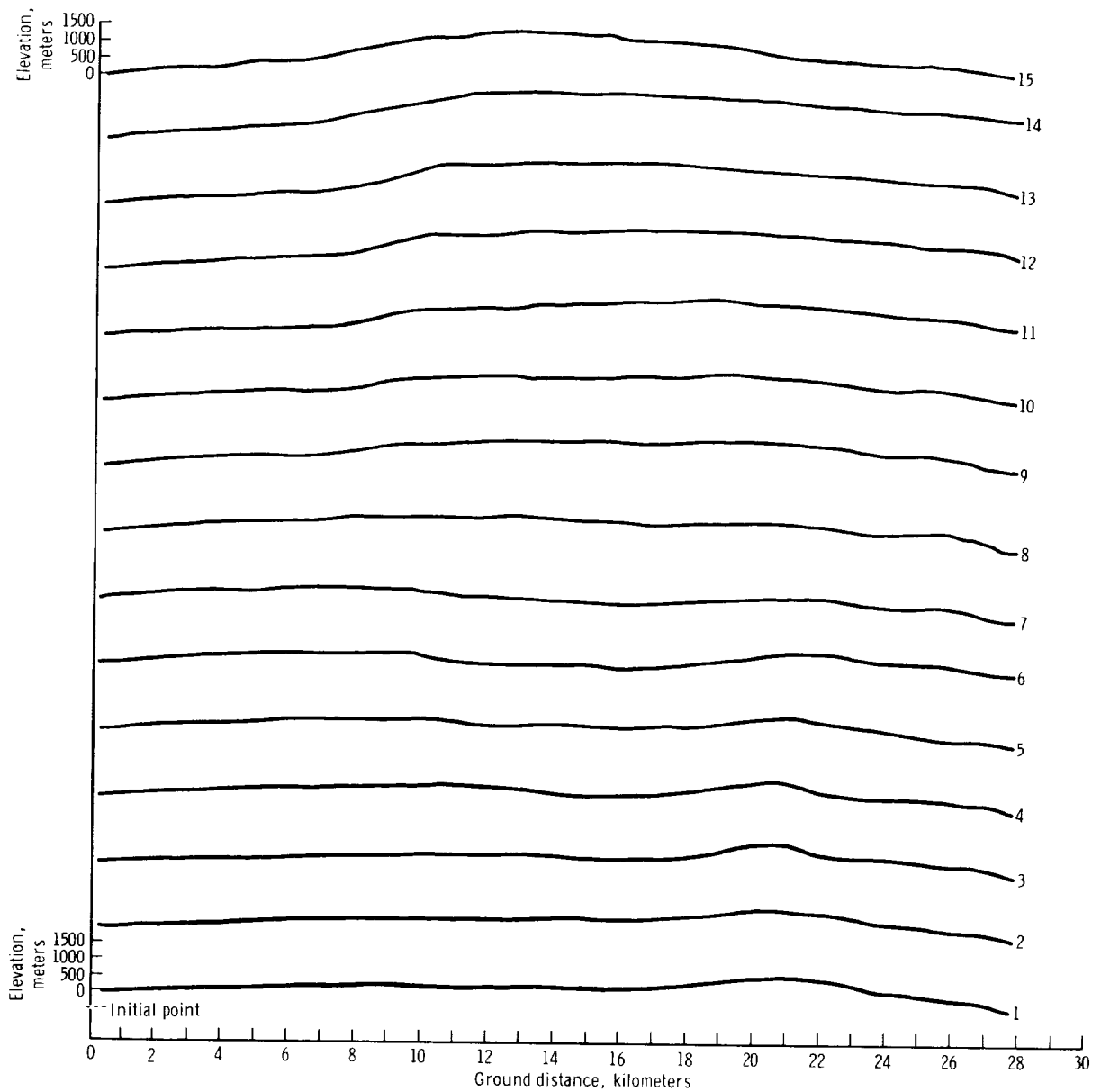


FIGURE 2-53.--Profiles of 15 scans plotted on XYZ plotter.

between the two profiles. Scan 1 was tilted to adjust the slightly rising, flat crater floor to almost horizontal and shows a marked diversion in the elevation of the rim and in the area outside the crater. Scan 8, when tilted to fit the equivalent photogrammetric scan, shows some agreement in small scale features but is too low in the beginning and in the end.

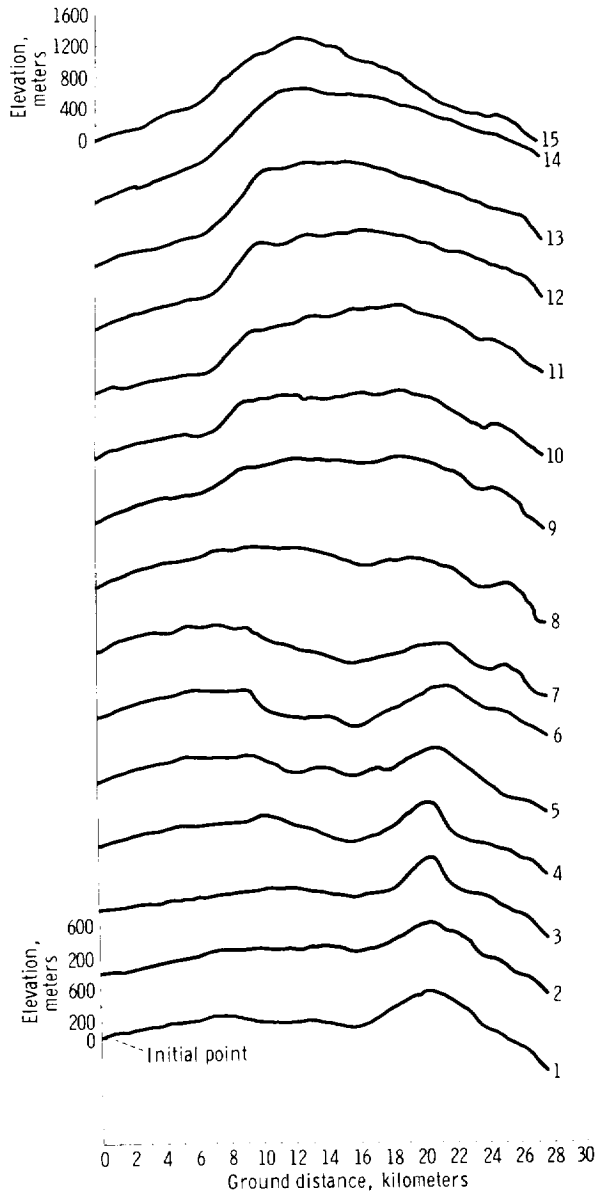


FIGURE 2-54.—Profiles of 15 scans plotted on XYZ plotter, 5X vertical exaggeration.

Comparison of Slopes From Lunar Orbiter Frame H-33, Framelet 739, With Slopes From Apollo 8 Frame 2082-D

An area lying within the site scanned on Apollo 8 film was scanned on Lunar Orbiter II film in an effort to compare slopes. Figure 2-57 shows the location of both sites. The large outline shows the Apollo 8 area scanned on frame 2082-D. Unfortunately, the differences in scale of the photographs make comparison difficult. Photometric reduction of the site on Lunar Orbiter II frame M-33 was impossible because of the extreme contrasts in brightness. Figure 2-58 shows plots from scans made on H-33 and the corresponding parts from scans made on frame 2082. Scan 15 (Lunar Orbiter photograph) should approximate scan 13 (Apollo photograph), while scan 1 should be equivalent to scan 10.

Evaluation

The photoclinometric profiles start at a relative zero elevation at each scan, and the heights are integrated over the entire length so that errors are accumulated. The measured points along the scan line are approximately 75 meters apart, and the computer program furnishes elevation differences to a fraction of a meter. At the scale of the scanned area, this precision represents noise of the system. To get more precision, reflecting small features, a small area would have to be scanned on an enlargement. This enlargement would have to be of very high quality in order not to lose resolution at the high spatial frequencies. An alternative way to increase precision is to scan a small area with a decreased spot size and increased frequency of points along the scan line. However, the reduced signal-to-noise ratio of the photomultiplier tube at low light levels may render this method unsuitable.

Errors in the photoclinometric slope derivation reported here may be caused by two main factors:

1. The use of a computer program written for Lunar Orbiter photography; or
2. The lack of some data (usually geometric) that are essential to photoclinometry.

The computer program in reference 2-43 was

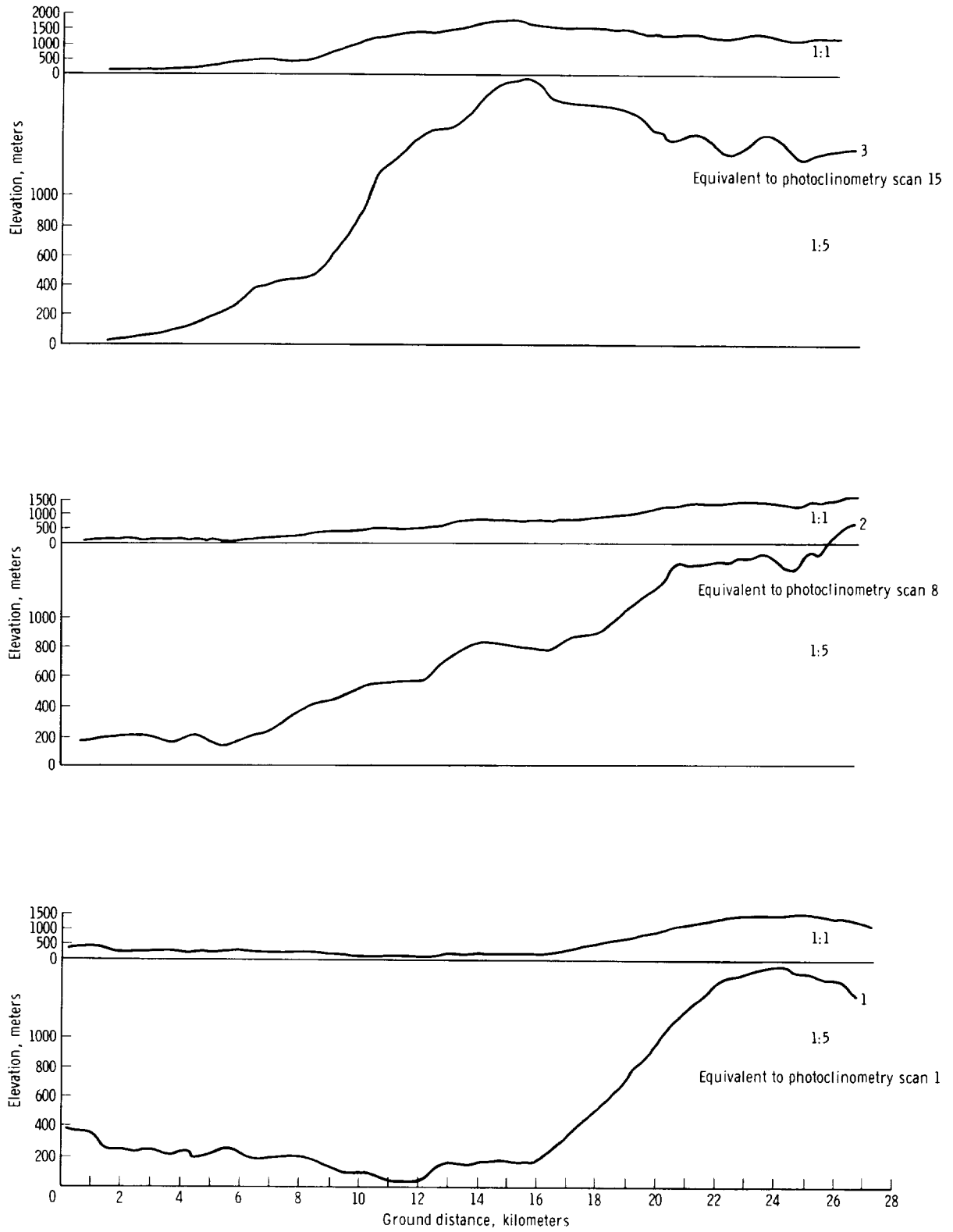


FIGURE 2-55.—Comparison of photogrammetric profiles and photoclinometric scans.

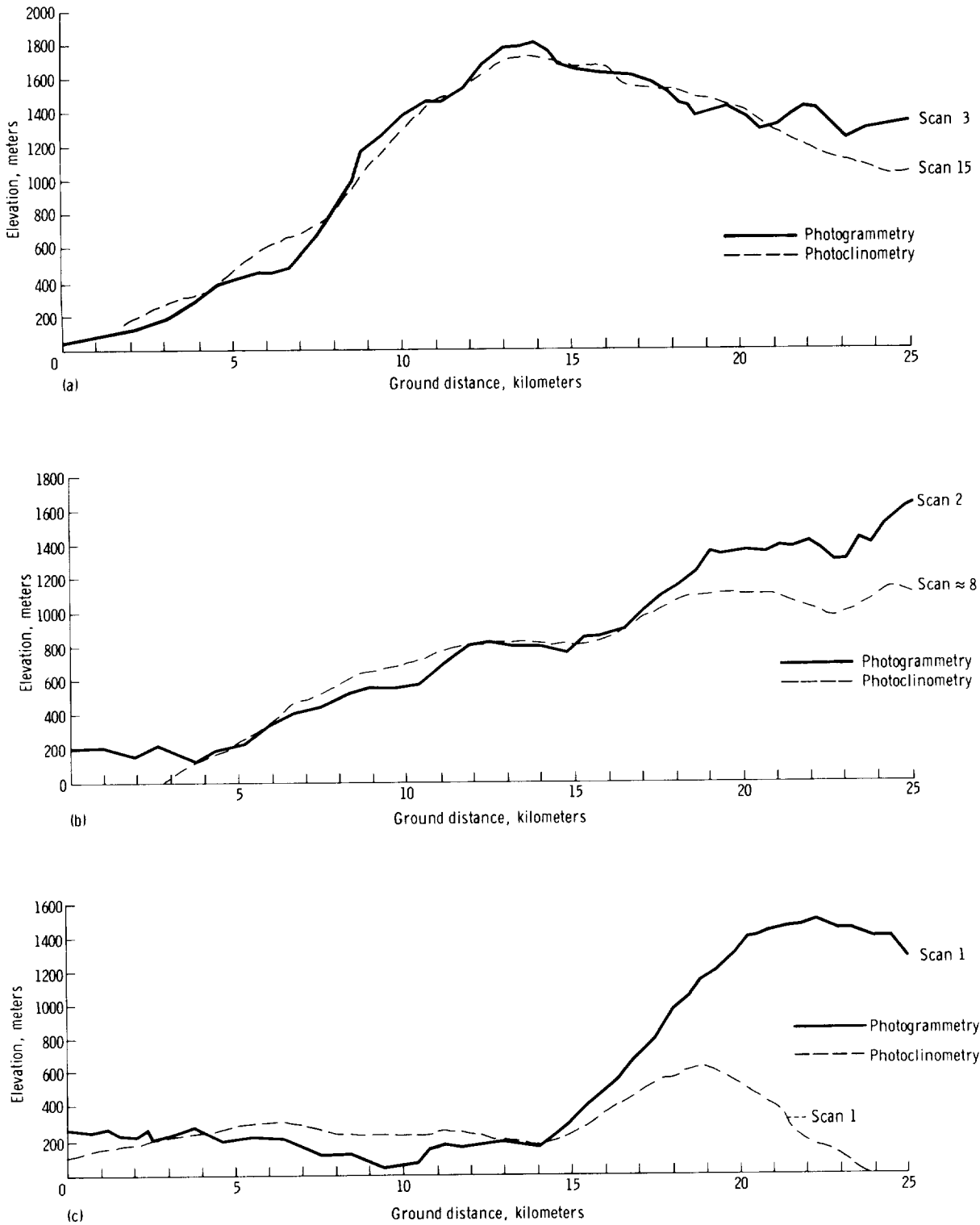


FIGURE 2-56.—Photogrammetric profiles compared with three photoclinometric scans. (a) Photogrammetric scan 3 and photoclinometric scan 15; (b) photogrammetric scan 2 and photoclinometric approximately scan 8; (c) photogrammetric scan 1 and photoclinometric scan 1.

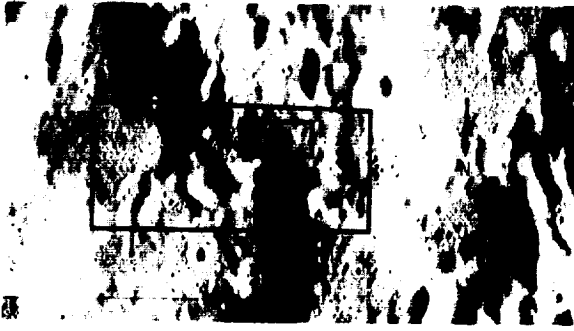


FIGURE 2-57.—Portion of Lunar Orbiter II frame H-33, showing areas of photoclinometric comparison.

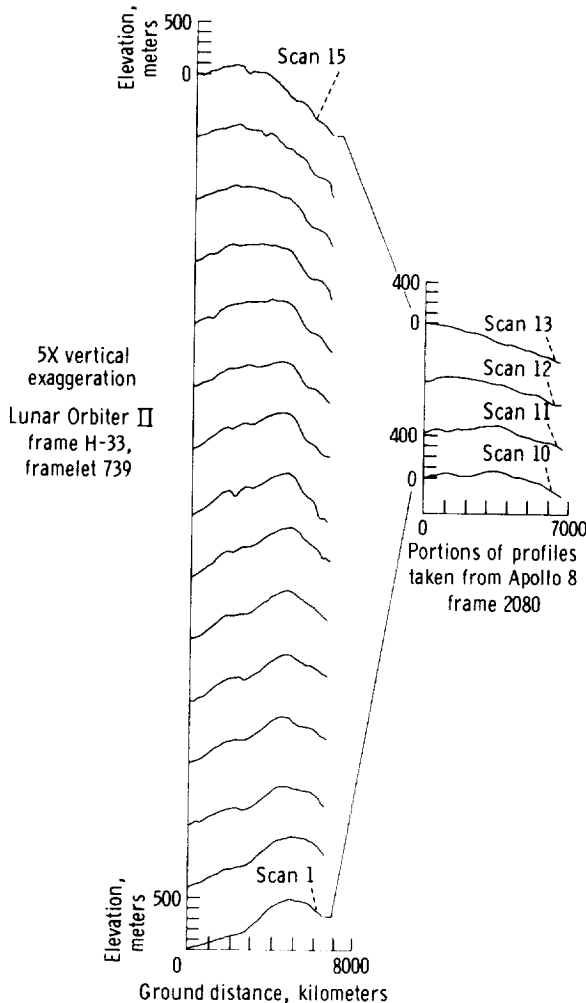


FIGURE 2-58.—Scan comparison of Lunar Orbiter II frame H-33, framelet 739, and Apollo 8 frame 2082.

written for high- and medium-resolution Lunar Orbiter photographs, mainly of the landing sites where low relief is predominant and small features are of interest. The application of this program to high-altitude, 70-mm Apollo 8 photography introduces errors which may be related to the following problems:

1. At the scale of Apollo 8 magazine D photography, variations in albedo are present in the photograph, but they are not corrected for in the computer program.

2. Lunar Orbiter chit areas, as commonly used for photoclinometry, involve phase-angle changes of less than 0.5° for high-resolution frames and approximately 3° for medium-resolution frames. The Apollo 8 film chit area spans 14° of phase-angle change.

3. The phase angles involved in the Apollo 8 photograph approach the lower limit of the phase-angle range set in the photoclinometry program. Midrange phase angles in magazine D photographs are not suitable for photoclinometric methods, because they occur on the back side of the Moon, where the roughness of the terrain results in large areas of shadow.

4. Erroneous interpretation of slope will have a large effect on integrated heights over a horizontal separation between points of 75 meters in the Apollo 8 photograph as opposed to a separation between points of only 0.6 meter in high-resolution Lunar Orbiter photographs.

5. The photometric function used in the computer program may not be correct for the back side of the Moon.

Additional causes for error may be found in one of the following areas:

1. Altitude given as 110 km may not be precise.
2. The time at which the photograph was taken was not accurately known; therefore, the latitude and longitude of the subsolar point may not be correct.
3. The photograph is assumed to be vertical. An unrecorded tilt may be present.
4. The latitude and longitude of features on the back side of the Moon are not accurately known.
5. The scan angle used was not accurate.
6. Calibration errors and loss of detail in the photographs may be introduced through the fourth-generation film used.

Vertical Resolution of Slope Profiles

The maximum vertical resolution of slope profiles can be calculated if the slope and the distance between successive points (approximately 75 meters) are known. Slopes of up to 7° would therefore have a vertical resolution of approximately 1 meter; slopes of up to 5° , approximately 7 meters; slopes of up to 20° , approximately 26 meters; and slopes of up to 30° , approximately 43 meters. Most slopes in Apollo 8 frame 2082 lie below 20° .

This vertical resolution is a theoretical limit which cannot be attained practically because of errors in the photometric function, the albedo, the density-to-brightness conversion, and noise in the scanning system.

Applications of Photoclinometry

Profiles derived by photoclinometric methods may be useful as an expression of topographic relief in the absence of stereoscopic photography. When detailed topographic data are required below the contour interval of a photogrammetric map, these data may be supplied by photoclinometry under the conditions previously outlined. The photoclinometric profiles should be referenced to photogrammetric control points. Also, the photoclinometric data are useful for statistical estimates of terrain roughness if a relatively high precision in the recorded heights has been achieved.

Advantages of Apollo 8 Photography

Photoclinometrically, Apollo 8 photography is superior to Lunar Orbiter photography for the following reasons:

1. In Lunar Orbiter photography, the size of the area scanned by the microdensitometer is limited by the framelet boundaries.
2. Each Lunar Orbiter framelet contains its own sensitometric data, which must be calibrated.
3. The Lunar Orbiter framelets contain erroneous density variations as a result of the transmission procedure used to reconstitute the images from the Lunar Orbiter spacecraft film.

Using Apollo film, sensitometric calibration data need to be calculated only once for all of the frames in a magazine. Density corrections for television lines are eliminated.

SELENODESY AND CARTOGRAPHY

EVALUATION OF THE PHOTOGRAPHY

D. W. G. ARTHUR

Although the Apollo 8 photography was not taken for selenodetic purposes, the photographs have some selenodetic applications. The small-scale photographs—frames 2473, 2474, 2484, 2485, 2491, 2505, and 2506 (magazine B)—are exposed from a direction (in the lunar frame of reference) which is quite new. Furthermore, the photographs cover sufficient area to determine without orbital data the spacecraft location from the photograph. The photographs have approximately the same resolution as the plates taken at the Paris Observatory. These plates have had extensive selenodetic application. Therefore, in spite of the small scale, these Apollo 8 photographs have some selenodetic applications when used in conjunction with Earth-based lunar photography. The same photographs have some usefulness for provisional mapping of part of the averted lunar hemisphere.

The high obliques—frames 2796 to 2819 and 2744 to 2759 (magazine C), and frames 2187, 2189, and 2202 to 2214 (magazine D)—have good cartographic possibilities, as do the steeper obliques, frames 2263 to 2266 (magazine E). The value of this photography will increase as more photographs are obtained from other directions.

APOLLO 8 CONTROL POINTS

RICHARD L. NANCE

For Apollo 8, a target for optical sightings on the lunar far side was called a control point (CP). Three control points were selected before the flight to make sightings easier. The control point identified as CP-1 was located 20° from the evening terminator and CP-2 was located 60° from the evening terminator. The control point identified as CP-3 was located 60° from the morning terminator. The command module pilot (CMP) exercised an option of selecting sighting targets in real time and selected new targets for CP-1 and CP-2. These control points can be positively identified on Apollo 8 photography (figs. 2-59 and 2-60), and the same points were probably sighted on all three revolutions.



FIGURE 2-59.—Control point 1.



FIGURE 2-60.—Control point 2.

Sightings on CP-3 were made on revolutions 6 and 7. On revolution 6, the position of CP-3, which was selected preflight (point 1 in fig. 2-61), was entered into the onboard computer. The optics were then automatically driven to view this location. Because of the high Sun angle at this location and because the Sun line was so close to the line of sight, primarily only albedo

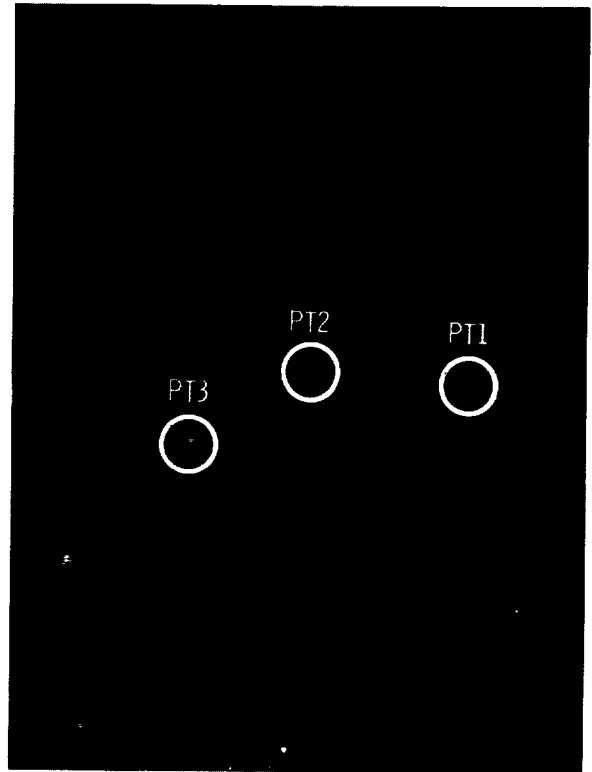


FIGURE 2-61.—Control point 3, showing points 1, 2, and 3.

differences could be seen, which made it difficult to identify the preselected CP. A bright spot (a crater with very high albedo) was sighted on revolution 6. During revolution 6, sextant photography was taken while sighting. Based on this photography, point 2 in figure 2-61 was probably sighted on during revolution 6. The poor visibility made it difficult to reacquire the same feature on revolution 7 as was sighted on revolution 6. Since sextant photography cannot be taken when the sextant is used for sighting, there is no sextant photography for revolution 7 to help in identification. Based on the different positions obtained on revolution 6 as compared to revolution 7 and based on similarity of albedo patterns, point 3 in figure 2-61 was possibly sighted on during revolution 7. Identification of point 3 is less certain than point 2. Because identification of CP-3 was difficult in real time and even more difficult on photography postflight, the identification of CP-3 is uncertain. Therefore, a lower level of confidence exists in the position of CP-3 than in that of CP-1 and CP-2.

TABLE 2-IV.—*Apollo 8 Control-Point Positions (Preliminary)*

Control point	Latitude, deg *	Longitude, deg *	Radius, km
CP-1 (average, revolutions 5, 6, and 7).....	-6.2537	-158.0650	1742.336
CP-2 (average, revolutions 5, 6, and 7).....	-9.7016	+163.2246	1738.093
CP-3, revolution 6, pt 2.....	-8.9229	+97.1466	1739.524
CP-3, revolution 7, pt 3.....	-8.9167	+96.8883	1737.464

* The sign convention used is that N lat and E long are positive.

From Apollo 8 data, the positions obtained for the three control points, which may be used in mapping the lunar far side, are shown in table 2-IV. Onboard optical sightings by the crew provide the basis for checking the positional accuracy of lunar charts compiled from small-scale photography. Photogrammetric reductions will extend these results, as will subsequent Apollo missions.

As compared with positional data available before Apollo 8, there was a great improvement in the accuracy of the positions of these features. These positions were derived from a combination

of an orbit determination to locate the command module (CM) and a program to locate the landmark relative to the CM. The former program uses Doppler tracking data, and the latter uses shaft and trunnion angles, which were measured with the onboard optical tracking instruments. It is possible to determine the positions both of the CM and of landmarks from optical tracking data. In Apollo 8, the instruments used were the scanning telescope (SCT), on revolutions 5 and 6, and the sextant, on revolution 7.

The positions (table 2-V) of these three features

TABLE 2-V.—*Apollo 8 Control-Point Map Positions*
[CP-1 and CP-2]

Lunar map	CP-1		CP-2	
	Latitude, °S	Longitude, °W	Latitude, °S	Longitude, °E
Army Map Service (AMS), Lunar Equatorial Zone Mosaic (LEZ), 1:2 500 000, 1968.....	05.00	158.50	09.50	163.90
ACIC Apollo Lunar Orbit Chart (ALO), 1:11 000 000, 1st ed., 1968.....	05.80	158.40	10.40	163.70
ACIC Apollo Lunar Orbital Map (LOM), 1:7 500 000, 1st ed., 1968.....	05.80	158.50	10.40	163.40
ACIC Lunar Farside Chart (LFC-1), 1:5 000 000, 2d ed., 1967.....	05.65	158.50	10.30	163.30

[CP-3]

Lunar map	Point 1		Point 2		Point 3	
	Latitude, °S	Longitude, °E	Latitude, °S	Longitude, °E	Latitude, °S	Longitude, °E
AMS LEZ (eastern limb), sheet 3 of 4.....	09.00	96.35	9.08	95.90	9.22	95.55
ACIC/ALO.....	08.80	96.10	9.05	95.80	9.10	95.55
ACIC/LOM.....	08.80	96.20	9.05	95.75	9.20	95.30
ACIC/LFC-1.....	09.05	96.10	8.77	96.07	8.83	95.67

were scaled from sheets from the four map series (refs. 2-45 to 2-48) which cover the lunar far side.

References 2-45, 2-46, and 2-47 are carried on board Apollo missions and are used for a gross form of navigation, to locate photographic targets, and to locate targets for optical sightings, respectively. Reference 2-48 is used for planning purposes.

To compare the positions, the Apollo 8 values were subtracted from the map values (table 2-VI). The Aeronautical Chart and Information Center

(ACIC) value in table 2-VI is from reference 2-47. In the last row of table 2-VI, the Army Map Service (AMS) and ACIC maps are compared. As shown in table 2-VI, the largest difference is 1.58°. Although it is realized that three points are a small sample from which to develop statistical parameters, the positional uncertainty (1 sigma) of the maps should be estimated as not larger than 2° (60 km). The estimated uncertainty used prior to Apollo 8 was 10° (300 km).

In addition to the three control points located

TABLE 2-VI.—Comparison of Apollo 8 and Map Positions

Comparison	Latitude	Difference	Longitude	Difference
CP-1				
AMS (Apollo 8)	-05.00° (-06.25°)	+1.25°	-158.50° (-158.06°)	-0.44°
ACIC (Apollo 8)	-05.80° (-06.25°)	+.45°	-158.50° (-158.06°)	-.44°
AMS (ACIC)	-05.00° (-05.80°)	+.80°	-158.50° (-158.50°)	.00°
CP-2				
AMS (Apollo 8)	-09.50° (-09.70°)	+0.20°	+163.90° (+163.22°)	+0.68°
ACIC (Apollo 8)	-10.40° (-09.70°)	-.70°	+163.40° (+163.22°)	+.18°
AMS (ACIC)	-09.50° (-10.40°)	+.90°	+163.90° (+163.40°)	+.50°
CP-3, point 2, revolution 6				
AMS (Apollo 8)	-9.08° (-8.92°)	-0.16°	+95.90° (+97.14°)	-1.24°
ACIC (Apollo 8)	-9.05° (-8.92°)	-.13°	+95.75° (+97.14°)	-1.39°
AMS (ACIC)	-9.08° (-9.05°)	-.03°	+95.90° (+95.75°)	-.15°
CP-3, point 3, revolution 7				
AMS (Apollo 8)	-9.22° (-8.91°)	-0.31°	+95.55° (+96.88°)	-1.33°
ACIC (Apollo 8)	-9.20° (-8.91°)	-.29°	+95.30° (+96.88°)	-1.58°
AMS (ACIC)	-9.22° (-9.20°)	-.02°	+95.59° (+95.30°)	+.29°
Landmark B-1				
AMS (Apollo 8)	+02.52° (+02.53°)	-0.01° (-.3 km)	+35.03° (+35.00°)	+0.03° (+.90 km)



FIGURE 2-62.—Apollo lunar landmark B-1.

by Apollo 8 data, the position of the B-1 landmark (fig. 2-62) was obtained. The B-1 landmark is on the lunar front side (table 2-VI). The optical sighting and orbit determination serve primarily to furnish information from which it is possible to evaluate the real-time navigational capability of Apollo.

THE FIGURE OF THE MOON

W. H. MICHAEL, JR.

Some information pertaining to lunar radii in the near-side equatorial region of the Moon available prior to the Apollo 8 mission is shown in figure 2-63, taken from reference 2-49. The data in figure 2-63 are plotted without consideration of latitude variations in order to indicate overall trends, but all data are for locations within $\pm 5^\circ$ of the lunar equator. The solid points on the figure are taken from an analysis of the angular velocity sensor data from Lunar Orbiter in conjunction with orbit determination procedures, and these radii are with respect to the center of mass of the Moon.

The Ranger VIII impact analysis point (ref. 2-50) is also with respect to the center of mass of the Moon. The solid curve represents results of a harmonic analysis of radii derived from Earth-based photography (ref. 2-51). This curve is thus

considered to be with respect to the center of figure of the Moon.

The trends illustrated in figure 2-63 indicate that the radii relative to the center of mass of the Moon are systematically less than those relative to the center of figure by an average of approximately 2 km. (The angular velocity sensor data in the 30° E to 40° E region are somewhat anomalous, but a highland area to the south of Mare Tranquillitatis may have influenced these results.) The radii relative to the center of mass are also less than what might be expected, based on the generally accepted value of about 1738 km for the mean radius of the visible disk of the Moon.

As pointed out in reference 2-49, these results may indicate a displacement of the center of mass of the Moon toward the Earth relative to the center of figure. If confirmed, this hypothesis should provide data for geophysical analyses, perhaps with implications pertaining to the origin and history of the Moon. The primary requirement is to obtain data for radii on the far side of the Moon.

Two types of data were obtained on Apollo 8 that should contain information relative to far-side lunar radii; namely, the sextant sightings of landmarks on the far side and the far-side photography. Photogrammetric reductions of the far-side photographs are in progress.

Some preliminary results from analyses of the landmark sightings are available, but the results given here are from an early stage of the analyses and are subject to later modification. The preliminary results on lunar radii from three landmark locations, consisting of average values of

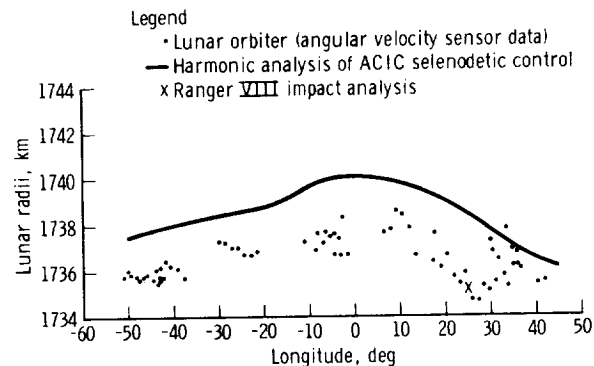


FIGURE 2-63.—Determinations of lunar radii in the equatorial region from Lunar Orbiter and other data.

TABLE 2-VII.—*Preliminary Results From Analyses of Apollo 8 Landmark Sightings*

Site	Latitude	Longitude	Radius, km
B-1.....	2.54° N	35.01° E	1737.5
CP-1.....	-6.28° S	-158.07° W	1742.0
CP-2.....	-9.71° S	163.21° E	1737.5

results from different orbital passes and somewhat different procedures, are shown in table 2-VII. These data are with respect to the center of mass of the Moon.

The B-1 landmark is on the near side of the Moon, and photogrammetric analyses of Lunar Orbiter photographs give a radius of 1735.2 km for this point compared with 1737.5 km given in the table. The 1735.2-km value seems to be consistent with the results in figure 2-63, indicating a possible bias in the 1737.5-km value in the table. Landmark CP-1, judging from its appearance in the Apollo 8 photography, seems to be representative of the mean surface level in its area. However, landmark CP-2 is a small crater inside a large crater, which is in turn inside a still larger crater of approximately 40 km in diameter; this point seems to be well below the mean surface level in its area.

Considering the results in table 2-VII independently, there is some evidence of larger lunar radii with respect to the center of mass for the far-side points. If only the B-1 site is biased, the evidence is somewhat strengthened. However, these data are not considered to be sufficiently convincing to confirm (or deny) the hypothesis concerning a displacement between the center of mass and the center of figure of the Moon.

PHOTOGRAMMETRY

PHOTOGRAMMETRIC DATA REDUCTION

PAUL E. NORMAN, MERRITT J. BENDER, AND
R. D. ESTEN

Introduction

The photography obtained from the Apollo 8

mission represents a number of firsts, among which are the following:

1. The first photography obtained from lunar orbit which included the return of the original negatives.

2. The first new lunar photography, for all practical purposes, since the Lunar Orbiter photography of almost 2 years ago.

3. The largest scale photography ever obtained of the lunar far side.

Because surveying and mapping, particularly by photogrammetric methods, play an important role in the NASA lunar exploration program, it is only logical to assess the value of the Apollo 8 photography from this standpoint. Such an assessment is of even greater importance in view of the limited availability of lunar photography that lends itself to the production of the required surveys and maps. As a result of these motivations, personnel of the MSC Mapping Sciences Laboratory undertook an investigation of the photogrammetric potential of the Apollo 8 photography. This investigation included an evaluation to determine what photography was suitable for photogrammetric data reduction, stellar calibrations of the Apollo 8 cameras, sample control extension to determine the value of the photography for establishing lunar control, and the production of a topographic map to assess the value of Apollo 8 photography for mapping. The results of these investigations, which will subsequently be described in more detail, show that the Apollo 8 Hasselblad photography represents a valuable medium for photogrammetric surveying and mapping of the lunar surface. Therefore, it is concluded that surveying and mapping based on Apollo mission photography can play an important role in the missions leading not only to the first lunar landing but also to subsequent lunar exploration.

Photogrammetric Evaluation of Photography

The first step in investigating the photogrammetric potential of Apollo 8 photography was to prepare a summary of the photography along with pertinent photogrammetric information. The evaluation was limited to photography obtained with the Hasselblad cameras, used with both 80-mm and 250-mm lenses. Other photography, such as the 16-mm sequence photography, was

not considered suitable for photogrammetric data reductions.

A description of the Apollo 8 mission, including the photographic aspects, is contained in the Introduction and chapter 4 of this document and will be only briefly summarized here. Most of the Hasselblad photography was obtained from a circular orbit of 60 n. mi. (111 km) with a 12° inclination with respect to the lunar equator. Photography was taken vertically in strips with the camera bracket mounted, as well as from an oblique hand-held position. An intervalometer was available for the strip photography to acquire exposures at 20-second intervals. In all, more than 600 exposures were acquired using both the 80-mm and the 250-mm lenses. The photography was exposed on 70-mm film, resulting in a format size of 55 by 55 mm. Representative scales for vertical photographs from the 111-km altitude are 1:1 400 000 for the photography taken with the 80-mm lens and 1:440 000 for the photography taken with the 250-mm lens. The photogrammetric evaluation yielded the following information for each photograph:

1. Frame number
2. Approximate location
3. Focal length of lens used
4. Approximate scale
5. Forward overlap and side overlap
6. Sun angle
7. Relationship to other coverage
8. Approximate tilt

Detailed information concerning the photographic coverage is included in appendix A. Of particular interest are two vertical strips which run from 150° W to 80° E. Selected vertical and oblique photography of features are also of scientific interest, such as that of the craters Langrenus and Tsiolkovsky. It should be noted that there was no time correlation with the orbit, nor were there specific attitude data for the camera.

Camera Calibration Data

Camera calibration data are an integral part of photogrammetric data reductions. The Apollo 8 Hasselblad camera had no special facilities for film flattening; the image plane is located in the removable magazine and, except for two V-shaped notches on one edge, has no fiducial marks. The

camera was located obliquely to the spacecraft window, and there was a pressure difference between the spacecraft and the outside environment. Furthermore, two different cameras and a variety of magazines were used for the photography. Ideally, the cameras should have been calibrated with all combinations of lenses and magazines used during the mission. What was done, in fact, was to select combinations of cameras, magazines, and lenses and to use these data for all cases. It was further hoped that the effect of the spacecraft window and the differential pressure between the spacecraft and the lunar surface could be determined by stellar photography acquired during the mission. Such photography was not obtained. Therefore, the effect of this condition will have to be estimated by comparing the plate residuals from the camera calibration with those obtained from data reductions.

The manufacturer furnished some calibration data on the camera with the 80-mm lens and an unspecified magazine. Because these data were incomplete, they were supplemented by stellar camera calibrations carried out at the Mapping Sciences Laboratory. The following camera/lens/magazine combinations were calibrated:

1. Camera 1024 with 80-mm lens and magazine C
2. Camera 1024 with 80-mm lens and magazine D
3. Camera 1024 with 250-mm lens and magazine B
4. Camera 1024 with 250-mm lens and magazine D
5. Camera 1020 with 80-mm lens and magazine D
6. Camera 1020 with 80-mm lens and magazine G

Camera 1024 was used with the intervalometer for the acquisition of the vertical strip photography. The results of these stellar calibrations are considered to be satisfactory, with the standard error of the plate residuals at the star images ranging from 10 μ to 14 μ .

Analytical Aerial Triangulation

Because one of the most valuable potential uses of the Apollo 8 photography is control extension, considerable effort was expended to investigate this aspect. There was no direct tie to orbit data,

nor was much lunar control available. There were, however, four points on the lunar surface with coordinates established by sextant observation from Apollo 8 (CP-1, CP-2, and CP-3, and landmark B-1). Since vertical photography was taken over three of these points, the investigation centered around these control points and an attempt to recover the orbital camera positions.

The three control points are located on the lunar far side. The coordinates of these points are listed in table 2-IV. The photography which covers these three control points was obtained from magazine D (revolution 4) and magazine C (revolution 8); the specific coverage is given in table 2-VIII.

Because no stereoscopic model contained more than one control point, it was decided to analytically triangulate short strips at CP-1 and CP-2 and to impose the constraint that adjusted coordinates of the exposure stations lie on the orbit.

TABLE 2-VIII.—*Photographic Coverage of Control Points*

Control point	Magazine D photographs *	Magazine C photographs *
CP-1.....	2052	2664
	2053	2665
	2054	2666
CP-2.....		2702
		2703
		2704
		2705
CP-3.....	2161	2771
	2162	2772
		2773

* By frame numbers.

With this in mind, photographs 2052 to 2055 and 2664 to 2667 were triangulated as a block at CP-1, and photographs 2091 to 2095 and 2702 to 2705 were triangulated as a block at CP-2. In both blocks, the exposure stations were constrained in latitude and height but allowed to adjust in longitude, that is, downtrack. In addition to enforcing CP-1 or CP-2, the exposure base as determined by the 20-second intervalometer was also enforced. Once the adjusted exposure stations were obtained, the positions were converted to time values; that is, to ground elapsed time (GET). The adjusted camera data for the block at CP-2 are found in table 2-IX.

The solutions seem satisfactory, although the results should be treated as preliminary. Although the 15 to 20 μ plate residuals might seem high for conventional aerial triangulation, it must be remembered that corrections were not applied for the differential pressure and the effect of the spacecraft window. Because the strips are continuous between CP-1 and CP-2, another check is afforded by computing the average exposure interval between the two points. The time interval between magazine D photographs 2055 and 2091, as determined from the two triangulations, proved to be 697 seconds. Thus, the exposure interval is 697/36, or 19.36 seconds. The time interval between magazine C photographs 2667 and 2702 proved to be 693 seconds, so the exposure interval is 693/35, or 19.80 seconds. These exposure intervals confirm the feasibility of this approach, and efforts are currently underway to refine the triangulation.

It is felt that these results show both that orbital data for the Apollo 8 vertical-strip photographs can be recovered and that the photography

TABLE 2-IX.—*Adjusted Camera Data (CP-2)*

Frame	GET, hr:min:sec	Latitude, deg	Longitude, deg	Radius, km	X-tilt, deg	Y-tilt, deg	Heading, deg	Sigma, μ m
2091.....	75:32:17	-11.155	-195.368	1849.05	-0.105	7.225	-94.632	20
2092.....	75:32:37	-11.244	-196.398	1848.92	-.213	7.394	-94.145	18
2093.....	75:32:57	-11.333	-197.415	1848.74	-.268	7.389	-93.707	21
2095.....	75:33:19	-11.432	-198.585	1848.63	-.253	7.736	-93.124	19
2702.....	83:26:10	-10.650	-194.170	1848.80	7.477	-14.276	-99.817	17
2703.....	83:26:30	-10.749	-195.191	1848.86	8.069	-12.848	-98.666	16
2704.....	83:26:50	-10.849	-196.213	1848.75	8.851	-11.388	-97.517	18
2705.....	83:27:10	-10.957	-197.241	1848.61	9.775	-9.964	-96.315	21

can be utilized to extend lunar control. This aspect of the investigation is continuing, and the next step will be to perform continuous triangulations from CP-1 to CP-2. An endeavor is also being made to acquire spacecraft attitude information and to include the information in the reduction.

Topographic Mapping

Another aspect of the investigation of the surveying and mapping potential of the Apollo 8 photography was its suitability for the production of topographic maps. Two approaches were used. One was a theoretical estimation of the relative horizontal and vertical accuracies obtainable, and the other was the production of a topographic map of a small, interesting area of the lunar surface.

A theoretical estimate of relative horizontal and vertical accuracies can be obtained by the use of the following equations:

$$m_p = \frac{H}{c} dx$$

and

$$m_h = \left(\frac{H}{B} \cdot \frac{H}{c} \right) dx$$

where

m_p = relative horizontal accuracy

H = flight height

dx = accuracy of image measurement

m_h = relative vertical accuracy

c = focal length of camera lens

B = space base between exposure

The horizontal accuracy can be estimated by using, for dx , the plate residuals from the triangulations. Using 20μ , one then gets $m_p \approx 30$ meters for the vertical photography taken with the 80-mm lens from the circular orbit of 60 n. mi. This value is probably optimistic, however, because the only present method of scaling the

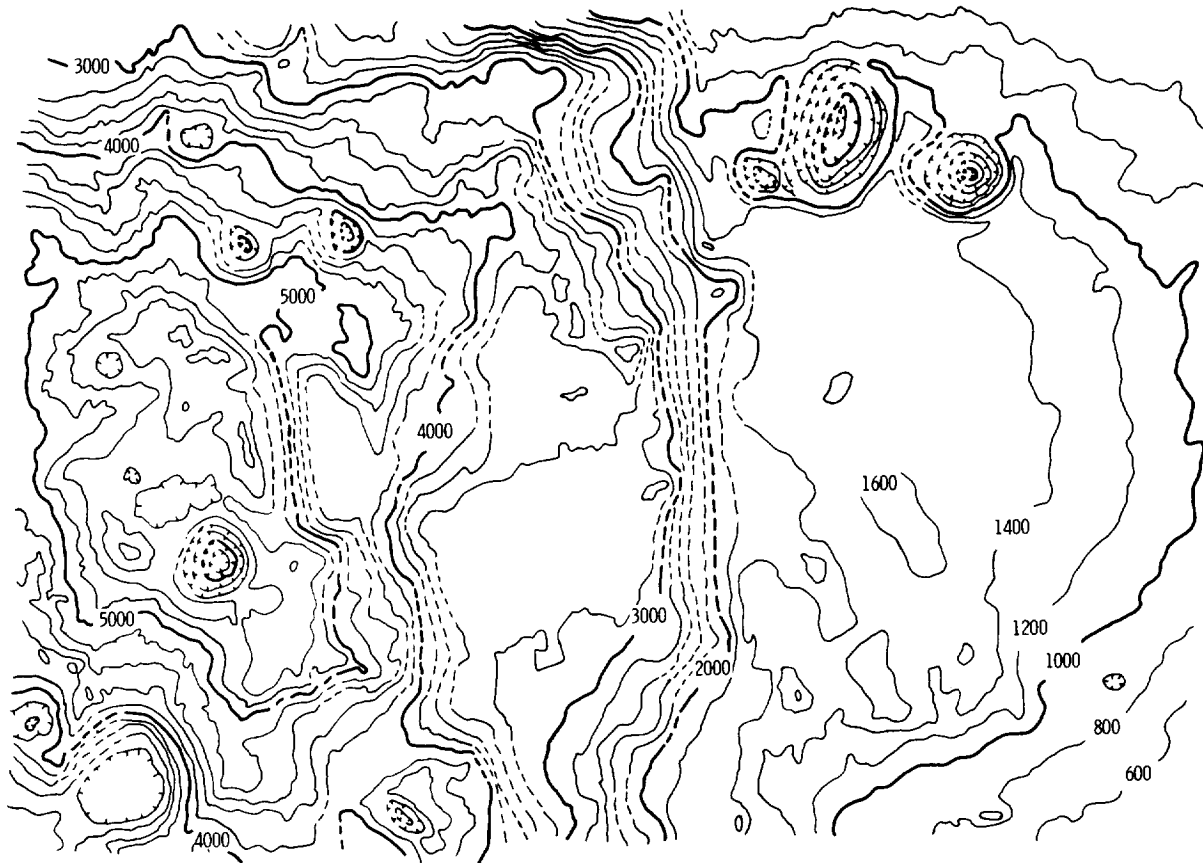


FIGURE 2-64.—Topographic map produced from Apollo 8 frames 2057-D to 2059-D.

stereoscopic models is by the use of the exposure interval and spacecraft velocity. Since both values contain uncertainties, the resultant model scale is approximate. However, it is believed that the horizontal position of points within a stereoscopic model (vertical photography taken with the 80-mm lens from 60 n. mi.) can be determined to a standard error of about ± 50 meters. For the relative heightening accuracy, the value of $H/B = 3.5$, $H/c = 1.4$, and dx again is 20μ . This gives $m_h = 100$ meters. This is an estimate of the accuracy of relative heights measured over a stereoscopic model of the vertical 80-mm photography taken from 60 n. mi. The datum in this case is local, because little information is available with which to level the stereoscopic models. No estimate was made of the attainable accuracy with the photography taken with the 250-mm lens, since no data reduction has been carried out with that photography. The 100-meter accuracy estimate of the 80-mm vertical photography is not good photogrammetrically. However, in this case, it is caused by a combination of the poor base/height ratio (B/H) of 0.3 and the 20μ plate residuals.

The topographic map (fig. 2-64) was produced from photographs 2057 to 2059 of magazine D, taken with the 80-mm lens. The contour interval is 200 meters. The contours are purely relative. However, they do show that the possible "lava tubes" run up and over crater walls and ridges. This, in itself, is interesting and points out the value of topographic maps that can be produced with the Apollo 8 photography.

PHOTOGRAMMETRY OF APOLLO 8 PHOTOGRAPHY

SHERMAN S. C. WU

Introduction

Apollo 8 mission photography is the first return-film photography of the lunar surface in the U.S. space program. The photography from this first manned lunar orbiting mission has good resolution and does not have the distortions that the previous GRE-film photographs of unmanned Lunar Orbiter photography had. For a preliminary scientific evaluation regarding the photogrammetric applications of photographs from the Apollo 8

mission, an attempt has been made to set up three models in the AP/C analytical plotter at the Center of Astrogeology in Flagstaff, Ariz.

The models selected include three different modes: the vertical case, the convergent case, and the oblique case. All the photography was taken with a Hasselblad camera using Kodak 70-mm film. Two camera focal lengths, 80 mm and 250 mm, were used. The vertical-case photography was selected from magazine D (frames 2081 and 2082), which was taken with the 80-mm lens using Estar thin-base type 3400 Panatomic X aerial film. The convergent-case photography was selected from the C magazine (frames 2703 and 2704), which was also taken with the 80-mm lens using type 3400 film. The oblique photography was selected from the A magazine (frames 2615 and 2616), which was taken with the 250-mm lens using SO-368 color film.

For this evaluation, fourth-generation transparencies were used. No camera calibration data were available at the time of this testing, and there is no established ground control for absolute orientation. One model of the vertical-case photography and one model of the convergent case were set up on the AP/C plotter. Contour maps of these two models have been compiled at a scale of 1:200 000. The model of vertical photography has a contour interval of 200 meters, and the model of convergent photography has a contour interval of 250 meters. Also, a relatively large-scale contour map was made of a special crater in the model of the vertical photography at a scale of 1:50 000 and a contour interval of 100 meters.

Twelve profiles in these two models have also been measured for comparison with similar profiles obtained with an isodensitometer, for study of surface roughness, and for determination of the accuracy of the photogrammetric method by repeated measurements.

The attempt to set up the oblique model was unsuccessful because the relative orientation computation would not converge in the AP/C computer. This phenomenon has several possible causes. First, the actual lens focal length is possibly different from the designed 250-mm lens. Second, the lens may cause large distortions. Third, the photographs were taken when the Apollo 8 spacecraft was not in lunar orbit. This

situation resulted in highly tilted photographs, a small model base, and a large difference in altitude between the two photographs of the model. However, this model could probably be set up on the AP/C plotter if the correct lens focal length and lens distortion values were available.

Most of the photography of the C and D magazines can be used in stereoscopic pairs for establishing photogrammetric models. However, to obtain accurate results, the complete camera calibration data are required. Ground control for the back side of the Moon may be established by the method of aerial triangulation using the vertical stereoscopic strip of magazine D and some parts of the convergent strip of magazine C.

Preliminary Photogrammetric Evaluation

Since the orbital flight height of the Apollo 8 spacecraft was about 110 km, the scale of the photography is about 1:1 375 000 for the 80-mm lens and 1:441 000 for the 250-mm lens. If the camera has a resolution of 50 lines/mm at the center of the photographs, then approximately 30 meters in ground resolution can be obtained with the 80-mm lens and approximately 10 meters with the 250-mm lens. Because the least reading in the AP/C plotter is 1μ , repeated observations in the plotter of a specific image point in the model have produced the unbelievable result of a 6μ or 7μ standard error for both horizontal position pointings and elevation readings, which is equivalent to about 8 meters on the ground. This result was obtained on the type 3400 film by an experienced AP/C plotter operator. Since the oblique model using color photography taken with the 250-mm lens did not set up on the AP/C plotter, the following discussion refers only to the models of vertical and convergent photography taken with the 80-mm lens, which set up easily.

Model of Vertical Photography (Magazine D)

Vertical photographs 2081-D and 2082-D (fig. 2-65) were selected for the first model. This model was selected so that profiles could be measured and a comparison made of the photogrammetric and photoclinometric methods. The photography from the D magazine taken with the 80-mm lens is black and white. The exposure time is 1/250 second with an f -stop of 5.6. The model coverage is on the back side of the Moon located at 10° S,

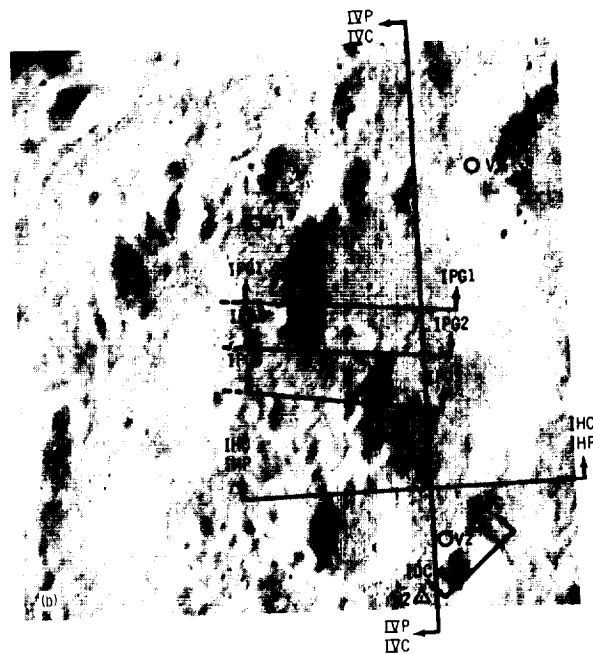
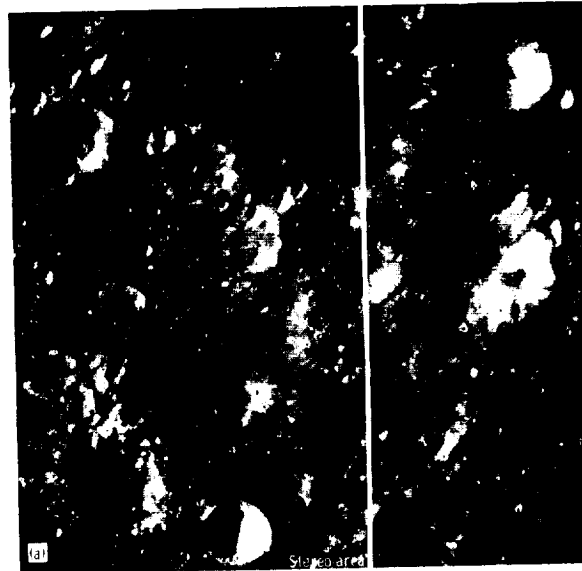


FIGURE 2-65.—Apollo 8 photographs used in model of vertical photography. (a) Apollo 8 frame 2081-D, (b) Apollo 8 frame 2082-D.

175° W. The ground coverage is about 2650 km². The Sun angles were 34° and 35° , respectively, at the time the photographs were taken. The contour map of the entire model is shown in figure 2-66. The model was scaled by measuring the distance

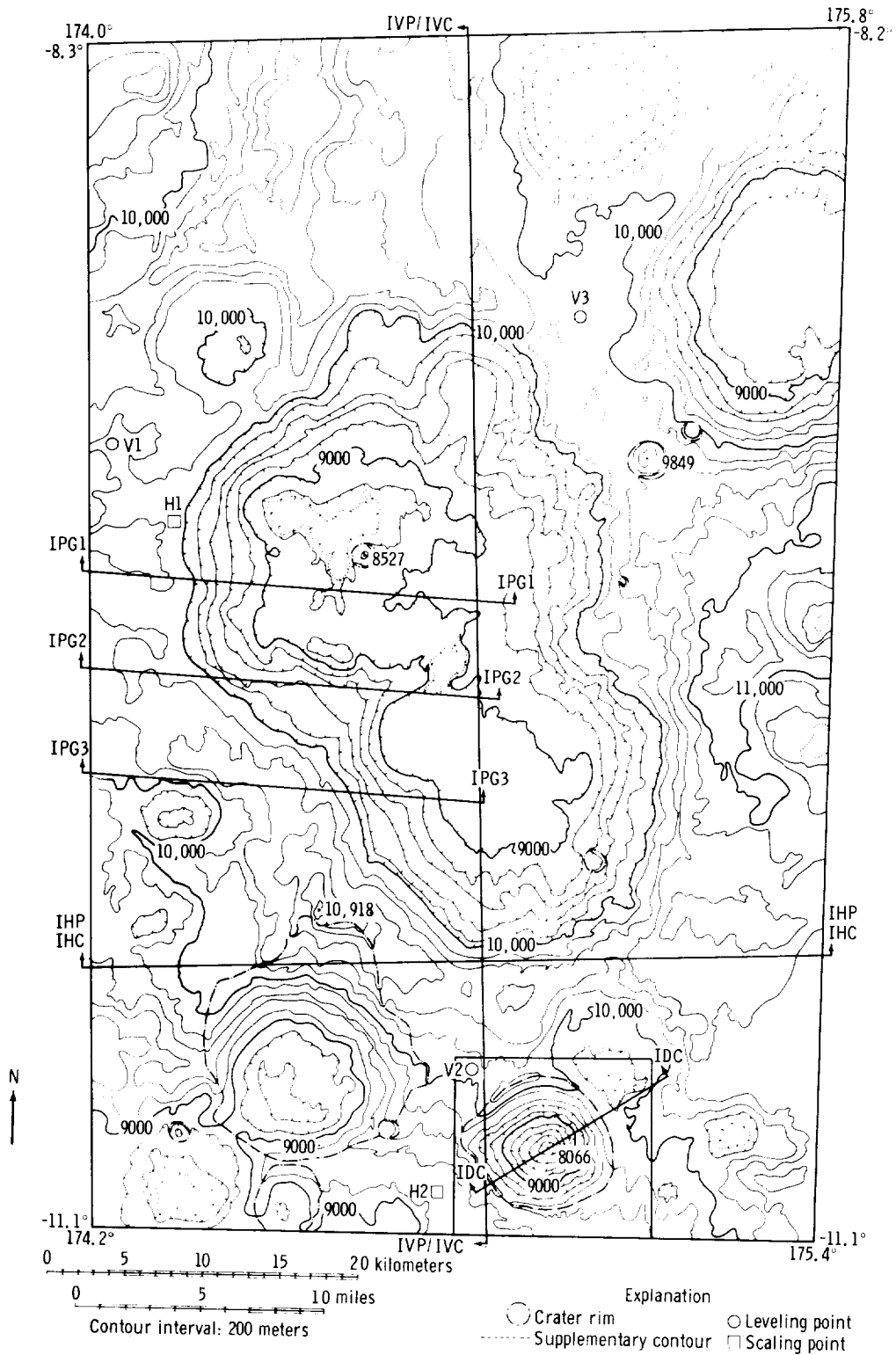


FIGURE 2-66.—Contour map of the entire model of vertical photography.

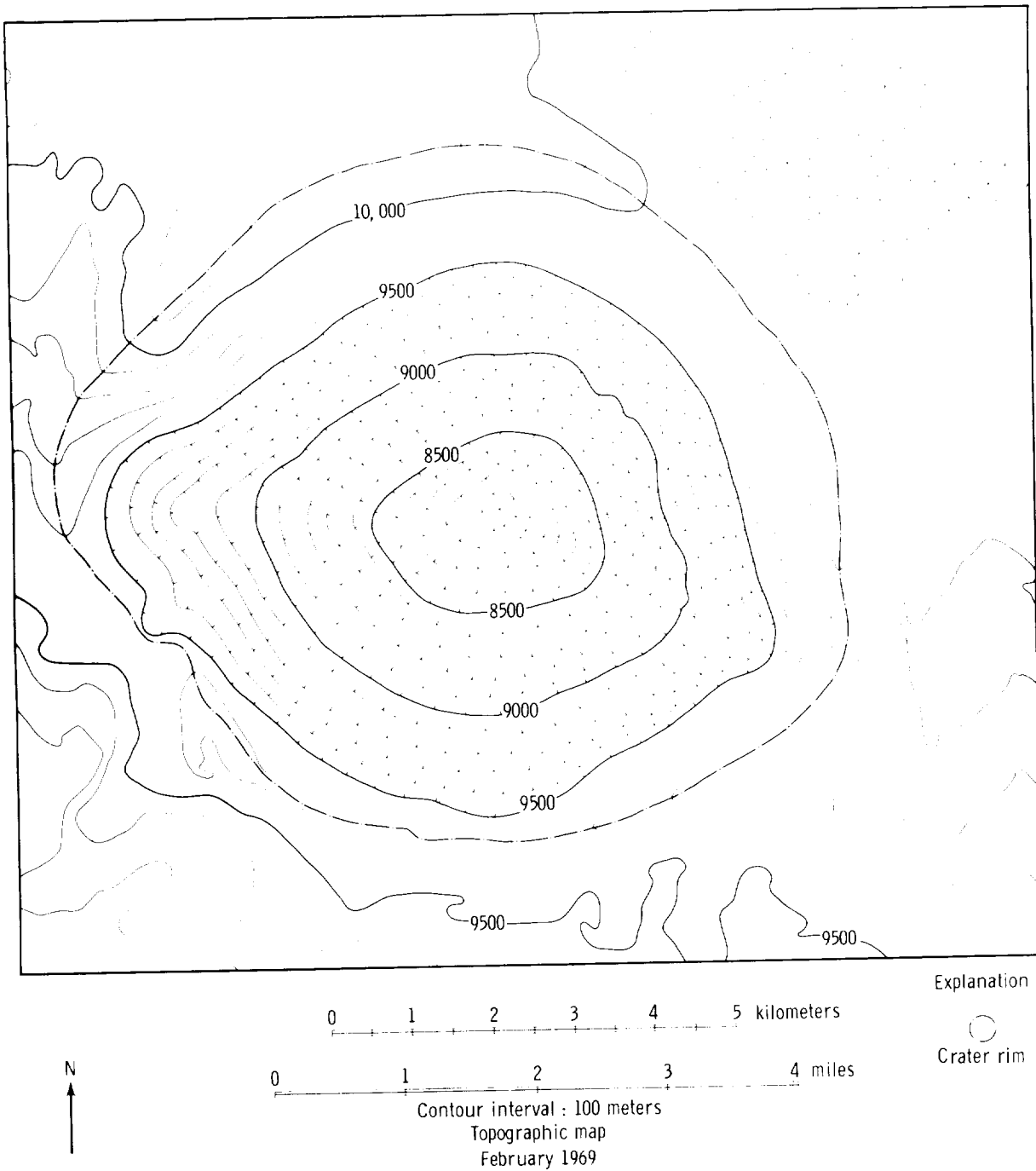


FIGURE 2-67.—Contour map of a special feature in the model of vertical photography.

between similar images identified on Lunar Orbiter II medium-resolution frame 33. Leveling of this model was performed by arbitrarily selecting three points (marked with dots on the map) which

appeared to be at the same elevation. An arbitrary elevation of 10 000 meters was assigned to these three points. The model scale is 1:1 407 789. This scale was magnified 7.0389 times to obtain an

original map scale of 1:200 000. Parameters from the output of the AP/C computer for the relative orientation and the absolute orientation transformation are listed in table 2-X.

Figure 2-67 is a contour map of a small crater compiled at a scale of 1:50 000 (the square area marked off in fig. 2-66) and shows the smallest contour interval that can be compiled. The scale on the full-sized map is a 28.1556 magnification of the model scale. The AP/C operator believes that a 50-meter contour interval could be obtained by using an extremely slow plotting speed and careful attention.

Profiles I-HP and I-HC of figures 2-68(a) and 2-68(b), respectively, were measured from the model of vertical photography at the same location, as indicated in figure 2-65(b), but profile I-HP was plotted directly from the AP/C plotter, and profile I-HC was measured point by point and then computed by the IBM 360 computer and plotted on the XYZ plotter. This process provides the geologist with information for performing a statistical analysis of surface roughness. Profiles I-VP and I-VC of figures 2-69(a) and 2-69(b), respectively, were measured in the same purpose as I-HP and I-HC, except that they

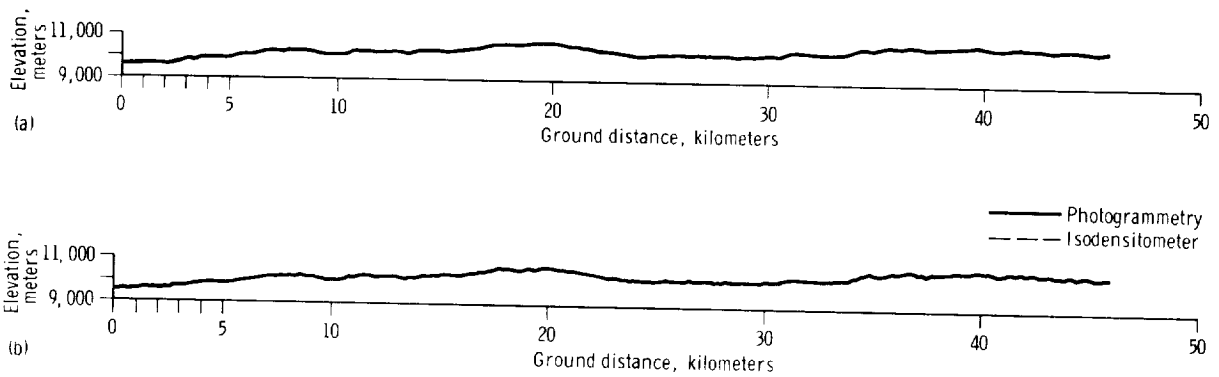


FIGURE 2-68.—Profiles in east-west direction in the model of vertical photography. (a) Profile I-HP, (b) profile I-HC.

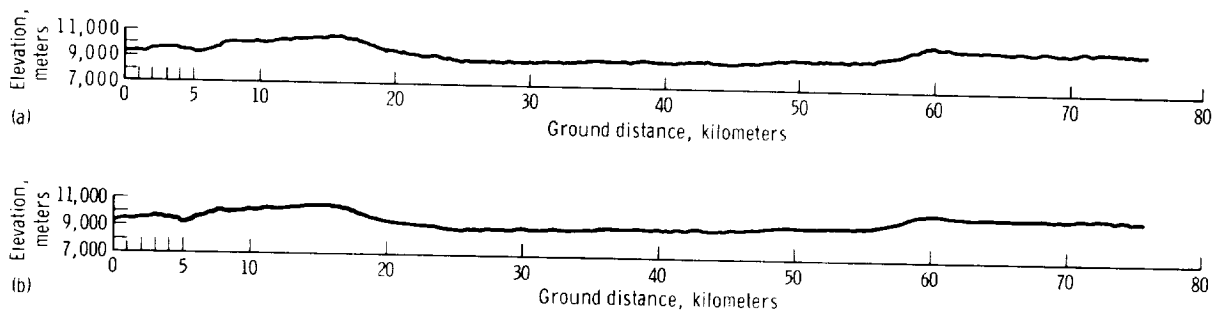


FIGURE 2-69.—Profiles in north-south direction in model of vertical photography. (a) Profile I-VP, (b) profile I-VC.

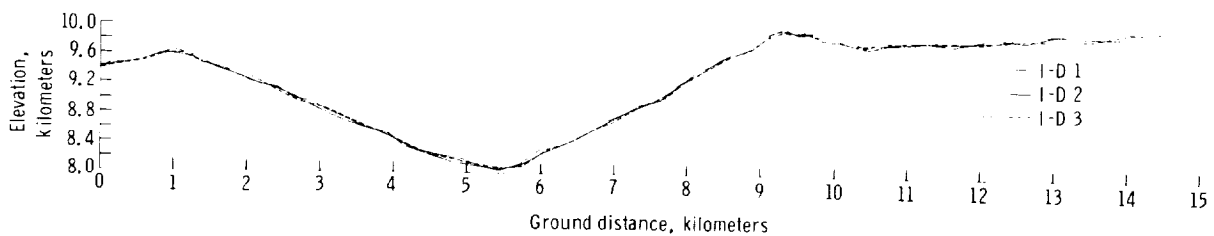


FIGURE 2-70.—Profiles of a crater in the model of vertical photography.

were measured in a south-north direction as indicated in figure 2-65(b).

Profiles I-D 1, I-D 2, and I-D 3, as shown in figure 2-70, were measured point by point and computed by the IBM 360 computer, then plotted on the XYZ plotter. These three profiles are exactly at the same location and were measured three times. These measurements, therefore, provide not only information for crater slope studies but also show the error of plotting in the model.

Model of Convergent Photography (Magazine C)

Photographs 2703 and 2704 from magazine C,

as shown in figure 2-71, were selected for the second model. This particular model was selected for evaluating the Apollo 8 convergent photography for photogrammetric processing. These are also black-and-white photographs taken with the 80-mm lens. This model covers the entire crater 302 at 11° S, 162° W. The scale of this model was also obtained from measurements made on Lunar Orbiter II medium-resolution frame 33. The Sun angles were 41° and 42°, respectively.

A contour map of this model, as shown in figure 2-72, was compiled using the same procedure for leveling as in the first model. The original map

TABLE 2-X.—Parameters of Orientations of the Model of Vertical Photography

Parameters	Relative orientation		Absolute orientation	
	Frame 2082	Frame 2081	Frame 2082	Frame 2081
Focal length, mm.....	80.000	80.000	80.000	80.000
B_x , mm.....	.000	25.725	-10.277	15.567
B_y , mm.....	.000	.348	-3.197	-2.876
B_z , mm.....	80.000	77.416	79.273	80.030
κ , deg.....	.0000	1.6750	.0181	1.6448
ω , deg.....	.0000	-.1714	2.3071	1.9232
ϕ , deg.....	.0000	2.8327	-7.3675	-4.6008

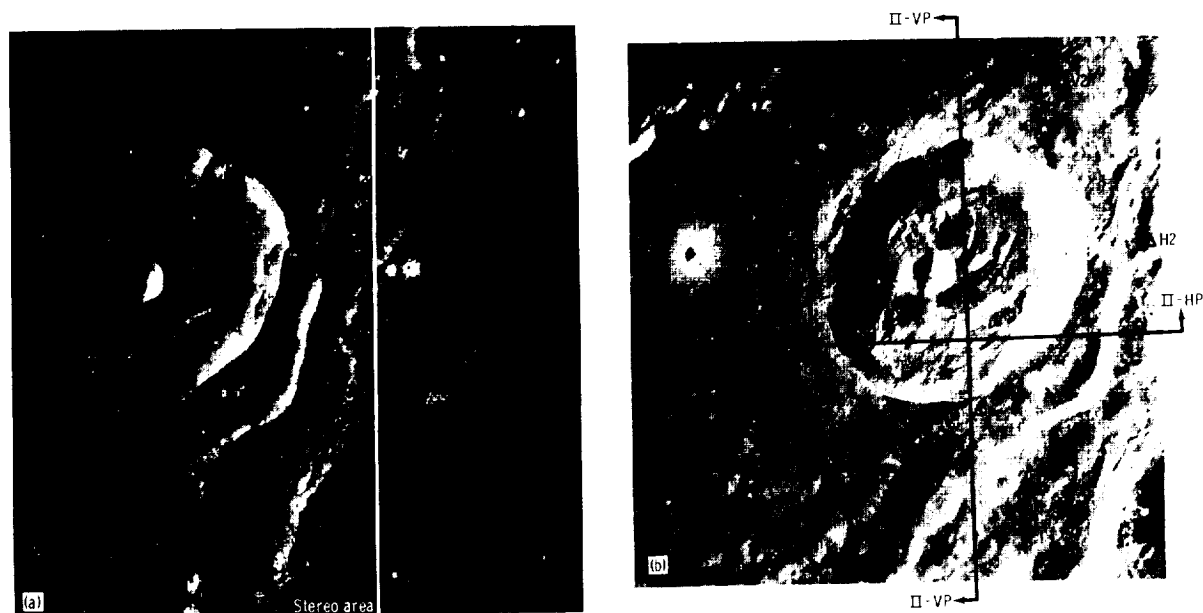


FIGURE 2-71.—Apollo 8 photographs used in model of convergent photography. (a) Apollo 8 frame 2703, (b) Apollo 8 frame 2704.

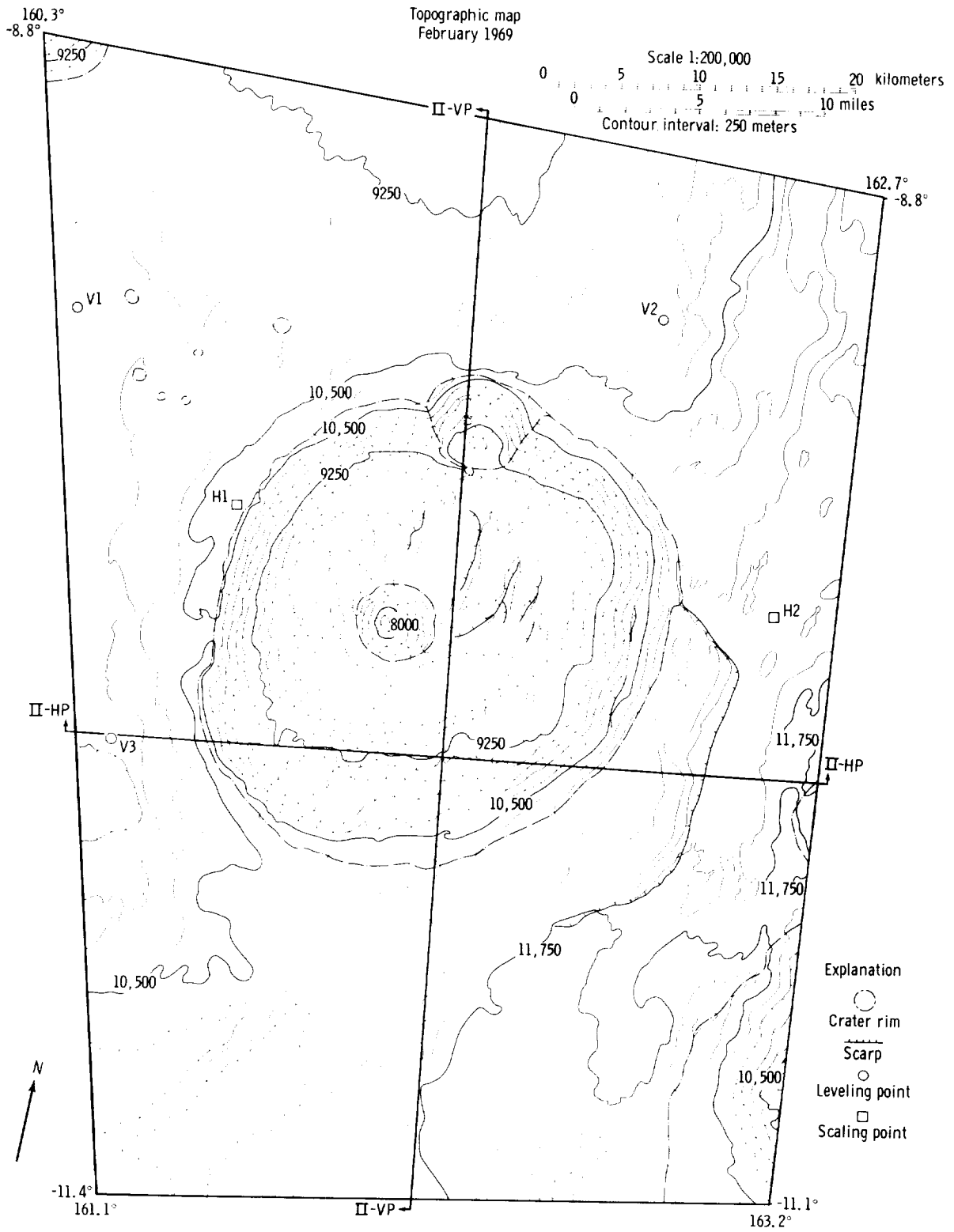


FIGURE 2-72.—Contour map of the model of convergent photography.

TABLE 2-XI.—Parameters of Orientations of the Model of Convergent Photography

Parameters	Relative orientation		Absolute orientation	
	Frame 2704	Frame 2703	Frame 2704	Frame 2703
Focal length, mm.....	80.000	80.000	80.000	80.000
B_x , mm.....	.000	18.079	3.831	21.978
B_y , mm.....	.000	.569	-5.506	-6.051
B_z , mm.....	80.000	79.793	79.719	78.608
κ , deg.....	.0000	1.8933	-.4543	1.4538
ω , deg.....	6.0000	5.7600	9.9119	9.7613
ϕ , deg.....	10.0000	13.5742	12.7690	16.2156

scale is 1:200 000, and the contour interval is 250 meters, larger than the first model. This may show the difference between vertical and convergent photography. The scale of the full-sized map is a 8.4480 magnification of the 1:1 689 600 model scale.

Parameters from the output of the AP/C computer after relative orientation and the absolute orientation transformation of this model are listed in table 2-XI.

Profiles II-HP and II-VP of figure 2-73 were plotted directly from the AP/C plotter in the east-west and south-north directions, respectively, as indicated in figure 2-71(b). No attempt was made to measure profiles analytically for surface

roughness studies or to test the repeatability of this model.

Comparison Between Photogrammetric and Photoclinometric Profiles

Profiles I-PG 1, I-PG 2, and I-PG 3, as shown in figure 2-74, were measured point by point from the model of vertical photography for comparison with profiles IDT-1, IDT-8, and IDT-15 measured with the microdensitometer. Since the profiles obtained from the microdensitometer measurements are not entirely covered in the stereoscopic model, a short distance on each profile could not be measured on the AP/C plotter, but the scales of both methods were checked very closely. Be-

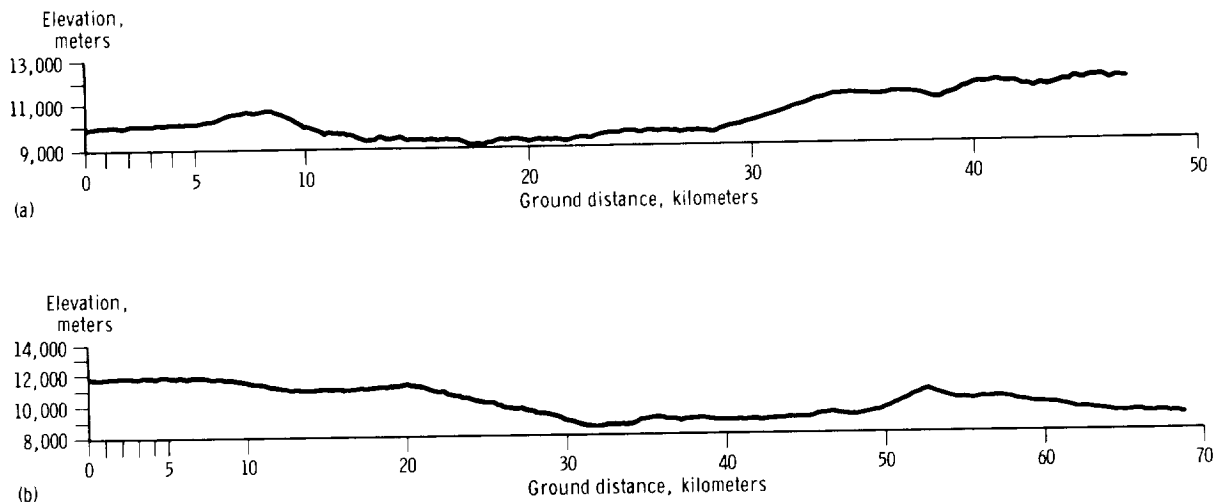
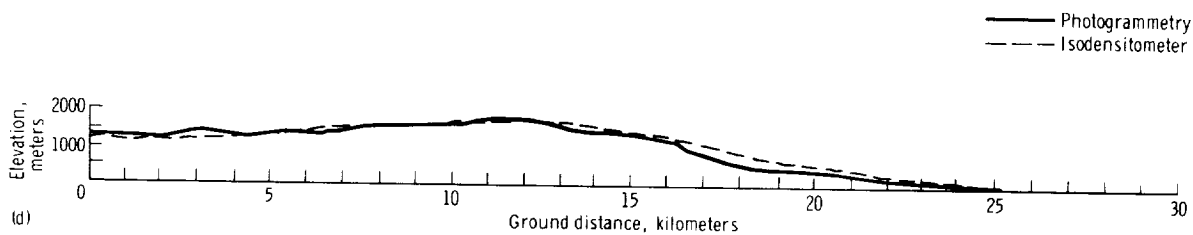
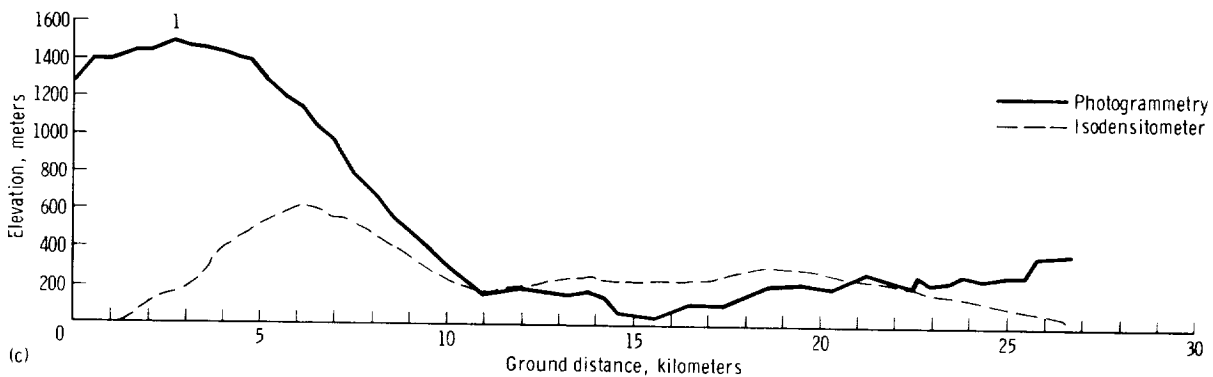
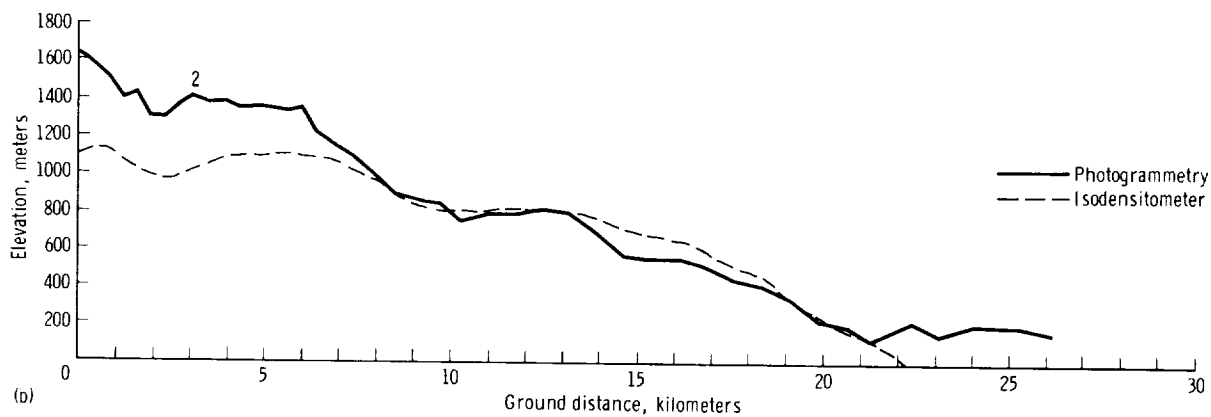
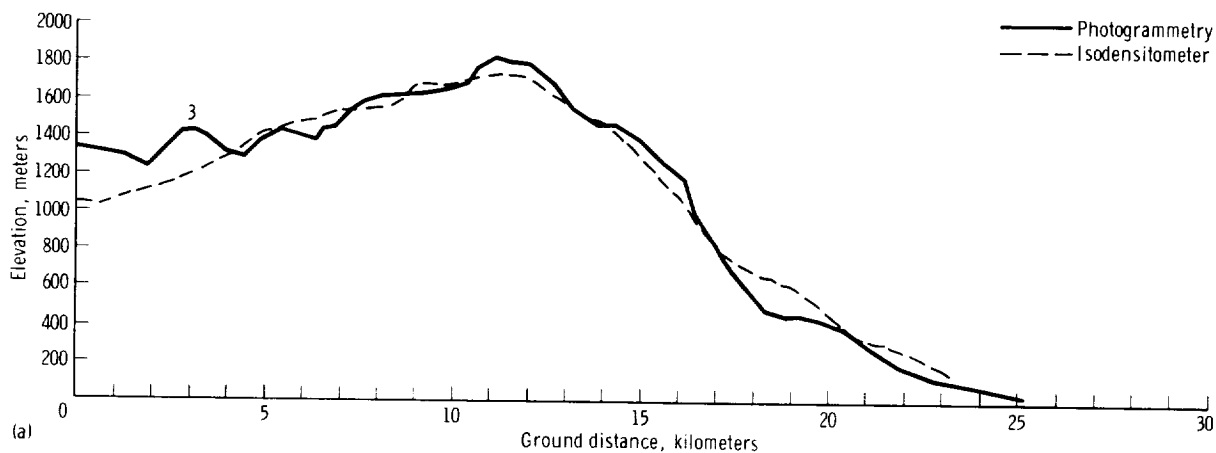


FIGURE 2-73.—Profiles in east-west and south-north directions in model of convergent photography. (a) Profile II-HP, (b) Profile II-VP.



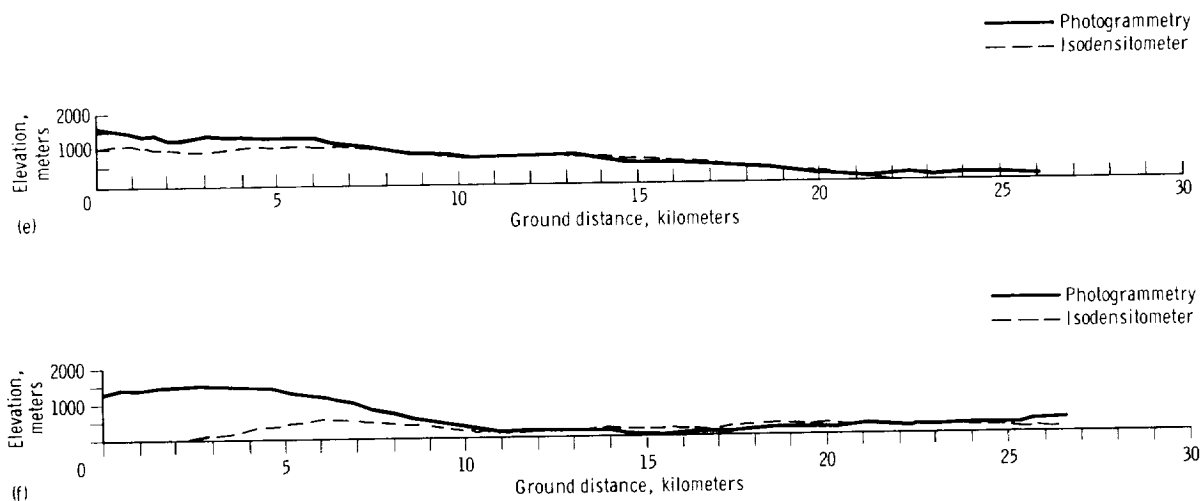


FIGURE 2-74.—Comparison between photogrammetric and photoclinometric methods. (a) Profile I-PG 1, (b) Profile I-PG 2, (c) Profile I-PG 3, (d) Profile I-PG 1 with reduced vertical scale, (e) Profile I-PG 2 with reduced vertical scale, (f) Profile I-PG 3 with reduced vertical scale.

cause of the lack of ground-control points, leveling procedures are arbitrary in both methods; therefore, slope comparison between each pair of profiles can only be made by rotating one to make the best fit with the other. Photogrammetric profile I-PG 3 compares well with IDT-15. Profiles I-PG 2 and IDT-8 are still somewhat similar. The most difference occurs between profiles I-PG 1 and IDT-1, especially at the east side (left).

Discussion

Camera Calibration

The sums of the squares of the residuals for the relative orientation of the two models from magazines D and C, taken with the 80-mm lens, are $0\mu^2$ and $21\mu^2$, respectively, as determined by the AP/C computer. In both cases, parallax measurements were made on 12 evenly distributed points over each model. However, for the oblique model of magazine A taken with the 250-mm lens, convergences for the relative orientation could not be obtained, even though parallax measurements were made only on six points. Camera calibration data for only the 80-mm lens were received after all the measurements were made. The calibrated focal length (CFL) is 79.95 mm, which is close to 80 mm. No indication is shown in the calibration data for the location of the principal point.

This may mean that the CFL of the 250-mm lens may differ very greatly from its designed value. The location of the principal point of the 250-mm lens may be farther away from the center of the photograph than for the 80-mm lens. Lens distortions of the 250-mm lens may be much more significant than the lens distortions of the 80-mm lens. These answers can only be obtained from a careful camera calibration using the standard photogrammetric calibration.

Two saw teeth appear at the lower edge of each photograph from the Apollo 8 mission. These two saw teeth may be used as references for the location of the photograph principal point and also for film shrinkage correction in both the X and the Y directions.

Establishment of Control Points

Because most overlapping pairs of photographs of magazine D and part of magazine C have good exposures for mapping purposes or for geological interpretation, a system of control points by photogrammetric methods can be established. This system of control points, which would be of great value in future mapping for geological purposes, can be accomplished by strip aerial triangulation using pure analytical methods or by instrumental triangulation, especially with the AP/C plotter.

*Absolute Orientation of a Model of Vertical
Photography With the Tracking Data
(Speed and Time Interval)*

If an assumption may be made that flight altitudes between each pair of adjacent camera stations in the orbit are approximately the same, then a model in the AP/C plotter can be leveled by iterations of absolute orientation until the same b_z is arrived at from both photographs and the x tilts W1 and W2 approach zero. During the iterations, scaling can be established simultaneously by comparing the base in the model and the base in space, which can be computed from the speed and time interval or from H and B/H.

**SIMULATION OF LUNAR MODULE
PHOTOGRAPHY AND LUNAR
MODULE LANDING CONDITIONS**

D. D. LLOYD

EXPERIMENT OPERATION

On revolution 3, a set of 39 photographs (frames 2271 to 2309) were taken out the right-hand rendezvous window using a bracket-mounted Hasselblad camera and the 250-mm lens. (These were the only 250-mm lens black-and-white photographs taken with a bracket-mounted camera.) The lunar module pilot (LMP) activated many of these photographs individually (fig. 2-75 and table 2-XII).

The f -stop was left unchanged at the maximum aperture of $f/5.6$. The initial 29 photographs (2271 to 2299) were taken at a shutter speed of 1/250 second. The final 10 photographs (2300 to 2309) were taken at a shutter speed of 1/60 second. The film used was black-and-white Panatomic X, SO-3400, magazine E. (These 10 photographs were the only SO-3400 film photographs taken at 1/60 second. All others were taken at 1/250 second.)

This sequence of photographs was taken at the same time that a landmark training sequence (maneuver and operation) was performed. The commander (CDR) was viewing the lunar surface north of landing site 1 through the left-hand rendezvous window. He viewed an area near Maskelyne F, and, in particular, a lunar feature at approximately 5° N, 34° E, consisting of a

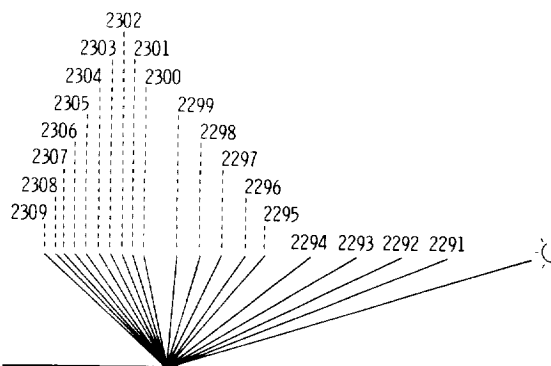


FIGURE 2-75.—Piggyback IMC experiment in maria with low Sun angle.

TABLE 2-XII.—*Approximate Time Intervals
of Photographs*

[Based on measurements of the photographs]

Frame	Time intervals, sec
2291	20
2292	20
2293	20
2294	10
2295	10
2296	10
2297	10
2298	10
2299 ^a	^b 27
2300	10
2301	10
2302	10
2303	10
2304	10
2305	25
2306	20
2307	20
2308	20
2309	20

^a Smallest scale factor.

^b Additional time required to change shutter exposure (1/250 to 1/60 sec).

peak or crater edge which is part of a crater pair. He viewed the lunar feature through the crew optical alinement sight (COAS), which is rigidly mounted to the spacecraft with its optical axis alined along the X -axis. To enable the CDR to view the lunar feature through the COAS, the

spacecraft was oriented with the optical axis of the COAS pointed roughly at the lunar feature. During the training sequence, the spacecraft traveled a considerable distance, creating a change in viewing direction of greater than 45°. Reorientation of the COAS required a rotation (roll) of the spacecraft. The CDR achieved this reorientation and roll by firing the spacecraft attitude control system, using the feedback loop of monitoring the lunar feature visually and adjusting the spacecraft orientation roll to suit his viewing convenience.

If, at the time each photograph was taken, the spacecraft were rolling at exactly the rate required to compensate for spacecraft travel relative to a viewed lunar feature, then the lunar feature would stay at a fixed position in the COAS and the picture taken by the camera would have zero image-motion smear. If, for example, the roll rate were 60 percent of the rate required to keep the same viewing of the lunar feature, then the smear would be reduced by 60 percent, leaving 0.4 uncompensated. (If a roll rate of 120 percent were achieved, then 0.2 of the smear would be uncompensated.)

If some of the 10 photographs taken at 1/60 second showed that a degree of compensation had been achieved, the possibility of high-resolution photography would be demonstrated.

Frames 2271, 2272, and 2273, taken at 1/250 second, were of separate interest. These photographs show maria near landing site 1 at Sun elevation angles similar to conditions that may occur at LM descent.

Photographs 2339 to 2343 of magazine E are of related interest. In particular, photograph 2341 shows an area of Mare Fecunditatis taken with a Sun elevation angle of approximately 17° and a look angle of approximately 26°. The camera was oriented so that zero phase occurred near the center of the photograph. The 80-mm lens was hand held with a shutter speed at 1/250 second and an *f*-stop of 5.6.

These photographs show lighting conditions similar to that which could be experienced during LM descent under one set of critical conditions. Albedo variations show up quite clearly near zero phase, and these variations explain much of the detail and definition observed by the astronauts in viewing the lunar surface compared to their

observations in constant albedo simulators. A second cause of definition would be shadow lining of features.

During a separate pitchup sequence on revolution 8, a series of photographs (2818 to 2821, magazine C) was taken under similar conditions, but with the 80-mm lens. The four photographs include an area close to zero phase and at Sun elevation angles similar to conditions that will occur at LM descent. (The portion of the photographs near zero phase is in Mare Tranquillitatis.)

Because the lens used was the 80-mm rather than the 250-mm lens used on the earlier set, the extent of the lunar surface covered per degree of lens field of view was larger and the resolution and detail correspondingly less.

HARDWARE AND IMAGE MOTION COMPENSATION CONSIDERATIONS

Hardware Limitations of Light-Collecting Capability

Because of limitations on weight and volume, there is a restriction on lens diameter and, thus, on lens light-collecting capability. The 250-mm lens carried on Apollo 8 had an aperture of *f*/5.6. The largest standard Zeiss lens available commercially (500 mm) has a lens diameter corresponding to *f*/8. To achieve *f*/5.6 with a 500-mm lens of reasonable optical quality would require a lens weighing approximately 10 pounds (the weight of the Lunar Orbiter lens). An aperture of *f*/5.6 is, therefore, a reasonable limit for long-focal-length, high-resolution lenses for early Apollo missions. Because light-power collection per unit area of film is proportional to the square of the *f*-stop, there is a limit on lens light-power collecting capability per unit area of film. This limitation generates a need for long exposure time in order to collect sufficient light energy per unit area of film crystals, which, in turn, generates a need for image motion compensation (IMC) for photography of regions of the Moon that are within 20° of the terminator.

Derivation of IMC: Requirements

On regions of the Moon where the Sun is below 20° elevation, there is a shortage of light for all high-resolution films at *f*/5.6 unless the shutter is held open for approximately 1/125 second. While the shutter is open for 1/125 second, the

spacecraft moves about 13 meters, producing a smear of approximately 13 meters if uncompensated. Without this smear (that is, with compensation) a resolution of approximately 2.7 meters with a 500-mm lens, or approximately 5.4 meters with a 250-mm lens, could be obtained.

A 100-mm lens would provide a basic resolution of approximately 13.2 meters. A combination of 13-meter smear (corresponding to 1/125 second) with 13.2-meter resolution provides significant image degradation of resolution and is near the upper limit of acceptable smear. (A smear equal to 40 percent of the basic resolution is more acceptable as a goal.) For 100- or 80-mm lenses, a shutter speed of 1/250 second or less should be used for all exposures until the combination of 1/250 second and maximum aperture requires more light. (A shutter speed of 1/250 second was selected for all regular photography during the Apollo 8 mission.)

When the 250-mm lens is used uncompensated for IMC, a shutter speed of 1/250 second produces an undesirable smear of 6.6 meters imposed upon the basic resolution of 5.4 meters for vertical photography; however, for nonvertical photographs at a range of 200 km, the basic resolution is approximately 10.8 meters, and the smear of 6.6 meters can be considered acceptable for most lighting conditions. (However, 1/250 second provides insufficient light when the angle of Sun elevation is less than 20°.)

Image motion compensation to reduce the 13 meters (produced with 1/125-second exposure) to 1.3 meters, 10-percent residual, is within the state of the art of IMC cameras. Better than 1-percent residual was achieved with the Lunar Orbiters. Image motion compensation based on spacecraft velocity and relative altitude derived from tracking data can do better than the required 10 percent residual, if the camera has a mechanism for moving the film to achieve compensation. Such a camera is desirable. Without compensation in the camera, the camera must be bracket mounted to the spacecraft and the spacecraft must be rolled to provide IMC. (This technique has limitations when an attempt is made to achieve a strip of photography.) The spacecraft is oriented toward the target of interest during the roll.

Two factors might generate uncertainties in spacecraft roll, which, in turn, might cause the

compensation to be less accurate than the 10 percent required. One of these could arise from uncertainties in the capability of the spacecraft to respond to the specified commands. (The control of the attitude engine thrust levels as it acts against the inertia of the spacecraft.) Fortunately, the uncertainty here is much less than 10 percent. (It is, in fact, less than 1 percent.) The second factor is in the uncertainties introduced by inaccurate geometric instructions to the spacecraft attitude control system.

The LM photography simulation/IMC experiment, performed as a piggyback operation added to the training sequence performed on revolution 3 of Apollo 8, was intended to provide an initial evaluation of any problems involved in achieving the desired spacecraft roll rate.

TECHNIQUES FOR PROVIDING THE REQUIRED GEOMETRIC INSTRUCTIONS

There are several possible techniques for providing the required geometric instructions to the spacecraft control system. The preferred method would be to obtain the instructions directly from a prestored computer software program. The necessary computer program is, however, not yet available.

Two alternative methods involve astronaut participation. In the first method, the astronaut substitutes for the desired computer software program. He inputs to the control geometric instructions based on printed instructions provided him preflight. In the second method, the astronaut watches the point of photographic interest with his eyes and fires the reaction control system to minimize relative rate. This sighting can be through a reflex camera or through a separate optical sighting instrument which looks down the same axis as the camera; for example, the COAS can be used to aim a rendezvous-window-mounted camera.

The LM photography simulation/IMC experiment performed on lunar revolution 3 of Apollo 8 used a downgraded modification of the second method. The method was downgraded in that the maneuver was not performed for the specific purpose of obtaining photographs and, naturally, it could not be optimized for the photographic purpose. The photographic experiment rode piggy-

back on a maneuver performed to optimize the viewing convenience of the astronaut. The significant part of the IMC experiment (that carried out with the shutter speed of 1/60 second) was, in fact, not started until the spacecraft was vertically over the target (table 2-XII). One effect of this delay was to cause glare on the film. A second effect was to cause low exposure, since the phase angle was never below 86°. A third effect is that the phase of correction of the roll may have been partially or fully missed.

MEASUREMENT OF RESIDUAL SMEAR

Method

Certain of the photographs taken to evaluate the piggyback IMC technique were measured by the Cornell Aeronautical Laboratory to determine the estimates of residual smear. The apparatus has a 1 μ slit providing a measurement accuracy of 1000 lines/mm. A model 1140 Mann microdensitometer was used to measure the change in transmittance of the film between shadows and the adjacent illuminated surface.

In this technique, the shadow edge is scanned in the direction of spacecraft travel, and the rate of change of transmittance with distance is used as a measure of modulation transfer factor (MTF) and, thus, resolution. The change of intensity is adjusted for the effect of Sun penumbra lighting.

Measurement Data Obtained

The previously mentioned method of estimating residual smear, using fourth-generation positive transparencies, obtained the following measurement data.

The resolution of the preexposure bar chart was 46 lines/mm. This chart, recorded preflight on the film by an 80-mm lens, was for comparison purposes to show basic unsmearred resolution.

Five measurements were taken on frame 2304 (26, 20, 19, 30, and 34 lines/mm). The average resolution was 26 lines/mm.

Uncompensated photography would have produced a film smear of 15 lines/mm at a vertical range of 102 km computed as follows:

$$\frac{1}{60} \times 1.6 \text{ km} \left(\frac{250 \text{ mm}}{102 \text{ km}} \right) = 66 \text{ m}\mu \quad \text{or } 15 \text{ lines/mm}$$

The value would be less at greater ranges.

Results

The piggyback IMC technique produced partial compensation and improved the resolution obtained in photograph 2304.

The data obtained from this experiment confirm that any reasonable operation of a technique for providing IMC will enable high-resolution photography to be obtained of the landed LM, the shape of its shadow, and the surrounding lunar surface.

SUMMARY

The Apollo 8 mission provided much new information which both supplements and complements the Lunar Orbiter material. In particular, the high-illumination photography is of great value.

The following are some of the valuable aspects of the high-illumination photography:

1. Inner walls of craters are seen better than before. (In the majority of Lunar Orbiter photographs, these walls are either overexposed or are in shadow.) Patterns resulting from downslope movement are obvious. Lunar rock layers show up clearly.

2. For the first time, it is possible to correlate brightness (reflectivity) and topography at comparatively high resolution.

3. Before the Apollo 8 mission, it was thought that photogrammetric analysis of lunar photographs would be restricted to photography obtained at Sun elevations lower than 45°. It has now been demonstrated that photogrammetric analysis can be made of photographs obtained even at the zero-phase point.

4. For the first time, ejecta (ray) patterns from small, bright craters are visible in detail. Ballistics of ejection may be determined for otherwise apparently similar craters which show distinctly different ray systems. Many more of these craters were visible than had been anticipated.

5. For the first time, surface brightness at zero-phase angle has been measured.

In addition, the following results were obtained from the photographs:

1. The photography has improved our knowledge of the topographic character of far-side features.

2. Several targets of opportunity yielded significant geologic information.

3. Stereoscopic coverage, permitting photo-

grammetry and excellent visual presentation, is clearly of great value and a unique contribution of the mission. The photogrammetry is by far the best ever obtained of the Moon.

4. Photogrammetry and photoclinometry can be compared in detail, and the prospect of evaluating the two against each other appears promising.

5. Whole-disk photography will be of value to extend selenodetic control over large areas of the east limb and back side of the Moon. Control based on supposed positions and pointing angles of the Lunar Orbiters has been shown to be very difficult to establish.

At the orbital height of Apollo 8, photographs taken with the 80-mm lens are most useful for geologic purposes from approximately 0° to 5° from the groundtrack and have some value out to approximately 10°. Photographs taken with the 250-mm lens are most useful out to approximately 10° and have some value out to approximately 14°. Photographs with the 250-mm lens are also useful when taken vertically if image motion is compensated for. Resolution with the 250-mm lens is about three times better than that with the 80-mm lens, but the field of view is only a ninth as great.

REFERENCES

- 2-1. WHITAKER, E. A.: Evaluation of the Russian Photographs of the Moon's Far Side. Univ. of Arizona, Commun. Lunar and Planetary Lab., vol. 1, no. 13, May 18, 1962, pp. 67-71.
- 2-2. WHITAKER, E. A.: Evaluation of the Soviet Photographs of the Moon's Far Side. The Moon, Meteorites, and Comets. Vol. IV of The Solar System, B. M. Middlehurst and G. P. Kuiper, eds., Univ. Chicago Press, 1963, pp. 123-128.
- 2-3. Commission 16 for the Physical Study of Planets and Satellites: Resolution No. 1. Trans. Astron. Union, vol. 11b, D. H. Sadler, ed., Academic Press, 1962, pp. 234-235.
- 2-4. LIPSKIY, Y. N.: Investigation of the Far Side of the Moon with the Aid of Rockets. The Moon, Meteorites, and Comets. Vol. IV of The Solar System, B. M. Middlehurst and G. P. Kuiper, eds., Univ. Chicago Press, 1963, pp. 90-122.
- 2-5. TRASK, NEWELL J.; AND ROWAN, LAWRENCE C.: Lunar Orbiter Photographs: Some Fundamental Observations. Science, vol. 158, no. 3808, Dec. 22, 1967, pp. 1529-1535.
- 2-6. OBERBECK, VERNE R.; AND QUAIDE, WILLIAM L.: Genetic Implications of Lunar Regolith Thickness Variations. Icarus, vol. 9, no. 3, Nov. 1968, pp. 446-465.
- 2-7. OETKING, PHILLIP: Photometric Studies of Diffusely Reflecting Surfaces With Applications to the Brightness of the Moon. J. Geophys. Res., vol. 71, no. 10, May 15, 1966, pp. 2505-2513.
- 2-8. LARSON, H. K.; AND MATEER, G. G.: Cross-Hatching—A Coupling of Gas Dynamics With the Ablation Process. Paper 68-670, Am. Inst. Aeron. and Astronaut. Fluid and Plasma Dynamics Conf. (Los Angeles, Calif.), June 1968.
- 2-9. SENFTLE, F.: Investigation of Infra-Red Absorption and Low-Angle X-Ray Scattering of Tektites. Semiannual Status Report, NGR 09-11-006, 1967.
- 2-10. GENTNER, W.; LIPPOLT, H. J.; AND SCHAEFFER, O. A.: The Potassium-Argon Age of a Glass Sample From the Nördlinger Ries. Z. Naturforschung, vol. 16a, no. 11, Nov. 1961, p. 1240.
- 2-11. YOUNG, GEORGE A.: The Physics of the Base Surge. U.S. Naval Ordnance Lab., White Oak, Md., NOL-TR 64-103, 1965.
- 2-12. O'KEEFE, JOHN A.: The Origin of Tektites. Space Sci. Rev., vol. 6, no. 2, 1966, pp. 174-221.
- 2-13. DUKE, M. B.: Petrology of the Basaltic Achondrite Meteorites. Ph.D. thesis, Calif. Institute of Technology, 1963.
- 2-14. MOORE, H. J.: Density of Small Craters on the Lunar Surface. Astrogeologic Studies. Part D: Studies for Space Flight Program. Geol. Survey, May 1964, pp. 34-51. (Also available as NASA CR-58623.)
- 2-15. KUIPER, GERARD P.: Volcanic Sublimates on Earth and Moon. Univ. of Arizona Commun. Lunar and Planetary Lab., vol. 3, no. 49, July 1965, pp. 36-60.
- 2-16. SHOEMAKER, E. M.; BATSON, R. M.; HOLT, H. E.; ET AL.: Colorimetric Observations of Lunar Surface. Surveyor III Mission Report, pt. II, sec. III, JPL TR 32-1177, June 1967, pp. 51-54. (Also available as NASA CR-88952.)
- 2-17. WRIGHT, W. H.: The Moon as Photographed by Light of Different Colours. Pub. Astron. Soc. Pacific, vol. 41, no. 241, 1929, pp. 125-132.
- 2-18. HARRIS, DANIEL L.: Photometry and Colorimetry of Planets and Satellites. Planets and Satellites. Vol. III of The Solar System, G. P. Kuiper and B. M. Middlehurst, eds., Univ. Chicago Press, 1961, pp. 272-342.
- 2-19. COFFEEN, DAVID L.: Wavelength Dependence of Polarization. IV: Volcanic Cinders and Particles. Univ. of Arizona, Commun. Lunar and Planetary Lab., vol. 4, no. 69, Dec. 29, 1964, pp. 157-167.
- 2-20. GEHRELS, T.; COFFEEN, T.; AND OWINGS, D.: Wavelength Dependence of Polarization. III. The Lunar

- Surface. *Astron. J.*, vol. 69, no. 10, Dec. 1964, pp. 826-852.
- 2-21. ADAMS, JOHN B.; AND FILICE, ALAN L.: Spectral Reflectance 0.4 to 2.0 Microns of Silicate Rock Powders. *J. Geophys. Res.*, vol. 72, no. 22, Nov. 15, 1967, pp. 5705-5715.
- 2-22. SALISBURY, JOHN W.; AND HUNT, GRAHAM R.: Martian Surface Materials: Effect of Particle Size on Spectral Behavior. *Science*, vol. 161, no. 3839, July 26, 1968, pp. 365-366.
- 2-23. NASH, DOUGLAS B.: Proton-Irradiation Darkening of Rock Powders: Contamination and Temperature Effects, and Applications to Solar-Wind Darkening of the Moon. *J. Geophys. Res.*, vol. 72, no. 12, June 15, 1967, pp. 3089-3104.
- 2-24. HAPKE, BRUCE: Lunar Surface: Composition Inferred From Optical Properties. *Science*, vol. 159, no. 3810, Jan. 5, 1968, pp. 76-79.
- 2-25. McCORD, T. B.: Color Differences on the Lunar Surface. Doctoral thesis, Calif. Institute of Technology, 1968, pp. 1-181.
- 2-26. WHITAKER, E. A.; AND KUIPER, G. P.: Interpretation of Ranger VII Records. Ranger VII, part II: Experimenters' Analyses and Interpretations. JPL TR 32-700, 1965, pp. 149-154. (Also available as NASA CR-62347.)
- 2-27. NATHAN, ROBERT: Digital Video-Data Handling. JPL TR 32-877, 1966. (Also available as NASA CR-71399.)
- 2-28. SELZER, R. H.: Digital Computer Processing of X-Ray Photographs. JPL TR 32-1028, 1966. (Also available as NASA CR-80521.)
- 2-29. MINNAERT, M. G. J. (H. M. KREMER-PRIEST, trans.; K. E. BRIAN JAY, revision): *The Nature of Light and Colour in the Open Air*. Dover Publications, Inc. (New York), c. 1954, pp. 230-234.
- 2-30. WHIPPLE, FRED L.: A Radio Telescope and the Heiligenschein. *Sky and Telescope*, vol. 37, no. 2, Feb. 1969, p. 85.
- 2-31. BARABASHOV, N. P.: The Albedo and Color of the Lunar Surface. *The Moon. A Russian View*. A. V. Markov, ed., Univ. of Chicago Press, c. 1962, pp. 123-156.
- 2-32. GEHRELS, T.: Photometric Studies of Asteroids. V. The Light-Curve and Phase Function of 20 Massalia. *Astrophys. J.*, vol. 123, no. 2, Mar. 1956, pp. 331-338.
- 2-33. GEHRELS, T.: Photometric Studies of Asteroids. VI. Photographic Magnitudes. *Astrophys. J.*, vol. 125, no. 2, Mar. 1957, pp. 550-570.
- 2-34. SYTINSKAYA, N. N.: Work Done by the Leningrad State University Astronomical Observatory on the Physiological Properties of the Eye. *Akademiia Nauk, SSSR, Izvestiia, Ser. Geogr. i Geofiz.*, vol. 6, no. 3, 1952, pp. 116-120.
- 2-35. FEDORETS, V. A.: Photographic Photometry of the Lunar Surface. *Uch. Zap. Kharkov Univ.*, vol. 42, 1952, p. 49.
- 2-36. STEINBACHER, R. H.; GUNTER, R. L.; SPENCER, R. L.; ET AL.: Surveyor I Mission Report. Part III: Television Data. JPL TR 32-1023, Nov. 1966. (Also available as NASA CR-81520.)
- 2-37. VAN DIGGELEN, J.: Photometric Properties of Lunar Crater Floors. NASA TT F-209, 1964.
- 2-38. HAPKE, BRUCE: A Theoretical Photometric Function for the Lunar Surface. *J. Geophys. Res.*, vol. 68, no. 15, Aug. 1, 1963, pp. 4571-4586.
- 2-39. WILLINGHAM, D.: The Lunar Reflectivity Model for Ranger Block III Analysis. NASA CR-59564, 1964.
- 2-40. LOWRY, E. M.: The Luminance Discrimination of the Human Eye. *J. Soc. Motion Pic. and Telev. Engrs.*, vol. 57, no. 3, Sept. 1951, pp. 187-196.
- 2-41. STEVENS, J. C.; AND STEVENS, S. S.: Brightness Function: Effects of Adaptation. *J. Optical Soc. Am.*, vol. 53, no. 3, Mar. 1963, pp. 375-385.
- 2-42. IRELAND, FRED H.; KINSLOW, WILLIAM; LEVIN, EDWIN; AND PAGE, DONALD: Experimental Study of the Effects of Surround Brightness and Size on Visual Performance. Final Report, Mar. 1966-Mar. 1967. (AMRL TR-67-102, CFSTI No. AD 666045), RCA for AMRL, Wright-Patterson AFB, Ohio, Sept. 1967.
- 2-43. LAMBIOTTE, J. J.; AND TAYLOR, G. R.: A Photometric Technique for Deriving Slopes From Lunar Orbiter Photography. Vol. 17, Use of Space Systems for Planetary Geology and Geophysics, Robert D. Enzmann, ed., AAS Science and Technology Series (Proceedings of symposium held in Boston, Mass., May 25-27, 1967), c. 1968, pp. 205-224.
- 2-44. ANON.: Lunar Orbiter II: Post Mission Photo Supporting Data. NASA CR-66478, Sept. 1967.
- 2-45. ANON.: Lunar Equatorial Zone Mosaic (LEZ) [Scale 1:2,500,000]. Army Map Service, 1968.
- 2-46. ANON.: Apollo Lunar Orbit Chart (ALO), Apollo Mission 8 [Scale 1:11,000,000]. Aeronautical Chart and Information Center, USAF, 1st ed., 1968.
- 2-47. ANON.: Apollo Lunar Orbital Map (LOM) [Scale 1:7,500,000]. Aeronautical Chart and Information Center, USAF, 1st ed., 1968.
- 2-48. ANON.: Lunar Farside Chart (LFC-1) [Scale 1:5,000,000]. Aeronautical Chart and Information Center, USAF, 2d ed., 1967.
- 2-49. MICHAEL, WILLIAM H., JR.: Physical Properties of the Moon as Determined From Lunar Orbiter Data. Presented at 14th General Assembly Int. Union Geodesy and Geophys. (Lucerne, Switzerland), Oct. 1967.
- 2-50. SJOGBREN, WILLIAM L.; TRASK, DONALD W.; VEGOS, CHARLES J.; AND WOLLENHAUPT, WILBUR R.: Physical Constants as Determined From Radio Tracking of the Ranger Lunar Probes. Vol. 11, Space Flight Mechanics Specialist Symposium, 1966, Maurice L. Anthony, ed., AAS Science and Technology Series, c. 1967, pp. 137-154.
- 2-51. BRAY, T. A.; AND GOUDAS, C. L.: A Contour Map Based on the Selenodetic Control System of A.C.I.C. Icarus, vol. 5, no. 5, Sept. 1966, pp. 526-535.



3

Astronomical and Earth Observations

ASTRONOMICAL OBSERVATIONS

L. DUNKELMAN AND ROBERT O. HILL

A demonstration of the visibility of lunar features in shadow regions is discussed in chapter 1. The ability to observe under high-contrast and also under very low light-level conditions during the lunar orbit portion of the flight requires further study. The photographic astronomical findings have already been discussed in chapter 2. In addition, the following visual observation is worthy of note.

During the Apollo 8 mission, the command module pilot (CMP) observed what is generally thought to be the zodiacal light and solar corona through the command module telescope just prior to sunrise on one of the early revolutions. The lunar module pilot (LMP) observed what he described as a cloud or bright area in the sky during lunar darkness on two successive revolutions. He sketched this area in his log and verbally described it during the photographic debriefing after the mission. Based on correlations of the spacecraft attitude and the LMP's position in the spacecraft, it appears that the LMP was looking at an area near the south celestial pole. His star sketch was roughly correlated with a star field. The identification of the observed area, if correct, indicates that the LMP observed one of the Magellanic clouds.

ASTRONOMICAL MOONWATCH DURING APOLLO 8

WILLIAM B. CHAPMAN

More than 30 professional observatories and 70 private observatories have been organized into

an international network of lunar observers by Barbara M. Middlehurst of the Lunar and Planetary Laboratory, University of Arizona. A system for reporting lunar transient events to observers and to the Science Support Room of the Science and Applications Directorate, NASA Manned Spacecraft Center, was organized through Robert Citron, Smithsonian Center for Short-Lived Phenomena, Cambridge, Mass. This communication system was employed when the Moon was under intense surveillance during the Apollo 8 mission. At this time, the early lunar phase mainly limited observation of events to those which occurred at favorable locations and which were in sunlight. Thus, astronomical observations of events were to some extent limited to those that might occur at Mare Crisium (selenographic coordinates latitude 18° N, longitude 55° E) and at Messier (2° S, 46° E).

However, on the unilluminated side of the Moon, observations of anomalous brightening near Aristarchus (23° N, 47° E) were reported during the Apollo 8 mission. Such phenomena were reported for December 21 and 22, 1968, by the Observatorio Nacional, Rio de Janeiro, Brazil. Similar phenomena near Aristarchus and also at Grimaldi (66° S, 67° W) were reported for December 22 to 25 by California members of Argus Astronet.

Because the Apollo 8 crew was watching both Aristarchus and Grimaldi, among other features, for transient events, the reported phenomena were not relayed to Apollo 8. However, Menelaus (17° N, 16° E) and Manilius (14° N, 9° E), which the crew was not particularly watching for transient events, were reported to have similar phenomena by Argus Astronet members. An observer

TABLE 3-I.—*Communications Report Summary*

Date, Dec. 1968	G.m.t., hr:min	Observer	Location	Report
21.....	21:00	Mourão	Brazil	Brightening in Aristarchus.
22.....	23:00	Mourilhe	Brazil	Light in Aristarchus.
23.....	23:28	Jean	Montreal	White light in Guericke.
23.....	01:30 to 02:00	Wick	South Dakota	Aristarchus pulsating.
23.....	02:00 to 02:30	Kohlenberger	California	Brightening and dimming in Aristarchus.
23.....	02:00 to 02:30	Harris	California	Brightening and dimming in Aristarchus.
23.....	02:40	Harris	California	SE quadrant of Grimaldi brightened.
23.....	01:56	Lehmann	South Dakota	Increase in Aristarchus brightness.
23.....	12:00 to 16:00	Sinvhal	India	Negative.
23.....	14:00 to 16:00	Kodaikanal	India	Negative.
23.....		Hvidovre	Denmark	Negative.
23.....		Kozyrev	U.S.S.R.	Negative.
23.....	03:00 to 03:06	Kohlenberger	California	Aristarchus went starlike.
24.....	03:00 to 06:00	Bunton	Hawaii	Negative.
24.....	03:23	Harris	California	Aristarchus brightening.
25.....	05:00 to 07:00	University of Michigan	Hawaii	Negative.
25.....	22:00	Jean	Montreal	White cone light on both sides of Pickering.

at Montreal, Canada, reported another similar phenomenon at 18° S, 12° W (near Guericke). However, since the reports of phenomena at these three sites were less substantial than those for Aristarchus, none of these reports was relayed to Apollo 8. A summary of observations, compiled by Citron, is given in table 3-I.

Prior to the flight of Apollo 8, the crew had been alerted to observe those sites within range of the spacecraft where lunar transient events had been reported. Sites where events were more common were plotted on the Apollo Target of Opportunity Flight Chart. Although these areas were observed on each revolution where spacecraft attitude and crew activities permitted, no transient events were reported by the Apollo 8 crew.

PRELIMINARY RESULTS OF APOLLO 8 OPTICAL TRACKING EXPERIMENT

HAROLD B. LIEMOHN

INTRODUCTION

Several observatories succeeded in sighting and photographing the Apollo 8 spacecraft during its lunar mission. This preliminary report contains a brief account of the sighting, tentative interpretations, and some conclusions about the program.

PARTICIPANTS

The participating observatories are shown in table 3-II. Astronet members provided amateur radio communications between U.S. observatories. About 25 amateur groups also participated in the observation efforts.

SIGHTINGS

During the translunar trajectory, the command and service module (CSM), the four quadrant panels for the spacecraft lunar-module adapter (SLA), and the Saturn IVB (S-IVB) booster rocket created a spectacular array of flashing objects. No one sighted the CSM in lunar orbit, but the weather was generally bad. On the return transearth trajectory, the brightness of the CSM again varied significantly. A record of the tracking success is shown in table 3-III.

On the first night, December 21, most observatories noted at least two 12th-magnitude objects which flashed to 8th to 10th magnitude occasionally. Both trailed and tracked photographs were made so that brightness and position data would be available as a function of time. Observatoire du Pic-du-Midi sighted the spacecraft briefly through a thin cloud layer at 17:10 G.m.t., and a strange white cloud appeared on the trajectory at 17:30 G.m.t. Catalina Observatory tracked at

TABLE 3-II.—Professional Observatories Participating in Apollo 8 Optical Tracking Experiment

Observatory	Location	Telescope	Personnel
Catalina Observatory	Tucson, Ariz.	61-in. NASA reflector.	Gerard P. Kuiper (Director), Elizabeth Roemer.
Corralitos Observatory	Las Cruces, N. Mex.	12- and 14-in. image orthicon.	Allen Hynek (Director), Justis Dunlap.
Dominion Astrophysical Observatory	Mount Kobau, British Columbia	72-in. Cassegrain reflector.	K. O. Wright (Director), Gordon Walker.
Haleakala Observatory	Mount Haleakala, Maui, Hawaii	60-in. image orthicon.	Robert L. Boggess (Director), John Erickson, Wayne Parsons.
High Altitude Observatory	Boulder, Colo.	12-in. camera, 20-in. refractor.	Gary Emerson.
Kitt Peak Observatory	Tucson, Ariz.	36-in. reflector.	Art Hoag (Director).
Lick Observatory	Mount Hamilton, Calif.	36-in. Crossley reflector.	E. J. Wampler.
Lowell Observatory	Flagstaff, Ariz.	72-in. reflector.	John Hall (Director), Peter Boyce, Otto Franz.
McDonald Observatory	Mount Locke, Tex.	82-in. reflector.	Harlan B. Smith (Director), Dan Weedman.
Observatoire du Pic-du-Midi	Hautes Pyrenees, France	43-in. reflector, 24-in. refractor.	M. Moutsoulas (Director), D. F. Gregory, C. Lowe, Zdenek Kopal.
Table Mountain Observatory	Table Mountain, Calif.	16- and 24-in. reflectors.	George Kocher, Charles Capen.
U.S. Naval Observatory	Flagstaff, Ariz.	61-in. astrometric reflector.	Gerald E. Kron (Director), Richard Walker, H. D. Ables, J. C. Christy, James Wray.

TABLE 3-III.—Apollo 8 Optical Tracking Record

[S indicates visual/photographic sighting; W indicates observation obscured by weather]

Observatory	Date, Dec. 1968					
	21	22	23	24	25	26
Catalina.....	S	S				W
Corralitos.....	S	S	S	W	W	W
Kitt Peak.....				W		
Lick.....	W	W	W	W	W	S
Lowell.....	S	S	S			W
McDonald.....		S				
Pic-du-Midi.....	S	W	W	W	W	W
Table Mountain.....	S	S	S			W
U.S. Naval.....	S	S	S			W
Mount Wilson.....	S	S	S	W	S	W
Fullerton.....						S

the sidereal rate and obtained trailed images of three objects on 25 plates of 4X emulsion. Flash durations of less than 1 second were noted visually, but photographs show bright periods lasting several seconds. Corralitos Observatory obtained photographs of the image-orthicon presentation, but did not detect flashing as a result of long integration time. The U.S. Naval Observatory detected four flashing objects surrounding a central dim object, but was unable to photograph more than three objects at one time. Table Mountain, Lowell, and Mount Wilson Observatories also reported sightings and made photographs.

On Sunday and Monday, December 22 and 23, only two sources were reported. Their brightness diminished proportionally to the square of the distance so that, near the Moon, the magnitude was approximately 14 to 15. Such sources would be very difficult to detect close to the lunar crescent. The two objects were separated by several minutes of arc on December 21 and by 20 to 30 minutes of arc on December 22. This is in apparent agreement with the motion of the CSM toward the dark limb and the motion of the S-IVB toward the bright limb.

The transearth trajectory was marked by a wide range of brightness on December 26. At Lick Observatory, 150 minutes of television tape were filmed with a video camera on the 120-inch telescope. Lick reported magnitudes varying from 10 to less than 17, the threshold of the Lick instrument. Fullerton, Calif., reported a highly variable source averaging about 11th magnitude and fading occasionally below the Fullerton instrument threshold of 13th magnitude. Fullerton saw

some flashes at about 05:30 G.m.t., which may have been as bright as fifth magnitude, but no photographs were obtained. Although most observatories were ready to operate that night, the weather in the Southwest was generally bad.

UNCONFIRMED INTERPRETATION

On December 21, the observatories undoubtedly detected some SLA panels, as well as the CSM and S-IVB. The S-IVB was kept in inertial hold, so that its brightness should have been fairly dim and steady. The CSM attitude changed slowly, so that its diffuse component changed slowly and any bright flashes would be widely spaced. The four SLA panels were blown off in opposite directions and tumbled wildly, which may account for most of the bright flashing sources. The bright cloud which was observed at 17:30 G.m.t. was produced by venting of the S-IVB.

On December 26, several tests were made of the orientation thrusters, which may account for some bright flashes. Also, if a water dump had taken place, the ensuing cloud of ice crystals would account for the bright flash which was reported. The solar position and spacecraft orientation were more favorable during this phase of the mission, so that the reflection was generally brighter than on December 21.

DISCUSSION OF PHOTOGRAPHS

The dates, times, and distances of the Apollo spacecraft from the Earth in the photographs presented as figures 3-1 to 3-9 are shown in table 3-IV.

TABLE 3-IV.—*Data for Selected Photographs*

Figure no.	G.m.t., hr:min	Date, Dec. 1968	Approximate distance from Earth, km
3-1.....	02:01	22	118 000
3-2.....	03:01	22	128 000
3-3.....	03:16	22	129 000
3-4.....	01:55	23	255 000
3-5.....	02:05	23	255 000
3-6.....	02:34	23	260 000
3-7.....	02:36	23	260 000
3-8.....	02:24	24	350 000
3-9.....	05:24	27	122 000

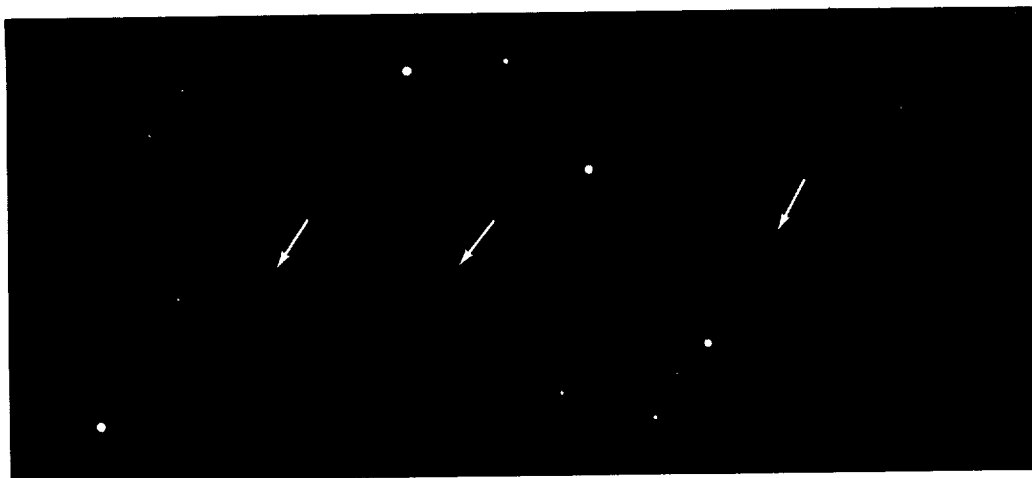


FIGURE 3-1.—CSM, S-IVB, and one SLA panel at 02:01 G.m.t. on December 22, 1968.

The photographs in figures 3-1, 3-4, and 3-5 were taken at Catalina Observatory, Tucson, Ariz., with the 61-inch NASA reflector. Corralitos Observatory, Las Cruces, N. Mex., supplied the photographs in figures 3-2 and 3-6. These photographs were taken with the Corralitos 24-inch reflector coupled to an image-orthicon light intensifier. The photographs in figures 3-3, 3-7, and 3-8 were taken at the U.S. Naval Observatory at Flagstaff, Ariz., with a 61-inch reflector. The photograph in figure 3-9 was taken at Lick Observatory, Mount Hamilton, Calif., with a 36-inch Crossley reflector.

In figure 3-1, the CSM (center), the S-IVB (right, very faint), and one SLA panel (left,

flashing) are trailed against the stellar background in this 2-minute exposure. They are separated by 3 minutes of arc, or a minimum of 100 km. North is at the top right of this photograph, and the apparent motion with respect to the star field is to the southeast (left).

In figure 3-2, two photographs taken 150 seconds apart are superimposed with the star field displaced vertically to show the apparent motion of five objects. Objects 1 and 2, which are not resolved here, are thought to be the CSM and one SLA panel; objects 3 and 5 are additional panels; and object 4 is the S-IVB booster. The apparent stellar magnitude of the objects ranges approximately between 11 and 14.

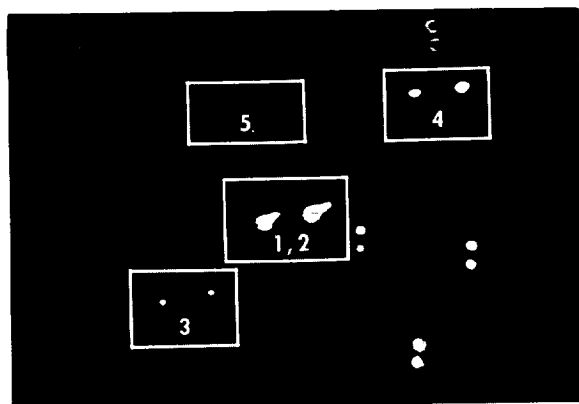


FIGURE 3-2.—CSM (1), SLA panels (2) (3) (5), and S-IVB (4) at 03:01 G.m.t. on December 22, 1968.

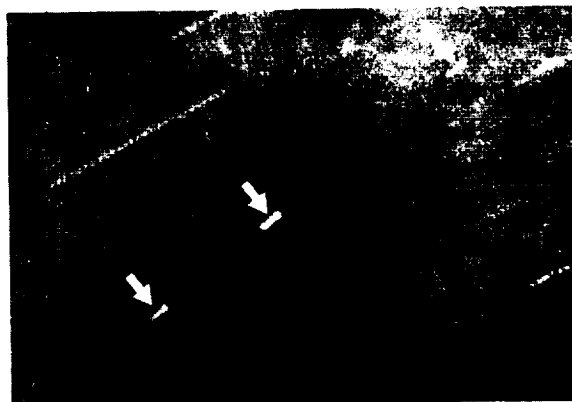


FIGURE 3-3.—CSM, S-IVB, and one SLA panel at 03:16 G.m.t. on December 22, 1968.

In figure 3-3, the CSM (center), the S-IVB booster (upper right), and one SLA panel (lower left) have an apparent stellar magnitude of 12 to 14. The dotted appearance of the images in this 5-minute exposure is caused by stepping the telescope drive at the apparent rate of motion of the spacecraft.

The CSM, which has an apparent stellar magnitude of 13 to 14, is trailed against the star field



FIGURE 3-4.—CSM at 01:55 G.m.t. on December 23, 1968.

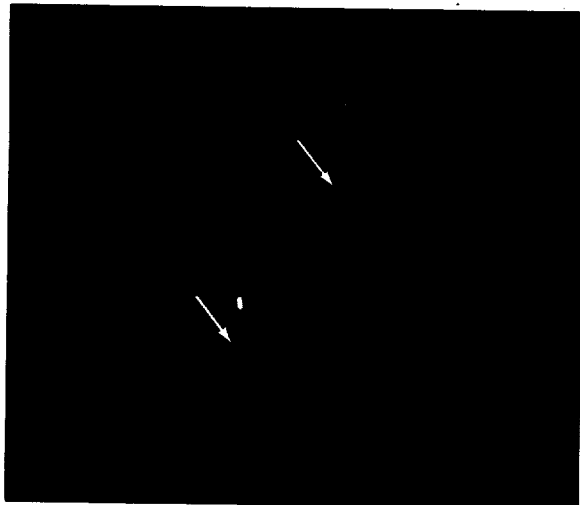


FIGURE 3-5.—CSM and S-IVB at 02:05 G.m.t. on December 23, 1968.

in the 2-minute exposure in figure 3-4. At this distance, the spacecraft is moving slightly faster than the sidereal rate, so that its apparent motion is toward the southwest with north at the top. The S-IVB booster is tumbling nearby and is not visible.

In figure 3-5, the telescope has been driven to compensate for the apparent motion of the CSM (below) and the S-IVB (above). The apparent separation is only 2.5 minutes of arc, but the linear separation is about 2000 km, since the S-IVB will pass in front of the Moon and the CSM will pass behind.

Apollo 8 is seen in figure 3-6 at 02:34 G.m.t. on December 23, about 260 000 km from the Earth. Four frames of the image-orthicon presentation spaced at 10-minute intervals have been superimposed to show the apparent motion of

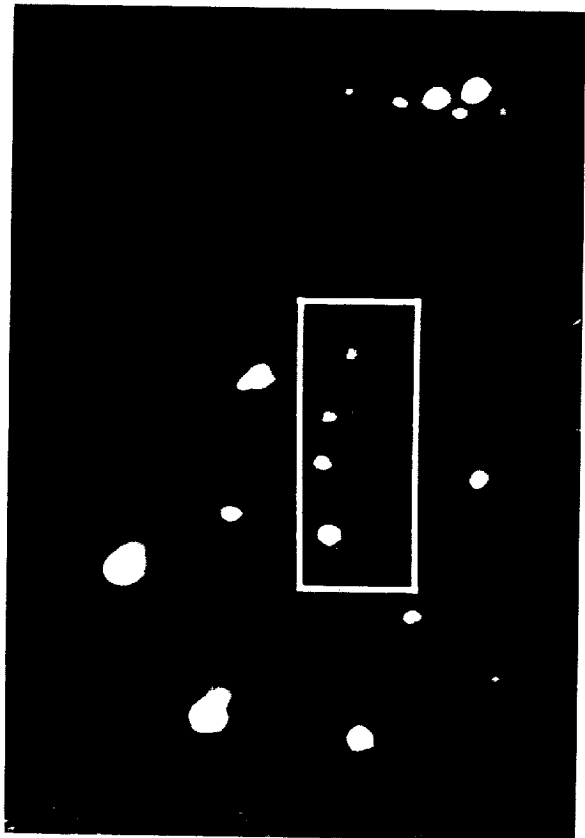


FIGURE 3-6.—Four frames superimposed to show apparent motion of CSM at 02:34 G.m.t. on December 23, 1968.

the CSM. The apparent curvature of the orbit is caused by the angular motion of the observatory.

In figure 3-7, the CSM (below) and the S-IVB (above) are moving to the southwest, with north at the top right. The vehicle reflections have an apparent stellar magnitude of 13 to 14, but because of the trailing, their image brightness is dimmed. Note that the brightness of the S-IVB varies considerably as it tumbles, whereas the brightness of the CSM changes slowly.

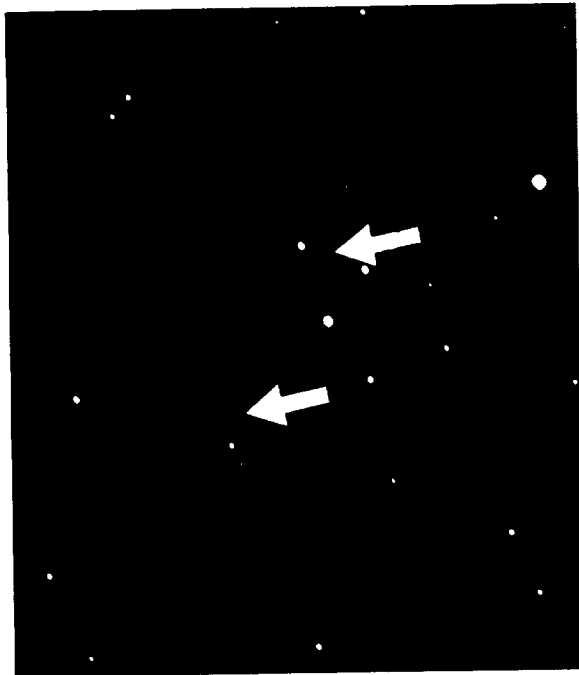


FIGURE 3-7.—CSM and S-IVB at 02:36 G.m.t. on December 23, 1968.

In the 5-minute exposure of figure 3-8, the CSM, which has an apparent stellar magnitude of 14 to 15, is being tracked, and the stars are trailed. The spacecraft is only 3° northeast of the Moon at this time, so that the gradation of the background brightness is caused by scattered moonlight.

Sixteen photographs of a television monitor taken at 10- to 20-second intervals were superimposed to obtain the dotted trail of the CSM, which has an apparent stellar magnitude of 10 to 12 (fig. 3-9). The motion is toward the northeast (upward).

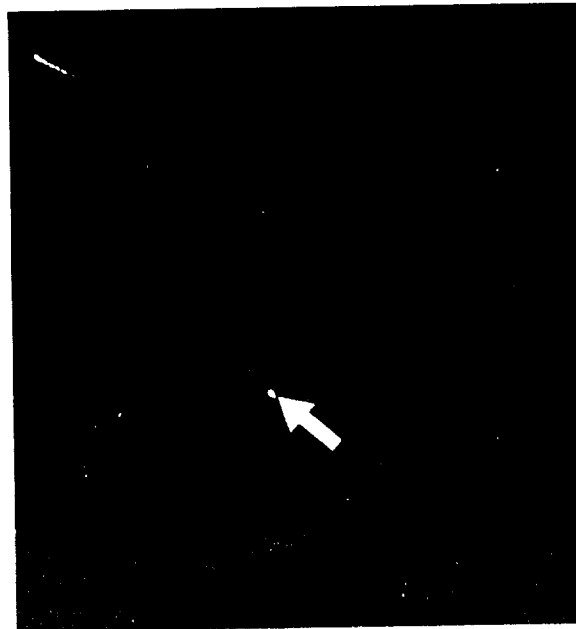


FIGURE 3-8.—CSM at 02:24 G.m.t. on December 24, 1968.

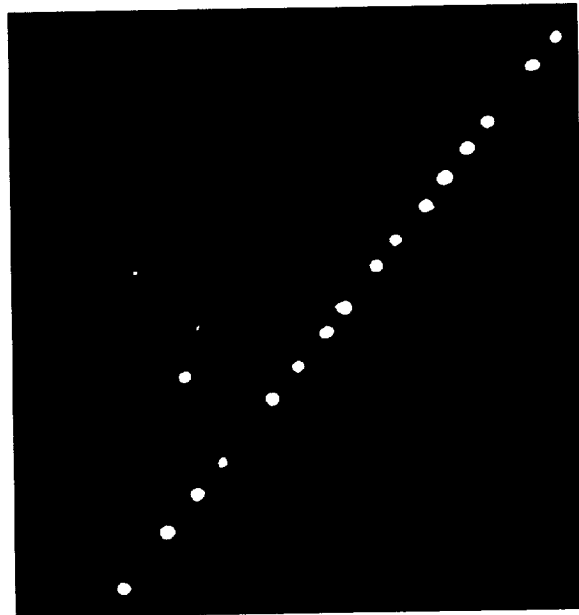


FIGURE 3-9.—Dotted trail of CSM at 05:24 G.m.t. on December 27, 1968.

CONCLUSIONS

The feasibility of optical tracking for Apollo missions to the Moon was confirmed by the observatory sightings. Unfortunately, the vagaries

of weather remain a deterrent to routine utility of optical tracking. The brightness estimates which were reported are in reasonable agreement with some crude theoretical estimates which preceded the flight. It is unlikely that the Apollo spacecraft can be monitored optically in lunar orbit, since the lunar crescent is too bright for discrimination. However, if the bright flashes can be attributed to special attitudes, thrusts, or water dumps, it may be possible to track optically for brief periods near the lunar disk.

The actual trajectory for this mission was very close to the nominal trajectory predicted in advance. Discrepancies of only a few minutes of arc were noted on December 21 and 26, but the shift remained well within the field of most telescopes. The accurate position data plus the rapidly varying source made identification and tracking relatively easy with moderate-sized instruments. The spacecraft position can be verified immediately with an accuracy of ± 10 arc seconds in a good star field, and an accuracy of ± 0.1 arc second is achievable with photographic plate measurements.

Future interest in optical tracking will depend on how effectively the data from Apollo 8 tracking can be used by NASA, whose interest was generated by the desire to determine the feasibility of visual boresighting on the spacecraft. Evidently, this is possible during translunar and transearth trajectories. During lunar orbit, it is unlikely unless special arrangements can be made to enhance the source brightness. Hopefully, this or some other technical application of optical tracking will prove useful.

SMITHSONIAN OBSERVATIONS OF APOLLO 8 NEAR EARTH

STAFF, SMITHSONIAN ASTROPHYSICAL
OBSERVATORY, AND
OTHA H. VAUGHAN, JR.

INTRODUCTION

On December 21, 1968, the Smithsonian Astrophysical Observatory (SAO) photographed events associated with the Apollo 8 translunar mission. The Baker-Nunn camera in Hawaii photographed the firing of the S-IVB that accelerated the spacecraft out of Earth orbit and into a translunar trajectory. Approximately 2 hours later, the

Baker-Nunn camera in San Fernando, Spain, made a series of photographs that show the CSM, the S-IVB rocket body, several SLA panels, and the large clouds formed by the ejection of the rocket's cryogenics. At that time, the distance of the objects from the Earth was of the order of 50 Mm. In addition, approximately 75 observations were made visually by Moonwatch observers in the United States, Great Britain, and Western Europe. This paper describes the Baker-Nunn camera system, the observations that were made, and the data derived.

THE BAKER-NUNN CAMERA

The Baker-Nunn camera (fig. 3-10) is an $f/1$ Schmidt-type system with a three-element correcting lens, a spherical mirror, and an aspherical focal surface. With a focal length of approximately 50 cm, the camera has a plate scale of approximately 2.4μ per second of arc. The Apollo 8 observations were made with Kodak 2475 recording film, more commonly known as Royal-X Pan extended red. The time of each exposure is recorded directly on the film and is related to



FIGURE 3-10.—Baker-Nunn satellite tracking camera and a typical installation.

TABLE 3-V.—Coordinates of Baker-Nunn Cameras

Station	Number	X, Mm	Y, Mm	Z, Mm
San Fernando, Spain.....	9004	5.105593	-0.555232	3.769674
Maui, Hawaii.....	9012	-5.466055	-2.404275	2.242170

Greenwich mean time at Cambridge with an accuracy of better than 1 msec.

Two of the observatory's Baker-Nunn cameras were used to make the observations described in this paper. Their coordinates (ref. 3-1) are given in table 3-V.

THE OBSERVATIONS

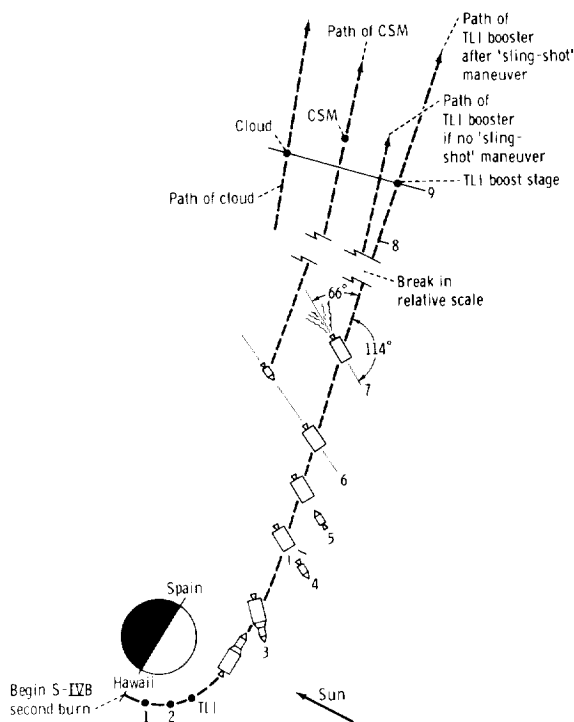
Mission Events Related to Mount Haleakala Photography

The Smithsonian astrophysical observing station on Mount Haleakala on the island of Maui, Hawaii, acquired the Apollo 8 spacecraft at 15:44:31 G.m.t., shortly after it appeared over the horizon. At that time, the translunar injection (TLI) burn of the S-IVB was already in progress. However, the spacecraft was still in the penumbra of the shadow of the Earth.

While the spacecraft was visible, the Baker-Nunn camera made 0.4-second exposures every 2 seconds. For accurate timing, each image was "chopped" at five points by the rotating shutter of the camera. The images are slightly trailed because of the rapid apparent motion of the spacecraft.

The photographic record continued for several minutes as the spacecraft reached its maximum elevation approximately 17° above the horizon and then finally disappeared below the station horizon. The sunlit exhaust from the booster was reported to be visually as bright as the full Moon.

Figure 3-11 is a schematic of selected events during the Hawaii and Spain photography. Figures 3-12 to 3-17 show six representative frames taken by the camera in Hawaii. In figure 3-12, the spacecraft appears as a chopped trail emerging from the shadow of the Earth. The second and third frames show "profiles" of the rocket exhaust. The effects of the chopping shutter are visible in figure 3-13, breaking the exhaust cone into dis-



1. Start of photography by Hawaii station, showing the TLI burn in progress.
2. End of photography by Hawaii station just prior to end of TLI burn.
3. Inertial attitude for separation of the CSM and TLI booster stage.
4. Separation of CSM and jettison of SLA panels; distance from surface of Earth approximately 7017 km.
5. Rotation of CSM to be able to observe the TLI booster and perform the mission.
6. Position of CSM and TLI booster stage after second evasive maneuver and prior to programmed liquid oxygen dump; CSM above and behind the TLI booster.
7. Attitude of TLI booster at time of programmed liquid oxygen dump event.
8. Start of San Fernando, Spain, photography.
9. Relative geometry of CSM, cloud, and TLI boost stage at approximately 18:28 G.m.t.

FIGURE 3-11.—Schematic of selected events of Hawaii and Spain photography during the Apollo 8 mission.

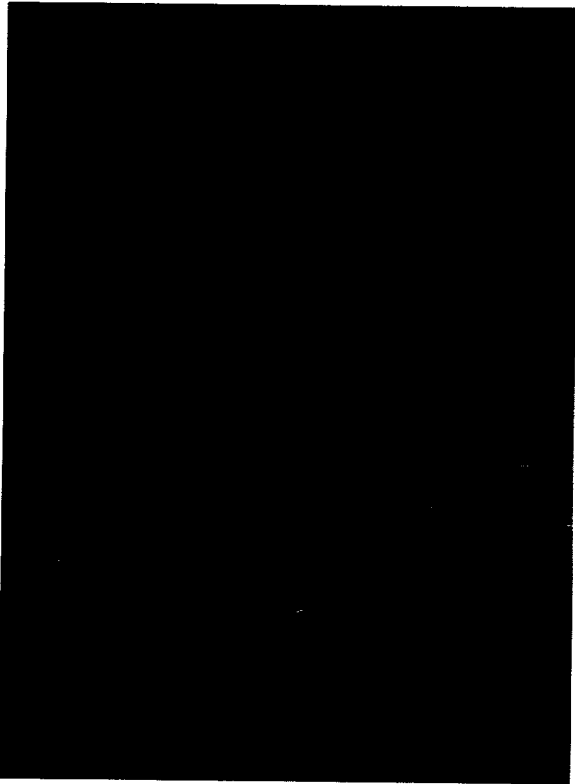


FIGURE 3-12.—CSM and S-IVB during burn of S-IVB J-2 engine.

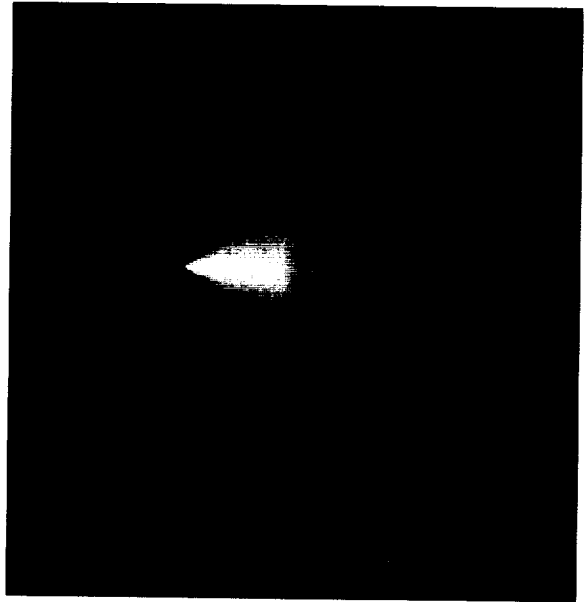


FIGURE 3-14.—CSM and S-IVB during translunar injection.

crete segments as the spacecraft moved across the sky. Figure 3-14 shows the CSM and S-IVB during TLI. Figures 3-15 and 3-16 show a somewhat changed geometry, the observations having been made nearly parallel to the velocity vector of the spacecraft. The slight trailing of the image blurred the ray structure in the vertical direction, but rays are clearly visible in the horizontal direction, parallel to the trailing.

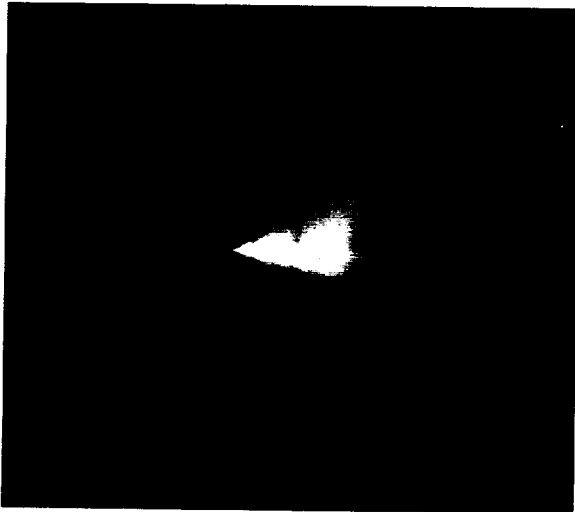


FIGURE 3-13.—CSM and S-IVB immediately after entering sunlight.

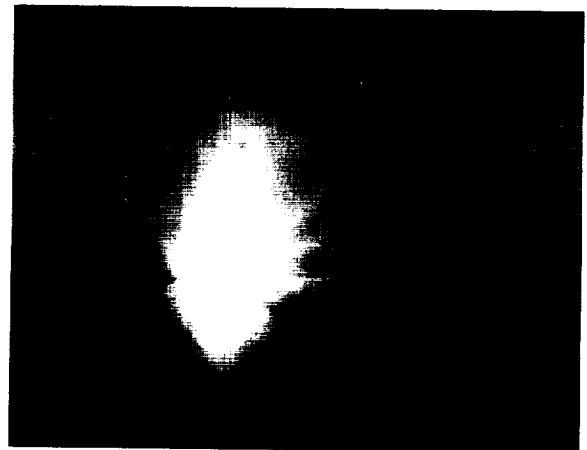


FIGURE 3-15.—Looking up exhaust plume during burn of S-IVB J-2 engine.



FIGURE 3-16.—S-IVB J-2 engine burn.

Finally, figure 3-17 shows the spacecraft just as it was disappearing behind a mountain on the horizon. The next frame (not reproduced here) still showed the ray structure even though the apex of the exhaust cone was obscured by the horizon.

The exposure times for the frames in figures 3-12 to 3-17 were as follows: figure 3-12, 15:44:31 G.m.t.; figure 3-13, 15:44:45; figure 3-14, 15:44:59; figure 3-15, 15:45:47; figure 3-16, 15:46:03; and figure 3-17, 15:46:09.

Mission Events Related to the San Fernando, Spain, Photographs

The Smithsonian astrophysical observing station at San Fernando, Spain, observed Apollo 8 for almost 2 hours beginning shortly after 18:00 G.m.t. on December 21.

Moonwatch Headquarters received a report that a cloud was first visible in England at about 17:48 G.m.t. and, at its brightest, reached approximately zero magnitude. A smaller cloud estimated at fourth magnitude was also reported.

At the time of first ground acquisition at 18:07:36 G.m.t., photography indicated that the "slingshot" maneuver of the S-IVB stage had been performed and that the liquid oxygen dump and portion of events for "safing" the S-IVB stage had been performed. In the following para-

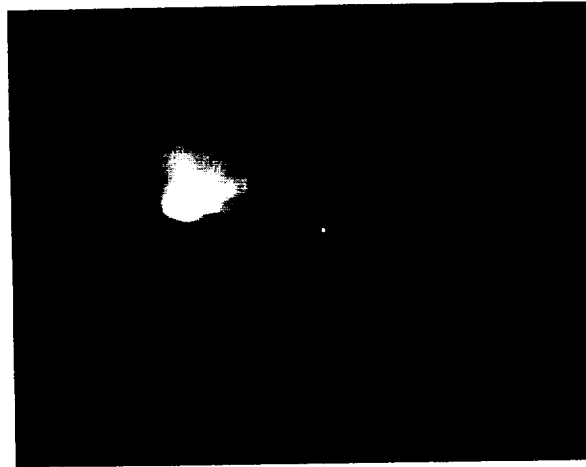


FIGURE 3-17.—Spacecraft immediately before disappearing behind mountain on horizon.

graphs, the events which occurred prior to the photography and those events which are related to the photography will be discussed.

At the time of the TLI (15:47:06 G.m.t.), which occurs at the S-IVB J-2 engine cutoff + 10 seconds (15:46:56), the CSM and the boost stage were traveling at a space-fixed velocity of 10 822.05 m/sec while at an altitude of 346.73 km (based on a spherical Earth radius of 6378.165 km (ref. 3-2). After a coast time of 10 seconds (approximately 15:47:16 G.m.t.), the vehicle began to orient itself for the local horizontal attitude maneuver and began orbital navigation. After coasting until 16:01:58, the CSM and boost vehicle began the required maneuver for separation attitude. While at this inertial attitude, the CSM and boost stage were separated and the SLA panels were jettisoned. Just prior to the actual separation event, the CSM and boost stage were traveling at a space-fixed velocity of 7616.85 m/sec while at an altitude of 7018.6 km from the surface of the Earth.

The CSM separated from the boost stage at 16:11:59 G.m.t., and the astronauts then used the four jet engines of the reaction control system (RCS) for separation propulsion. After performing a null burn and the programmed evasive maneuver, at approximately 16:31:00, the CSM was about 300 meters from the TLI boost stage. At 16:46:56, the boost stage began its programmed liquid hydrogen vent prior to performing the "slingshot"

maneuver. This event is a nonpropulsive vent and, at the time of the start of this event, there were approximately 1440 kg liquid hydrogen and ullage gaseous hydrogen on board the boost stage. The liquid hydrogen vent operation lasted until 17:01:56, at which time it was terminated. A total of 1437 kg of liquid and gaseous hydrogen was vented. The astronauts observed this event and noted it as "spectacular . . . , spewing out from all sides like a huge water sprinkler." At 17:36:00, a second evasive maneuver, which had been requested by the astronauts, was performed. This maneuver placed the CSM at approximately 1000 meters slant range above and behind the TLI boost stage (fig. 3-11).

At 17:46:60 G.m.t., the liquid hydrogen continuous vent valves were opened prior to the start of the programmed liquid oxygen dump. At 17:58:56, the "slingshot" ΔV mode of the boost stage was started by opening the main liquid oxygen valve and using ullage gas pressurization to force the liquid oxygen through the engine injector plate and out through the nozzle throat and the expansion skirt of the J-2 engine. At 17:59:25, the J-2 engine start sphere was vented, and a total of 1.8 kg of gaseous hydrogen was dumped. This event took approximately 150 seconds. During the main liquid oxygen dump through the engine, a steady-state liquid flow rate of 1.4 m³/sec was reached in 40 seconds. After 126 seconds of dump, gas ingestion was indicated by a sudden flow-rate increase. After 150 seconds of dump, approximately 3329 kg of liquid oxygen had been dumped. Ullage gases continued to be dumped until the time of programmed liquid oxygen dump ending (by closing the main liquid oxygen valve) at 18:03:56. At this time, approximately 200 kg of gaseous oxygen ullage gases remained in the liquid oxygen tank.

At 18:03:59 G.m.t., the liquid oxygen nonpropulsive vent valve was opened and remained open for the duration of the mission. At 18:04:04, cold helium gas was dumped overboard through the liquid hydrogen tank and its vent system. Approximately 64 kg were dumped, and the time required for this dump was approximately 3000 seconds.

At 18:16:56 G.m.t., the S-IVB auxiliary propulsion system (APS) ullage engines 1 and 2 were commanded to start a burn. Module engine 1

burned until 18:29:34, and module engine 2 burned until 18:29:08. Approximately 220 kg of propellants were consumed during this burn sequence. The "slingshot" maneuver resulting from the liquid hydrogen vent, the liquid oxygen dump, and the APS ullage burn caused the TLI boost stage to acquire a retrovelocity of 41.9 m/sec.

At 18:19:16 G.m.t., the CSM could be seen on the tracking film, and by 18:20:54, the S-IVB was visible emerging from the cloud formed by the liquid oxygen dump.

At 18:54:03 G.m.t., the ambient helium in the liquid oxygen and liquid hydrogen tank repressurization spheres was dumped via the liquid hydrogen tank. This dump lasted for 200 seconds, and approximately 28 kg of helium was dumped during this time.

At 18:57:24 G.m.t., the J-2 engine control sphere was vented. This event requires about 300 seconds vent duration. Approximately 0.9 kg of helium was vented. After all of the programmed dumps of propellants and other gases from the TLI boost stage had been completed, the inert stage weighed 23 670 kg. The last frame that shows the S-IVB was taken at 19:07:52. The CSM is last seen on a frame taken at 19:08:24, and the cloud disappeared at about 19:54:26. Observations ended approximately 4 minutes later. Two other objects are visible intermittently, one of them between 18:21:18 and 18:33:04, and the other between 18:35:32 and 18:49:03.

Figure 3-18, a frame exposed for 1.6 seconds, is typical of the frames taken between about 18:20 and 19:07. The large cloud maintained its characteristic "mushroom" shape during most of the observing period. Slightly above it and to the right is the smaller butterfly-shaped cloud with the brighter S-IVB at its center. Between the S-IVB and the large cloud, almost directly on line with the "stem" of the large cloud, is the starlike CSM.

DATA

Thirty-four positions of the CSM and 32 positions of the S-IVB were precisely measured in Cambridge; the observatory's standard procedures for photoreducing satellite images were used (ref. 3-3).

Tables 3-VI, 3-VII, and 3-VIII list observed positions of the CSM, the S-IVB, and two SLA



FIGURE 3-18.—S-IVB, showing cloud formed by blowdown maneuver.

panels. The accuracy of the observations from Maui, Hawaii (station 9012), is assumed to be ± 150 arcsec because of the absence of a point source. The reductions from San Fernando, Spain (station 9004), are considered to be of precisely reduced quality with an assigned standard deviation of ± 4 arcsec.

The time accuracy of the observations (G.m.t.) depends primarily on the stability of the station clock and on the reception of the time signals. Uncertainties estimated according to these criteria vary from ± 0.5 to ± 20 msec, with an average value of ± 2 msec (ref. 3-4).

The positions in columns 4 and 5 of tables 3-VI 3-VII, and 3-VIII refer to the mean equator and equinox of 1950.0 in the fundamental system of FK-4 (ref. 3-5). All satellite positions after August 31, 1962, have been reduced with the SAO Star Catalog (ref. 3-6), which is in the FK-4 system.

TABLE 3-VI.—CSM Positions

Date, yr:mo:day	G.m.t., hr:min:sec	rms, msec ^a	Right ascension, hr:min:sec ^b	Declination, hr:min:sec ^b	rms, sec of arc ^c	Station
1968 12 21	15 44 31.4460	10	11 42 42.000	-50 43 0.00	150	9012
12 21	15 44 33.4480	10	11 51 24.000	-50 18 0.00	150	9012
12 21	15 44 35.4510	10	12 1 24.000	-49 37 0.00	150	9012
12 21	15 44 37.4530	10	12 10 54.000	-49 0 0.00	150	9012
12 21	15 44 43.4620	10	12 38 18.000	-46 42 0.00	150	9012
12 21	15 44 45.4650	10	12 47 24.000	-45 52 0.00	150	9012
12 21	15 44 49.4700	10	13 4 24.000	-43 56 0.00	150	9012
12 21	15 44 59.4850	10	13 45 0.000	-38 26 0.00	150	9012
12 21	15 45 9.5020	10	14 19 36.000	-32 16 0.00	150	9012
12 21	15 45 23.5200	10	14 58 30.000	-23 29 0.00	150	9012
12 21	15 45 33.5330	10	15 20 30.000	-17 44 0.00	150	9012
12 21	15 45 45.5480	10	15 42 6.000	-11 43 0.00	150	9012
12 21	15 45 57.5620	10	15 59 54.000	-6 39 0.00	150	9012
12 21	15 46 9.5790	10	16 14 12.000	-2 33 0.00	150	9012
12 21	18 19 16.0247	1	20 22 14.963	1 50 51.07	4	9004
12 21	18 21 10.7077	1	20 23 6.045	1 45 14.33	4	9004
12 21	18 22 41.1831	1	20 23 44.607	1 42 47.21	4	9004
12 21	18 25 27.6893	1	20 24 57.796	1 36 37.94	4	9004
12 21	18 26 29.8132	1	20 25 23.845	1 34 18.78	4	9004
12 21	18 27 28.6320	1	20 25 45.787	1 32 54.85	4	9004
12 21	18 28 .6320	1	20 25 59.243	1 31 50.29	4	9004
12 21	18 29 4.6319	1	20 26 25.610	1 29 27.34	4	9004
12 21	18 29 36.6317	1	20 26 38.522	1 28 15.01	4	9004
12 21	18 32 48.6313	1	20 28 .114	1 20 55.64	4	9004
12 21	18 33 56.3477	1	20 28 22.423	1 19 9.76	4	9004

TABLE 3-VI.—CSM Positions—Continued

Date, yr:mo:day	G.m.t., hr:min:sec	rms, msec ^a	Right ascension, hr:min:sec ^b	Declination, hr:min:sec ^b	rms, sec of arc ^c	Station
12 21	18 34 44.3482	1	20 28 41.027	1 17 29.80	4	9004
12 21	18 35 32.3480	1	20 28 59.799	1 15 54.40	4	9004
12 21	18 36 20.3479	1	20 29 18.293	1 14 15.10	4	9004
12 21	18 37 24.3484	1	20 29 43.296	1 12 37.71	4	9004
12 21	18 38 44.3477	1	20 30 15.788	1 8 40.58	4	9004
12 21	18 39 3.3233	1	20 30 22.873	1 8 6.28	4	9004
12 21	18 39 55.0126	1	20 30 42.298	1 6 22.29	4	9004
12 21	18 40 59.0137	1	20 31 5.512	1 4 13.15	4	9004
12 21	18 41 47.0147	1	20 31 21.552	1 4 .88	4	9004
12 21	18 44 19.5074	1	20 32 18.422	0 57 47.00	4	9004
12 21	18 47 59.1986	1	20 33 36.888	0 50 55.07	4	9004
12 21	18 48 47.1998	1	20 33 50.418	0 50 46.04	4	9004
12 21	18 51 37.8318	1	20 34 50.575	0 44 13.70	4	9004
12 21	18 52 41.8321	1	20 35 11.905	0 42 16.72	4	9004
12 21	18 53 13.8324	1	20 35 19.331	0 42 .28	4	9004
12 21	18 54 15.0331	1	20 35 39.447	0 40 20.34	4	9004
12 21	18 55 3.0330	1	20 35 54.996	0 38 47.97	4	9004
12 21	18 55 51.0358	1	20 36 6.567	0 42 35.59	4	9004
12 21	18 57 11.0351	1	20 36 38.483	0 37 38.58	4	9004
12 21	18 58 11.6707	1	20 36 56.309	0 33 16.88	4	9004
12 21	19 2 43.4079	1	20 38 21.351	0 26 16.73	4	9004
12 21	19 5 19.5754	1	20 39 9.068	0 21 20.45	4	9004
12 21	19 17 2.4777	1	20 42 32.605	0 2 45.48	4	9004
12 21	19 18 4.8330	1	20 42 51.020	0 1 6.74	4	9004
12 21	19 19 48.4194	1	20 43 47.052	-0 5 20.71	4	9004
12 21	19 20 27.6810	1	20 43 29.032	-0 2 19.24	4	9004

^a Standard error of time.

^b Topocentric coordinates with reference to mean equator and equinox of 1950.0.

^c Standard error of position.

The positions have not been corrected for parallax refraction; the correction seldom exceeds 2 seconds of arc.

From these data, preliminary orbital elements were derived by using the December 10, 1968, version of the SAO differential orbit improvement (DOI) program (refs. 3-7 and 3-8). The following are the preliminary orbital elements for the CSM:

1. T_0 = December 21,
18:46:05.061 G.m.t.
2. Argument of perigee = $(29.15^\circ \pm 11)$
 $+0.011455^\circ (T - T_0)$

3. Right ascension of ascending node =
 $(141.590^\circ \pm 0.016^\circ) - 0.0073^\circ (T - T_0)$
4. Inclination = 30.739436°
5. Eccentricity = 0.975975
6. Mean anomaly (in revolutions) =
 $(0.007819 \pm 0.000051) + (0.06245 \pm 0.00055) (T - T_0)$

The standard error of unit weight is 6.56 with 34 observations used. The following are the preliminary orbital elements for the S-IVB:

1. T_0 = December 21, 18:46:05.061 G.m.t.

TABLE 3-VII.—*S-IVB Positions*

Date, yr:mo:day	G.m.t., hr:min:sec	rms, msec ^a	Right ascension, hr:min:sec ^b	Declination, hr:min:sec ^b	rms, sec of arc ^c	Station
1968 12 21	18 19 16.0254	1	20 22 4.834	1 52 24.25	4	9004
12 21	18 21 10.7088	1	20 22 55.616	1 48 10.34	4	9004
12 21	18 21 18.7087	1	20 22 58.942	1 47 52.46	4	9004
12 21	18 22 41.1847	1	20 23 34.536	1 44 49.46	4	9004
12 21	18 25 11.6904	1	20 24 38.285	1 39 25.32	4	9004
12 21	18 25 27.6907	1	20 24 45.102	1 38 49.80	4	9004
12 21	18 26 29.8137	1	20 25 10.550	1 36 30.39	4	9004
12 21	18 27 28.6334	1	20 25 34.863	1 34 33.66	4	9004
12 21	18 28 .6333	1	20 25 47.552	1 33 20.26	4	9004
12 21	18 29 4.6334	1	20 26 13.638	1 31 14.65	4	9004
12 21	18 29 36.6332	1	20 26 26.750	1 30 1.51	4	9004
12 21	18 32 48.6334	1	20 27 42.829	1 23 26.50	4	9004
12 21	18 33 4.6331	1	20 27 49.015	1 22 54.26	4	9004
12 21	18 33 56.3495	1	20 28 7.468	1 21 19.53	4	9004
12 21	18 34 44.3500	1	20 28 26.002	1 19 46.43	4	9004
12 21	18 35 32.3500	1	20 28 43.953	1 18 12.40	4	9004
12 21	18 36 20.3499	1	20 29 2.222	1 16 33.71	4	9004
12 21	18 37 8.3500	1	20 29 20.076	1 15 3.56	4	9004
12 21	18 37 24.3501	1	20 29 26.000	1 14 31.94	4	9004
12 21	18 37 56.3499	1	20 29 37.637	1 13 29.79	4	9004
12 21	18 38 44.3504	1	20 29 55.333	1 11 59.20	4	9004
12 21	18 39 3.3246	1	20 30 2.141	1 11 20.95	4	9004
12 21	18 39 55.0154	1	20 30 21.032	1 9 43.33	4	9004
12 21	18 40 59.0165	1	20 30 44.240	1 7 42.82	4	9004
12 21	18 44 19.5089	1	20 31 55.135	1 1 28.08	4	9004
12 21	18 47 59.2018	1	20 33 10.566	0 54 51.42	4	9004
12 21	18 48 47.2021	1	20 33 26.739	0 53 25.72	4	9004
12 21	18 49 3.2019	1	20 33 31.983	0 52 55.67	4	9004
12 21	19 2 43.4107	1	20 37 52.541	0 29 46.10	4	9004
12 21	19 5 19.5787	1	20 38 38.885	0 25 37.19	4	9004
12 21	19 17 2.4813	1	20 41 57.844	0 7 46.69	4	9004
12 21	19 18 4.8367	1	20 42 15.566	0 6 8.19	4	9004
12 21	19 19 48.4260	1	20 42 42.679	0 3 44.71	4	9004
12 21	19 20 27.6848	1	20 42 52.920	0 2 47.54	4	9004

^a Standard error of time.

^b Topocentric coordinates with reference to mean equator and equinox of 1950.0.

^c Standard error of position.

2. Argument of perigee = $(28.098^\circ \pm 0.087^\circ) + 0.011455^\circ (T - T_0)$
3. Right ascension of ascending node = $(141.5563^\circ \pm 0.0033^\circ) - 0.00731^\circ (T - T_0)$
4. Inclination = $30.816^\circ \pm 0.044^\circ$
5. Eccentricity = 0.975975

$$6. \text{ Mean anomaly (in revolutions)} = (0.008313 \pm 0.000048) + (0.06655 \pm 0.00053) (T - T_0)$$

The standard error of unit weight is 0.97 with 32 observations used.

TABLE 3-VIII.—*Adapter-Panel Positions*

Date, yr:mo:day	G.m.t., hr:min:sec	rms, msec ^a	Right ascension, hr:min:sec ^b	Declination, hr:min:sec ^b	rms, sec of arc ^c	Station
Panel A						
1968 12 21	18 21 18.7083	1	20 23 8.247	1 47 9.39	4	9004
12 21	18 25 11.6899	1	20 24 49.543	1 38 22.26	4	9004
12 21	18 28 .6322	1	20 26 .398	1 32 16.21	4	9004
12 21	18 29 4.6322	1	20 26 25.966	1 29 54.69	4	9004
12 21	18 33 4.6318	1	20 28 2.994	1 21 29.68	4	9004
12 21	18 36 20.3482	1	20 29 18.952	1 14 46.80	4	9004
12 21	18 53 13.8328	1	20 35 19.672	0 42 41.13	4	9004
Panel B						
1968 12 21	18 35 32.3475	1	20 29 2.991	1 15 8.56	4	9004
12 21	18 36 20.3474	1	20 29 21.251	1 13 28.90	4	9004
12 21	18 36 52.3475	1	20 29 33.476	1 12 27.75	4	9004
12 21	18 37 8.3474	1	20 29 39.498	1 11 55.65	4	9004
12 21	18 37 24.3475	1	20 29 45.796	1 11 23.64	4	9004
12 21	18 37 56.3473	1	20 29 57.783	1 10 18.15	4	9004
12 21	18 48 47.1989	1	20 33 52.875	0 49 24.85	4	9004
12 21	18 49 3.1987	1	20 33 56.879	0 48 54.11	4	9004
12 21	18 55 3.0325	1	20 35 58.943	0 38 4.38	4	9004
12 21	18 55 51.0320	1	20 36 14.755	0 36 41.56	4	9004

^a Standard error of time.

^b Topocentric coordinates with reference to mean equator and equinox of 1950.0.

^c Standard error of position.

Elements accompanied by errors of two significant figures have been determined by the DOI program. The values of the motions of the argument of perigee and the right ascension of the node are theoretical, being those given in the revision to the Apollo 8 Spacecraft Operational Trajectory (Vol. 1, "Mission Profile for Dec. 21 Launch").

In the SAO computer program, the inclination and the argument of perigee are referred to the true equator of date; the right ascension of the ascending node, however, is reckoned from the mean equinox of 1950.0 along the corresponding mean equator to the intersection with the moving true equator of date, and then along the true equator of date. To transform from right ascension

of the node as determined by the DOI to right ascension of the node referred to the mean equinox of date

$$\Omega = \Omega(\text{DOI}) + 3.508^\circ \times 10^{-5}(\text{MJD} - 33\,281)$$

where Ω is the right ascension of the node in degrees and MJD is the modified Julian day.

Densitometer scans were made in two directions across the image of the cloud on approximately 12 frames of the Spanish films. The density profiles identified the approximate position of the point of greatest density in each image. They also permitted a reasonably accurate determination of the extent of the cloud in two arbitrary directions, approximately parallel and perpendicular to the direction of apparent motion. Table 3-IX gives

TABLE 3-IX.—*Angular Extent of Cloud and Angular Separation of Density Maximum From S-IVB*

G.m.t., hr:min:sec	Length, arcsec	Width, arcsec	Separation, arcsec
18:14:57			334.4
18:20:02			549.8
18:25:11			574.8
18:30:08	2508	1254	647.9
18:36:04	2508	1254	773.3
18:40:11	2508	1254	856.9
19:02:59	2194	1097	
19:09:28	2194	1097	

the angular extent of the cloud and the angular separation of the density maximum from the S-IVB in seconds of arc.

During the period covered in table 3-IX, the slant range from the observing station to the objects increased from 42 to 54 Mm, approximately. At the same time, the height of the objects above the surface of the Earth increased approximately from 39 to 54 Mm.

DISCUSSION

The Hawaiian photographs of the TLI firing of the S-IVB show that most of the illumination originates from a relatively thin conical surface.

During the observations, Apollo 8 was approximately 165 km above the surface of the Earth, where the ambient density is 5×10^{-7} g/m³. The S-IVB was exhausting approximately 1100 kg/sec at a velocity, relative to the rocket, of the order of 5 km/sec. If the exhaust gases were contained in a cylinder of 1-mile radius immediately after ejection, the initial density of the gas cloud would be 15 g/m³. The exhaust gases would, therefore, expand, because their density exceeded that of the ambient atmosphere by a factor of 3×10^7 . The density of the gas cloud would become equal to that of the ambient atmosphere after the gas had expanded to a radius of approximately 5 km. This is very close to the distance at which the photographs indicate that the gas cloud had become too diffuse to scatter an appreciable amount of light.

The dynamics of the gas-cloud expansion can

be estimated as follows. At an altitude of 165 km, one ambient neutral particle collides with another every 0.15 second. The gas cloud will possess a kinetic temperature perhaps a little greater than that of the ambient atmosphere. During the expansion, an ambient particle will collide with a plume particle about every 0.001 second; therefore, the ambient particles will be "scooped up" by the expanding cloud, and a shock front will form at a radius of the order of 1 km. Many collisions between plume particles occur during the expansion, and it is not, therefore, an expansion of the free-molecule type. The expansion front must take the form of a conical surface because of the downstream (or possibly upstream) translational velocity of the gas cloud. The velocity of this front must be of the order of $2/(\gamma-1)$ times the acoustic velocity in the gas cloud (where γ is the ratio of specific heats), which implies a speed of the order of 5 km/sec. This figure fits well with the large cone angle that is observed in the exhaust plume.

The brightness of the object was described as "much greater than that of the full Moon." An apparent magnitude of -15 (as compared to -27 for the Sun and -13 for the full Moon) implies that the scattering process must be capable of producing about 1 percent of the light incident from the Sun (assuming an isotropic scattering process). It would be difficult to accomplish this by an inelastic type of scattering process because of the narrowness of absorption lines. It is more likely that Rayleigh scattering from crystals of ice is the required mechanism.

The rocket exhaust consists largely of water vapor, and at the front of the expanding gas cloud, cooling must occur that may be sufficient to produce ice crystals. Such condensation fronts are often observed in wind tunnels. Hotter gas farther behind the front will melt these crystals so that the crystals will be confined to the expansion front. The photographs indicate that the ice crystals are confined to a depth of 500 to 1000 meters behind the front. If these ice crystals are about 0.1 μ size, then a rough calculation indicates that there could be a sufficient number of them to produce such a bright object. An upper limit on the size of about 0.1 μ arises from the observation that the scattering process appears to be isotropic.

Finally, the rayed structure that appears in the exhaust plume when it is viewed end-on probably arises from the mechanisms for injecting fuel into the combustion chamber. If a plasma-type instability were present, it would probably occur in a helical fashion and would not, therefore, be seen in this type of observation.

The Spain photography shows the effect of the release of unburned cryogenic materials in vacuum at an altitude of approximately 43 000 km above the Earth. At the time of the photograph seen in figure 3-18, the gas cloud was approximately 214 by 99 km in size and the S-IVB auxiliary propulsion units were burning. The exhaust plumes

of these units can be seen in the photograph as the butterfly-shaped objects near the S-IVB.

A detailed study of this type of photography by gas dynamicists will allow a better understanding of the venting of materials in hard vacuum and their effects on spacecraft which may happen to be near during the venting schedules.

Because of the many questions raised by this type of photography from the Apollo 8 mission, more extensive coverage is indicated for future manned missions. The results will depend heavily both on the timing of the space-vehicle maneuvers with respect to sunrise and sunset at the observation stations and on the illumination aloft.

REFERENCES

- 3-1. LUNDQUIST, C. A.; AND VEIS, G.: Geodetic Parameters for a 1966 Smithsonian Standard Earth. SAO Special Rept. no. 200, Dec. 1966.
- 3-2. ANON.: Saturn V Launch Vehicle Flight Evaluation Report, AS-503 Apollo 8 Mission. MPR-SAT-FE-69-1, Feb. 1969.
- 3-3. HAEFNER, R. R.: The Precise Reduction of Baker-Nunn Films at the Smithsonian Astrophysical Observatory. The Use of Artificial Satellites for Geodesy. Vol. II, George Veis, ed., National Technical University (Athens), 1967, pp. 81, 83-94.
- 3-4. LAMBECK, K.; AND McGRATH, L. J., JR.: Reduction and Accuracy of Baker-Nunn Observations of Geos 1. Geodetic Satellite Results During 1967, Charles A. Lundquist, ed., SAO Special Rept. no. 264, Dec. 1967, pp. 145-161. (Also available as NASA CR-97155.)
- 3-5. FRICKE, W.; AND KOPFF, A.: Fourth Fundamental Catalogue. Veröff Astron. Recheu-Inst., Heidelberg, no. 10.
- 3-6. STAFF OF SMITHSONIAN ASTROPHYSICAL OBSERVATORY: Smithsonian Astrophysical Observatory Star Catalog. Smithsonian Publication 4652. Smithsonian Institution (Washington, D.C.), Mar. 1966.
- 3-7. GAPOSCHKIN, E. M.: Publication of Orbits Derived From Photoreduced Baker-Nunn Observations. SAO Special Rept. no. 232, Dec. 1966. (Also available as NASA CR-82799.)
- 3-8. VEIS, G.: The Deflection of the Vertical of Major Geodetic Datums and the Semimajor Axis of the Earth's Ellipsoid as Obtained From Satellite Observations. Space Research V, D. G. King-Hele, P. Muller, and G. Righini, eds., North-Holland Publ. Co. (Amsterdam), 1965, pp. 849-875.

4

Background

INTRODUCTION

RICHARD J. ALLENBY

Under the guidance of the future Project Scientist, James H. Sasser, an ad hoc Lunar Science Working Group was convened September 6, 1968, at the Manned Spacecraft Center (MSC) to consider and recommend lunar-surface areas of scientific interest for which photography was desirable.

An ad hoc Astronomy Working Group was convened by Richard J. Allenby at NASA Headquarters on September 25 to recommend astronomical tasks. These ad hoc working groups, with expanded memberships, later were incorporated into the three formal working groups (fig. 4-1). Under a science management plan approved by

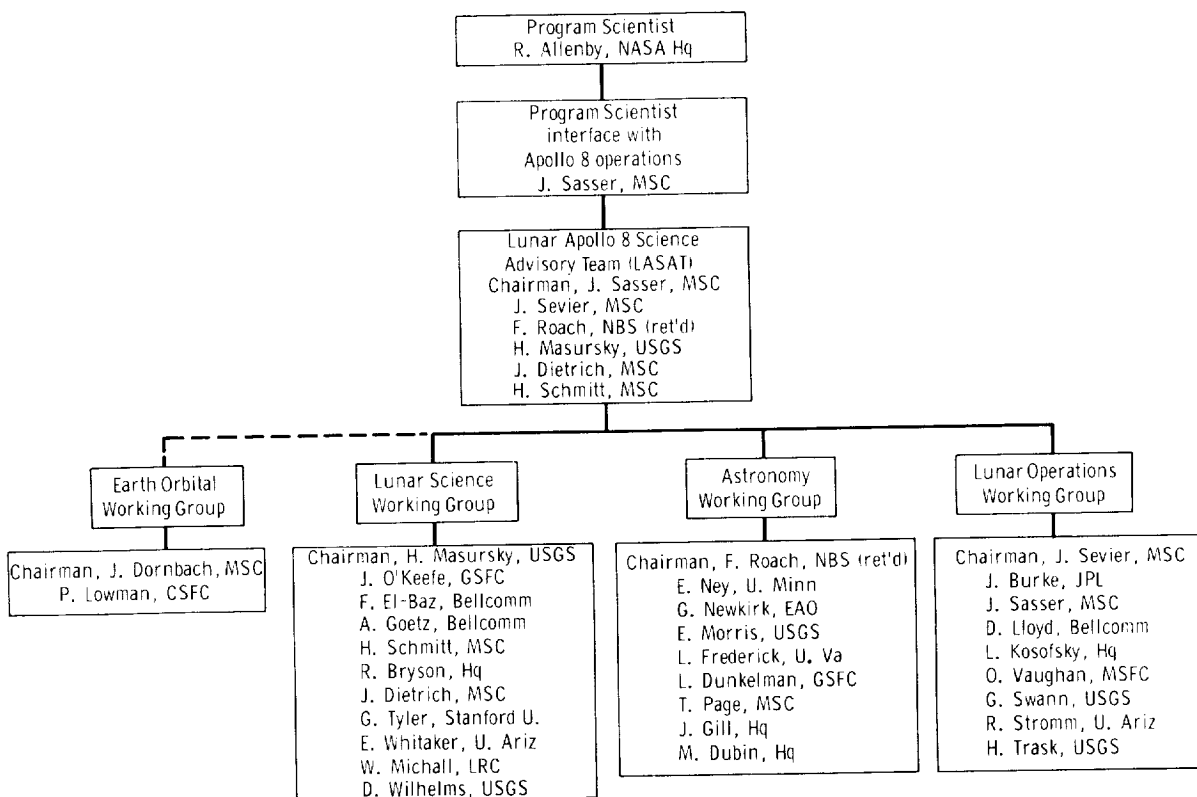


FIGURE 4-1.—Apollo 8 science management plan.

the Associate Administrator for Science, John E. Naugle, on December 17, 1968, the working groups were organized to reflect the key areas of interest in:

1. Operational photography related to present and future Apollo landing sites
2. Scientific photography
3. Astronomy

The obvious overlapping interests of these groups were coordinated by the advisory team chaired by James H. Sasser. This advisory team was also responsible for briefing the astronauts on the proposed tasks and for consulting with and advising the crew and the flight operations team on scientific problems during the mission.

The mission flight plan for Apollo 8 provided alternatives as a series of success "steps." The success of each step determined the actions to follow. Thus, if problems that precluded a lunar-orbital mission arose before translunar injection, an Earth-orbital mission would be conducted. The Earth Orbital Working Group was established to prepare plans for this alternative.

By launch time, a series of scientific tasks had been formulated and included in the flight plan. The instruments available for these scientific tasks were the following cameras and ancillary equipment carried in the command module:

1. One 16-mm Maurer data acquisition camera (primarily for operational sequence photography)
 - a. One 200-mm lens
 - b. One 75-mm lens
 - c. One 18-mm lens
 - d. One 5-mm lens
 - e. Nine magazines SO-368 color film (outdoor)
 - f. Two magazines SO-168 color film (high-speed interior)
2. Two 70-mm Hasselblad electric cameras
 - a. One 250-mm lens
 - b. Two 80-mm lenses
 - c. One magazine SO-121 color film (outdoor)
 - d. Two magazines SO-368 color film (outdoor)
 - e. Three magazines type 3400 black-and-white film (Pan-X)
 - f. One magazine type 2485 black-and-white film (high-speed)
 - g. One red-blue filter holder
 - h. One polarizing filter

- i. One 2A filter
- j. One 47B blue filter
- k. One 25A red filter
- l. One intervalometer (20-second interval)
3. One camera mounting bracket
4. One spotmeter (narrow-angle exposure meter)
5. One television camera

Briefing papers had been prepared covering phenomena that the crew should search for visually. Oral briefings on some of these subjects were inserted into the astronauts' crowded preflight schedule. It was clearly understood by everyone connected with the mission that the science tasks would be performed only on a "target of opportunity" basis. It was also apparent that the astronauts might be "overprogramed" and would have difficulty performing all of the tasks requested, even if no unexpected problems arose during the mission. The crew's performance was outstanding, although they were tired when they arrived in orbit. The lunar module pilot (LMP) did an excellent job of acquiring most of the lunar surface photography. Although the nighttime pass for astronomical photography was canceled because of crew fatigue, the command module pilot's (CMP) visual studies of an orbital sunrise were of scientific value. A summary of the proposed versus accomplished scientific tasks is shown in table 4-I.

PHOTOGRAPHIC OBJECTIVES

ROBERT O. HILL AND LEWIS C. WADE

Obtaining vertical and oblique overlapping photographs on at least two orbits was a primary photographic objective of the Apollo 8 mission. The purpose of the overlapping, or stereoscopic strip, photography was to provide a means for determining the positions of lunar far-side features in latitude, longitude, and elevation. The positions were to be determined with respect to the control points sighted with the sextant as a part of the lunar navigation task and with respect to selenographic control points on the front side established from Lunar Orbiter and telescopic photography. The results of these studies are covered in chapter 2. In addition, terminator-to-terminator photographs were to provide a means for relating points on the eastern limb of the Moon to features in the Apollo landing zone. Additional information

TABLE 4-I.—*Scientific Tasks Proposed for the Apollo 8 Mission*

Proposed	Accomplished
Take pictures or photographic sequences of approximately 50 targets of opportunity (of 185 targets identified, 50 were opportune for a Dec. 21 launch).	Approximately 30 of planned targets photographed.
Using intervalometer and bracket, photograph lunar terminator to terminator vertical stereoscopic strip.	Accomplished with excellent results.
Using intervalometer and bracket, photograph lunar oblique stereoscopic strip with color film.	Taken as vertical strip with black-and-white film and no stop changes; results enhanced by extended-range developing techniques.
Track and photograph a lunar landmark, using rotation of spacecraft for image motion compensation.	Accomplished.
Photograph lunar surface in earthshine.	Not attempted; however, surface detail visually distinguishable in both earthshine and Sun shadows.
Observe and photograph transient lunar surface phenomena.	None observed.
Photograph zodiacal light.	Not attempted.
Photograph solar corona.	Not attempted.
Photograph gegenschein.	Not attempted.
Use the spotmeter to verify preplanned lunar surface lens exposure schedule.	As predicted, spotmeter output of limited value for lunar surface exposures because of narrow view angle.
Obtain zero-phase-angle surface pictures.	Accomplished.
Red-blue surface study (use of dual filter holder to obtain evidence of color).	Not attempted until transearth injection; data unsatisfactory.
Take star-field photographs to aid in window contamination studies.	Not attempted.
Obtain translunar and transearth pictures of Earth.	Accomplished.
Use high-speed film to determine total film radiation dosage during the mission.	Accomplished.
Visually search for the following geologic phenomena:	Crew exceptional on visual observations:
Anomalous crater shapes.	Differences in crater shapes and apparent ages noted.
Volcanic evidence.	Area resembling volcanic flow noted.
Structure.	Possible faulting and collapsed volcanic pipes noted.
Transitory phenomena (light flashes, volcanic eruptions, phosphorescence, etc.).	Looked for; none observed.
Visually search for the following dim-sky phenomena:	Sunrise phenomena observed through tracking telescope.
Solar corona-zodiacal light.	Nothing observed.
Gegenschein-Moulton point.	Occultations noted; no evidence of atmosphere.
Atmosphere evidence by star occultation.	Looked for; not seen.
Visually search for evidence of the sunset horizon glow such as first seen by Surveyor.	Effects of rocket-motor operations and dumps noted.
Visually search for evidence of contamination.	

that was to be obtained from this photography included albedo data and an evaluation of near-terminator topographic analysis capability.

The areas to be covered by the stereoscopic strip photography were dependent on the day of launch. The photography was to consist of one pass with the camera optical axis near vertical and one pass with the camera optical axis inclined

20° from the vertical. The photographs were to be taken at 20-second intervals with a shutter speed of 1/250 second. The vertical pass was scheduled on the fourth revolution. In the flight plan, the landmark evaluation exercise preempted the last 20 minutes of photography that would have permitted camera operation all the way to the near-side terminator.

The convergent strip, using SO-368 color film, was scheduled for the ninth revolution. The camera was to be started 6 minutes after the far-side terminator and was to be operated to approximately longitude 60° E. In the flight plan, continuing the convergent stereoscopic strip to the near-side terminator was precluded by television activities scheduled for the ninth revolution.

On both passes, an extra exposure was to be manually triggered approximately every 5 minutes and the time of the exposure recorded. Both passes were to require a full magazine of film.

Photographic targets of opportunity are those recommended if time and circumstances permit their accomplishment. All lunar surface areas where Apollo 8 photographic coverage was desired were plotted on a Target of Opportunity Planning Chart. These recommended targets were launch-day dependent. To determine which targets can be photographed on a given launch date, it is necessary to determine the lunar lighting limits, the orbital inclination, and the spacecraft attitude during orbit. With these three basic parameters and by considering the position of the photographer in the spacecraft, targets were sequenced by revolution during lunar orbit. At the same time, camera lens and film combinations were determined. Changes in configuration of lens and film were kept to a minimum by this method.

To assist the crew, the data developed were printed on the Apollo Target of Opportunity Chart, which was carried on board the spacecraft. This chart also contained data for recommended film exposures (*f*-stop changes); regions to make spotmeter measurements; special symbols for non-sequenced targets, such as potential lunar transient events; and all supplemental data required to accomplish the recommended photography.

NOTES ON FILM SELECTION AND USE

JAMES L. DRAGG AND ROBERT O. HILL

Film type SO-368 has been used extensively during past manned missions for both 70-mm still and 16-mm sequence photography. Several factors entered into its selection for the lunar surface photography when a color emulsion was desired: past experience in exposing and processing, which gave a high confidence level; wide exposure lati-

tude; availability with Estar thin base; scheduled use in the 16-mm camera, which made possible the use of the same exposure settings with both 16-mm and 70-mm cameras; and high recommendation by personnel of the MSC Photographic Technology Laboratory. Film type SO-368 was scheduled for use during the ninth-revolution stereoscopic strip photography and for a limited number of targets of opportunity. In addition, use of this emulsion was planned for operational photography of the S-IVB and for Earth photographs. Two magazines of 70-mm and nine of 16-mm SO-368 were on board.

Kodak Panatomic X aerial film, type 3400 (Estar thin base), is a panchromatic negative film that has high contrast and extended red sensitivity. The high acutance and very high resolution of this film favor a small-negative format. It is rated at 65 lines/mm on 1.6:1 contrast targets, 60 percent better than the resolution quoted by Kodak for Plus X aerial film, type 3401 (Estar thin base), which was also recommended.

The Panatomic X film was selected for the following reasons: (1) it possessed maximum resolution consistent with lunar-surface exposure requirements, which indicated a shutter speed of 1/250 second to eliminate image motion; (2) it was available on Estar thin base; (3) it yielded exposure values roughly consistent with other selected emulsions; and (4) black-and-white film was preferred over color film for lunar photometric studies.

The SO-121, slower speed, high-definition, color-reversal film (Estar thin base) was used quite successfully for the Apollo 6 strip photography. Its advantage over SO-368 is that it has about twice the resolution. The exposure latitude is not as great as that of SO-368; thus, it was not deemed as desirable for lunar surface photography. The SO-121 film was carried on Apollo 8 because (1) it represents maximum resolution for color-reversal emulsions; (2) it was primarily intended for use in Earth orbit in the event that Apollo 8 remained there; (3) it was available on Estar thin base; and (4) the exposures were consistent with other onboard films.

Kodak 2485 high-speed recording film (Estar-AH base) is an extremely high-speed panchromatic film with extended red sensitivity. It was selected for the Apollo 8 mission for possible

photography of various astronomical phenomena (gegenschein, zodiacal light, stars, and solar corona), the lunar surface in earthshine, and other low-light-level subjects. An emulsion with as high a speed as possible compatible with the predicted radiation dosage, 0.5 rad, was required. The Kodak 2485 film was selected primarily because of its high speed. Also, it was available on 4-mil base (which proved to be compatible with the Hasselblad thin-base film magazine), and it appeared to be compatible with the radiation expected on Apollo 8.

USE OF TYPE 2485 FILM

L. DUNKELMAN AND ROBERT O. HILL

The fastest lens on board the spacecraft was the $f/2.8$ standard 80-mm lens used with the Hasselblad camera. While a lens of approximately $f/1$ would have been much more suitable, it was determined from ground-based photography that exposure times of 90 seconds would be acceptable. This determination was made from (1) the results of experiments in which daytime photographs of the faint dayglow and of stars were obtained with type 2485 film from an Aerobee rocket, and (2) determinations from ground-based photography taken during clear, moonless nights at Greenbelt, Md., and at Flagstaff, Ariz., of the region of the sky (Gemini and neighboring Milky Way) where the antisolar point would be during the Apollo 8 mission.

The flight film was precalibrated 3 days before the launch of Apollo 8 by photographing, with the flight camera, a calibrated nine-step gray target, the luminance of which ranged from 1×10^{-13} to 1×10^{-11} of the brightness of the solar surface. The faintest portions of the gray scale included luminances well below that of the gegenschein in order to provide for quantitative analysis of the most critical of the possible astronomical observational tasks.

During the planning stage for Apollo 8, a calculation based on the predicted radiation environment for the December 21, 1968, launch gave 0.5 rad as an upper limit. The energy spectrum indicated that more than 99 percent of the radiation would consist of energetic protons. Film data produced by the manufacturer of type 2485 film indicated 0.4 as the upper limit of density

increase that would be caused by this level of radiation. The head and tail portions of the returned flight film were developed at the NASA Manned Spacecraft Center by using the procedures established prior to flight; namely, D-19 developer at 75° F for 12 minutes in a small tank. The Hurter-Driffeld curves of the flight and control film have been compared. The measured radiation of approximately 0.2 rad simply raised the flight film calibration curve by 0.18 density. There was no appreciable effect on the detectable threshold of the faintest calibration exposures.

CALIBRATION INFORMATION

JAMES DAVIS AND ALAN WELLS

INTRODUCTION

This section presents manufacturing specifications and tolerances, along with performance parameters measured at the factory prior to delivery, for the electric Hasselblad camera assemblies. Some of the measured parameters were obtained from a typical lens; others were obtained from the flight hardware. Some parameters were merely checked to insure conformity with tolerances, and the measured values were not recorded.

SPECIFICATIONS AND TOLERANCES

Specifications and tolerances for the Planar $f/2.8$, 80-mm lens included the following:

1. Flange focal distance (FFD), 74.90 ± 0.02 mm.
2. Calibrated focal length (CFL), 79.9 ± 0.8 mm.
3. Relative aperture, $f/2.8$ (± 3 percent).
4. Average spectral transmittance over the range 400 to 700 millimicrons, 80 percent minimum.
5. Field of view, 37.9° side and 51.8° diagonal.
6. Relative illumination at 22° field angle at full aperture, 35 percent minimum; at $f/11$, 75 percent minimum.
7. Sine-wave modulation transfer factors (MTF) at 20 cycles/mm, full aperture (mean between tangential and radial image elements), minimum on axis, 0.50; minimum at 22°, 0.35.

Aperture tolerances are shown in table 4-II, and nominal versus effective exposure times for

TABLE 4-II.—Planar $f/2.8$, 80-mm Lens Aperture Tolerances

f -stop	Equivalent circular diameter, mm
2.8.....	21.20 (± 5 percent)
4.....	14.99 (+12.25 percent, -10.56 percent)
5.6.....	10.60 (+12.25 percent, -10.56 percent)
8.....	7.50 (+12.25 percent, -10.56 percent)
11.....	5.30 (+12.25 percent, -10.56 percent)
16.....	3.75 (+12.25 percent, -10.56 percent)
22.....	2.65 (+14.90 percent, -12.83 percent)

TABLE 4-III.—Planar $f/2.8$, 80-mm Lens Shutter

Nominal exposure time, sec	Effective exposure time, msec ^a
1/500	2.15
1/250	4.11
1/125	8.01
1/60	15.83
1/30	31.50
1/15	62.70
1/8	125.2
1/4	250.2
1/2	500.2
1	1000.2

^a ± 10 percent.

the between-the-lens shutter are given in table 4-III.

No specific tolerance information is available for the Sonnar $f/5.6$, 250-mm lens, but it provides three times more magnification than the 80-mm lens; has relative apertures of $f/5.6$, $f/8$, $f/11$, $f/16$, $f/22$, $f/32$, and $f/45$; has the same type shutter as the 80-mm lens; and has a field of view of 12.5° side and 17.6° diagonal.

MEASUREMENTS FROM A TYPICAL LENS

The following information is based on measurements using a Planar $f/2.8$, 80-mm lens, serial number (S/N) 4289861, and must be considered the best available to date since measurements of these parameters were not made on the flight lenses. Figure 4-2 shows the spectral transmittance curve for this lens. No information is available concerning measurement method or accuracy.

Figure 4-3 shows the relative illumination curve for this lens. The curve for $f/11$ resembles the cosine⁴ degeneration curve, but it is generally slightly higher. The curve shown for $f/2.8$ should be the composite curve of cosine⁴ degeneration and vignetting effects. Information for the curves at the other relative apertures was not supplied by the manufacturer. If there is no vignetting,

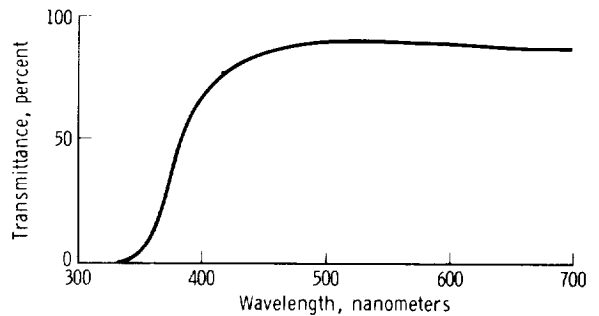


FIGURE 4-2.—Spectral transmittance curve for Planar lens, S/N 4289861.

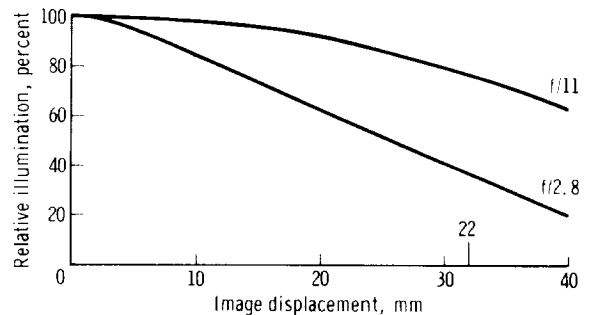


FIGURE 4-3.—Relative illumination curve for Planar lens, S/N 4289861.

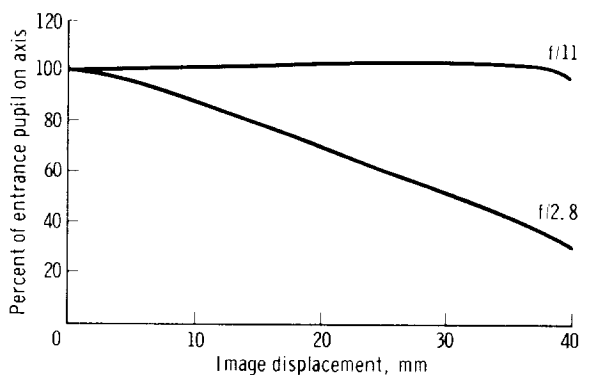


FIGURE 4-4.—Effective area of entrance pupil in percent of the entrance pupil on axis for Planar lens, S/N 4289861.

of 79.87 ± 0.08 mm. For distortion relative to the principal point of autocollimation (PPA), see figure 4-5. Sine-wave MTF at the spatial frequency of 20 cycles/mm for various image

field positions is given in figures 4-6 and 4-7. Nominal versus effective exposure times for the Compur CS-1210-722 shutter, S/N 177, are given in table 4-IV.

The CFL of the Planar $f/2.8$, 80-mm lens is 79.95 ± 0.08 mm. For distortion relative to the PPA for full aperture, see figure 4-8. Sine-wave MTF at 20 cycles/mm for various image field positions is given in figures 4-9 and 4-10.

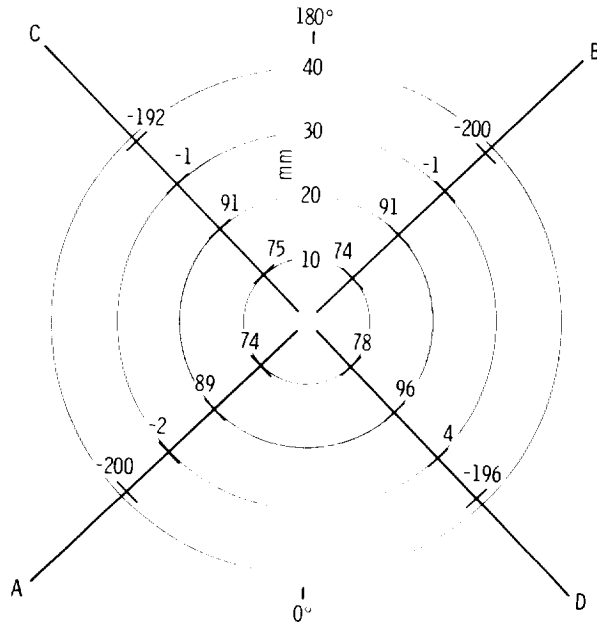


FIGURE 4-8.—Distortion μ relative to PPA for $f/2.8$, view from rear, positive direction away from center, for Planar lens, S/N 4488999.

TABLE 4-V.—*Exposure Times for Compur Shutter, S/N 175*

Nominal exposure time, sec	Effective exposure time, msec *
1/500	2.33
1/250	4.05
1/125	7.95
1/60	15.41
1/30	28.04
1/15	55.48
1/8	122.4
1/4	250.8
1/2	505.4
1	928.0

* Average of 10 releases.

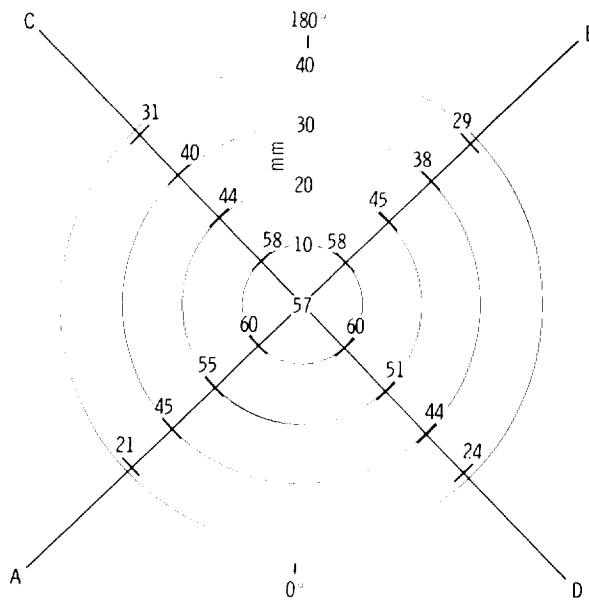


FIGURE 4-9.—Sine wave MTF at 20 cycles/mm for radial image components, percent, for Planar lens, S/N 4488999.

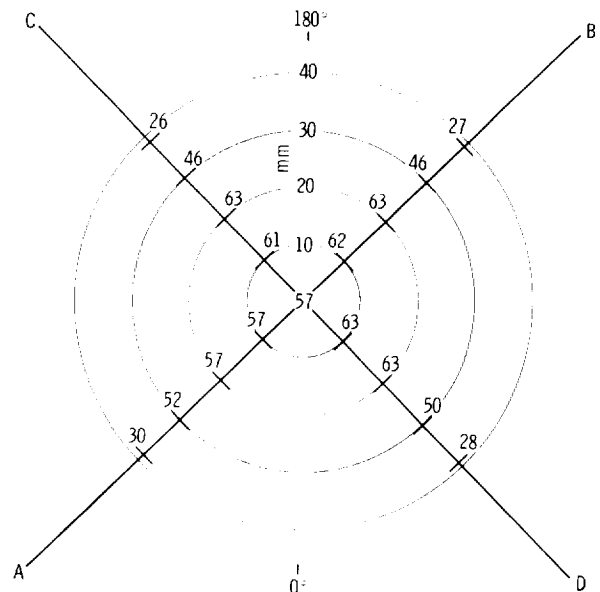
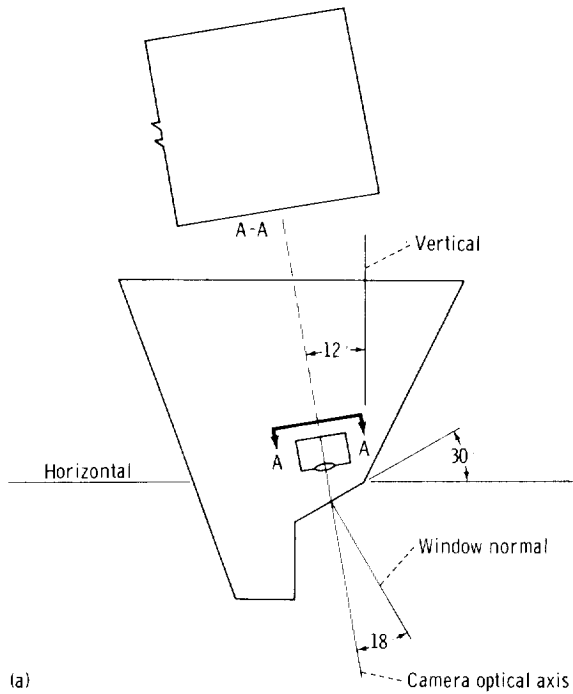
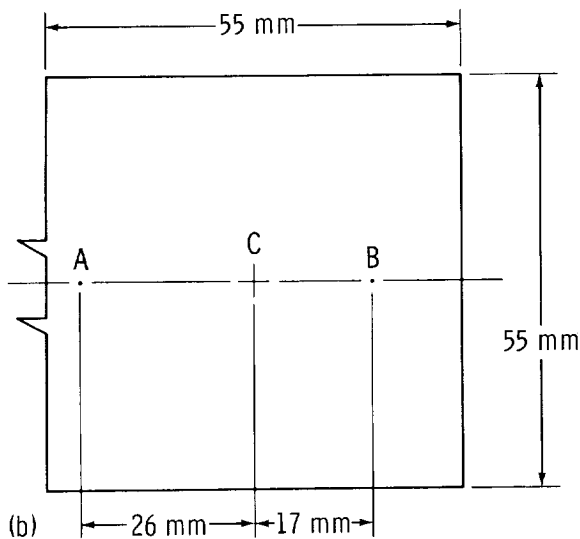


FIGURE 4-10.—Sine wave MTF at 20 cycles/mm for tangential image components, percent, for Planar lens, S/N 4488999.

For nominal versus effective exposure times for the Compur CS-1210-722 shutter, S/N 175, see table 4-V.



(a)



(b)

FIGURE 4-11.—Relationship of bracket-installed Hasselblad camera to spacecraft window. (a) Configuration, (b) resulting image formation.

SPECTRAL TRANSMITTANCE OF THE LENS/WINDOW COMBINATION

Figure 4-11 shows the relationship of the electric Hasselblad camera to the spacecraft window when the camera is installed in the bracket. The spectral transmission of the window varies with the incidence angle of the impinging light. Spectral transmittance curves for the window are available for incidence angles 0° and 45° . The spectral transmittance curve for the camera lens, on-axis, is available. Spectral transmittance of the lens, off-axis, can be obtained by multiplying the on-axis curve by the relative illumination factor for the desired off-axis angle (field angle). The spectral transmittance of the lens/window system is shown in figure 4-12 for window incidence angles 0° and 45° . Data are being obtained for window transmission at each 5° . The condition of 0° incidence on the spacecraft window results in the formation of the image at point A in the film format (fig. 4-11(b)). The corresponding lens field angle is 18° . In the same way, a 30° angle of incidence at the window

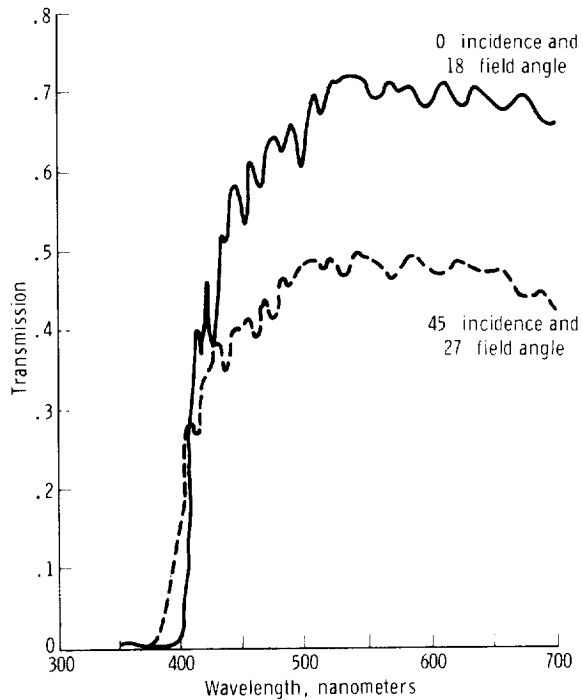


FIGURE 4-12.—Transmission versus wavelength for lens/window combination (80-mm focal length, $f/11$).

produces an image at point *B*, at 12° field angle. The on-axis image point *C* is formed by light at an 18° angle of incidence on the window.

For all the points just discussed, the window incidence angle and the lens field angle are both in the same plane. The plane also contains the camera optical axis and is mutually perpendicular to the window and to the film plane.

For points to either side of line *A-B* in figure 4-11(b), each of the two angles is in a different plane; and the solution for the locus of points in the film plane which satisfies the same conditions as, for example, point *B*, is a complex problem in geometry. For points in the corners of the format near point *B*, the window incidence angle approaches 45°.

Common points which satisfy given conditions occur in pairs, symmetrical about line *A-B*. A correction matrix could be formed for one-half of the image format, which is valid for the other half if mirrored. However, each point in the matrix is unique, requiring the solution of a different complex geometrical problem, involving compound angles, for each point. To obtain a suitable density of points in the correction matrix would require a large number of computations.

FILM SENSITOMETRIC CALIBRATION

JAMES L. DRAGG

The Apollo 8 photography affords the first opportunity for analyses of the intensity and spectral distribution of lunar scene light free from modulation caused by atmospheric effects (Earth telescopic photography) and by electronic transmission and reconstruction (Ranger, Surveyor, and Lunar Orbiter). To provide for these analyses, a series of sensitometric strips was exposed onto the flight film and related film, allowing the extraction of quantitative information relating film densitometric measures to exposure values.

Assistance in establishing the sensitometric requirements was provided by the MSC Photographic Technology Laboratory, which also provided for the placement of the sensitometry and subsequent original negative film measurements and has been of valuable assistance to sensitometric analyses.

The primary function of a calibration sensitometric strip is to reconstruct the density (*D*)

versus exposure (*E*) relationship (*D* log *E* or Hurter-Driffield—H and D—curve) which pertains to the specific processing chemistry, temperature, and processing time for the flight film and subsequent duplication printing. Contingencies allowing for lunar photography, Earth photography, and lunar photography with the red (29) and blue (47B) filters were considered in establishing sensitometric requirements for Apollo 8 film types 3400, 2485, SO-121, and SO-368.

The spectral distribution of light reflected from the Moon was approximated by addition of filters nos. 80A and 82 to the 2850° K sensitometer illuminant to convert to an approximately 4750° K source. Daylight sensitometry was provided by application of a Corning 5900 filter to the sensitometer illuminant to convert to a color temperature of approximately 5600° K. Sensitometric strips with red and blue filters utilized the 4750° K source. No provision was made for the spectral transmission of the camera lens and spacecraft window. However, all sensitometric exposures used a Wratten 2B filter to simulate the cutoff of the spacecraft window. Sensitometry was performed through a carbon step wedge of 21 steps. Values for the steps

TABLE 4-VI.—*Density of Carbon Step Wedge*

Step	Density
0	0
1	.15
2	.33
3	.48
4	.62
5	.77
6	.93
7	1.08
8	1.24
9	1.38
10	1.54
11	1.70
12	1.86
13	2.00
14	2.16
15	2.34
16	2.49
17	2.65
18	2.81
19	2.98
20	3.14

are listed in table 4-VI. Actual sensitometry applied to the films was as indicated in table 4-VII.

Provision was made for head-versus-tail, premission-versus-postmission, and stored-versus-flight-film comparisons of sensitometry at 4750° K. Sensitometric data on original negatives for

magazines C, D, and E have been supplied by the Photographic Technology Laboratory. Some comparative results ($D \log E$ curves) are shown in figures 4-13, 4-14, and 4-15.

The differences observed between sensitometric strips and control strips in figure 4-14 are larger than would be expected. However, all

TABLE 4-VII.—Magazine Sensitometric Strips

Magazines	Strip no.	Where exposed	When exposed	Filters	Absolute log E , step 11
A and F.	1	Head	Premission	80A, 82, 2B	$\bar{2}.82$
	2	Head	Premission	C5900, 2B	$\bar{2}.87$
	3	Tail	Postmission	80A, 82, 2B	$\bar{2}.82$
B.	1	Head	Postmission	80A, 82, 2B	$\bar{2}.82$
	2	Head	Premission	80A, 82, 2B	$\bar{2}.82$
	3	Head	Premission	C5900, 2B	$\bar{2}.87$
C and E.	1	Head	Postmission	80A, 82, 2B	$\bar{2}.82$
	2	Head	Premission	80A, 82, 2B, 47B	$\bar{2}.45$
	3	Head	Premission	80A, 82, 2B, 29	$\bar{2}.75$
	4	Head	Premission	80A, 82, 2B	$\bar{2}.82$
	5	Head	Premission	C5900, 2B	$\bar{2}.87$
D.	1	Head	Postmission	80A, 82, 2B	$\bar{2}.82$
	2	Head	Premission	80A, 82, 2B, 47B	$\bar{2}.45$
	3	Head	Premission	80A, 82, 2B, 29	$\bar{2}.75$
	4	Head	Premission	80A, 82, 2B	$\bar{2}.82$
	5	Head	Premission	C5900, 2B	$\bar{2}.87$
	6	Tail	Premission	80A, 82, 2B	$\bar{2}.82$

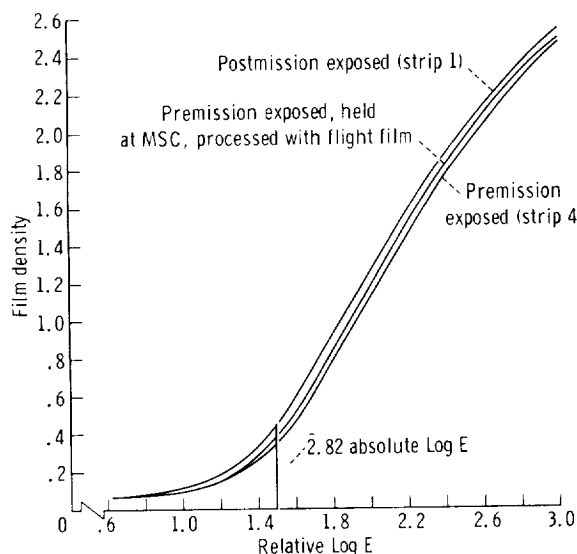


FIGURE 4-13.— $D \log E$ curves for Apollo 8 magazine E original negative.

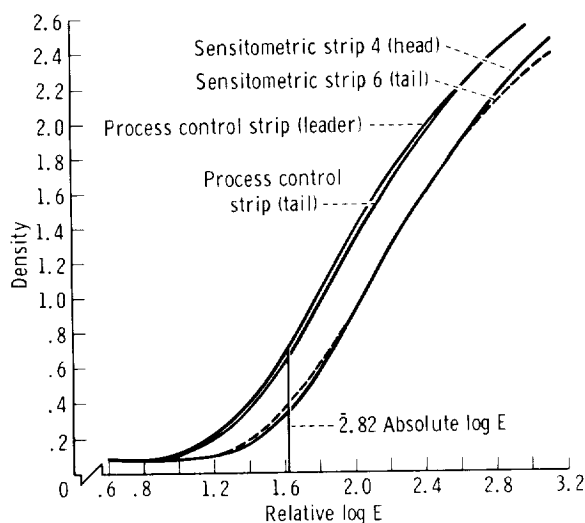


FIGURE 4-14.— $D \log E$ curves for Apollo 8 magazine D original negative, comparing sensitometric strips and process control strips.

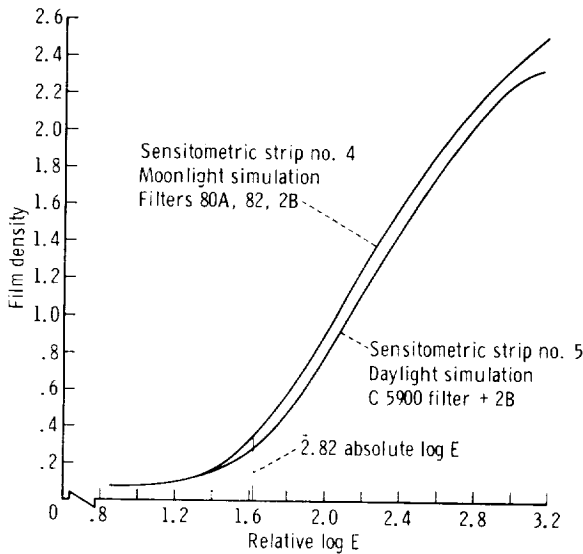


FIGURE 4-15.— $D \log E$ curves for Apollo 8 magazine D original negative.

results have not yet been received, and analyses are continuing. The use of the premission exposures with 80A, 82, and 2B filters are currently recommended for photometric reductions.

CAMERA EXPOSURE CALCULATIONS

GEORGE R. BLACKMAN

The relative aperture settings were determined preflight for use with the 70-mm film types and were applicable for the 80-mm lens, and for the 250-mm lens up to and including the $f/5.6$ aperture, which is the largest that can be used. These data were printed on the photographic Target of Opportunity Chart with the f -stop changes indicated as a function of selenographic longitude. Although underexposures were expected near the terminators, it was decided that the shutter rate should remain fixed at 1/250 second. At slower shutter speeds, loss of image resolution could be expected because of image smear. With the wide latitude inherent in the film types selected, adequate exposure control could be maintained with aperture regulation only.

Three sets of f -stop changes were recommended to correspond to each of the general

camera-pointing orientations: vertical, east and west oblique on groundtrack, and north and south oblique off track.

Computing the exposures (f -stops) involved two operations:

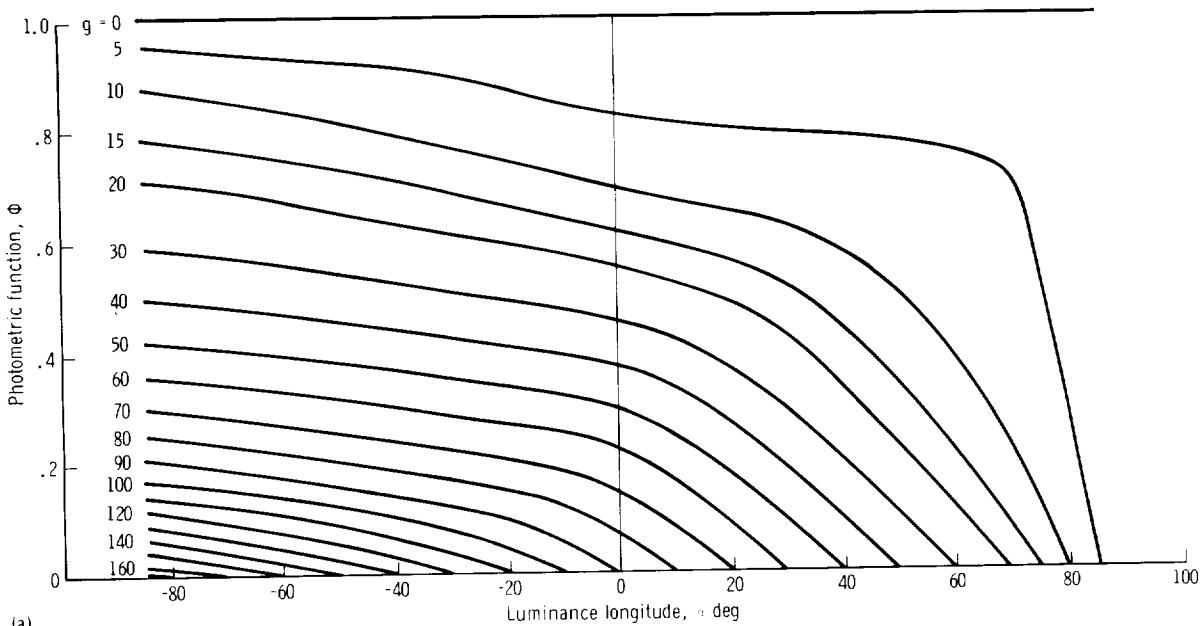
1. Prediction of the average value and range of the film-plane illumination (exposure) for each condition of solar illumination/viewing geometry and surface albedo to be encountered.

2. Evaluation of the sensitivity of each film type to the predicted illumination and subsequent selection of the appropriate camera setting required to achieve the optimum exposure at the film plane.

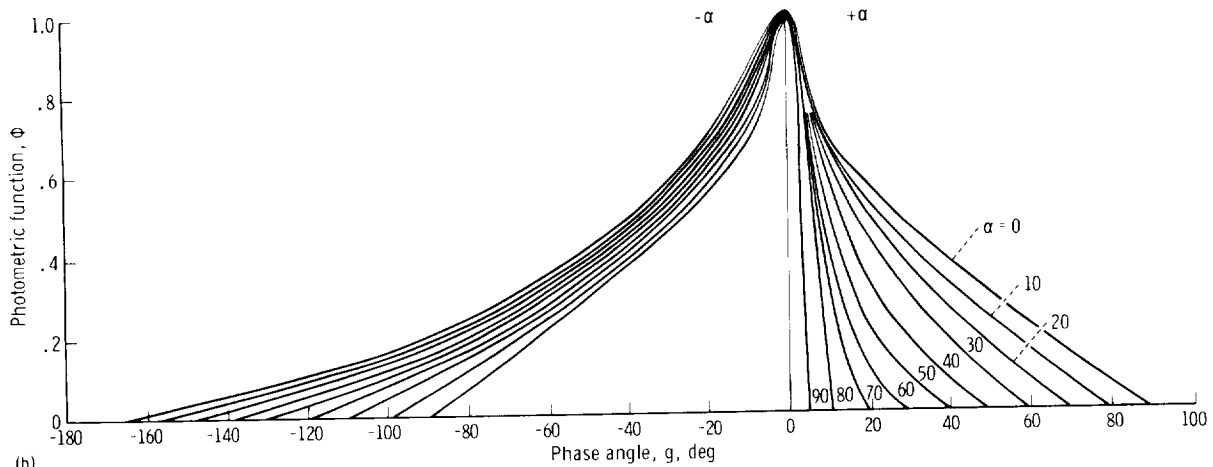
A matrix of exposure values was generated that accounted for all possible combinations of camera/scene conditions. These conditions were treated as $E = STt\rho\phi/4f^2$, where E is the exposure in meter-candle-seconds (m-cd-s), S is the average solar illumination at the surface in meter-candles (m-cd), T is the percent transmittance of the lens and spacecraft window, t is the shutter speed in seconds, ρ is the surface albedo, ϕ is the lunar photometric function, and f is the relative aperture. Values used for Apollo 8 were 14×10^4 m-cd for S , 0.747 for T , and 0.004 second for t . The relative aperture was variable, with full stops from $f/2.8$ to $f/16$. The percent of albedo ρ varied from 0.05 to 0.25, and ϕ varied from 0 to 1.0.

For each scheduled photographic target, the solar illumination/viewing geometry was computed for entry into the lunar photometric function (fig. 4-16), and the albedo noted from existing data. Since albedo data were not available for the lunar back side, those values were derived through the correlation of brightness measurements from front- and far-side Lunar Orbiter photography and controlled to the existing albedo data applicable to the front side. By referring to the locations of these two values in the matrix (photometric function and albedo), the predicted film plane exposure could be determined for each of the camera stops ($f/2.8$ to $f/16$). The next step was to decide which of these f -stops should be used for each particular scene as dictated by the sensitivity of the specified film type.

The film response (sensitivity) to the incident exposure was derived through analysis of plots



(a)



(b)

FIGURE 4-16.—Photometric function. (a) ϕ versus α (JPL), (b) ϕ versus g (JPL).

of density D versus the logarithm of the exposure ($D \log E$ curves) resulting from the controlled exposure and processing of calibrated sensitometric strips on the same film types to be used during the mission (figs. 4-17 to 4-19).

The analysis for each film type was conducted as follows. First, it was determined that the range of exposure that could be expected from a given lunar scene would not exceed $2\frac{1}{2}$ stops. The latitudes of the film types were found

to provide the adequate tolerance necessary to record all surface detail in any one scene, dependent only on the provision that a suitable minimum level of intensity entered the system. Four stops for the 3400 (black and white) film and SO-121 color film and five stops for the SO-368 color film were found to be the latitude ranges of the films. Consequently, the f -stop selected for a given scene could be off by as much as one full stop on either the 3400 or SO-121

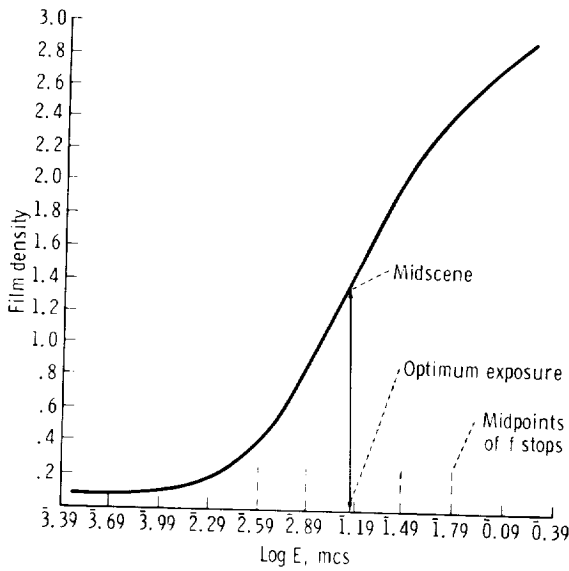


FIGURE 4-17.— $-D \log E$ curve for 3400 film.

films or by $1\frac{1}{2}$ stops on the SO-368 film and still suitably record all the information within the scene.

The next step was to decide, within the range of exposures to which the film is sensitive, the exposure value which most closely defined the

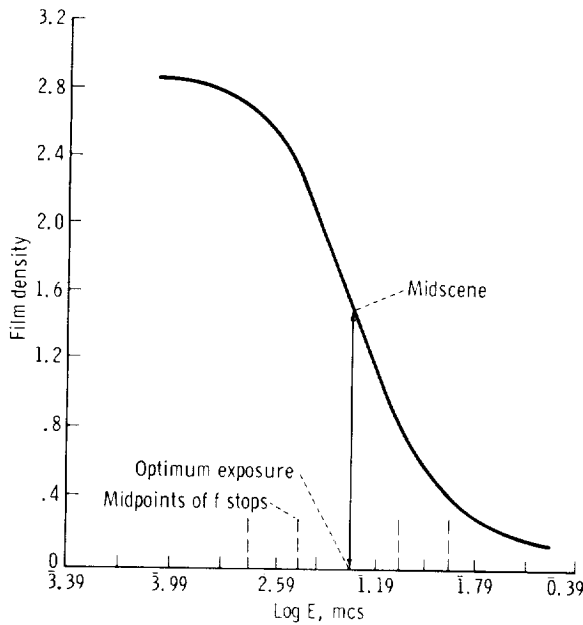


FIGURE 4-18.— $-D \log E$ curve for SO-121 film.

inflection point between overexposure and underexposure. Again, if the appropriate f -stop is chosen, this value could be correlated to the average brightness of the lunar scene (midscene exposure). The $\log E$ midscene values determined for each of the films are $\bar{2}.89$ for SO-368, $\bar{1}.00$ for SO-121, and $\bar{1}.19$ for 3400.

The f -stops were selected by relating back to the computed exposure matrix and treating the scheduled photographic targets individually. The selected f -stops were those that represented exposure values nearest to those of the midscene values derived for the specified film type.

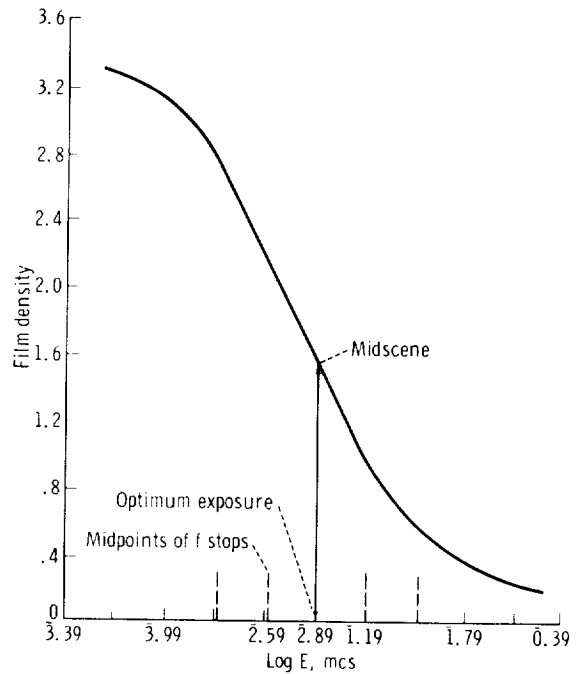


FIGURE 4-19.— $-D \log E$ curve for SO-368 film.

For the vertical and ontrack oblique stereoscopic strips, the midscene exposures progressed as a symmetrical curve of near-zero value at the terminators and increased to maximum value at that point on the groundtrack nearest the subsolar point. Only differences in the surface albedo caused local fluctuations in the smooth progression of the curve. For those cases, determining the f -stop change points was straightforward and considerably more accurate than was the case with the targets of opportunity (north and south obliques).

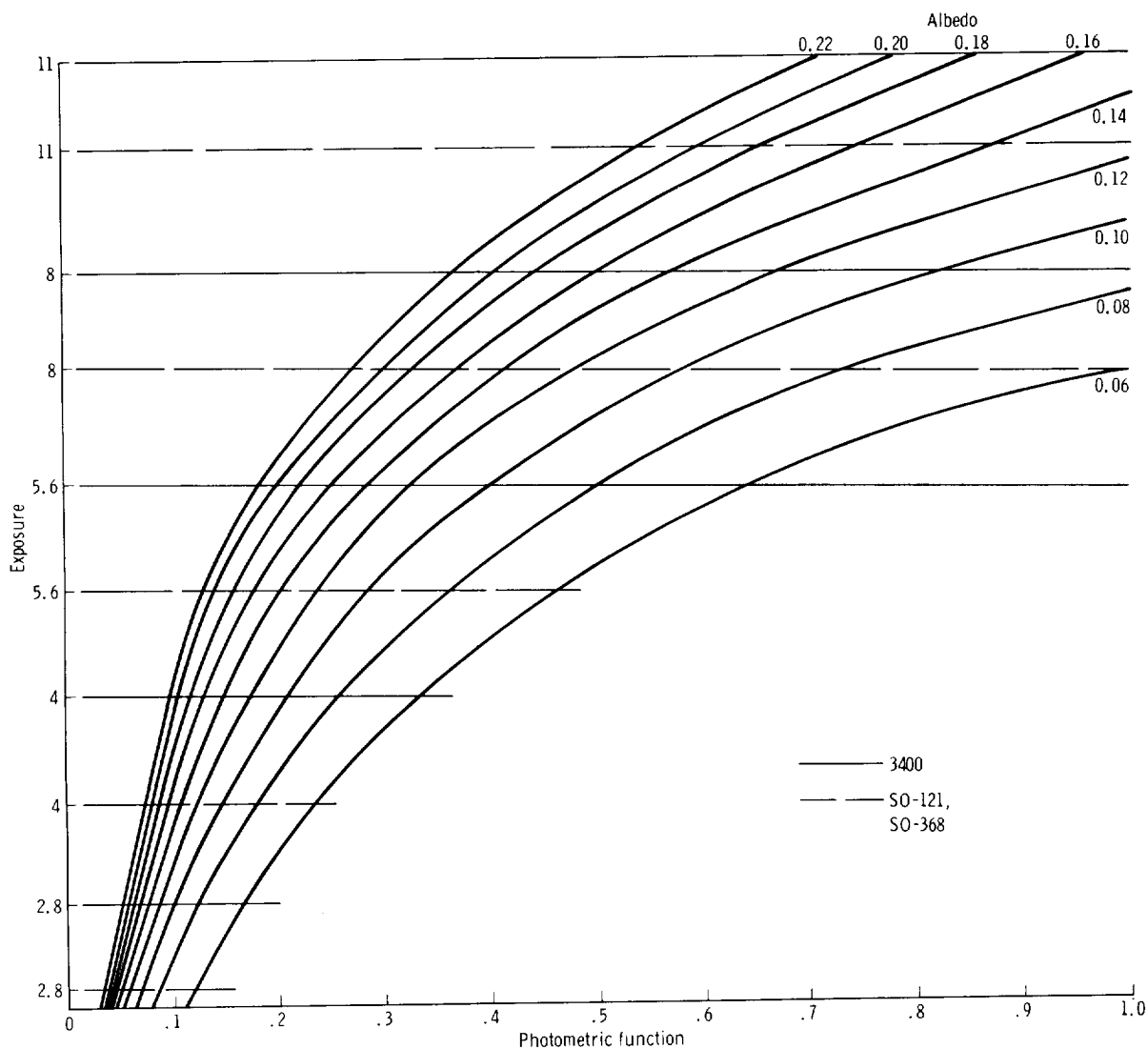


FIGURE 4-20.—Exposure matrix.

The stops for the targets of opportunity were calculated in essentially the same manner. Unfortunately, it is not possible to compile one set of exposure-change points that would apply to all targets north and south of the ground-track. Extreme differences in scene brightness occur when the camera pointing angles are in any plane other than one that is approximately parallel to the plane containing the solar illumination vector and the subsolar point. This is especially critical within the region bounded by $\pm 35^\circ$ of longitude from the subsolar point. Some compromise had to be made. Many instances

existed where, on one revolution, a target close to the groundtrack required an $f/8$ exposure; and, on a later revolution, a target some distance off track, but at approximately the same longitude, would require an $f/2.8$ exposure. For cases of this nature, an intermediate stop was chosen biased toward the more important of the two targets. Dependence was made on the wide latitude of the film to salvage the greater part of each of the two images.

The capability was established for providing f -stop values in real time by translating the exposure matrix into a graph (fig. 4-20) and

instituting techniques for determining the scene geometry from 1:5 000 000-scale maps. The f -stop change locations were superimposed on the graph; and, consequently, the appropriate selection could be determined directly as a function of the photometric function and albedo that applied to any given target. Procedures were established and simulated for revising the entire set of exposure recommendations that were on the flight chart if an off-nominal situation should occur.

EXPOSURE EVALUATIONS

JAMES L. DRAGG AND HAROLD L. PRIOR

Questions have arisen from Apollo 8 as to whether multiple aperture settings are required and whether high- or low-gamma processing is desired. To investigate these alternatives and also to evaluate the exposures obtained, a task was initiated to examine the exposures of magazines C, D, and E. All three magazines are type 3400 black-and-white film. Second-generation master positives were obtained for the evaluation. Each magazine was evaluated by

scanning each frame¹ with a McBeth TD 102 densitometer for minimum, maximum (exclusive of shadow), and average visual diffuse densities. The average was taken of six points distributed over the frame. The maximum was generally near one of the frame corners where lens transmission was least. All densities are correlated for relative exposure against the preexposed sensitometric strip, approximating a 4750° K source with a Wratten 2B filter. Correlation against the original negative was performed by reference to sensitometric curves supplied by the Photographic Technology Laboratory.

Magazine C

Magazine C includes the second, or forward-looking, pass of the stereoscopic strip photography in which a real-time decision was made by the Apollo 8 crew to bracket-mount the camera and expose at a constant aperture of $f/5.6$. To

¹ Earth, full-Moon, and low-horizon photographs were not evaluated. Also, several frames of magazine E were too dense on the positive for evaluation.

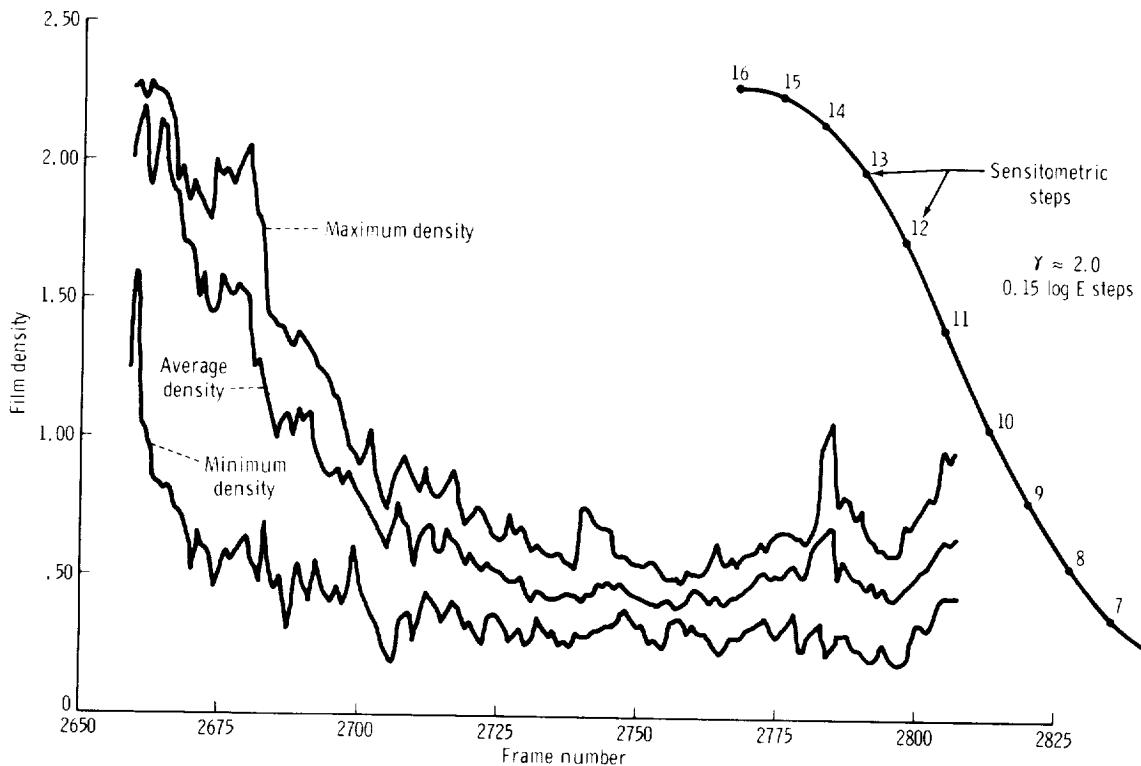


FIGURE 4-21. ---Density versus frame number for Apollo 8 magazine C master positive.

allow for the deviation from planned multiple aperture settings and provide maximum probability for image recovery, the Photographic Technology Laboratory deviated from the planned high-gamma processing and processed this magazine at low gamma. The density plots of magazine C are shown in figure 4-21. A shift in *D*-max occurred at the termination of the stereoscopic strip at frame 2740. Discounting shadow, all but the first few near-terminator frames are well exposed. Correlation to the original negative (fig. 4-22) shows all frames from 2667 to 2807 are recovered on essentially the "straight line" portion of the curve. The maximum exposures of all frames are well recorded, and two full stops and possibly more² were available on the linear-

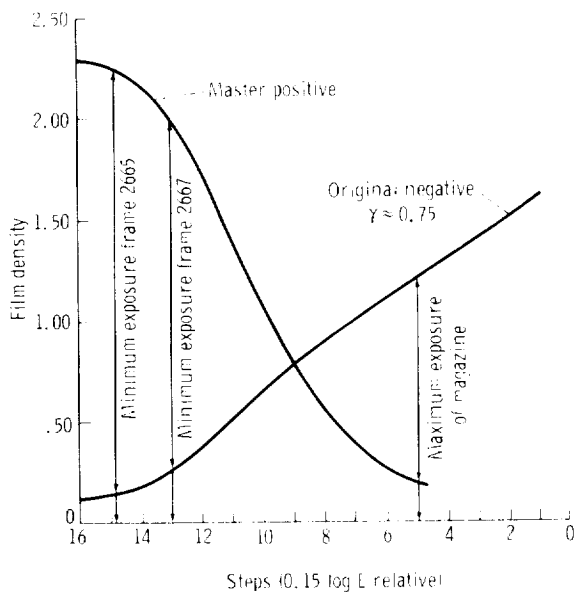


FIGURE 4-22.—Density versus steps for Apollo 8 magazine C.

² Data from the Photographic Technology Laboratory indicate a relatively straight-line-portion usefulness up to a density of about 2.1 on the original, or a total of about 10 stops.

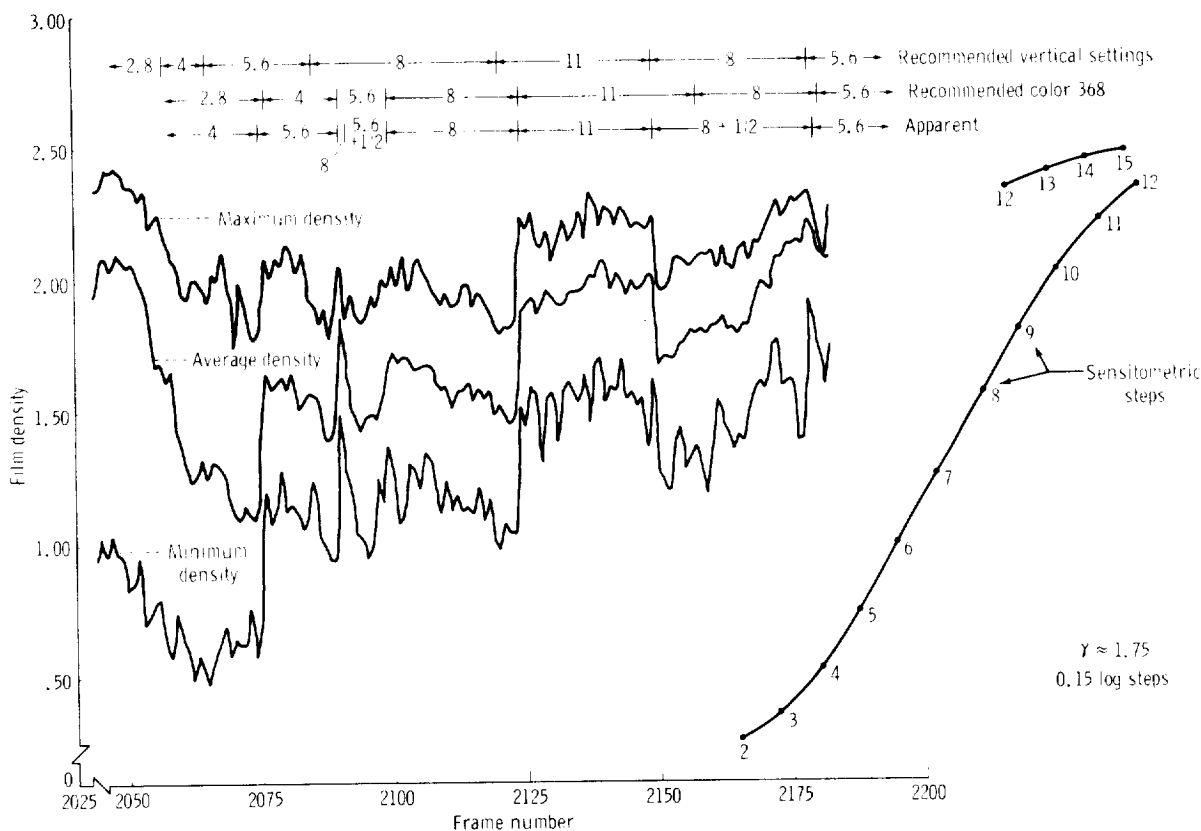


FIGURE 4-23.—Density versus frame number for Apollo 8 magazine D master positive.

response portion of the curve at the maximum exposure end. It is noted that all of the imagery fell into a relative log E range of 1.65, or about 5.5 stops, and also that 75 percent of the imagery fell within a relative log E range of 0.8, or about 2.7 stops. Therefore, it is concluded that this magazine could have been exposed at either $f/4$ or $f/2.8$ and have maintained linear response at the maximum exposure end. This, then, might have produced a beneficial effect on the near-terminator photography.

Magazine D

Magazine D includes the vertical stereoscopic strip pass and was processed at high gamma according to premission planning. The high-gamma processing was principally planned to accommodate the planned red-blue filter photographs where very small exposure differences were to be measured and correlated. The plot (fig. 4-23) of the densities of magazine D reveals several interesting factors. Correlation of verified aperture changes to the mission map gives clear evidence that aperture changes were made at

locations specified for the recommended forward-looking color film (SO-368) pass as opposed to the recommended vertical 3400 pass, which was exercised. The exception was in the change from $f/11$ to $f/8$, which occurred as recommended. The recommended change from $f/8$ to $f/5.6$ occurred at the same location for both and was apparently exercised as recommended. It is also apparent that half-stop apertures were used. The apertures shown in figure 4-23 are the apparent ones used, although absolute exposure uncertainty might shift all apparent stops potentially as a unit by up to one stop. Assuming the apparent apertures are correct, an adjustment has been applied³ for each frame to place it at the planned exposure levels, as shown in figure 4-24. Note that the exposures are now more uniform, with the primary exception being the $f/11$ sequence. A deliberate bias was planned for this sequence, which includes zero-phase photography, to insure proper exposure of zero phase (in view

³ No correction has been applied resulting from changes in lens transmissions at different apertures.

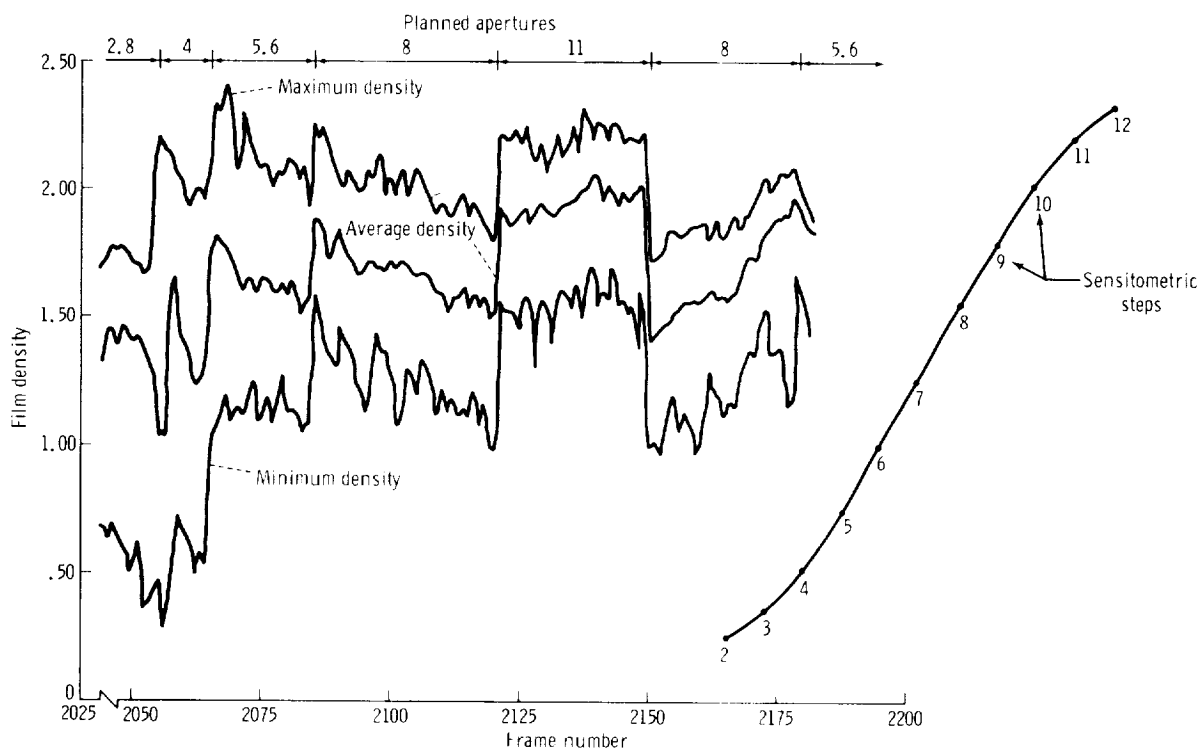


FIGURE 4-24. —Apollo 8 magazine D master positive exposures corrected to reflect planned apertures.

of uncertainties in the photometric function at zero phase) and to allow for potentially high albedos on the lunar far side. No degradation in the imagery occurred as a result of the apertures used, however, and all frames (except near-terminator frames) are adequately recorded in the linear-response portion of the film, as indicated in figure 4-25. To compare the effect of magazine D viewing geometry against magazine C, all frames from magazine D have been adjusted in exposure (fig. 4-26) to reflect the condition of those images taken at a constant $f/5.6$ aperture, as was magazine C. The results are compared (fig. 4-27) against the high-gamma process of magazine D and the low-gamma process of magazine C. Maximum exposures would have been recorded in the linear-response portion of either film process. The low-gamma process would have yielded significantly better exposures near the terminator. It would also appear that sufficient film latitude was available to expose

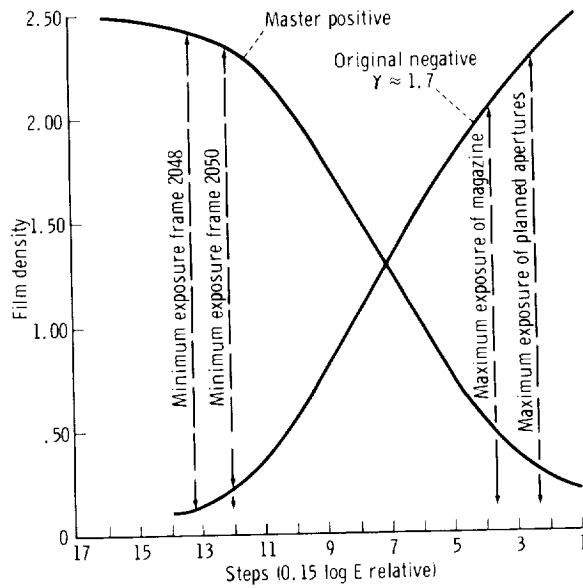


FIGURE 4-25.—Density versus steps for Apollo 8 magazine D.

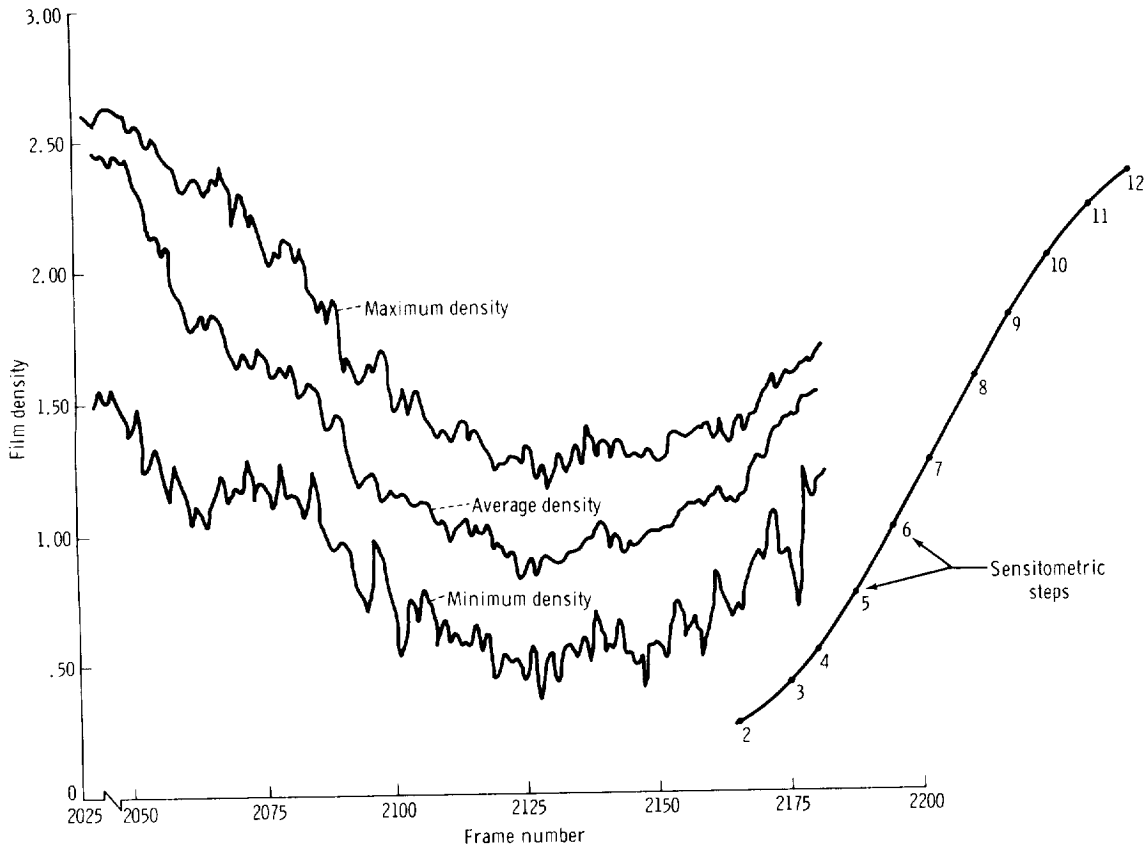


FIGURE 4-26.—Predicted densities of Apollo 8 magazine D exposed at constant $f/5.6$ aperture.

at $f/4$ with high-gamma processing and to $f/2.8$ with the low-gamma process.

Magazine E

Magazine E was used for target-of-opportunity coverage and processed at high gamma. On the positive used, several frames were too dense for the type of analysis that was performed. Other frames are plotted in figure 4-28. Exposures are not correlated back to the original negative, but this can be approximately accomplished by reference to the magazine D original curve of figure 4-27. The planned targets of opportunity are well recorded in the linear portion of the response curve. Other sequences near the terminator have adequate response in the bright areas, but may be underexposed in the darker areas. The training sequence was apparently underexposed in the earlier portions but was properly exposed when the exposure time was adjusted to 1/60 second at frame 2300.

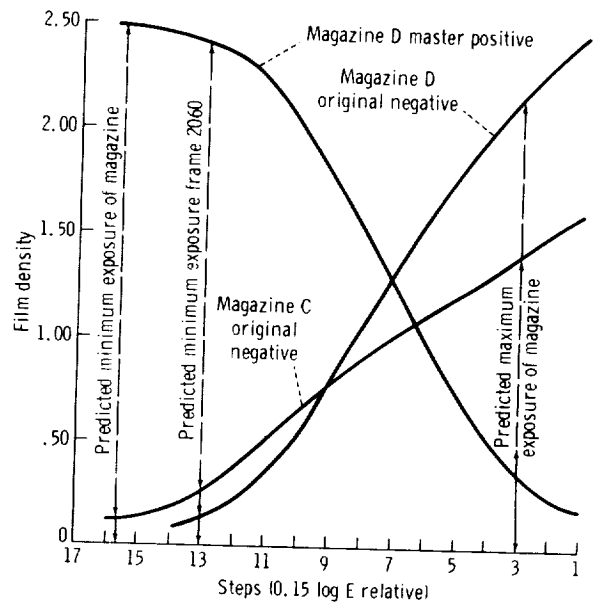


FIGURE 4-27.—Predicted exposures of Apollo 8 magazine D exposed at constant $f/5.6$ aperture and extrapolation to magazine C processing.

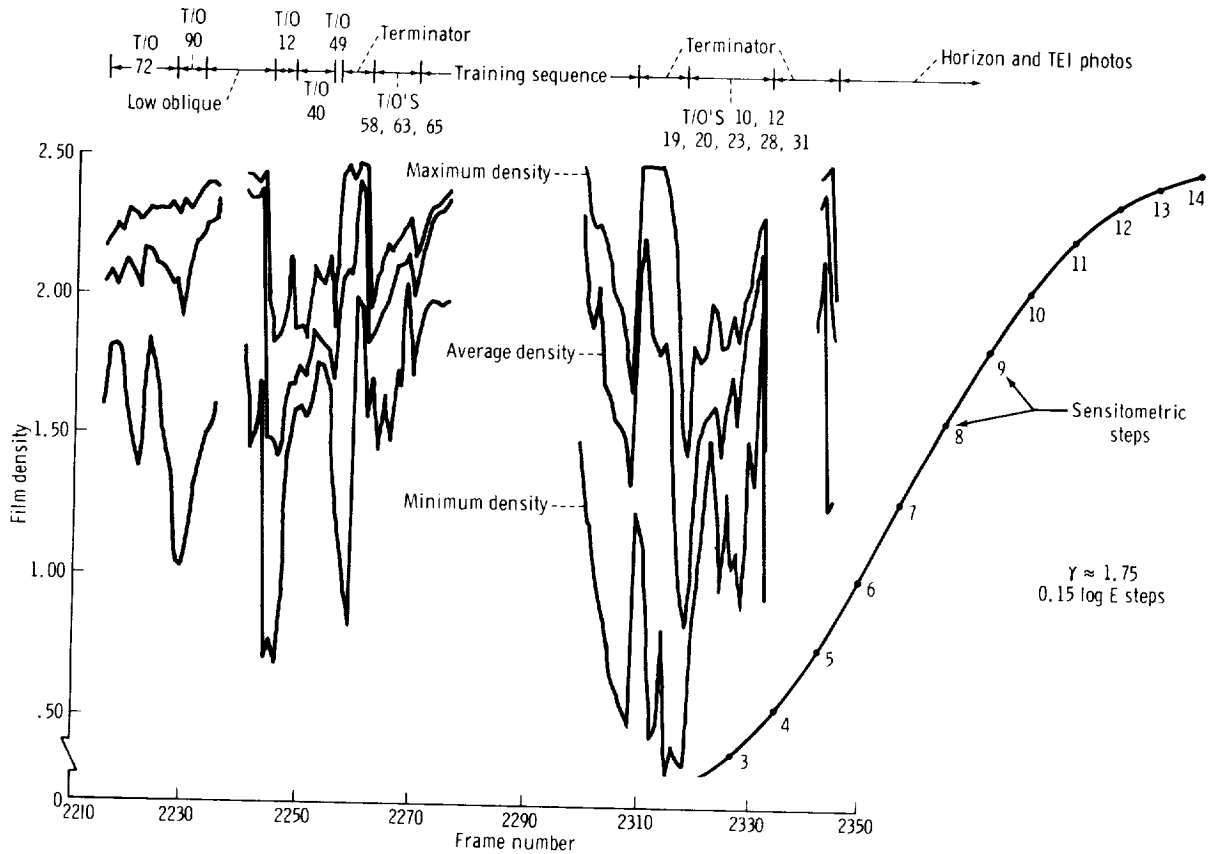


FIGURE 4-28.—Density versus frame number for Apollo 8 magazine E master positive.

APOLLO CAMERA RESOLUTION TESTS

A. F. H. GOETZ

Film from three different magazines exposed during the Apollo 8 red-blue color experiment showed all red frames to be severely out of focus. This phenomenon had not been anticipated. However, all frames were taken after transearth injection (TEI) with the 250-mm lens instead of the 80-mm lens as planned. Lens resolution measurements to clarify the focus problem were performed on the Apollo 8 flight hardware at the Manned Spacecraft Center by this author.

Measurements were made in the Flight Crew Support Division camera facility at MSC. A Gaertner L360n optical bench and collimator and an Air Force resolution target were used. Using a collimator allows resolution tests to be made at the infinity (∞) camera focus setting, which was the setting used during flight.

Tests were conducted using camera back and 80-mm lens no. 1020, 250-mm lens no. 11, magazine G no. 123, and type 3400 film. The twin-filter slide holder no. 1001, carrying the standard 47B (blue) and 29+0.6ND (red) filters, was used.

Focal-length tests were also made by placing a microscope near the image plane of the camera. Assuming a nominal focal length without a filter, the 80-mm lens focuses at 80.02 mm in the blue and at 79.82 mm in the red. The 250-mm lens focuses at 250.22 mm in the blue and 249.62 mm in the red. The red focus was difficult to locate and was nowhere sharp. This fact was borne out in the resolution tests.

Table 4-VIII lists the results of the resolution tests. Because a number of frames were overexposed, some values will appear low. Overexposure is denoted by a plus sign after the value. Where both red and blue values were overexposed, the same exposures were used in each case.

The source of the red, out-of-focus images is now quite apparent. The 250-mm lens used on board Apollo 8 is obviously a poor achromat, showing a resolution of only 5 to possibly 15 lines/mm at 6600 Å. However, the 80-mm lens appears to be well suited for lunar color measurements, exhibiting, at $f/4$, 57 lines/mm resolution in both red and blue wavelength regions.

TABLE 4-VIII.—Results of Resolution Tests

Focus	f -stop	Resolution for filter, lines/mm		
		None	Red	Blue
80-mm lens				
∞	2.8		36	36+
∞	4.0	80	57	57
∞	5.6			50+
$\frac{1}{4}$ distance from ∞ between 50 ft and ∞	2.8		32+	40
$\frac{1}{2}$ distance between 50 ft and ∞	2.8		25+	40
50 ft.....	2.8		Completely out of focus.	Completely out of focus.
250-mm lens				
∞	5.6	13+	5+	40+
$\frac{1}{2}$ distance between 50 ft and ∞	5.6		8+	23+
200 ft.....	5.6		9+	8+
150 ft.....	5.6		Completely out of focus.	Completely out of focus.

PROCESSING OF APOLLO 8 ONBOARD FILM

RICHARD W. UNDERWOOD

INTRODUCTION

The Apollo 8 spacecraft carried a total of five different types of film:

1. SO-368 Ektachrome MS, 70-mm and 16-mm
2. SO-168 Ektachrome EF, 16-mm
3. SO-121 Ektachrome, High-resolution Aerial, 70-mm
4. Type 3400 Panatomic X, Aerial, 70-mm
5. Type 2485, High-speed Recording, 70-mm

All films required different processing techniques and equipment. Standards for processing these films are determined before the flights. Standard processes are usually specified by the manufacturer, but modified because of the specific user (MSC) requirements and sensitometric tests of the actual flight film emulsions. Films are kept under low-temperature refrigeration from the time of emulsion coating until processing, except for the time they are actually in the Apollo spacecraft.

Prior to loading the film magazines, preflight sensitometry is applied at MSC. During the mission strict surveillance of the spacecraft environment is maintained in order to determine if it will in any way change the film sensitivity, thus necessitating a change in processing techniques.

After the return of the films to MSC by courier, the film magazines are downloaded. Post-flight sensitometry is applied where and when appropriate, and the films are then carefully processed to predetermined standards.

The SO-368 and SO-168 films were processed in the MSC General Photography Laboratory, and the SO-121, 3400, and 2485 films were processed in the MSC Precision Laboratory.

SO-368 PROCESSING

The SO-368 film was processed by using Kodak ME-2A chemistry at 75° F. The 70-mm film was processed at 3½ ft/min and the 16-mm at 34 ft/min. No problems were encountered,

and the results are excellent for the film/chemistry combination.

SO-168 PROCESSING

The SO-168 film is the Kodak Ektachrome EF emulsion on a thin base. The ASA (film speed) is adjusted up to 1000 from the manufacturer's specified level of 160. This adjustment requires a substantial modification of the processing technique. The film is intended for use within the Apollo spacecraft using available light. A high-temperature processor is used with modified Kodak ME-4 chemistry. The machine transports film at 42 ft/min with the color developer at 110° F, first developer at 98° F, prehardener at 95° F, and the other chemicals at normal temperatures. The operation was smooth, and no problems were encountered.

SO-121 PROCESSING

The Kodak 1411-M color Versamat is required for SO-121 film. The EA-4 (MX-672) chemistry is modified based on the particular emulsion coating, or "batch." In the case of the Apollo 8 film, the processing times and temperatures given in table 4-IX were used.

TABLE 4-IX.—*Processing Times and Temperatures Used for Apollo 8 Film*

Process	Temperature, °F	Time, min:sec
Prehardener.....	95	2:30
Neutralizer.....	95	1:15
1st developer.....	100	2:30
1st stop.....	100	1:15
Wash.....	95	1:15
Color developer.....	110	2:30
2d stop.....	110	1:15
Wash.....	95	1:15
Bleach.....	110	1:15
Fixer.....	110	1:15
Wash.....	95	2:30
Dry.....	125	2:30

The film was processed at a rate of 3.2 ft/min. The original flight film was spliced with other films and leaders to insure proper transit of the machine, as follows:

1. Scratch test, 10 feet
2. Head leader threads entire machine, 80 feet
3. Head precision sensitometry, 3 feet
4. Flight film, 38 feet
5. Tail precision sensitometry, 3 feet
6. Colorimetric, resolution, photogrammetric, sensitometric frisket, 20 feet
7. Trailer, 80 feet

No problems were encountered.

TYPE 3400 PROCESSING

The Kodak M-11C black-and-white Versamat was used to process the 3400 film. Kodak MS MX-641-1 developer and Hunt Starfix comprised the chemistry.

Preflight sensitometric tests on the particular flight emulsion, the requirements of experimenters, and the photometric requirements brought about the establishment of an aerial exposure index of 13.1, a maximum density of 3.32, and a gamma of 1.70. This resulted in a processing at 85° F and at 13.75 ft/min, or 18.5 seconds of development time. Magazines D and E were processed according to the established procedure outlined previously. Magazine C was not normally exposed. The LMP set the aperture at $f/5.6$ and the speed at 1/250 second, and the magazine was exposed at these settings during the entire eighth revolution of the Moon. The Photographic Technology Laboratory recommended that a low-gamma developer be used in processing this magazine to bring out the photographic detail.

A low-gamma developer was formulated and tested in the Precision Laboratory. Photographic simulation secured from a high-altitude aircraft flying over West Texas arid areas was used to verify the process and technique. The final process for the M-11C Versamat indicated that the special low-gamma developer should run at 5 ft/min in two development tanks at 75° F or 100 seconds of development plus 150 seconds of fix (Hunt Starfix). This resulted in the gamma being lowered from 1.70 to 0.70; maximum density dropped from 3.32 to 2.25, and the aerial exposure index was recomputed from 13.1 to 28.8. The resulting negatives show far more

visual detail than the two films processed by conventional means.

TYPE 2485 PROCESSING

Processing techniques for the very high-speed type 2485 film had been established in cooperation with personnel of the Goddard Space Flight Center. The film has previously been used for, and its intended use on the Apollo 8 flight was for, the recording of astronomical phenomena. A Versamat Model M-11C cycle using standard D-19 developer at 3 ft/min (150 seconds) in two tanks at 95° F would produce a gamma of 1.95. A 0.5-base fog rise, attributed to radiation fogging, was anticipated.

The LMP did not use the film for the programmed astronomical experiments, but he did use the film for general lunar surface photography; he exposed the film for an ASA (speed) of 80, not 2000 to 6000 as the film is rated by the manufacturer. This is approximately six stops overexposure, or far beyond the normal latitude of the film.

The Precision Laboratory formulated a special chemistry and photographic technique in order to "save" the data recorded. After 6 days of experimental testing, a chemistry and processing technique evolved; but when this technique was attempted in the Versamat Model M-11C processor, the chemistry could not be changed fast enough to prevent the image from destroying itself. It was then decided to use Nikor spiral film reels in a large chemical tank. The processing was at 68° F. Steps included wetting agent, bleach, neutralizer, wash, developer, fix, second wash, and second drying (in the Versamat). The bleach technique removed the effect of the vastly overexposed emulsion by destroying the external latent image and then overdeveloping the internal molecular latent image in order to produce a more nearly normal negative. The technique proved highly successful, and normal images resulted. The standard graininess of type 2485 film is slightly reduced by silver halide solvents in the developer removing the large bleached grains.

The head and tail sensitometry had been removed and was processed normally. The "bleach process" would have destroyed these data, which

were of value in determining radiation effects on the emulsion. A negligible radiation effect was shown, which favors use of this emulsion on future long-duration space flights.

STEREOSCOPIC STRIP PHOTOGRAPHY

PAUL E. NORMAN, ROBERT O. HILL, AND
LEWIS C. WADE

As discussed previously, one Apollo 8 photographic objective was to obtain two strips of stereoscopic photography from terminator to terminator. For operational reasons, this requirement was reduced to one partial strip using black-and-white film (from terminator to about 60° from the opposite terminator) and one strip using color emulsion, which was curtailed to allow for television transmission on the ninth revolution. By taking an exposure every 20 seconds, using the intervalometer, each photograph overlaps the previous photograph by approximately 60 percent. This allows viewing of each point on the surface from at least two photographic positions separated by approximately 30 km along the orbit. At an orbital altitude of 110 km, this method produces a base-to-height ratio (B/H) of about 0.27, acceptable for stereoscopic viewing

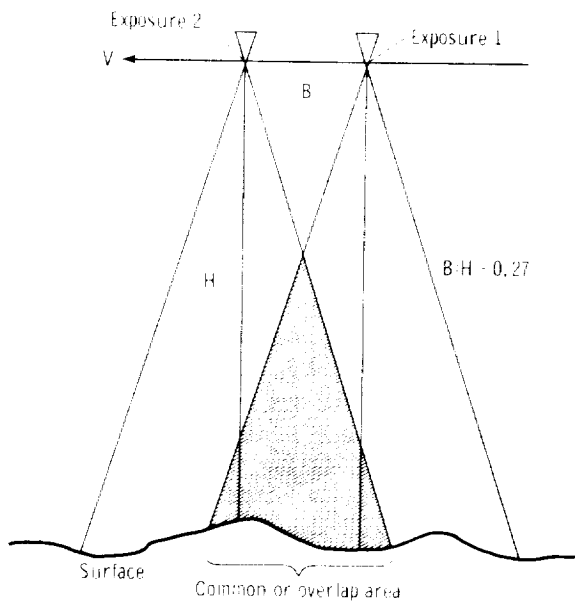


FIGURE 4-29. Geometry of vertical strip.

(fig. 4-29). By combining the vertical strip with the second, or convergent, strip, the geometry of the stereoscopic view could be made stronger. Hence, the ability to measure height differences would be better by a factor of two (fig. 4-30).

The vertical strip was accomplished as planned on the fourth revolution. It extends from the far-side terminator (longitude 150° W) to about 45° from the near-side terminator (approximately longitude 75° E). The photography is of good quality and appears to have good forward lap in all areas. The extra exposure was triggered as planned every 5 minutes.

The planned convergent strip on the ninth revolution was deleted from the flight plan because of the need for crew rest. The commander (CDR) did bracket-mount the 70-mm camera and took photographs in a near-vertical orientation on the eighth revolution, using a fixed camera exposure of $f/5.6$ and $1/250$ second. This procedure resulted in good-quality photography after special processing by the Photographic Technology Laboratory, and this photography provides additional stereoscopic coverage along the groundtrack.

With the two stereoscopic strips, it is possible to position far-side features with respect to the

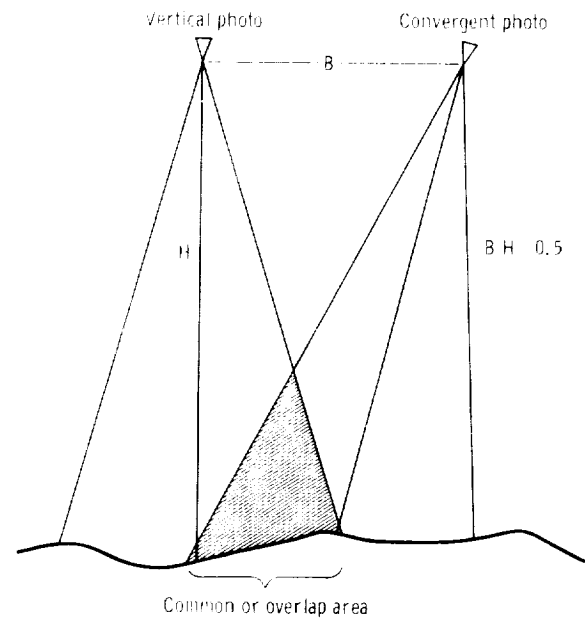


FIGURE 4-30. Geometry of combined vertical and convergent strips.

control points. Because of the early launch date and termination of both passes at approximately longitude 75° E, information that can be gained concerning relative positions of eastern-limb and Apollo-zone features depends on the photography obtained after transearth injection. Both passes included many frames taken with a zero phase angle in the field of view. The photometric "washout" was less than generally expected, and surface detail remains readily apparent. Many small craters exhibit considerable albedo differences with respect to the surrounding terrain, so sufficient surface detail is available to permit photogrammetric reconstruction of the surface.

Some 16-mm color sequence photography was taken through the rendezvous window during the mission. A plot of the coverage of these magazines, as well as that of the 70-mm stereoscopic strip photography, may be found in appendix A of this report.

PHOTOGRAPHIC TARGETS OF OPPORTUNITY

LEWIS C. WADE

Lunar photographic targets of opportunity (T/O) are all photographic targets outside the strips of stereoscopic photographs along the groundtrack of Apollo 8. Within the brief time allotted for planning, the various organizations involved in lunar-surface analysis for Apollo 8 compiled lists of sites where additional photography, at the scale and resolution available from the spacecraft, would be helpful.

Lists of proposed photographic sites were submitted by the following organizations:

1. U.S. Geological Survey, Flagstaff, Ariz.
2. Branch of Astrogeology, U.S. Geological Survey
3. Science and Applications Directorate, NASA MSC
4. Bellcomm, Inc.
5. NASA Headquarters

The targets were selected to provide either detailed coverage of specific features or broad coverage of areas to improve on Lunar Orbiter IV photographs. All requested sites were plotted, and serial designations were assigned.

Most of the proposed photographic sites were on the Earth-facing hemisphere. This area has been studied for many years through telescopes, and most of the hemisphere is covered by Lunar Orbiter IV photographs with resolutions from 70 to 150 meters.

For each daily launch window, the advancing terminator and changing orbit trace define a different set of targets. Apollo Target of Opportunity (ATO) Flight Charts were prepared for each launch date in the December 1968 window. The December 21, 1968, ATO is discussed in the section of this chapter entitled "Photographic Objectives."

The targets shown on the December 21, 1968, ATO are numbered identically to those shown on the Target of Opportunity Planning Chart. Table A-I (in app. A) briefly describes and locates these targets. A target shown on the ATO as requiring more than one photograph usually indicates that a number of targets from the planning chart have been included in the same sequence of photographs. This procedure was followed to minimize crew workload in taking T/O photography.

In all, there were 51 targets, either a single photograph or a series of photographs, that might be taken for a December 21, 1968, launch. The majority of these 51 targets were programmed to be taken during the fourth and ninth lunar orbits. Vertical stereoscopic photography was planned for the fourth orbit, and convergent stereoscopic photography was planned for the ninth orbit. The loss of photography on the ninth orbit resulted in some loss of T/O photography, as discussed subsequently.

Approximately 60 percent of the targets selected for a December 21, 1968, launch date were photographed. In addition, many crew-selected targets were photographed. All 70-mm black-and-white and color photography targets of opportunity are shown on the charts in appendix A. The list in table A-II relates the frames to target number. Most of the targets photographed are to the south of the groundtrack, and most of the targets not photographed are to the north. The loss of targets to the north is the result of two events. It was known prior to launch that targets to the north of the track would be the most difficult to obtain, since the LMP would

look mostly southward. This, combined with the loss of photographic opportunities during the ninth orbit, resulted in the small number of targets photographed to the north of the track. The two most unfortunate losses to the north of the track are the loss of T/O 59 using the red-blue filters and the loss of T/O 67, a prime photographic area to supplement Lunar Orbiter photography. This latter area was photographed by the LMP as Apollo 8 left lunar orbit. Most targets were photographed with the requested

lens configuration and desired type of film. With few exceptions, the exposures used were good, and the data content of the photography is completely satisfactory.

Discussions during the crew photographic debriefing indicated that the preplanned exposure data worked well, and that targets, when time was available, could be photographed at a higher rate than was planned. Most of the targets of opportunity were photographed in the first few revolutions of the Moon.

APPENDIX A

Data Availability

This appendix contains a nearly complete index of Apollo 8 photographic coverage compiled for the benefit of those groups and individuals who wish to obtain photographic prints for further study. Inquiries from scientists in the United States should be directed to the following address:

National Space Science Data Center
Goddard Space Flight Center
Code 601.4
Greenbelt, Md. 20771

The 70-mm photographs can be obtained either as positive or negative film copies on 70-mm black-and-white film or as 8- by 10-inch black-and-white paper prints. The 16-mm sequence films are available as 16-mm positive or negative copies. Although the Apollo 8 mission included color photography, only black-and-white copies of these films are generally available from the Data Center. As previously noted in this report, the astronauts commented that the lunar surface is devoid of color, and that black-and-white film more closely depicts the appearance of the lunar scene. The results of the mission have clearly shown that it is very difficult to recover the true color of the lunar surface with existing color films. Even with optimal film processing, the color emulsion layers introduce false color because they are sensitive to varying surface brightness as well as to color.

Limited quantities of black-and-white reproductions can often be furnished without charge to researchers performing studies that require the photographs. Color reproductions or reproductions in nonstandard formats will be made available at cost to qualified users. Scientists requiring photographic data for research should

inform the Data Center of their needs and identify the nature of their study; their affiliation with any scientific organization, university, or company; and any contracts they may have with the Government for the performance of the investigation.

Requests for photographs should include the following information, which can be found in the charts and tables that comprise this index:

1. Mode (stereoscopic strips, sequence photography, or targets of opportunity)
2. Frame number of 70-mm photography, including mission number and letter designation of magazine
3. Magazine designation of 16-mm sequence photography
4. Format of photography (positive or negative, films or prints), and size of product

Requests for Apollo 8 photography from outside the United States should be directed to the following address:

World Data Center A for Rockets
and Satellites
Goddard Space Flight Center
Code 601
Greenbelt, Md. 20771

Many general-interest requests may be satisfied with materials available in printed form. Requests of this type should be directed to the following address:

Office of Public Affairs
National Aeronautics and Space
Administration
Code F
Washington, D.C. 20546

Inquiries or requests regarding the pictures of the Earth taken from Apollo 8 should be directed to the following address:

Technology Application Center
University of New Mexico
Albuquerque, N. Mex. 87106

Prints of the Apollo 8 photography may be viewed at the National Space Science Data Center at Goddard Space Flight Center in Greenbelt, Md. The Data Center will also supply requesters with copies of the charts included in the cover pocket. Charts were prepared under the direction of the Department of Defense by the Aeronautical Chart and Information Center (ACIC), U.S. Air Force, for NASA. The scale of these Mercator Projections is 1:7 500 000 at the equator and the grid interval is 5°.

Table A-I lists all Apollo targets of opportunity (T/O) by number and gives the description and location of each. A T/O flight chart, a copy of which was used as a reference on board the Apollo 8 spacecraft, shows the targets of opportunity that were available for photography on the Apollo 8 launch date, December 21, 1968.

Four charts published by ACIC as the "Apollo 8 Mission Lunar Photography Index," copies of which are included in the cover pocket, illustrate the coverage of the 70-mm stereoscopic strip photography, the 16-mm sequence photography, and the 70-mm photography of targets of opportunity. The T/O photography is outlined on two of the charts, one covering magazines A, B, and G, and the other covering magazines C, D, and E.

Table A-II shows the extent of Apollo 8 T/O coverage by giving the magazines and frame numbers of photographs taken of specific targets. Tables A-III to A-IX are detailed indices of the 70-mm T/O photography. Each table represents one film magazine with consecutively

numbered frames. Where possible in these tables, the approximate selenographic coordinates of the principal point of each photograph have been given. Also, the revolution during which the magazine A and B photographs (tables A-III and A-IV) were taken is unknown; therefore, a Sun angle for the third revolution was used in these tables. Where a shutter speed and *f*-stop are not indicated, it is probable that the shutter speed and *f*-stop for the corresponding area on the Apollo Target of Opportunity Flight Chart were used.

The frame numbers given in tables A-II to A-IX are those plotted on the 70-mm index charts. The coverage shown on the 16-mm sequence photography chart has not been listed by frame.

The following abbreviations are used in the 70-mm index tables:

alt	altitude
CS	convergent stereoscopic photograph
exp	exposure
H.O.	high oblique
hor	horizon
LO	Lunar Orbiter
L.O.	low oblique
lat	latitude
long	longitude
NV	near vertical
PP	principal point
rev	revolution
SSP	subsolar point
TEC	transearth coast
TEI	transearth injection
term.	terminator
TLC	translunar coast
T/O	target of opportunity
vert.	vertical
VS	vertical stereoscopic photograph
(?)	indicates uncertainty

This appendix is concluded with black-and-white contact-print reproductions of all Apollo 8 70-mm photography.

TABLE A-I.—*Apollo Targets of Opportunity*

T/O no.	Description	T/O location	
		Latitude	Longitude
1.	Steep terra dome	001.6° N	130.3° W
2.	Swirly Mare Orientale material	017.3° N	134.7° W
3.	Fresh crater interior	001.5° S	133.9° W
4.	Rim of crater from T/O 3	000.6° N	136.7° W
5.	Mare Orientale secondaries	021.0° N	140.8° W
6.	Mare Orientale secondaries	010.1° N	140.9° W
7.	Mare Orientale secondaries	013.3° N	145.1° W
8.	Two fresh craters and landslide	014.9° S	152.0° W
9.	Steep dome	019.3° S	154.6° W
10.	Various targets	020.9° S	161.0° W
11.	Basin with pitted plains, fill on floor	002.9° S	162.9° W
12.	Fresh crater with trails of bird's-foot secondaries	009.1° S	164.0° W
13.	55-km young crater	010.3° S	165.5° W
14.	12-km central peak in 40-km crater	021.0° S	172.4° W
15.	25-km central peak in 85-km crater	004.7° S	173.7° W
16.	18-km central peak in 60-km crater	020.6° S	177.5° W
17.	Cluster of equi-age craters	019.0° N	175.5° E
18.	Fractured tumescent floors (2 craters)	014.0° N	173.9° E
19.	Patches of 2-km bulbous hills with mare	017.4° S	174.3° E
20.	15-km young craters on rim of Mendeleev	014.1° S	173.5° E
21.	Patches of bulbous hills in small crater in mare	027.1° S	173.3° E
22.	Mare fill in 150-km crater	018.4° S	172.9° E
23.	Fractured tumescent floor	017.1° S	167.8° E
24.	Steep dome	010.0° S	165.8° E
25.	30- by 50-km central peak	010.1° S	161.7° E
26.	Bulbous hills and ridges in bottom	026.1° S	158.2° E
27.	Old crater	012.7° N	153.6° E
28.	Mare on floor of 100-km crater, and bright crater	019.2° S	147.5° E
29.	Fractured tumescent crater floors (2 craters)	004.2° S	146.1° E
30.	Large crater floored by old pitted plains; other detail	003.7° N	139.8° E
31.	Tsiolkovsky secondaries	017.3° S	139.2° E
32.	Medium-age crater	004.1° S	138.4° E
33.	Medium-age crater	002.0° S	138.1° E
34.	Various crater materials	006.0° N	136.8° E
35.	Medium-age crater	010.2° S	135.9° E
36.	Fractured tumescent crater floor	015.0° S	129.3° E
37.	Crater chains	000.3° S	129.5° E
38.	Dark, probable flows of old crater near Tsiolkovsky	026.9° S	128.5° E
39.	Push-through crater materials	012.2° S	128.4° E
40.	Fractured mare dome and other features, Tsiolkovsky	020.1° S	128.0° E
41.	Crater chains	005.7° S	128.0° E
42.	Landslide N of Tsiolkovsky	019.0° S	124.4° E
43.	Soviet Mountains	003.5° S	123.1° E
44.	Young crater, priority below 40 and 43 strips	017.4° S	122.7° E
45.	Soviet Mountains	005.7° S	121.9° E
46.	Crater much like Copernicus	003.9° N	121.2° E
47.	Fractured tumescent floor	012.9° N	117.9° E
48.	Young crater on large medium-age crater wall	010.8° S	117.1° E
49.	Fairly young 20-km crater	020.0° S	116.4° E
50.	Lobachevsky interior, may be dark	009.3° N	112.4° E
51.	Bright spot in Luna III photos	000.2° S	107.5° E
52.	Mare patches and light-dark crater	027.2° S	104.0° E

TABLE A-I.—*Apollo Targets of Opportunity*—Continued

T/O no.	Description	T/O location	
		Latitude	Longitude
53	C or E crater with landslide.	009.6° N	102.0° E
54	Probable young crater.	022.3° S	100.3° E
55	Very bright small crater.	004.8° N	099.8° E
56	Very bright small crater.	009.7° S	098.0° E
57	Very bright small crater.	008.0° N	096.1° E
58	Fresh large crater with secondaries.	017.9° S	093.7° E
59	Mare Smythii, ring craters.	002.9° S	083.8° E
60	Mare Marginis, N edge.	017.6° N	086.0° E
61	Center of Mare Marginis.	013.1° N	085.5° E
62	Humboldt.	027.9° S	080.7° E
63	Behaim, especially central peak.	017.0° S	078.4° E
64	Very bright crater NW of La Pérouse.	010.1° S	074.2° E
65	Kapteyn.	010.5° S	070.6° E
66	E Mare Crisium rim, fill-in for poor LO IV photos.	015.0° N	068.9° E
67	S Mare Crisium rim, fill-in for poor LO IV photos.	004.6° N	057.7° E
68	Langrenus, to compare with Copernicus.	008.8° S	060.7° E
69	Langrenus C, large dark-halo crater.	005.2° S	060.4° E
70	Mare Crisium.	010.5° N	057.7° E
71	Petavius B, missing rim material.	019.1° S	057.4° E
72	McClure crater cluster.	013.4° S	051.4° E
73	N of Colombo, fill-in for poor LO IV photos.	012.8° S	046.3° E
74	Mare Crisium rim E and NE of Taruntius, fill-in for poor LO IV photos.	009.4° N	049.2° E
75	Messier double crater, elongate S rays.	001.8° S	047.4° E
76	Proclus, excluded-ray zone.	016.4° N	047.0° E
77	Palus Somni domes.	016.0° N	043.1° E
78	Da Vinci, peninsula, various terrain, LO IV photos not good.	009.8° N	043.3° E
78a	Secchi, peninsula, LO IV photos not good.	001.2° N	042.9° E
79	Palus Somni, irregular crater.	012.8° N	042.7° E
80	W of Lubbock, sharp irregular depression and hills.	002.2° S	040.0° E
81	N of Gutenberg G; small, sharp hills.	004.3° S	040.0° E
82	NW of Gutenberg.	006.0° S	040.1° E
83	Crater Bohnenberger, irregular terrain.	016.2° S	040.1° E
84	NW of Gutenberg, volcanics(?).	006.3° S	038.8° E
85	Gaudibert A and B, "Sabine and Ritter" type with dark deposits and fresh rocks.	012.3° S	038.4° E
86	Gaudibert complex crater with troughs.	010.9° S	037.7° E
87	Cauchy dome.	007.4° N	038.3° E
88	Small, bright crater N of Censorinus F.	002.6° S	037.3° E
89	Censorinus S, irregular crater with bulbous hills.	004.2° S	036.1° E
90	Capella.	007.6° S	035.0° E
91	Censorinus C, irregular crater with irregular depressions and domes.	003.2° S	034.1° E
92	Maskelyne A, irregular crater with irregular depression and domes.	000.0° S	034.1° E
92a	Landing site 1, redesignate.	004.7° N	035.4° E
92b	Landing site 1, prime.	003.9° N	034.9° E
93	Isidorus, for comparison with Capella.	007.9° S	033.5° E
94	Daguerre, double ring ghost with young deposits.	010.3° S	033.6° E
95	Isidorus B, irregular crater with irregular depressions and hills.	004.7° S	032.9° E
96	Censorinus H, sharp depressions.	001.6° S	032.8° E
97	Crater Censorinus, landing site.	000.2° S	032.5° E
98	Isidorus C, irregular volcanic crater.	005.1° S	031.6° E
99	Censorinus T, sharp irregular depressions.	002.5° S	031.5° E

TABLE A-I.—*Apollo Targets of Opportunity—Continued*

T/O no.	Description	T/O location	
		Latitude	Longitude
100	Censorinus J, paired craters with mare fill	001.5° S	032.4° E
101	Maskelyne B, dark halo	003.3° N	029.7° E
102	Maskelyne K, dark halo	002.1° N	029.0° E
103	Torricelli B, dark crater	002.3° S	029.1° E
104	Crater Mädler	010.9° S	029.9° E
105	Crater Torricelli	004.6° S	028.4° E
106	Crater Jansen	013.7° N	028.7° E
107	Jansen, miscellaneous volcanic objects	015.2° N	028.7° E
108	Littrow, landing site	021.9° N	028.9° E
108a	Posidonius, raised floor	031.7° N	030.1° E
108b	Dawes, single frame on LO IV photography	017.2° N	026.4° E
109	Theophilus, rim	009.0° S	027.7° E
110	Theophilus, plains on rim	008.9° S	026.4° E
111	Theophilus, floor	011.3° S	026.3° E
112	Moltke, dark crater	000.5° S	024.2° E
112a	Landing site 2, redesignate	000.6° S	024.9° E
112b	Landing site 2, prime	000.7° N	023.5° E
113	S of Moltke, irregular depressions	001.8° S	023.9° E
114	Surveyor V	002.6° N	023.0° E
115	Hypatia, irregular crater	003.9° S	022.5° E
116	Transient SW of Plinius	011.9° N	021.6° E
117	Alfraganus A, S complex of depressions and domes	003.7° S	020.4° E
118	Alfraganus A, N complex of depressions and domes	002.2° S	020.2° E
119	E of Alfraganus	005.3° S	020.2° E
120	Dionysius W	002.9° N	017.2° E
121	Descartes, hilly and furrowed material	009.3° S	016.1° E
122	Julius Caesar, interior deposits	008.2° N	015.6° E
123	Ariadaeus, rille-cutting hills	006.1° N	014.4° E
124	Taylor B, hills and furrows	005.1° S	014.0° E
125	Abulfeda, single frame on LO V photography	014.2° S	014.1° E
126	Boscovich, fresh volcanics	009.3° N	011.1° E
127	Ariadaeus, intersection of faults	007.5° N	010.5° E
128	Godin and nearby hills	001.8° N	010.0° E
129	W of Godin, domes	001.0° N	009.2° E
130	Big plateau SE of Dembowski	002.1° N	008.2° E
131	Bright hills W of Agrippa S	005.2° N	007.6° E
	NOTE.—S is letter designation of crater secondary to Agrippa, not south.		
132	Mounds and grooves N of Pickering	001.3° S	007.6° E
133	Hyginus N, irregular crater	010.5° N	007.4° E
134	Manilius D, dark crater	013.2° N	006.8° E
135	Airy, dark interior	018.0° S	005.7° E
136	Triesnecker	004.2° N	003.5° E
137	NE of Müller, terra domes	006.9° S	002.9° E
138	Müller	007.9° S	001.3° E
139	Ukert	007.7° N	001.5° E
140	Hadley Rille	025.2° N	002.8° E
141	Murchison, interior volcanics	004.4° N	000.3° W
142	Landing site 3, prime	000.4° N	001.5° W
143	Surveyor VI	000.5° N	001.9° W
144	Herschel	005.8° S	002.0° W
145	Alphonsus transient, cutting faults	013.7° S	002.5° W

TABLE A. I. *Apollo Targets of Opportunity* Concluded

T/O no.	Description	T/O location	
		Latitude	Longitude
146.....	Rima Bode I dome, sinuous rille deposits.....	006.7° N	003.1° W
147.....	Textures W of Rima Bode I.....	006.8° N	004.2° W
148.....	Dark deposits SW of Rima Bode II.....	010.8° N	005.2° W
149.....	Davy G, fresh chain.....	010.9° S	005.5° W
150.....	Mösting.....	000.9° S	005.8° W
151.....	Lalande.....	004.2° S	008.6° W
152.....	Eratosthenes.....	014.1° N	011.3° W
153.....	Mare Ridge SE of Copernicus.....	005.8° N	012.5° W
154.....	Copernicus CD, dark deposits S of LO V single frame.....	005.7° N	015.4° W
155.....	Gambart and to W.....	000.3° N	015.6° W
156.....	Fra Mauro N hill, probably volcanic.....	002.3° S	015.5° W
157.....	Very bright crater S of Parry.....	008.5° S	015.9° W
158.....	Boupland ψ hill, probably volcanic.....	011.6° S	020.1° W
159.....	Darney δ hill, probably volcanic.....	013.5° S	021.1° W
160.....	Copernicus, south rim and wall.....	008.5° N	020.0° W
161.....	Surveyor III.....	003.0° S	023.3° W
162.....	Reinhold.....	002.2° N	023.2° W
163.....	SW Copernicus, miscellaneous.....	004.7° N	024.1° W
164.....	Riphaeus Mountains, volcanics and bedrock.....	006.0° S	026.0° W
165.....	Lansberg.....	001.1° S	026.6° W
166.....	Kunowsky D, irregular crater.....	001.4° N	029.0° W
167.....	Sinuous rille near Eneke.....	008.3° N	032.8° W
168.....	Dome W of Milichius.....	011.1° N	033.1° W
169.....	Spiral chain NE of Kepler.....	009.3° N	034.7° W
170.....	Landing site 4, redesignate.....	003.4° S	035.8° W
171.....	Landing site 4, prime.....	003.6° S	036.5° W
172.....	Eneke.....	004.2° N	036.6° W
172a.....	Vitello.....	030.4° S	037.4° W
172b.....	Gassendi interior.....	027.9° S	039.6° W
173.....	Kepler.....	008.0° N	037.8° W
174.....	Landing site 5, prime.....	001.6° N	041.7° W
175.....	III P-12, redesignate.....	002.8° S	042.4° W
176.....	Surveyor I.....	002.6° S	043.2° W
177.....	Craters E of Marius.....	011.2° N	044.9° W
178.....	Craters E of Marius.....	012.3° N	045.9° W
179.....	Craters E of Marius.....	014.2° N	047.6° W
180.....	Aristarchus, bright and transient.....	023.4° N	047.4° W
181.....	Hansteen, bright hills.....	012.2° S	050.1° W
182.....	Marius Hills, N.....	013.4° N	051.9° W
183.....	Marius Hills, S.....	011.2° N	054.6° W
184.....	Hevelius.....	002.0° N	067.4° W
185.....	Grimaldi, interior fill.....	006.0° S	068.0° W

TABLE A-II.—*Apollo 8 Target-of-Opportunity Coverage by Frame Number*

T/O no.	Magazine A	Magazine B	Magazine C	Magazine D	Magazine E
10					2319
11			2827		
12		2412 to 2415			2244 to 2247, 2318
14					2320
15					
16					
19					2322, 2323, 2324
20					2321
21					
23					2325
26					
28				2197	2327
29				2197	
30					
31				2197	2328
32				2197, 2198	
33				2197, 2198	
34					
35			2730	2197, 2198	
36				2197, 2198	2249 to 2251
37				2197, 2198	
38				2214	
40		2447 to 2451			2248, 2252 to 2255
41				2197, 2198	
44				2197 to 2199	
45				2198 to 2200	
49		2446		2214	2256
51					
52		2455 to 2462		2212 to 2214	
54				2195, 2213	
55					
57					
58				2189, 2201, 2190, 2193	2262 to 2265
59				2202 to 2205, 2207	2331, 2332
63				2189, 2193	2268, 2269
64					
65				2181, 2182, 2203	2270
66				2206	
67				2204 to 2206	2334 to 2338, 2344 to 2350
68	2613 to 2616			2184, 2203	
71					
72					2215 to 2227
80			2805 to 2826		2340 to 2343, 2257 to 2261
87					2244
90					2228 to 2242

TABLE A-III.—*Apollo 8 Magazine A, SO-368 Film*

Rev	Frame (AS8-16-)	Lat	Long	Mode	Direction	f-stop	Shutter speed, sec	Sun angle, deg	Other coverage	Area	Remarks
TLC	2581			High alt Earth	NV					E coast, Florida, Cuba, Bahamas	Good exp
TLC	2582									S-IVB	Good exp
TLC	2583									S-IVB	80-mm, good exp
TLC	2584									S-IVB	Good exp
TLC	2585									S-IVB	Good exp
TLC	2586									S-IVB	Good exp
TLC	2587			High alt Earth						Africa, South America	Good exp
TLC	2588			High alt Earth						Africa, South America	Good exp
TLC	2589			High alt Earth						Africa, South America	Good exp
TLC	2590			High alt Earth						Africa, South America	Good exp
TLC	2591									S-IVB	Good exp
TLC	2592									S-IVB	Good exp
TLC	2593									Earth	Good exp
TLC	2594			High alt Earth						Earth	Good exp
TLC	2595			High alt Earth						Earth	Good exp
TLC	2596			Earth						Earth	Good exp
TLC	2597			Earth						Earth	Good exp
TLC	2598			Earth						Earth	Good exp
TLC	2599			Earth						Earth	Good exp
TLC	2600			Earth						Earth	Good exp
TLC	2601			Earth						Earth	Good exp
TLC	2602			Earth						Earth	Good exp
TLC	2603			Earth						Earth	Good exp
TLC	2604			Earth						Earth	Good exp
TLC	2605			Earth						Earth	Good exp
TLC	2606			Earth						Earth	Good exp
TLC	2607			Earth						Earth	Good exp
TLC	2608			Earth						Earth	Good exp
TLC	2609			Earth						Earth	250-mm, good exp Good exp

TABLE A-IV.—Apollo 8 Magazine B, SO-368 Film^a

Rev	Frame (AS8-14-)	Lat	Long	Mode	Direction	f-stop	Shutter speed, sec	Sun angle, deg	Other coverage	Area	Remarks
	2383			H.O.	W	5.6	1/250	Near SSP			Earth above hor, good 250-mm
	2384			H.O.	W	5.6	1/250	Near SSP			Earth above hor, good 250-mm
	2385			H.O.	W	5.6	1/250				80-mm
	2386			H.O.	W	5.6	1/250				80-mm
	2387			H.O.	W	5.6	1/250				80-mm
	2388			H.O.	W	5.6	1/250				80-mm
	2389	13° S	105° E	H.O.	WSW	5.6	1/250	70	LO II S-14	NE of Humboldt	80-mm
	2390	13° S	105° E	H.O.	WSW	5.6	1/250	70	LO I S-1, S-9	NE of Humboldt	80-mm
	2391	13° S	105° E	H.O.	WSW	5.6	1/250	70	LO II S-14	NE of Humboldt	80-mm
	2392	13° S	105° E	H.O.	WSW	5.6	1/250	70	LO I S-1, S-9	NE of Humboldt	80-mm
	2393	13° S	105° E	H.O.	WSW	5.6	1/250	70	LO II S-14	NE of Humboldt	80-mm
	2394	13° S	105° E	H.O.	WSW	5.6	1/250	70	LO I S-1, S-9	NE of Humboldt	80-mm
	2395	13° S	105° E	H.O.	WSW	5.6	1/250	70	LO II S-14	NE of Humboldt	80-mm
	2396	13° S	105° E	H.O.	WSW	5.6	1/250	70	LO I S-1, S-9	NE of Humboldt	80-mm
	2397	3° S	154° W	Vert	Vert	5.6	1/250	6	LO I S-1, S-9	Far side	Near term., 250-mm
	2398	3° S	154° W	Vert	Vert	5.6	1/250	6	LO I S-3	Far side	Near term., 250-mm
	2399	3° S	155° W	Vert	Vert	5.6	1/250	6	LO V A8, 10, 12	Far side	Near term., 250-mm
	2400	3° S	155.5° W	Vert	Vert	5.6	1/250	7	LO I, S-3	Far side	Near term., 250-mm
	2401	3° S	156° W	Vert	Vert	5.6	1/250	7	LO V A8, 10, 12	Far side	Near term., 250-mm
	2402	157° S	3° W	Vert	Vert	5.6	1/250	7	LO I S-3	Far side	Near term., 250-mm
	2403	5° S	157° W	NV	NV	5.6	1/250	0	LO V A8, 10, 12	Far side	Dark

2404	5°	S	157.5°	W	NV	NV	5.6	1/250	0	LO I S-3	Far side	Dark
2405	5°	S	159.5°	W	NV	NV	10	LO V A8, 10, 12 LO I S-3	Far side	Dark
2406	6°	S	160°	W	NV	NV	10	LO V A8, 10, 12	Far side	Dark
2407	6°	S	160°	W	NV	NV	10	LO V A8, 10, 12 LO I S-3	Far side	Dark
2408	5°	S	161.5°	W	NV	NV	11	LO V A8, 10, 12 LO I S-3	Far side	Dark
2409	4°	S	162°	W	NV	NV	12	LO V A8, 10, 12 LO I S-3	Far side	Dark
2410	6.5°	S	163°	W	NV	NV	12	LO V A8, 10, 12 LO I S-3	Far side	Dark
2411	6.5°	S	163°	W	NV	NV	12	LO V A8, 10, 12 LO I S-3	Far side	Dark
2412	7.5°	S	165°	W	Oblique	Oblique	15	LO V A8, 10, 12 LO I S-3	Far side	Dark, T/O 12
2413	6.5°	S	165°	W	NV	NV	15	LO V A8, 10, 12 LO I S-3	Far side	Dark, T/O 12
2414	7.5°	S	166°	W	NV	NV	15	LO V A8, 10, 12 LO I S-3	Far side	Dark, T/O 12
2415	7°	S	167°	W	NV	NV	17	LO V A8, 10, 12 LO I S-3	Far side	Dark, T/O 12
2416	7.5°	S	171°	W	NV	NV	21	LO V A8, 10, 12 LO I S-3	Far side	Dark
2417	8.5°	S	171.5°	W	Oblique	Oblique	21	LO II S-3 LO I S-3	Far side	Dark
2418	8°	S	170.5°	W	NV	NV	21	LO I S-3	Far side	Dark
2419	8°	S	175°	W	NV	NV	25	LO II S-3 LO I S-3	Far side	Dark
2420	10°	S	175°	W	NV	NV	25	LO II S-3 LO I S-3	Far side	Somewhat dark
2421	10°	S	175°	W	NV	NV	25	LO II S-3 LO I S-3	Far side	Somewhat dark
2422	9°	S	177.5°	W	NV	NV	27	LO I S-3 LO II S-3	Far side	Somewhat dark
2423	8.5°	S	180°	W	NV	NV	31	LO II S-3, S-5	Far side	Somewhat dark
2424	9°	S	178°	E	NV	NV	33	LO II S-3, S-5	Far side	Somewhat dark
2425	9°	S	177°	E	NV	NV	34	LO II S-3, S-5	Far side	Somewhat dark
2426	10°	S	174°	E	NV	NV	36	LO II S-3, S-5	Far side	Somewhat dark
2427	10°	S	174°	E	NV	NV	37	LO II S-3, S-5	Far side	Somewhat dark
2428	10°	S	172.5°	E	NV	NV	38	LO II S-3, S-5	Far side	Somewhat dark
2429	10.5°	S	169°	E	NV	NV	42	LO II S-3, S-5	Far side	Good exp

TABLE A-IV.—*Apollo 8 Magazine B, SO-368 Film*^a—Continued

Rev	Frame (ASS-14-)	Lat	Long	Mode	Direction	<i>f</i> -stop	Shutter speed, sec	Sun angle, deg	Other coverage	Area	Remarks
.....	2430	10° S	166° E	NV	NV	44	LO I S-9	Far side	Good exp
.....	2431	10° S	164° E	NV	NV	47	LO II S-3, S-5 LO I S-9	Far side	Good exp
.....	2432	11° S	165° E	NV	NV	45	LO II S-3, S-5 LO I S-9	Far side	Good exp
.....	2433	10° S	161.5° E	NV	NV	48	LO II S-3, S-5 LO I S-9	Far side	Good exp
.....	2434	10° S	161° E	NV	NV	50	LO II S-3, S-5 LO I S-9	Far side	Good exp
.....	2435	11° S	157° E	NV	NV	48	LO II S-3, S-5 LO I S-9	Far side	Good exp
.....	2436	12° S	152.5° E	NV	NV	49	LO II S-3, S-5 LO I S-9	Far side	Good exp
.....	2437	12° S	152° E	NV	NV	53	LO II S-3, S-5 LO I S-9	Far side	Good exp
.....	2438	12° S	150° E	Oblique	WNW	53	LO II S-3, S-5 LO I S-9	Far side	Good exp
.....	2439	12° S	150° E	Oblique	WNW	54	LO II S-3, S-5 LO I S-9	Far side	Good exp
.....	2440	13° S	143° E	Oblique	WNW	71	LO II S-5 LO I S-9	Far side	Good exp
.....	2441	12.5° S	140° E	Oblique	WNW	68	LO II S-5 LO I S-9	Far side	Good exp
.....	2442	12.5° S	137.5° E	Oblique	W	69	LO II S-5 LO I S-9	Far side	Good exp
.....	2443	13° S	132° E	Oblique	W	70	LO II S-5 LO I S-9	Far side	Good exp
.....	2444	13° S	127° E	Oblique	NE	71	LO II S-5 LO I S-9	Far side	Good exp
.....	2445	13° S	127° E	Oblique	SW	76	LO II S-5 LO I S-9	Far side	Good exp
.....	2446	13° S	127° E	Oblique	SW	75	LO II S-5 LO I S-9	Far side	Good exp, T/O 49
.....	2447	21° S	128° E	H.O.	S	63	LO II S-5 LO I S-9	Tsiolkovsky	Good exp, T/O 47
.....	2448	21° S	128° E	H.O.	S	63	LO II S-5 LO I S-9	Tsiolkovsky	Good exp, T/O 47
.....	2449	21° S	128° E	H.O.	S	69	LO II S-5 LO I S-9	Tsiolkovsky	Good exp, T/O 40
.....	2450	21° S	128° E	H.O.	S	69	LO II S-5 LO I S-9	Tsiolkovsky	Good exp, T/O 40
.....	2451	21° S	128° E	H.O.	S	69	LO II S-5 LO I S-9	Far side	Good exp, T/O 40
.....	2452	11° S	113° E	H.O.	W	77	LO II S-5 LO I S-9	Far side	Good exp

TEC	2494	High alt Moon	Blue filter
TEC	2495	High alt Moon	Blue filter
TEC	2496	High alt Moon	Blue filter
TEC	2497	High alt Moon	Blue filter
TEC	2498	High alt Moon	Red filter
TEC	2499	High alt Moon	Red filter
TEC	2500	High alt Moon	Red filter
TEC	2501	High alt Moon	Red filter
TEC	2502	High alt Moon	Red filter
TEC	2503	High alt Moon	Red filter
TEC	2504	High alt Moon	Blue filter
TEC	2505	High alt Moon	Good exp
TEC	2506	High alt Moon	Good exp
TEC	2507	TEC	Earth
TEC	2508	TEC	Earth
TEC	2509	TEC	Earth
TEC	2510	TEC	Earth
TEC	2511	TEC	Earth
TEC	2512	TEC	Earth
TEC	2513	TEC	Earth
TEC	2514	TEC	Earth
TEC	2515	TEC	Earth
TEC	2516	TEC	Earth
TEC	2517	TEC	Earth
TEC	2518	TEC	Earth
TEC	2519	TEC	Earth
TEC	2520	TEC	Earth
TEC	2521	TEC	Earth
TEC	2522	TEC	Earth
TEC	2523	TEC	Earth
TEC	2524	TEC	Earth
TEC	2525	TEC	Earth

TABLE A-IV.—Apollo 8 Magazine B, SO-368 Film^a—Concluded

Rev	Frame (AS8-14-)	Lat	Long	Mode	Direction	f-stop	Shutter speed, sec	Sun angle, deg	Other coverage	Area	Remarks
TEC	2526	TEC	Earth
TEC	2527	TEC	Earth
TEC	2528	TEC	Earth
TEC	2529	TEC	Earth
TEC	2530	TEC	Earth
TEC	2531	TEC	Earth
TEC	2532	TEC	Earth
TEC	2533	TEC	Earth
TEC	2534	TEC	Earth

^a Entire roll shot with 250-mm lens, except 2385 to 2396, which were shot with 80-mm lens.

TABLE A-V.—*Apollo 8 Magazine C, 3400 Film*

Rev	Frame (AS8-17-)	Lat	Long	Mode	Direction	f-stop	Shutter speed, sec	Sun angle, deg	Other coverage	Area	Remarks
8	2659	3° S	152° W	CS		5.6	1/250	0	LO I S-3	Far side	Entire roll shot with 80-mm lens
8	2660			CS		5.6	1/250	1	LO V A-12	Far side	
8	2661			CS		5.6	1/250	2		Far side	
8	2662			CS		5.6	1/250	2		Far side	
8	2663			CS		5.6	1/250	3		Far side	
8	2664	4° S	157° W	CS		5.6	1/250	3	LO I S-3	Far side	
8	2665			CS		5.6	1/250	4	LO V A-12	Far side	
8	2666			CS		5.6	1/250	5		Far side	
8	2667			CS		5.6	1/250	6		Far side	
8	2668			CS		5.6	1/250	7		Far side	
8	2669	6° S	162° W	CS		5.6	1/250	8	LO I S-3	Far side	
8	2670			CS		5.6	1/250	9		Far side	
8	2671			CS		5.6	1/250	10		Far side	
8	2672			CS		5.6	1/250	11		Far side	
8	2673			CS		5.6	1/250	12		Far side	
8	2674			CS		5.6	1/250	13		Far side	
8	2675	7° S	169° W	CS		5.6	1/250	14	LO I S-3	Far side	
8	2676			CS		5.6	1/250	15	LO II S-3	Far side	
8	2677			CS		5.6	1/250	16		Far side	
8	2678			CS		5.6	1/250	17		Far side	
8	2679			CS		5.6	1/250	18		Far side	
8	2680	8° S	174° W	CS		5.6	1/250	19	LO I S-3	Far side	
8	2681			CS		5.6	1/250	20	LO II S-3	Far side	
8	2682			CS		5.6	1/250	21		Far side	
8	2683			CS		5.6	1/250	22		Far side	
8	2684			CS		5.6	1/250	23		Far side	
8	2685	9° S	179° W	CS		5.6	1/250	24	LO II S-3	Far side	
8	2686			CS		5.6	1/250	25		Far side	
8	2687			CS		5.6	1/250	26		Far side	
8	2688			CS		5.6	1/250	27		Far side	
8	2689			CS		5.6	1/250	28		Far side	
8	2690	9° S	176° E	CS		5.6	1/250	29	LO II S-3, S-5	Far side	
8	2691			CS		5.6	1/250	30		Far side	
8	2692			CS		5.6	1/250	31		Far side	

TABLE A-V.—Apollo 8 Magazine C, 3400 Film—Continued

Rev	Frame (AS8-17-)	Lat	Long	Mode	Direction	f-stop	Shutter speed, sec	Sun angle, deg	Other coverage	Area	Remarks
8	2693			CS		5.6	1/250	32		Far side	
8	2694	10° S	172° E	CS		5.6	1/250	33		Far side	
8	2695			CS		5.6	1/250	34		Far side	
8	2696			CS		5.6	1/250	35		Far side	
8	2697			CS		5.6	1/250	36		Far side	
8	2698			CS		5.6	1/250	37		Far side	
8	2699			CS		5.6	1/250	38		Far side	
8	2700	11° S	167° E	CS		5.6	1/250	38	LO I S-9	Far side	
8	2701			CS		5.6	1/250	39	LO II S-3, S-5	Far side	
8	2702			CS		5.6	1/250	40		Far side	
8	2703			CS		5.6	1/250	41		Far side	
8	2704			CS		5.6	1/250	42		Far side	
8	2705	11° S	162° E	CS		5.6	1/250	43	LO I S-9	Far side	
8	2706			CS		5.6	1/250	44	LO II S-3, S-5	Far side	
8	2707			CS		5.6	1/250	45		Far side	
8	2708			CS		5.6	1/250	46		Far side	
8	2709			CS		5.6	1/250	47		Far side	
8	2710	12° S	157° E	CS		5.6	1/250	48	LO I S-9	Far side	
8	2711			CS		5.6	1/250	49	LO II S-5	Far side	
8	2712			CS		5.6	1/250	50		Far side	
8	2713			CS		5.6	1/250	51		Far side	
8	2714	12° S	152° E	CS		5.6	1/250	52	LO I S-9	Far side	
8	2715			CS		5.6	1/250	53	LO II S-5	Far side	
8	2716			CS		5.6	1/250	54		Far side	
8	2717			CS		5.6	1/250	55		Far side	
8	2718			CS		5.6	1/250	56		Far side	
8	2719			CS		5.6	1/250	57		Far side	
8	2720	12° S	147° E	CS		5.6	1/250	57.5	LO I S-9	Far side	
8	2721			CS		5.6	1/250	58	LO II S-5	Far side	
8	2722			CS		5.6	1/250	59		Far side	
8	2723			CS		5.6	1/250	60		Far side	
8	2724			CS		5.6	1/250	61		Far side	

TABLE A-V.—Apollo 8 Magazine C, 3400 Film—Continued

Rev	Frame (AS8-17-)	Lat	Long	Mode	Direction	f-stop	Shutter speed, sec	Sun angle, deg	Other coverage	Area	Remarks
8	2756			H.O.		5.6	1/250	77		Far side	
8	2757			H.O.		5.6	1/250	76		Far side	
8	2758			H.O.	Forward	5.6	1/250	76			
8	2759			H.O.		5.6	1/250	75			
8	2760			H.O.		5.6	1/250	75			
8	2761	8° S	102° E	CS	Forward	5.6	1/250	74	LO II S-14	SE of Mare Smythii	Start CN
8	2762			CS		5.6	1/250	74			
8	2763			CS		5.6	1/250	73			
8	2764			CS		5.6	1/250	73			
8	2765	8° S	100° E	CS	Looking N	5.6	1/250	72	LO II S-14	SE of Mare Smythii	
8	2766			CS		5.6	1/250	72			
8	2767			CS		5.6	1/250	71			
8	2768			CS		5.6	1/250	71			
8	2769			CS		5.6	1/250	70			
8	2770			CS		5.6	1/250	70			
8	2771			CS		5.6	1/250	69			
8	2772	7° S	96° E	CS	Rear (E), looking N	5.6	1/250	69	LO II S-14	SE of Mare Smythii	
8	2773			CS		5.6	1/250	69			
8	2774			CS		5.6	1/250	68			
8	2775			CS		5.6	1/250	68			
8	2776			CS		5.6	1/250	67			
8	2777	10° S	95° E	CS	Rear (E)	5.6	1/250	66	LO II S-14	SE of Mare Smythii	
8	2778			CS		5.6	1/250	65			
8	2779			CS		5.6	1/250	64			
8	2780	11° S	91° E	CS	Rear (E)	5.6	1/250	63.5	LO II S-14	SE of Mare Smythii	
8	2781			CS		5.6	1/250	60			
8	2782			CS		5.6	1/250	58			
8	2783			CS		5.6	1/250	57			
8	2784			CS		5.6	1/250	55			
8	2785	9° S	80° E	CS	Rear (E)	5.6	1/250	53	LO II S-14 LO IV 27, 34	Kästner R	

TABLE A-V.—Apollo 8 Magazine C, 3400 Film—Continued

Rev	Frame (AS8-17-)	Lat	Long	Mode	Direction	f-stop	Shutter speed, sec	Sun angle, deg	Other coverage	Area	Remarks
S	2811			H.O.		5.6	1/250				
S	2812			H.O.		5.6	1/250	21		Secchi	T/O 80
S	2813			H.O.		5.6	1/250				T/O 80
S	2814			H.O.		5.6	1/250				T/O 80
S	2815			H.O.	Forward	5.6	1/250	17	LO V A 1, S 6 LO II S-1, S 2, P-1	Secchi	T/O 80
S	2816			H.O.		5.6	1/250		LO III P-2 LO IV 65, 66, 72, 73		
S	2817			H.O.		5.6	1/250		LO V 3, 1, 5, 1, 8A, 8B		
S	2818			H.O.		5.6	1/250	15		Tarminius F	T/O 80
S	2819			H.O.		5.6	1/250		LO I A-1, A-2, S 6		T/O 80
S	2820			H.O.	Forward	5.6	1/250	10	LO II P 1, P-2, S-2 LO IV 65, 66, 72, 73, 77, 78 LO V 8, 9, 11, 12	Maskelyne F	T/O 80
S	2821			H.O.		5.6	1/250		LO I S-9, A-3 LO II P-2, P-5, P-6 LO III P-1, P-5, P-6 LO IV 72, 73, 77, 78 LO V V9, 11A, 11B, 12, 13, 16A, 16B		T/O 80

TABLE A-VI.—Apollo 8 Magazine D, 3400 Film

Rev	Frame (AS8-12-)	Lat	Long	Mode	Direction	f-stop	Shutter speed, sec	Sun angle, deg	Other coverage	Area	Remarks
4	2044	4° S	148° W	VS		2.8	1/250	0	LO I S-3	Far side	Used 80-mm lens on VS pass
4	2045			VS		2.8	1/250	0		Far side	
4	2046	4° S	150° W	VS		2.8	1/250	0	LO V A-8, A-12	Far side	
4	2047			VS		2.8	1/250	1		Far side	
4	2048			VS		2.8	1/250	2		Far side	
4	2049			VS		2.8	1/250	4		Far side	
4	2050			VS		2.8	1/250	4		Far side	
4	2051			VS		2.8	1/250	5		Far side	
4	2052	5° S	157° W	VS		2.8	1/250	6		Far side	
4	2053			VS		2.8	1/250	7	LO I S-3	Far side	
4	2054			VS		2.8	1/250	8		Far side	
4	2055			VS		2.8	1/250	9		Far side	
4	2056			VS		2.8	1/250	10		Far side	
4	2057			VS		2.8	1/250	11		Far side	
4	2058			VS		2.8	1/250	12		Far side	
4	2059			VS		2.8	1/250	13		Far side	
4	2060			VS		4	1/250	14		Far side	
4	2061			VS		4	1/250	14		Far side	Exp change
4	2062	6° S	167° W	VS		4	1/250	15		Far side	
4	2063			VS		4	1/250	16	LO I S-3	Far side	
4	2064			VS		4	1/250	17		Far side	Extra frame
4	2065			VS		4	1/250	18		Far side	
4	2066			VS		4	1/250	19		Far side	
4	2067			VS		4	1/250	20		Far side	
4	2068			VS		4	1/250	21		Far side	
4	2069	8° S	173° W	VS		4	1/250	22		Far side	
4	2070			VS		4	1/250	23	LO I S-3	Far side	
4	2071			VS		4	1/250	24	LO II S-3	Far side	
4	2072			VS		4	1/250	25		Far side	
4	2073			VS		4	1/250	26		Far side	
4	2074			VS		4	1/250	27		Far side	
4	2075			VS		4	1/250	28		Far side	
4	2076	9° S	180° W	VS		4	1/250	29		Far side	
4	2077			VS		5.6	1/250	29	LO II S-3, S-5	Far side	Exp change
4	2078			VS		5.6	1/250	30		Far side	
4				VS		5.6	1/250	31		Far side	

4	2079	VS			5.6	1/250	32	Far side		
4	2080	VS			5.6	1/250	33	Far side		
4	2081	VS			5.6	1/250	34	Far side		
4	2082	VS			5.6	1/250	35	Far side		
4	2083	VS			5.6	1/250	35	Far side		
4	2084	VS			5.6	1/250	36	Far side		
4	2085	VS			5.6	1/250	37	Far side		
4	2086	VS			5.6	1/250	38	Far side		
4	2087	VS			5.6	1/250	39	Far side		
4	2088	VS	11° S	168° E	5.6	1/250	40	Far side	LO I S-9 LO II S-3, S-5	
4	2089	VS			5.6	1/250	41	Far side		Exp change
4	2090	VS			8	1/250	42	Far side		
4	2091	VS			8	1/250	43	Far side		
4	2092	VS			8	1/250	44	Far side		
4	2093	VS			8	1/250	45	Far side		
4	2094	VS			8	1/250	46	Far side		Extra frame
4	2095	VS			8	1/250	47	Far side		
4	2096	VS			8	1/250	48	Far side		
4	2097	VS			8	1/250	49	Far side		
4	2098	VS			8	1/250	50	Far side		
4	2099	VS			8	1/250	51	Far side		
4	2100	VS	12° S	157° E	8	1/250	51.5	Far side	LO I S-9 LO II S-3, S-5	
4	2101	VS			8	1/250	52	Far side		
4	2102	VS			8	1/250	53	Far side		
4	2103	VS			8	1/250	54	Far side		
4	2104	VS			8	1/250	55	Far side		
4	2105	VS			8	1/250	56	Far side		
4	2106	VS			8	1/250	57	Far side		
4	2107	VS			8	1/250	58	Far side		
4	2108	VS			8	1/250	59	Far side		
4	2109	VS			8	1/250	60	Far side		
4	2110	VS			8	1/250	61	Far side		
4	2111	VS	13° S	147° E	8	1/250	61	Far side	LO I S-9 LO II S-5	Extra frame
4	2112	VS			8	1/250	62	Far side		
4	2113	VS			8	1/250	63	Far side		
4	2114	VS			8	1/250	64	Far side		
4	2115	VS			8	1/250	65	Far side		
4	2116	VS			8	1/250	66	Far side		
4	2117	VS	14° S	140° E	8	1/250	66.5	Far side	LO I S-9 LO II S-5 LO III S-21.5	
4	2118	VS			8	1/250	67	Far side		

TABLE A-VI.—Apollo 8 Magazine D, 3400 Film—Continued

Rev	Frame (AS8-12-)	Lat	Long	Mode	Direction	f-stop	Shutter speed, sec	Sun angle, deg	Other coverage	Area	Remarks
4	2119			VS		8	1/250	68		Far side	
4	2120			VS		8	1/250	69		Far side	
4	2121			VS		8	1/250	70		Far side	
4	2122	13° S	134° E	VS		8	1/250	71.5	LO I S-9 LO III S-21.5	Far side	
4	2123			VS		8	1/250	72		Far side	
4	2124			VS		11	1/250	73		Far side	
4	2125			VS		11	1/250	74		Far side	
4	2126			VS		11	1/250	75		Far side	
4	2127			VS		11	1/250	76		Far side	
4	2128			VS		11	1/250	76		Far side	
4	2129	12° S	127° E	VS		11	1/250	77	LO I S-9 LO III S-21.5	Far side	
4	2130			VS		11	1/250	77		Far side	
4	2131			VS		11	1/250	78		Far side	
4	2132			VS		11	1/250	78		Far side	
4	2133			VS		11	1/250	79		Far side	
4	2134			VS		11	1/250	79		Far side	
4	2135			VS		11	1/250	80		Far side	
4	2136	12° S	120° E	VS		11	1/250	80	LO I S-9 LO III S-21.5	Far side	
4	2137			VS		11	1/250	80		Far side	Start spacecraft roll
4	2138			VS		11	1/250	79		Far side	
4	2139			VS		11	1/250	79		Far side	
4	2140			VS		11	1/250	78		Far side	
4	2141	12° S	113° E	VS		11	1/250	78	LO I S-9 LO II S-14 LO III S-21.5	Far side	
4	2142			VS		11	1/250	77		Far side	
4	2143			VS		11	1/250	77		Far side	
4	2144			VS		11	1/250	76		Far side	
4	2145			VS		11	1/250	76		Far side	
4	2146	11° S	108° E	VS		11	1/250	75	LO III S-21.5 LO II S-14 LO I S-9	Far side	
4	2147			VS		11	1/250	75		Far side	
4	2148			VS		11	1/250	74		Far side	

TABLE A-VI.—Apollo 8 Magazine D, 3400 Film—Continued

Rev	Frame (AS8-12-)	Lat	Long	Mode	Direction	f-stop	Shutter speed, sec	Sun angle, deg	Other coverage	Area	Remarks
4	2184	8° S	67° E	H.O. hor	Forward, W	11	1/250	37	LO IV 39, 184, 185	W of Langrenus	T/O 68
4	2185					11	1/250			Earth	
4	2186					11	1/250			Earth	
10 (TEI)	2187	40° S	153° E			11	1/250	47		S of Tsiolkovsky	
10 (TEI)	2188					11	1/250			Earth and lunar hor	
10 (TEI)	2189	26° S	72° E	H.O. hor	S	11	1/250	35	LO IV 27, 33, 34, 38, 39, 46, 52, 53, 59, 60, 64, 184, 185	Humboldt	T/O 58, T/O 63
10 (TEI)	2190	20° S	79° E	H.O. hor	S	11	1/250	45		Humboldt	T/O 58
10 (TEI)	2191					11	1/250	43	LO IV 9, 10, 11, 12, 5, 6, 8	Mare Australe	Overexposed 230-mm lens
10 (TEI)	2192	40° S	100° E	H.O.	S	11	1/250	50	LO IV 27, 33, 34, 38, 39, 46, 52, 53, 59, 60, 64, 184, 185	Humboldt	T/O 58, T/O 63
10 (TEI)	2193	27° S	90° E	L.O.	S	11	1/250	51	LO IV S-121.5 LO V 4, 10, 11, 12, 27, 33	Mare Australe	
10 (TEI)	2194	33° S	100° E		S	11	1/250	61	LO I S-9	E of Mare Australe	T/O 54
10 (TEI)	2195	26° S	107° E		S	11	1/250	68	LO III S-21.5 LO I S-9	Tsiolkovsky	
10 (TEI)	2196	21° S	130° E	H.O. hor	E	11	1/250	80	LO II S-5 LO IV 146, 147 LO I S-9	N of Tsiolkovsky	Overexposed, 250- mm lens, T/O 28, 29, 31, 32, 33, 35, 36, 37, 41, 44
10 (TEI)	2197	8° S	127° E	H.O. hor	E	11	1/250	82	LO II S-3, S-4		T/O 32, 33, 35, 36, 37, 41, 44 T/O 44, 45 T/O 45
10 (TEI)	2198	8° S	126° E	H.O. hor	E	11	1/250	82.5	LO II S-5, S-14	N of Tsiolkovsky	
10 (TEI)	2199	8° S	127° E	L.O.	E	11	1/250	74	LO I S-1, S-9	N of Tsiolkovsky	
10 (TEI)	2200	11° S	108° E	L.O.	E	11	1/250		LO II S-14	Far side	

APPENDIX A

10 (TEI)	2201	10° S	100° E	NV	11	1/250	68	LO I S-1 LO II S-14	E of Mare Smythii	T/O 58
10 (TEI)	2202	5° S	90° E	NV	11	1/250	60	LO I S-1 LO II S-14	Mare Smythii	T/O 59
10 (TEI)	2203	9° S	68° E	NV	11	1/250	37	LO I S-4	Langrenus	T/O 65, 59, 68
10 (TEI)	2204	3° S	73° E	NV	N	11	1/250	43	LO IV 28, 34	Gilbert	T/O 59, 67
10 (TEI)	2205	3° N	73° E	NV	N	11	1/250	43	LO IV 35, 39, 40, 46	Gilbert	T/O 59, 67
10 (TEI)	2206	7° N	74° E	NV	N	11	1/250	43	LO IV 47, 53, 54, 165	Mare Undarum	T/O 66, 59, 67
10 (TEI)	2207	7° N	82° E	NV	NW	11	1/250	52	LO IV 177, 178, 184, 185	Neper	T/O 59
10 (TEI)	2208	9° N	86° E	NV	NW	11	1/250	54	LO IV 191, 192	Neper, Goddard	
10 (TEI)	2209	24° N	100° E	H.O. hor	N	11	1/250	56	LO II S-14 LO IV 17, 18, 20, 24, 165	Joliot-Curie, Lomonosov	
10 (TEI)	2210	36° S	85° E	L.O.	S	11	1/250	40	LO IV 9, 10, 11, 12, 27, 33, 34, 38, 39	Mare Australe, Abel	
10 (TEI)	2211	35° S	90° E	L.O.	S	11	1/250	42	LO I S-9 LO IV 9, 10, 11, 12, 27, 35	Mare Australe	
10 (TEI)	2212	37° S	101° E	L.O.	S	11	1/250	47	LO I S-9 LO IV 9, 10, 11, 12, 27, 35	Mare Australe	T/O 52
10 (TEI)	2213	35° S	110° E	H.O. hor	SE	11	1/250	53	LO I S-9 LO IV 9, 10, 11, 12, 27, 35	Mare Australe	T/O 52, 54
10 (TEI)	2214	36° S	116° E	H.O. hor	SE	11	1/250	53	LO I S-9 LO IV 9, 10, 11, 12, 27, 35	Mare Australe	T/O 38, 49, 52

TABLE A-VII.—Apollo 8 Magazine E, 3400 Film

Rev	Frame (ASS-13-)	Lat	Long	Mode	Direction	f-stop	Shutter speed, sec	Sun angle, deg	Other coverage	Area	Remarks
.....	2215	10.25° S	55.5° E	L.O.	S	5.6	1/250	23	LO IV 60, 65	Colombo	T/O 72
.....	2216	10.25° S	55.33° E	L.O.	S	5.6	1/250	22	LO IV 60, 65	Colombo	T/O 72
.....	2217	10° S	53.75° E	L.O.	S	5.6	1/250	21	LO IV 60, 65	Colombo	T/O 72
.....	2218	11.5° S	51.5° E	L.O.	S	5.6	1/250	19	LO IV 60, 65	Colombo	T/O 72
.....	2219	11.75° S	50.75° E	L.O.	S	5.6	1/250	19	LO IV 60, 65	Colombo	T/O 72
.....	2220	11.92° S	49.5° E	L.O.	S	5.6	1/250	18	LO IV 60, 65	Colombo	T/O 72
.....	2221	12.5° S	48° E	L.O.	S	5.6	1/250	17	LO IV 60, 65	Colombo	T/O 72
.....	2222	11.5° S	47.5° E	L.O.	S	5.6	1/250	15	LO IV 60, 65	Colombo	T/O 72
.....	2223	11.92° S	46.5° E	L.O.	S	5.6	1/250	14	LO IV 60, 65	Colombo	T/O 72
.....	2224	11.25° S	45° E	L.O.	S	5.6	1/250	13	LO IV 60, 65	Colombo	T/O 72
.....	2225	10.75° S	44.75° E	L.O.	S	5.6	1/250	12	LO IV 60, 65	Colombo	T/O 72
.....	2226	10.75° S	42.25° E	L.O.	S	5.6	1/250	11	LO IV 60, 65	Colombo	T/O 72
.....	2227	12.5° S	42.5° E	L.O.	S	5.6	1/250	10	LO IV 60, 65	Colombo	T/O 72
.....	2228	6° S	38.5° E	L.O.	S	5.6	1/250	7	LO IV 60, 65	Pyrenees Mts.	Term. shot including T/O 90
.....	2229	5.5° S	37° E	L.O.	S	5.6	1/250	6	LO IV 60, 65	Pyrenees Mts.	
.....	2230	5.5° S	36.5° E	L.O.	S	5.6	1/250	6	LO IV 60, 65	Pyrenees Mts.	
.....	2231	6° S	35.5° E	L.O.	S	5.6	1/250	4	LO IV 60, 65	Pyrenees Mts.	
.....	2232	PP in darkness		L.O.	S	5.6	1/250	3	LO IV 65	Pyrenees Mts.	
.....	2233	PP in darkness		L.O.	S	5.6	1/250	3	LO IV 65	Pyrenees Mts.	
.....	2234	PP in darkness		L.O.	S	5.6	1/250	2	LO IV 65	Pyrenees Mts.	
.....	2235	PP in darkness		L.O.	S	5.6	1/250	2	LO IV 65	Pyrenees Mts.	
.....	2236	PP in darkness		L.O.	S	5.6	1/250	2	LO IV 65	Pyrenees Mts.	
.....	2237	PP in darkness		L.O.	S	5.6	1/250	2	LO IV 65	Pyrenees Mts.	
.....	2238	PP in darkness		L.O.	S	5.6	1/250	2	LO IV 65	Pyrenees Mts.	
.....	2239	PP in darkness		L.O.	S	5.6	1/250	2	LO IV 65	Pyrenees Mts.	
.....	2240	PP in darkness		L.O.	S	5.6	1/250	2	LO IV 65	Pyrenees Mts.	
.....	2241	PP in darkness		L.O.	S	5.6	1/250	2	LO IV 65	Pyrenees Mts.	
.....	2242	PP in darkness		L.O.	S	5.6	1/250	2	LO IV 65	Pyrenees Mts.	
.....	2243	15° S	35° E	H.O.	S	5.6	1/250	3	LO IV 65	Fracastorius	T/O 12
.....	2244	12° S	162° W	L.O.	S	5.6	1/250	10	LO II 75		T/O 12
.....	2245	11° S	164.5° W	L.O.	S	5.6	1/250	15	LO I S-3		T/O 12
.....	2246	15° S	165° W	H.O.	S	5.6	1/250	12	LO I S-3		T/O 12
.....	2247	14° S	167° W	H.O.	S	5.6	1/250	15	LO I S-3		T/O 12
.....	2248	18° S	130° E	L.O.	S	8	1/250	70	LO I S-9	Tsiolkovsky	T/O 40
.....	2249	17.5° S	127° E	L.O.	S	8	1/250	72	LO III S-21.5 LO I S-9 LO III S-21.5	Tsiolkovsky	T/O 36(?)

APPENDIX A

2250	17°	S	126.5° E	L.O.	S	8	1/250	73	LO I S-9 LO III S-21.5	Tsiolkovsky	T/O 36(?)
2251	17°	S	125° E	L.O.	S	8	1/250	74	LO I S-9 LO III S-21.5	Tsiolkovsky	T/O 40
2252	20°	S	129° E	H.O.	S	8	1/250	71	LO I S-9 LO III S-21.5	Tsiolkovsky	T/O 40
2253	20°	S	126.5° E	H.O.	S	8	1/250	70	LO I S-9 LO III S-21.5	Tsiolkovsky	T/O 40
2254	21°	S	126.5° E	H.O.	S	8	1/250	70	LO I S-9 LO III S-21.5	Tsiolkovsky	T/O 40
2255	20°	S	124.5° E	H.O.	S	8	1/250	70	LO I S-9 LO III S-21.5	Tsiolkovsky	T/O 40
2256	20°	S	116.5° E	L.O.	S	8	1/250	72	LO I S-9 LO III S-21.5	W of Tsiolkovsky	T/O 49
2257	0.5°	N	35.5° E	NV	S	5.6	1/250	5	LO I S-6, S-7, A-2	Western edge of Mare Fecundi- tatis	Term. shot
2258	0.5°	N	35.25° E	NV	S	5.6	1/250	4	LO IV V-6, V-12	Western edge of Mare Fecundi- tatis	
2259	0.5°	N	39.75° E	NV	S	5.6	1/250	3	LO IV 72, 73	Western edge of Mare Fecundi- tatis	
2260	0.5°	N	34° E	NV	S	5.6	1/250	2		Western edge of Mare Fecundi- tatis	
2261	0.5°	N	33.5° E	NV	S	5.6	1/250	1		Western edge of Mare Fecundi- tatis	
2262	15°	S	93° E	L.O.	S	5.6	1/250	63	LO II S-14	NE of Humboldt	T/O 58
2263	14°	S	90.5° E	L.O.	S	5.6	1/250	62	LO II S-14	NE of Humboldt	T/O 58
2264	18°	S	93° E	H.O.	S	5.6	1/250	62	LO II S-14	NE of Humboldt	T/O 58
2265	18°	S	91.5° E	H.O.	S	5.6	1/250	60	LO II S-14	NE of Humboldt	T/O 58
2266	13.5°	S	79.5° E	L.O.	S	8	1/250	47	LO IV 178		
2267	13.5°	S	78.5° E	L.O.	S	8	1/250	46	LO IV 178		T/O 63
2268	14.5°	S	78° E	L.O.	S	8	1/250	45	LO IV 178		T/O 63
2269	18°	S	79° E	H.O.	S	8	1/250	45	LO IV 178		T/O 65
2270	11°	S	71° E	L.O.	S	8	1/250	39	LO IV 184		Training sequence
2271				H.O.	W	5.6 (?)	(?)	8	LO I S-6, S-7	Mare Tranquil- litatis	Training sequence
2272			Principal line runs from 42° E, 30.25° N, to 33.5° E, 4.5° N	H.O.	W	5.6 (?)	1/250		LO II P-2	Mare Tranquil- litatis	Training sequence
2273				H.O.	W	5.6 (?)	1/250		LO IV 73, 76	Mare Tranquil- litatis	Training sequence

TABLE A-VII.—Apollo 8 Magazine E, 3400 Film—Continued

Rev	Frame (AS8-13-)	Lat	Long	Mode	Direction	f-stop	Shutter speed, sec	Sun angle, deg	Other coverage	Area	Remarks
.....	2274			H.O.	W	5.6 (?)	1/250 (?)	5	LO V V-5.1, V-6, V-9.1, V-11a, V-11b, V-12	Mare Tranquil- litatis	Training sequence
.....	2275			H.O.	W	5.6 (?)	1/250 (?)	LO V V-5.1, V-6, V-9.1, V-11a, V-11b, V-12	Mare Tranquil- litatis	Training sequence
.....	2276			H.O.	W	5.6 (?)	1/250 (?)	LO V V-5.1, V-6, V-9.1, V-11a, V-11b, V-12	Mare Tranquil- litatis	Training sequence
.....	2277			H.O.	W	5.6 (?)	1/250 (?)	LO V V-5.1, V-6, V-9.1, V-11a, V-11b, V-12	Mare Tranquil- litatis	Training sequence
.....	2278		Principal line runs from 42° E, 30.25° N, to 33.5° E, 4.5° N	H.O.	W	5.6 (?)	1/250 (?)	LO V V-5.1, V-6, V-9.1, V-11a, V-11b, V-12	Mare Tranquil- litatis	Training sequence
.....	2279			H.O.	W	5.6 (?)	1/250 (?)	LO V V-5.1, V-6, V-9.1, V-11a, V-11b, V-12	Mare Tranquil- litatis	Training sequence
.....	2280			H.O.	W	5.6 (?)	1/250 (?)	2	LO V V-5.1, V-6, V-9.1, V-11a, V-11b, V-12	Mare Tranquil- litatis	Training sequence
.....	2281			H.O.	W	5.6 (?)	1/250 (?)	2	LO V V-5.1, V-6, V-9.1, V-11a, V-11b, V-12	Mare Tranquil- litatis	Training sequence
.....	2282			L.O.	W	5.6 (?)	1/250 (?)	LO V V-5.1, V-6, V-9.1, V-11a, V-11b, V-12	Mare Tranquil- litatis	Training sequence

2283	L.O.	W	5.6 (?)	1/250 (?)	LO V V-5.1, V-6, V-9.1, V-11a, V-11b, V-12	Mare Tranquil- litatis	Training sequence
2284	L.O.	W	5.6 (?)	1/250 (?)	LO V V-5.1, V-6, V-9.1, V-11a,	Mare Tranquil- litatis	Training sequence
2285	L.O.	W	5.6 (?)	1/250 (?)	V-11b, V-12 LO V V-5.1, V-6, V-9.1, V-11a,	Mare Tranquil- litatis	Training sequence
2286	L.O.	W	5.6 (?)	1/250 (?)	V-11b, V-12 LO V V-5.1, V-6, V-9.1, V-11a,	Mare Tranquil- litatis	Training sequence
2287	L.O.	W	5.6 (?)	1/250 (?)	V-11b, V-12 LO V V-5.1, V-6, V-9.1, V-11a,	Mare Tranquil- litatis	Training sequence
2288	L.O.	W	5.6 (?)	1/250 (?)	V-11b, V-12 LO V V-5.1, V-6, V-9.1, V-11a,	Mare Tranquil- litatis	Training sequence
2289	L.O.	W	5.6 (?)	1/250 (?)	V-11b, V-12 LO V V-5.1, V-6, V-9.1, V-11a,	Mare Tranquil- litatis	Training sequence
2290	L.O.	NW	5.6 (?)	1/250 (?)	V-11b, V-12 LO V V-5.1, V-6, V-9.1, V-11a,	Mare Tranquil- litatis	Training sequence
2291	L.O.	NW	5.6 (?)	1/250 (?)	V-11b, V-12 LO V V-5.1, V-6, V-9.1, V-11a,	Mare Tranquil- litatis	Training sequence
2292	L.O.	NW	5.6 (?)	1/250 (?)	V-11b, V-12 LO V V-5.1, V-6, V-9.1, V-11a,	Mare Tranquil- litatis	Training sequence
2293	L.O.	NW	5.6 (?)	1/250 (?)	V-11b, V-12 LO V V-5.1, V-6, V-9.1, V-11a,	Mare Tranquil- litatis	Training sequence

Principal line runs
from 42° E, 30.25°
N, to 33.5° E, 4.5°
N

TABLE A-VII.—Apollo 8 Magazine E, 3400 Film—Continued

Rev	Frame (AS8-13-)	Lat	Long	Mode	Direction	f-stop	Shutter speed, sec	Sun angle, deg	Other coverage	Area	Remarks
.....	2294			L.O.	NW	5.6 (?)	1/250 (?)	LO V V-5.1, V-6, V-9.1, V-11a, V-11b, V-12	Mare Tranquil- litatis	Training sequence
.....	2295			L.O.	NW	5.6 (?)	1/250 (?)	LO V V-5.1, V-6, V-9.1, V-11a, V-11b, V-12	Mare Tranquil- litatis	Training sequence
.....	2296			L.O.	NW	5.6 (?)	1/250 (?)	LO V V-5.1, V-6, V-9.1, V-11a, V-11b, V-12	Mare Tranquil- litatis	Training sequence
.....	2297			L.O.	NW	5.6 (?)	1/250 (?)	LO V V-5.1, V-6, V-9.1, V-11a, V-11b, V-12	Mare Tranquil- litatis	Training sequence
.....	2298		Principal line runs from 42° E, 30.25° N, to 33.5° E, 4.5° N	NV	NW	5.6 (?)	1/250 (?)	LO V V-5.1, V-6, V-9.1, V-11a, V-11b, V-12	Mare Tranquil- litatis	Training sequence
.....	2299			NV	NW	5.6 (?)	1/250 (?)	LO V V-5.1, V-6, V-9.1, V-11a, V-11b, V-12	Mare Tranquil- litatis	Training sequence
.....	2300			NV	NE	5.6 (?)	1/250 (?)	2	LO V V-5.1, V-6, V-9.1, V-11a, V-11b, V-12	Mare Tranquil- litatis	Training sequence
.....	2301			NV	NE	5.6 (?)	1/250 (?)	LO V V-5.1, V-6, V-9.1, V-11a, V-11b, V-12	Mare Tranquil- litatis	Training sequence
.....	2302			NV	NE	5.6 (?)	1/250 (?)	LO V V-5.1, V-6, V-9.1, V-11a, V-11b, V-12	Mare Tranquil- litatis	Training sequence

2303	L.O.	NE	5.6	1/250 (?)	LO V V-5.1, V-6, V-9.1, V-11a, V-11b, V-12	Mare Tranquil- littatis	Training sequence
2304	L.O.	NE	5.6	1/250 (?)	LO V V-5.1, V-6, V-9.1, V-11a, V-11b, V-12	Mare Tranquil- littatis	Training sequence
2305	L.O.	NE	5.6	1/250 (?)	LO V V-5.1, V-6, V-9.1, V-11a, V-11b, V-12	Mare Tranquil- littatis	Training sequence
2306	L.O.	NE	5.6	1/250 (?)	LO V V-5.1, V-6, V-9.1, V-11a, V-11b, V-12	Mare Tranquil- littatis	Training sequence
2307	L.O.	NE	5.6	1/250 (?)	LO V V-5.1, V-6, V-9.1, V-11a, V-11b, V-12	Mare Tranquil- littatis	Training sequence
2308	L.O.	NE	5.6	1/250 (?)	LO V V-5.1, V-6, V-9.1, V-11a, V-11b, V-12	Mare Tranquil- littatis	Training sequence
2309	L.O.	NE	5.6	1/250 (?)	LO V V-5.1, V-6, V-9.1, V-11a, V-11b, V-12	Mare Tranquil- littatis	Training sequence
2310	L.O.	S	5.6	1/250	LO I S-3	Mare Tranquil- littatis	Term. shot (far side)
2311	L.O.	S	5.6	1/250	LO I S-3		Term. (far side)
2312	L.O.	S	5.6	1/250	LO I S-3		
2313	L.O.	S	5.6	1/250	LO I S-3		
2314	L.O.	S	5.6	1/250	LO I S-3		
2315	L.O.	S	5.6	1/250	LO I S-3		
2316	L.O.	S	5.6	1/250	LO I S-3		
2317	L.O.	S	5.6	1/250	LO I S-3		
2318	L.O.	S	5.6	1/250	LO I S-3		
2319	L.O.	S	5.6	1/250	LO I S-3		
2320	H.O.	S	5.6	1/250	LO I S-3		
2321	H.O.	SE	5.6		LO I S-3		T/O 12
2322	L.O.	SW	5.6		LO II S-5		T/O 10
2323	L.O.	SE	5.6		LO II S-5		T/O 20
2324	L.O.	SE	5.6		LO II S-5		T/O 19
2325	L.O.	SE	5.6		LO II S-5		T/O 19
							T/O 23

Principal line runs
from 42° E, 30.25°
N, to 33.5° E, 4.5°
N

TABLE A-VII.—Apollo 8 Magazine E, 3400 Film—Continued

Rev	Frame (AS8-13-)	Lat	Long	Mode	Direction	f-stop	Shutter speed, sec	Sun angle, deg	Other coverage	Area	Remarks
.....	2326	16° S	158° E	L.O.	SE	5.6	51	LO II S-5	E of Tsiolkovsky	T/O 28
.....	2327	19° S	144° E	L.O.	SE	8	1/250	61	LO III MR-121
.....	2328	17° S	140° E	L.O.	SE	8	1/250	57	LO I MR-115	E of Tsiolkovsky	T/O 31(?)
.....	2329	PP in space	H.O.	SW	1/250	LO I S-9	Looking toward Gibbs	Moon/Earth shot
.....	2330	0°	107°20'E	H.O.	N	1/250	76	LO II S-14	E of Mare
.....	2331	1.5° N	90° E	L.O.	N	8	1/250	59	LO II S-14	Smythii to hor
.....	2332	2.5° N	87.5° E	L.O.	N	8	1/250	57	LO III S-21.5	T/O 59 (in part)
.....	2333	H.O.	LO I S-1
.....	2334	PP in darkness	L.O.	N	5.6	1/250	1	LO II S-14	Overexposed frame, insufficient detail to plot
.....	2335	11.5° N	31° E	L.O.	N	5.6	1/250	1	LO IV 78	Northern part of Mare Tranquil- litas	Term. (near side)
.....	2336	12° N	31° E	H.O.	N	5.6	1/250	1	LO IV 78	Northern part of Mare Tranquil- litas
.....	2337	15° N	31.5° E	H.O.	N	5.6	1/250	1	LO IV 78	Northern part of Mare Tranquil- litas
.....	2338	PP on horizon	H.O.	N	5.6	1/250	1	LO IV 78	Northern part of Mare Tranquil- litas
.....	2339	1° S	54° E	H.O.	W	5.6	1/250	25	LO I S-4, S-5, S-6	Mare Tranquil- litas
.....	2340	0.5° S	50° E	H.O.	W	5.6	1/250	20	LO II S-1 LO III P-2 LO IV 53, 54, 60, 61	Mare Tranquil- litas

2341	PP on horizon	H.O.	W	5.6	1/250	17	LO V V-3.1, V-5.1, V-6, V-8a, V-8b LO I A-1, S-6, S-7		
2342	0.5° N 38°	E H.O.	W	5.6	1/250	10	LO II P-2 LO III P-2		
2343	2° N 35°	E H.O.	W	5.6	1/250	5	LO IV V-5.1, V-6, V-11a, 11b, V-12, V-9.1		
2344	PP on horizon	H.O.	NW	5.6	1/250	6	LO IV V-5.1, V-6, V-11a, V-11b, V-12, V-9.1		
2345	PP in space	H.O.	NW	5.6	1/250	3	LO IV 63, 73, 78	Mare Tranquil- litas	
2346	PP in space	H.O.	NW	4	1/250	1	LO V V-9.1	NW of Mare Tranquillitatis	
2347	PP in space	H.O.	W	4	1/250	1	LO V V-9.1		
2348	14.3° N 30°	E H.O.	N	2.8	1/250	1	LO V V-9.1		Term. shot near side
2349	13° N 30.25°	E L.O.	N	2.8		1	LO V V-9.1	NW of Mare Tranquillitatis	
2350	15° N 30°	E L.O.	N	2.8		1	LO V V-9.1	NW of Mare Tranquillitatis	
2351	PP on horizon	L.O.	N	2.8		1	LO V V-9.1	NW of Mare Tranquillitatis	
2352	TEI							Moon	80-mm lens
2353	TEI							Moon	80-mm lens
2354	TEI							Moon	80-mm lens
2355	TEI							Moon	80-mm lens
2356	TEI							Moon	80-mm lens
2357	TEI							Moon	80-mm lens
2358	TEI							Moon	80-mm lens
2359	TEI							Moon	250-mm lens
2360	TEI							Moon	250-mm lens
2361	TEI							Moon	250-mm lens
2362	TEI							Moon	250-mm lens
2363	TEI							Moon	250-mm lens
2364	TEI							Moon	250-mm lens
2365	TEI							Moon	250-mm lens
2366	TEI							Moon	250-mm lens
2367	TEI							Moon	250-mm lens
2368	TEI							Moon	250-mm lens
2369	TEI							Earth	250-mm lens

TABLE A-VII.—*Apollo 8 Magazine E, 3400 Film—Concluded*

Rev	Frame (AS8-13-)	Lat	Long	Mode	Direction	f-stop	Shutter speed, sec	Sun angle, deg	Other coverage	Area	Remarks
TEI	2370	TEI	Earth	250-mm lens
TEI	2371	TEI	Earth	250-mm lens
TEI	2372	TEI	Earth	250-mm lens
TEI	2373	TEI	Earth	250-mm lens
TEI	2374	TEI	Earth	250-mm lens
TEI	2375	TEI	Earth	250-mm lens
TEI	2376	Earth	250-mm lens
TEI	2377	Earth	250-mm lens
TEI	2378	Earth	250-mm lens
TEI	2379	Earth	250-mm lens
TEI	2380	Earth	250-mm lens
TEI	2381	Earth	250-mm lens
TEI	2382	Earth	250-mm lens

TABLE A-VIII.—*Apollo 8 Magazine F, SO-121 Film*

Rev	Frame (AS8-15-)	Lat	Long	Mode	Direction	f-stop	Shutter speed, sec	Sun angle, deg	Other coverage	Area	Remarks
TLC...	2535									Earth	80-mm lens
TLC...	2536									Earth	80-mm lens
TLC...	2537									Earth	80-mm lens
TLC...	2538									Earth	80-mm lens
TLC...	2539									Earth	80-mm lens
TLC...	2540									Earth	80-mm lens
TLC...	2541									Earth	80-mm lens
TLC...	2542									Earth	80-mm lens
TLC...	2543									Earth	80-mm lens
TLC...	2544									Earth	80-mm lens
TEC...	2545									Moon	80-mm lens
TEC...	2546									Moon	80-mm lens
TEC...	2547									Moon	80-mm lens
TEC...	2548									Moon	80-mm lens
TEC...	2549									Moon	80-mm lens
TEC...	2550									Moon	80-mm lens
TEC...	2551									Moon	80-mm lens
TEC...	2552									Moon	80-mm lens
TEC...	2553									Moon	80-mm lens
TEC...	2554									Moon	80-mm lens
TEC...	2555									Moon	80-mm lens
TEC...	2556									Moon	80-mm lens
TEC...	2557									Moon	80-mm lens
TEC...	2558									Moon	80-mm lens
TEC...	2559									Moon	80-mm lens
TEC...	2560									Moon	80-mm lens
TEC...	2561									Moon	80-mm lens
TEC...	2562									Moon	80-mm lens
TEC...	2563									Moon	80-mm lens
	to										
TEC...	2573									Earth	250-mm lens
	2574									Earth	250-mm lens
	to										
	2580									Earth	250-mm lens

TABLE A-IX.—Apollo 8 Magazine G, 2458 Film

Rev	Frame (AS8-18-)	Lat	Long	Mode	Direction	f-stop	Shutter speed, sec	Sun angle, deg	Other coverage	Area	Remarks
	2828	8° S	149° W	NV	S		1/250	0		Far side	Term.
	2829	9° S	149° W	NV	S		1/250	0		Far side	Term.
	2830	10° S	149° W	L.O.	S		1/250	0		Far side	Term.
	2831	11° S	149° W	L.O.	S		1/250	0		Far side	Term.
	2832	15° S	148° W	L.O.	S		1/250	0		Far side	Term.
	2833			H.O.	S		1/250			Far side	Term.
	2834	16° S	158° W	H.O.	S		1/250	8		Far side	
	2835	16° S	171° W	L.O.	S		1/250	20		Far side	
	2836	19° S	179° W	H.O.	S		1/250	28		Far side	
	2837	16° S	175° E	L.O.	S		1/250	34		Far side	
	2838	14° S	174° E	L.O.	S		1/250	36		Far side	T/O 20 (partial)
	2839	20° S	174° E	H.O.	S		1/250	34		Far side	
	2840	16° S	173° E	L.O.	S		1/250	36		Far side	T/O 20 (partial)
	2841	15° S	172° E	L.O.	S		1/250	37		Far side	T/O 20 (partial)
	2842	17° S	167° E	L.O.	S		1/250	42		Far side	T/O 23
	2843	21° S	157° E	L.O.	S		1/250	48		Far side	Uncertain
	2844	15° S	155° E	L.O.	E		1/250	54		Far side	
	* 2845	06° S	85° E	NV			1/250	57			T/O 59
	2846	08.5° S	81° E	NV	S		1/250	48			
	2847	11° S	78° E	NV	S		1/250	47			
	2848	14° S	76° E	NV	S		1/250	44			T/O 65
	2849	16° S	75° E	NV	S		1/250	42		Far side	T/O 62 (partial) T/O 58
	2850			H.O.	E		1/250				
	2851	14° N	67° E	L.O.	N		1/250	35		Mare Nectaris Mare Crisium Mare Crisium	Slightly blurred, not plotted
	2852	Not plotted, same area as 2853		L.O.	N						
	2853	10° N	72° E	L.O.	N		1/250	47		Mare Crisium E of Mare Smythii	Slightly blurred
	2854	03° S	110° E	H.O.	E		1/250	3		E of Mare Smythii	Slightly blurred
	2855										
	2856	26° N	58° E	H.O.	N		1/250	20	Possible filter	Mare Crisium	
	2857	34° N	63° E	H.O.	N		1/250	20	Possible filter	Mare Crisium	
	2858			H.O.	E		1/250		Possible filter	Mare Crisium	
	2859			H.O.	E		1/250			Mare Fecunditatis	
	2860	39° N	63° E	H.O.	NE		1/250			Messier, Messier A	
	2861			H.O.	NE		1/250			Palus Somni	
	2862			H.O.	NE		1/250			Newcomb	T/O 67 (partial)
	2863	3° N	66° E	L.O.	N		1/250	35		Geminus	

2864	13° N	65° E	L.O.	N	1/250	33		PP in space T/O 54
2865	24° N	67° E	H.O.	N	1/250	30		
2866	36° N	68° E	H.O.	N	1/250	25		
2867			H.O.	N	1/250	55	Far side	
2868	24° S	95° E	H.O.	SW	1/250	58	Far side	
2869	16° S	92° E	L.O.	SW	1/250	65	Mare Smythii	T/O 56
2870	4° S	95° E	L.O.	S	1/250	65	Joliot-Curie	T/O 55
2871	11° N	97° E	H.O.	NW	1/250	65	Joliot-Curie	
2872	34° N	113° E	H.O.	NW	1/250	50	Eastern portion of Mare Crisium	Blurred
2873			L.O.	N			Eastern portion of Mare Crisium	Not plotted
2874				N				Blurred
2875			H.O.					Blurred
2876			H.O.					Blurred, not plotted
2877							Mare Smythii	Slightly blurred
2878	13° N	64° E	L.O.	N		33	Mare Crisium	Slightly blurred
2879	13° N	64° E	L.O.	N		33	Mare Crisium	
2880	05° S	58° E	NV	S		28	Langrenus	T/O 68
2881	03° S	56° E	NV	S		28	Langrenus	
2882			H.O.	N			Gauss	Exp change
2883			H.O.	N			Gauss	
2884			H.O.	NW		57	Joliot-Curie	Exp change
2885	22° N	94° E	H.O.	N			Joliot-Curie	Very high hor photo
2886			H.O.	N				Unable to locate
2887			H.O.				Entire Moon	Exp change
2888							Entire Moon	Exp change
2889							Entire Moon	Exp change
2890							Entire Moon	Exp change
2891							Entire Moon	Exp change
2892							Entire Moon	Exp change
2893	22° N	94° E			1/250		Entire Moon	Exp change
2894							Entire Moon	Exp change
2895							Entire Moon	Exp change
2896							Entire Moon	Exp change
2897							Entire Moon	Exp change
2898							Entire Moon	Exp change
2899							Entire Moon	Exp change
2900							Entire Moon	Exp change
2901							Entire Moon	Exp change
2902							Entire Moon	Scale change

See footnotes at end of table.

TABLE A-IX.—*Apollo 8 Magazine G, 2458 Film—Concluded*

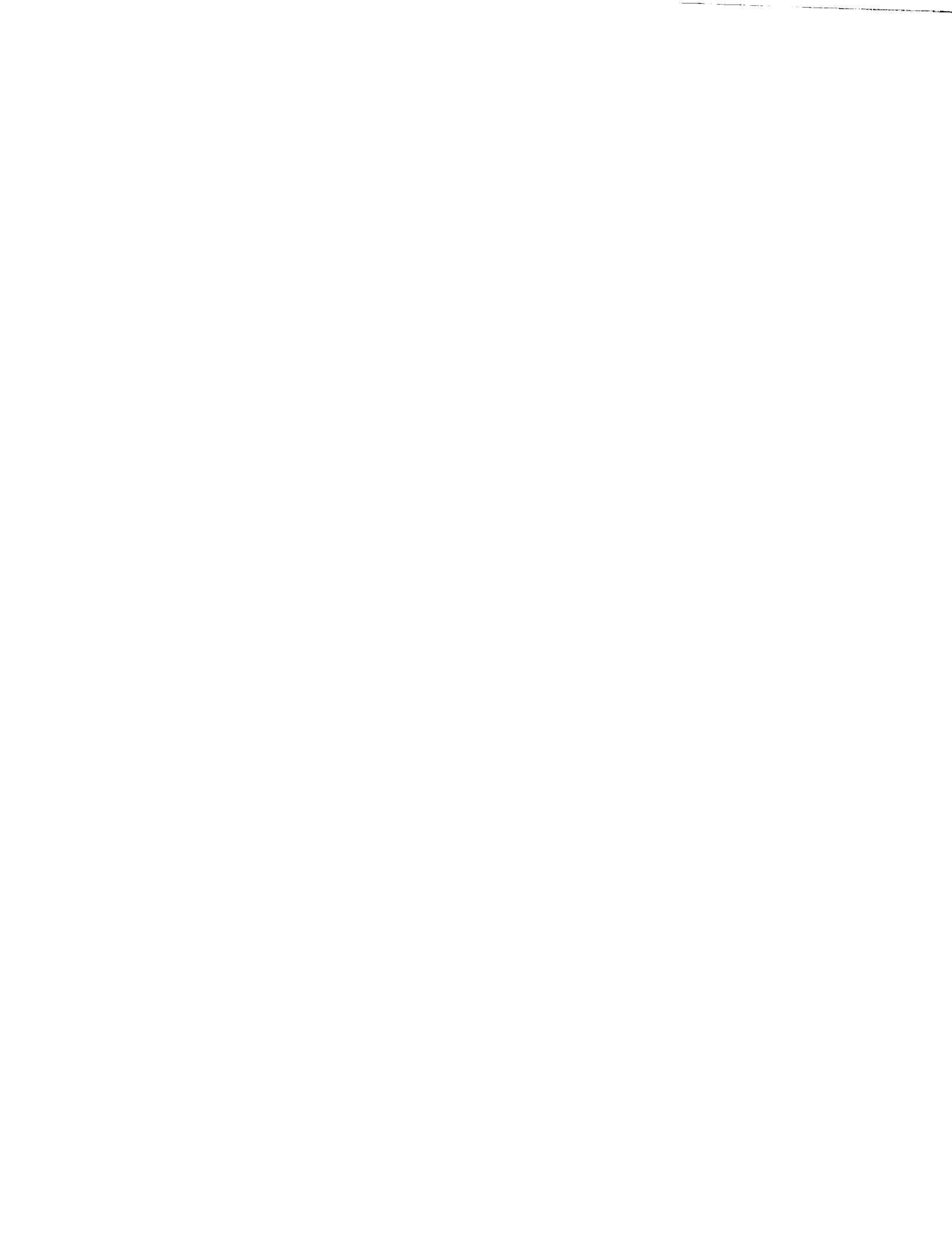
Rev	Frame (AS8-18-)	Lat	Long	Mode	Direction	f-stop	Shutter speed, sec	Sun angle, deg	Other coverage	Area	Remarks
.....	2903	Possible filter
.....	2904	Possible filter
.....	2905	Possible filter
.....	2906	Possible filter
.....	2907	Possible filter
.....	2908	Possible filter	Exp change

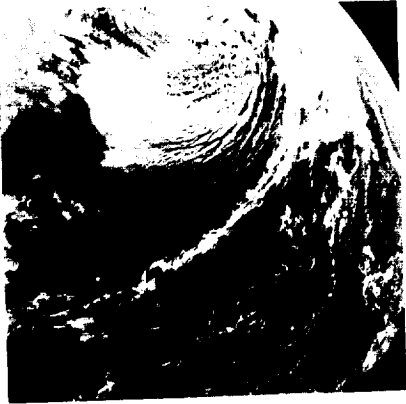
* Between frames 2844 and 2845, there are 20 very dark exposures of the lunar surface. These are not numbered and are too dark to be of value. No attempt was made to plot or index these frames.

MAGAZINE

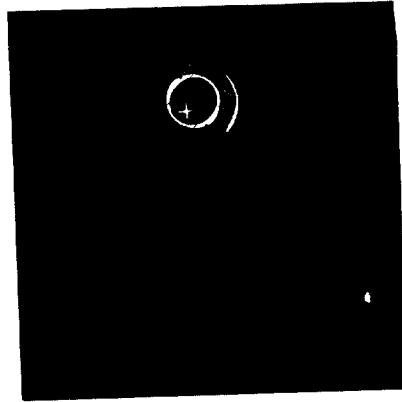
A

AS8-16-2581 to 2658

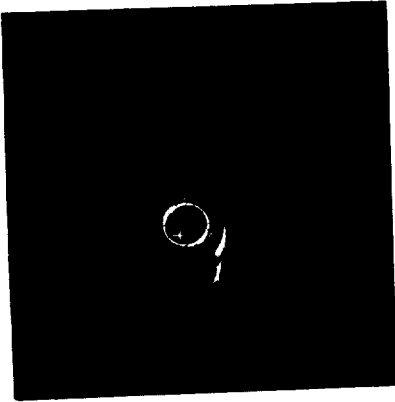




AS8-16-2581



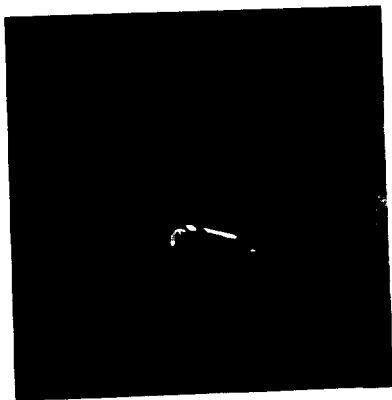
AS8-16-2582



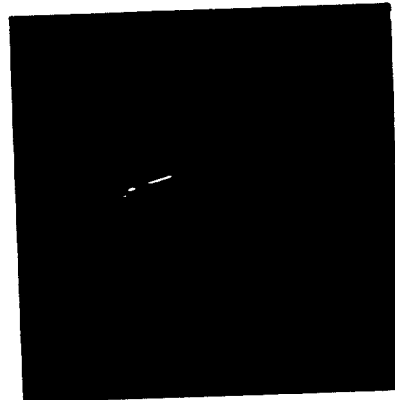
AS8-16-2583



AS8-16-2584



AS8-16-2585

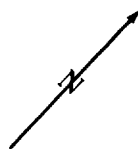


AS8-16-2586

(Available in color.)



AS8-16-2587



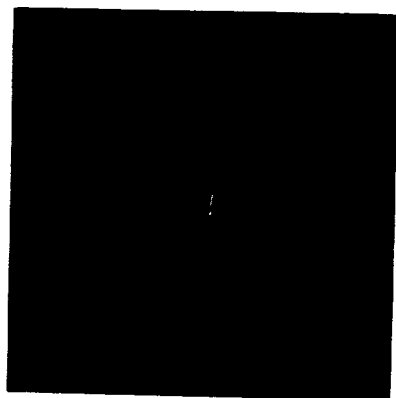
AS8-16-2588



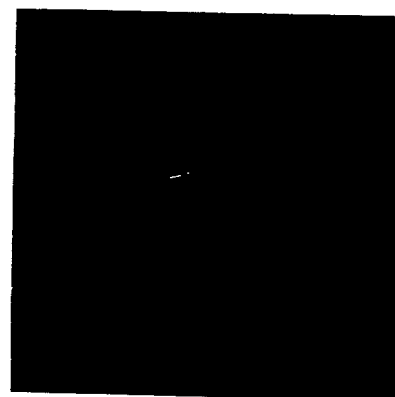
AS8-16-2589



AS8-16-2590



AS8-16-2591

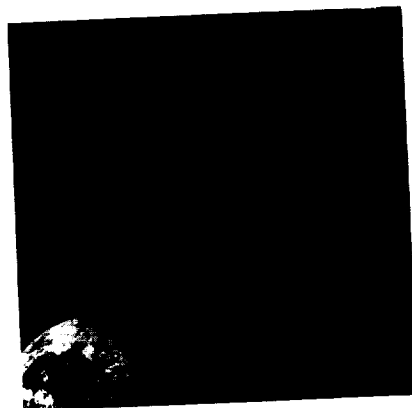


AS8-16-2592

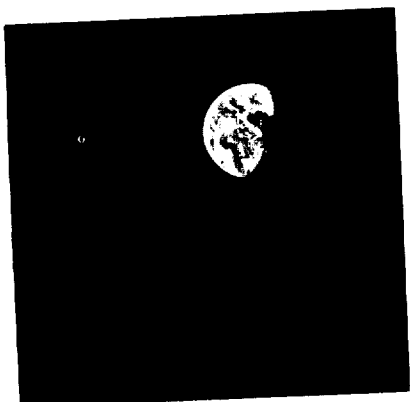
(Available in color.)



AS8-16-2593



AS8-16-2594



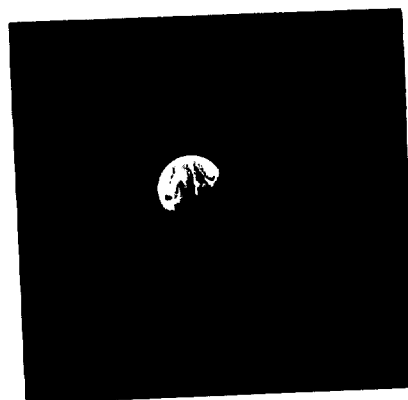
AS8-16-2595



AS8-16-2596

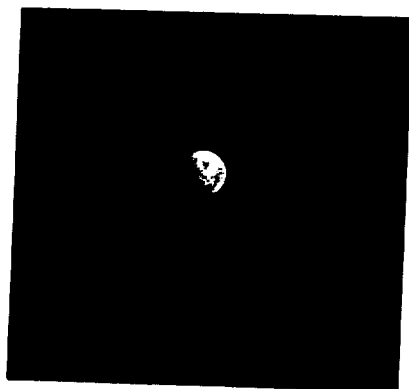


AS8-16-2597



AS8-16-2598

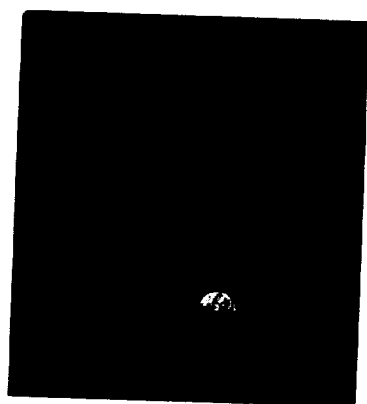
(Available in color.)



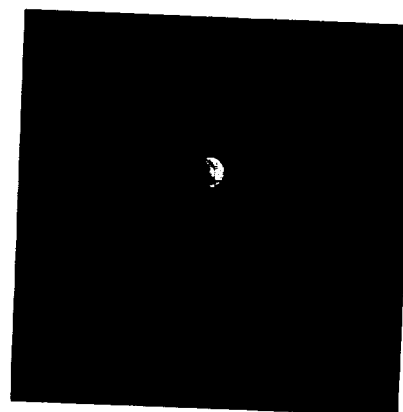
AS8-16-2599



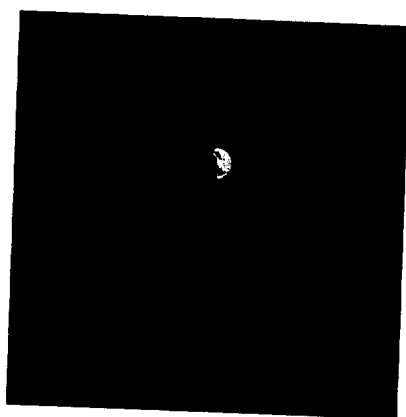
AS8-16-2600



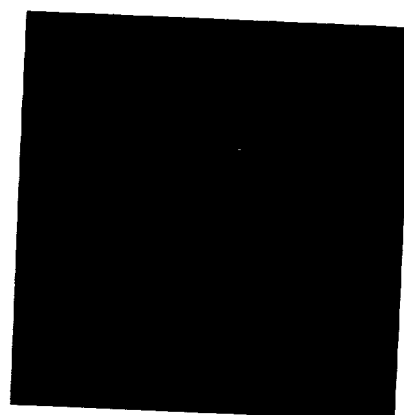
AS8-16-2601



AS8-16-2602

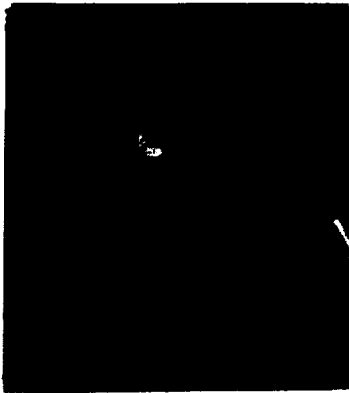


AS8-16-2603

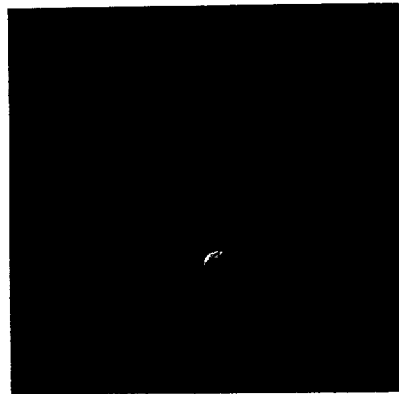


AS8-16-2604

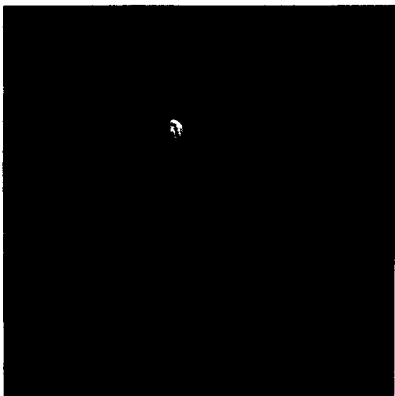
(Available in color.)



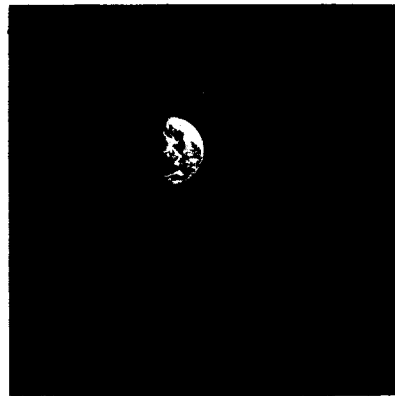
AS8-16-2605



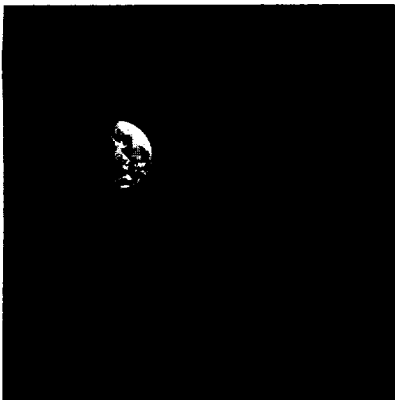
AS8-16-2606



AS8-16-2607



AS8-16-2608

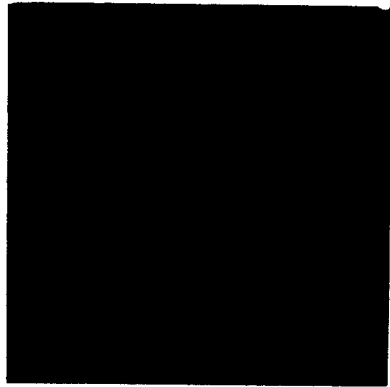


AS8-16-2609

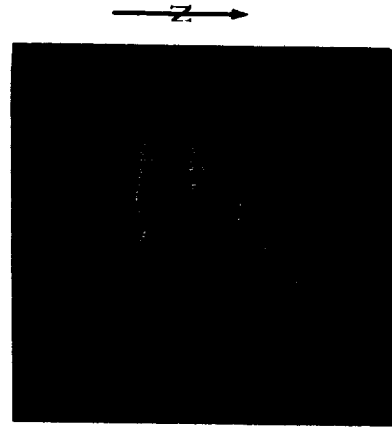


AS8-16-2610

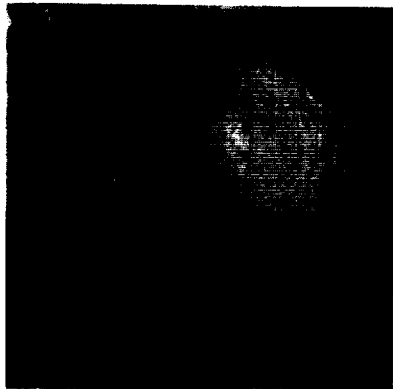
(Available in color.)



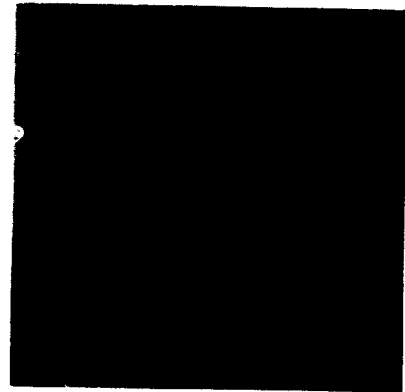
AS8-16-2611



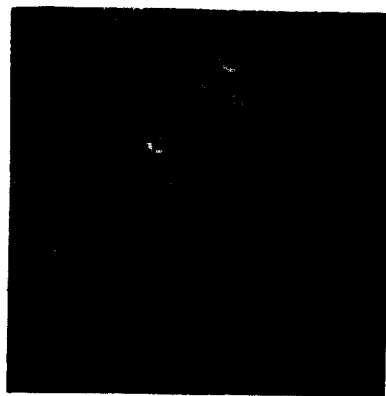
AS8-16-2612



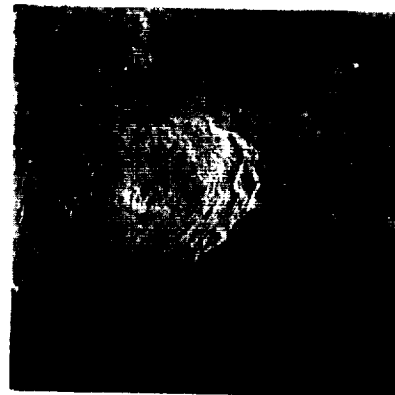
AS8-16-2613



AS8-16-2614



AS8-16-2615



AS8-16-2616

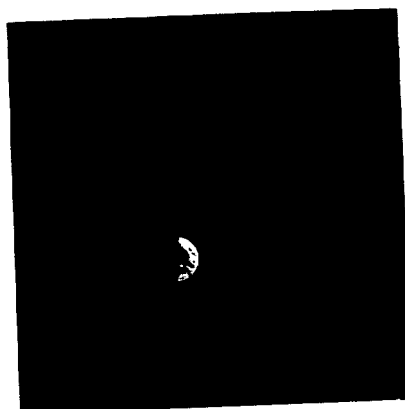
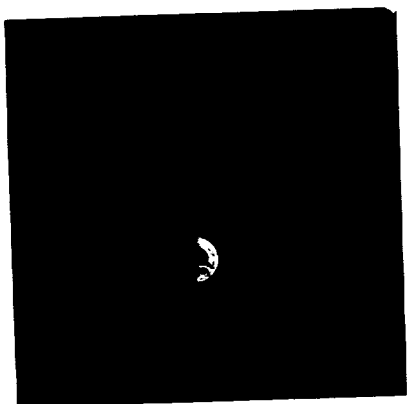
(Available in color.)

BLANK

BLANK

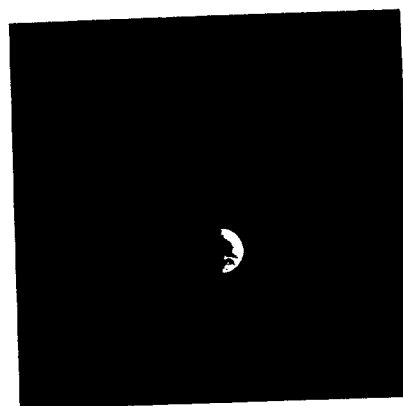
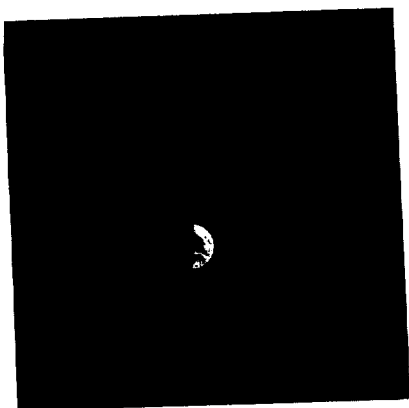
AS8-16-2617

AS8-16-2618



AS8-16-2619

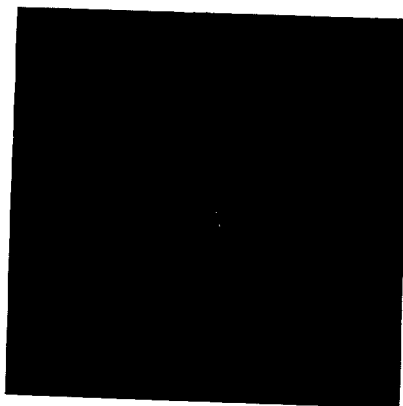
AS8-16-2620



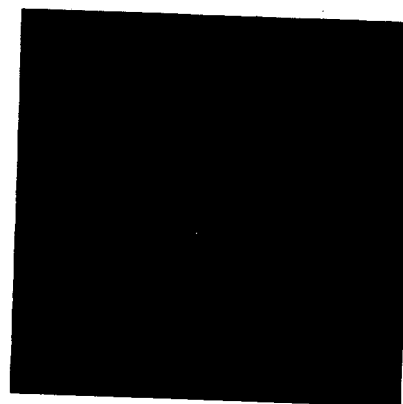
AS8-16-2621

AS8-16-2622

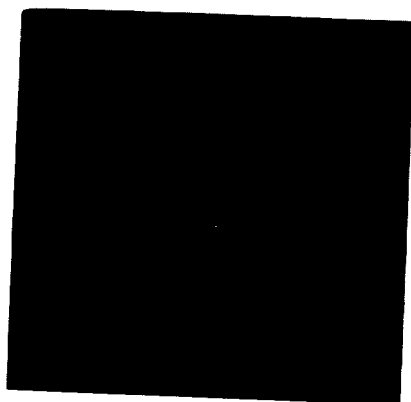
(Available in color.)



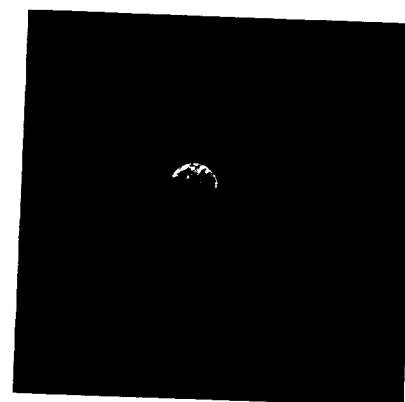
AS8-16-2623



AS8-16-2624



AS8-16-2625



AS8-16-2626

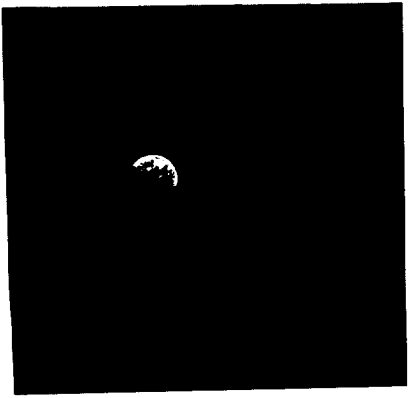


AS8-16-2627



AS8-16-2628

(Available in color.)



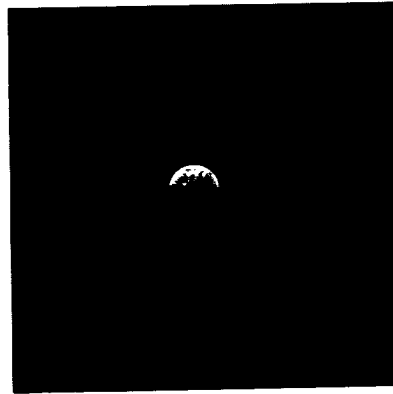
AS8-16-2629



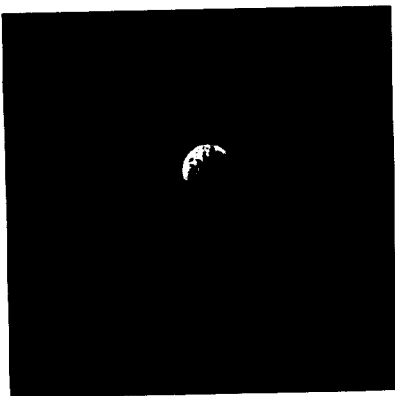
AS8-16-2630



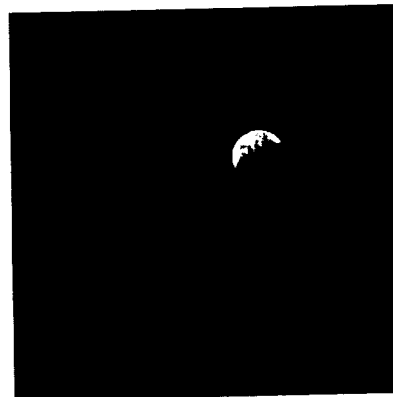
AS8-16-2631



AS8-16-2632

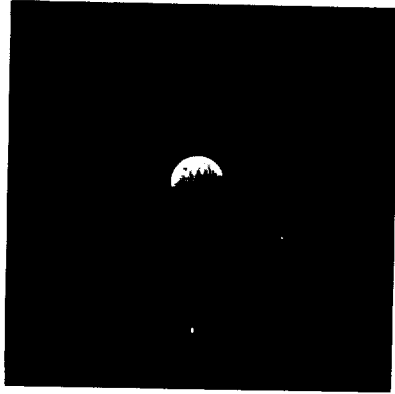


AS8-16-2633

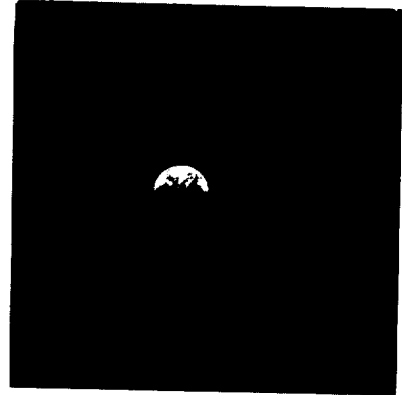


AS8-16-2634

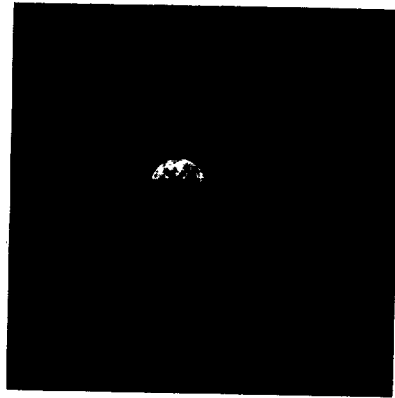
(Available in color.)



AS8-16-2635



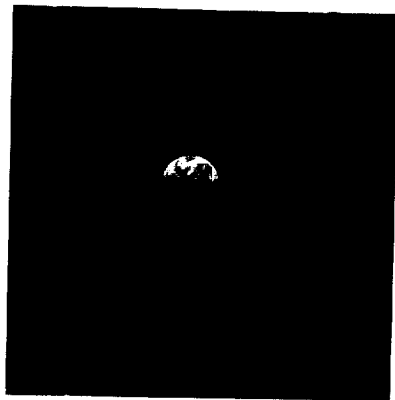
AS8-16-2636



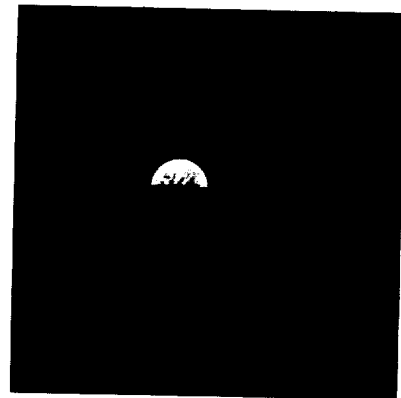
AS8-16-2637



AS8-16-2638

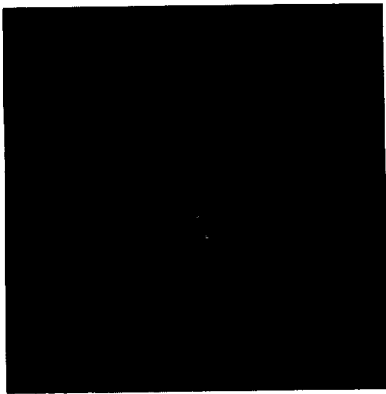


AS8-16-2639

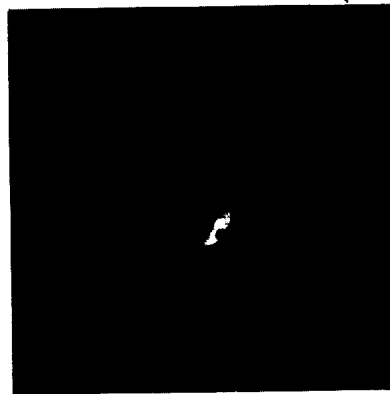


AS8-16-2640

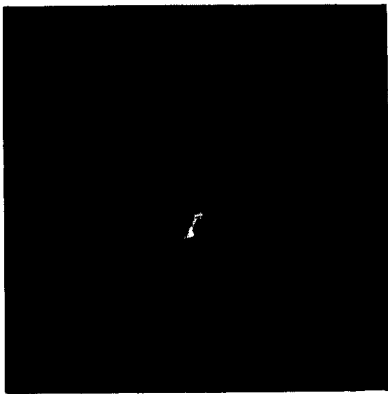
(Available in color.)



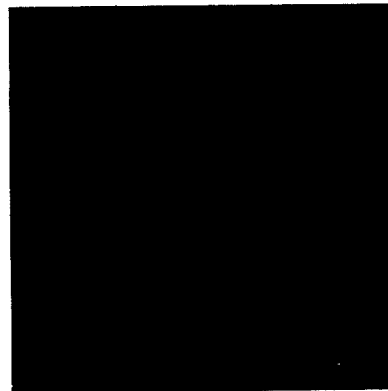
AS8-16-2641



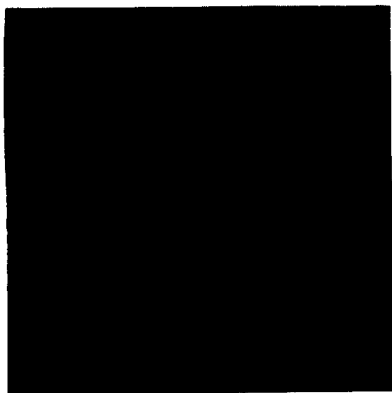
AS8-16-2642



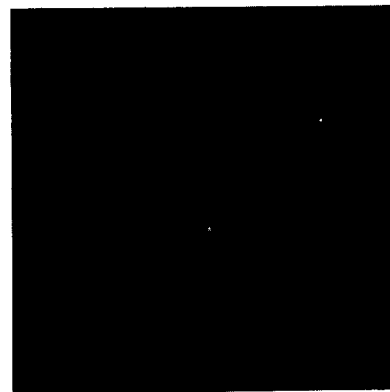
AS8-16-2643



AS8-16-2644

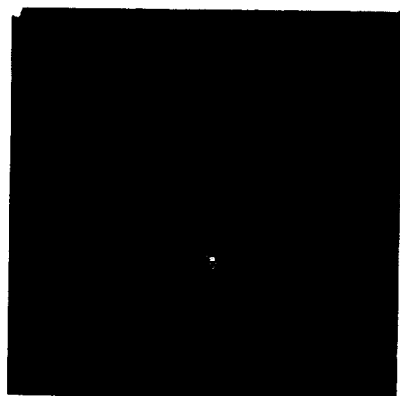


AS8-16-2645

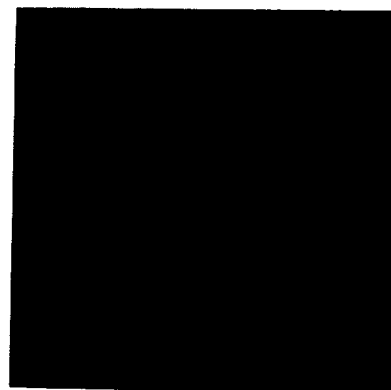


AS8-16-2646

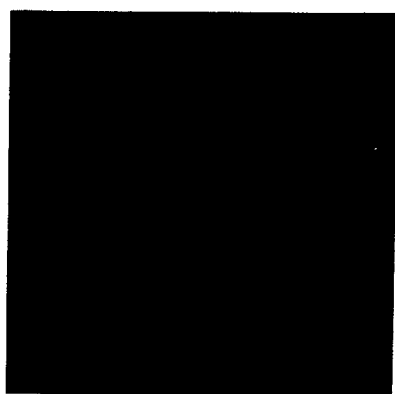
(Available in color.)



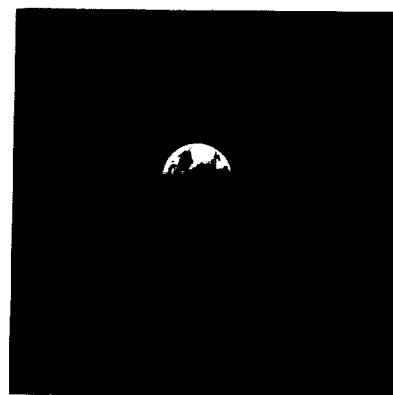
AS8-16-2647



AS8-16-2648



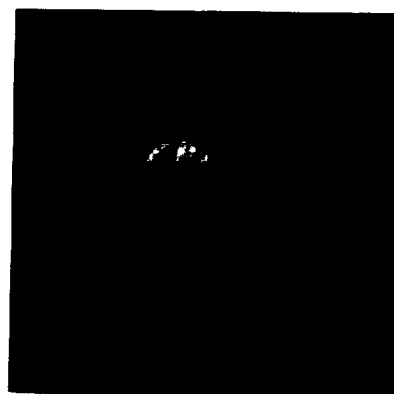
AS8-16-2649



AS8-16-2650

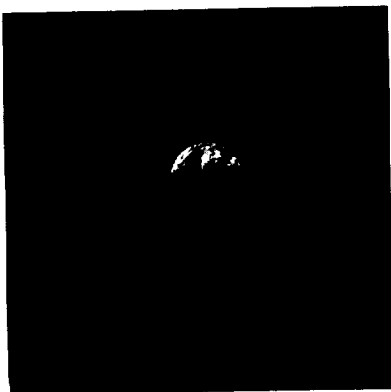


AS8-16-2651



AS8-16-2652

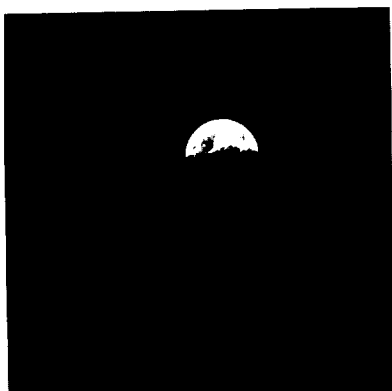
(Available in color.)



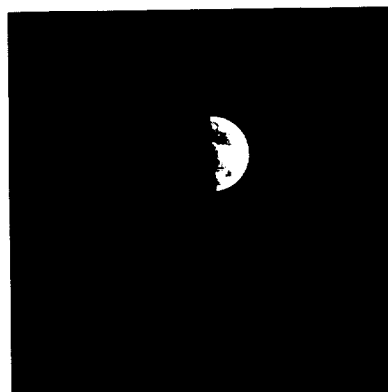
AS8-16-2653



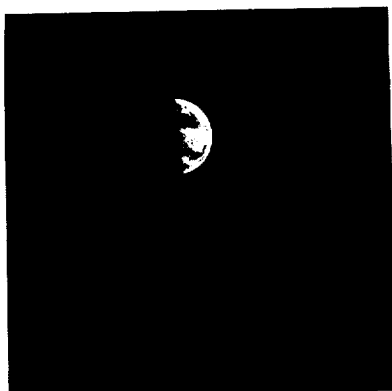
AS8-16-2654



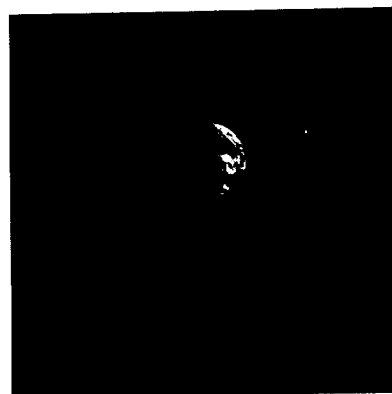
AS8-16-2655



AS8-16-2656



AS8-16-2657



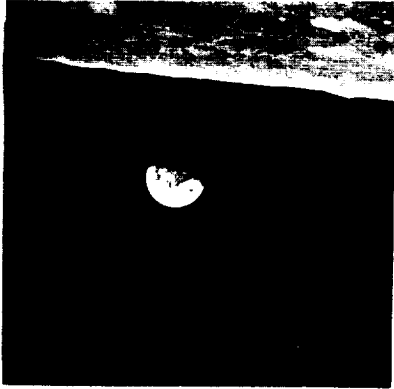
AS8-16-2658

(Available in color.)

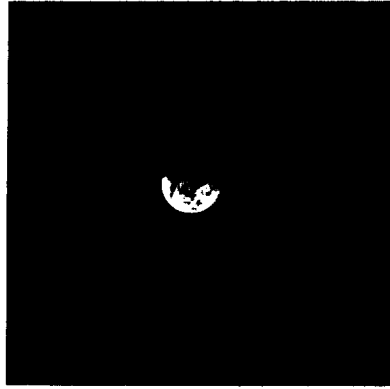
MAGAZINE

B

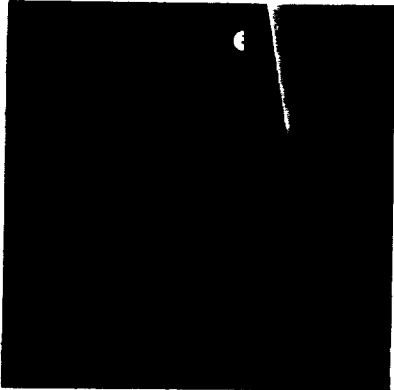
AS8-14-2383 to 2534



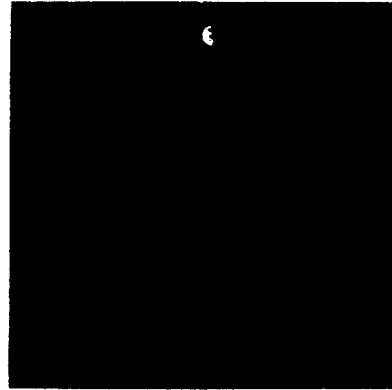
AS8-14-2383



AS8-14-2384



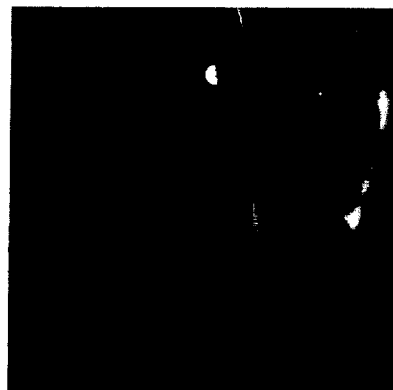
AS8-14-2385



AS8-14-2386

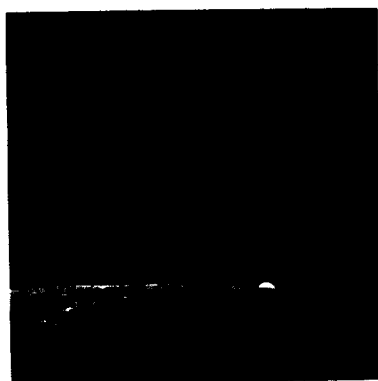


AS8-14-2387

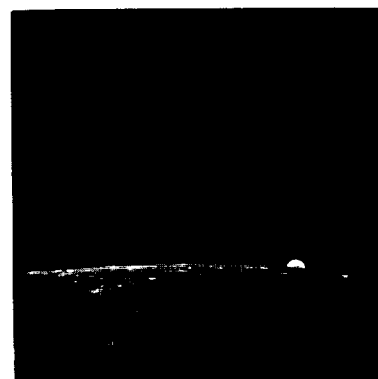


AS8-14-2388

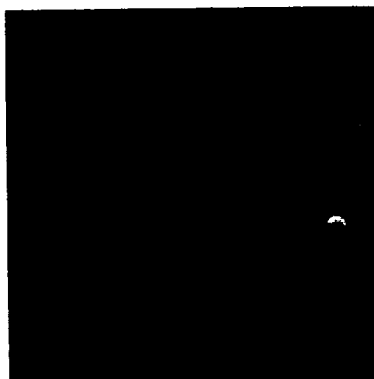
(Available in color.)



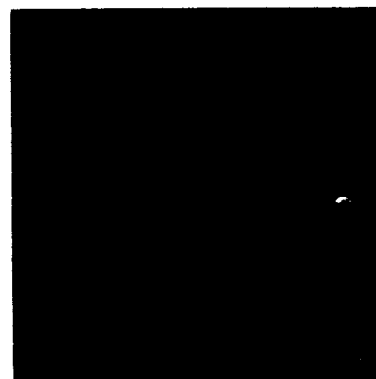
AS8-14-2389



AS8-14-2390



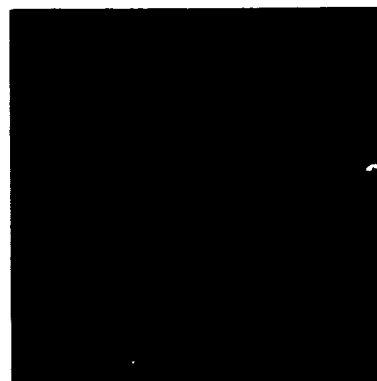
AS8-14-2391



AS8-14-2392

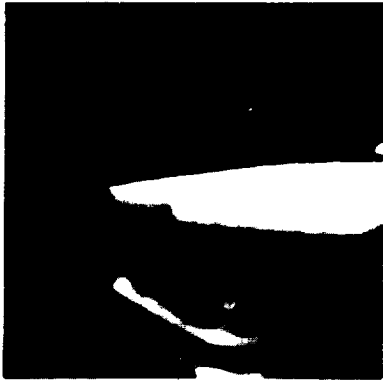


AS8-14-2393



AS8-14-2394

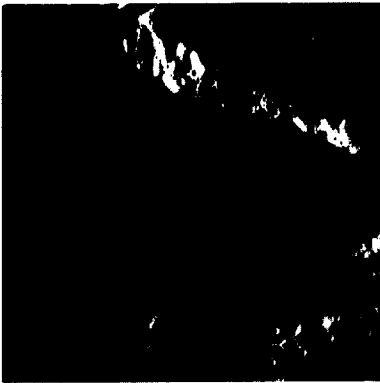
(Available in color.)



AS8-14-2395



AS8-14-2396



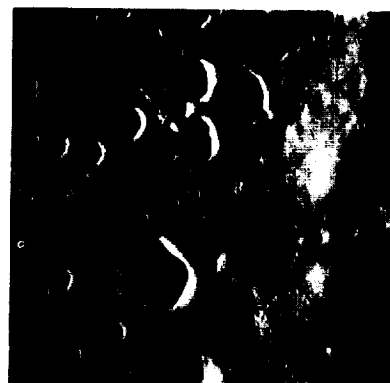
AS8-14-2397



AS8-14-2398

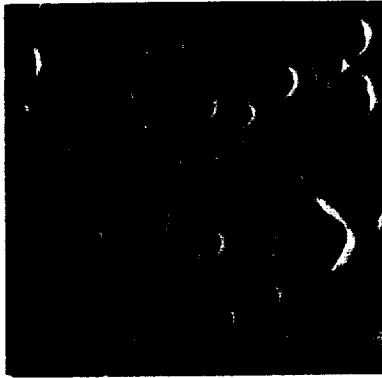


AS8-14-2399

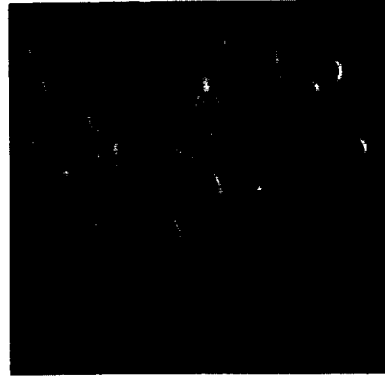


AS8-14-2400

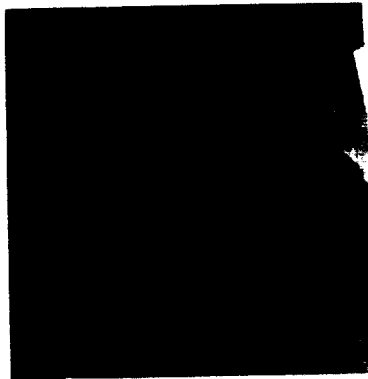
(Available in color.)



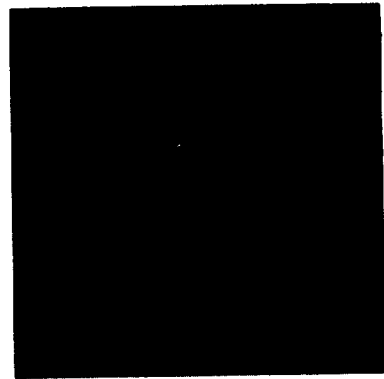
AS8-14-2401



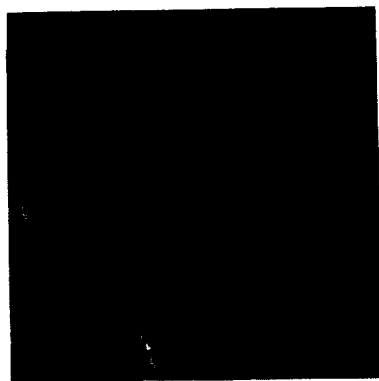
AS8-14-2402



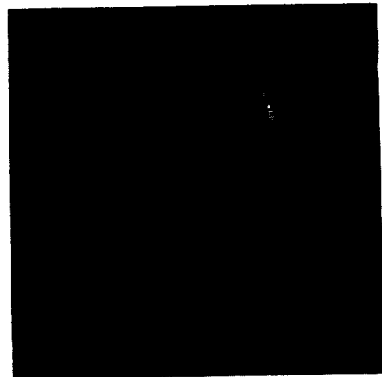
AS8-14-2403



AS8-14-2404

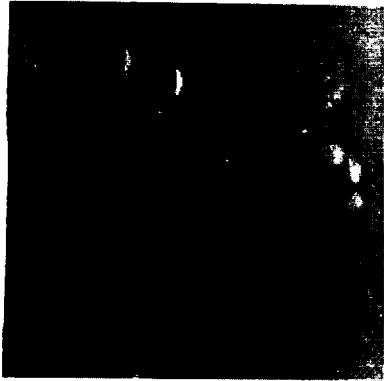


AS8-14-2405



AS8-14-2406

(Available in color.)



AS8-14-2407



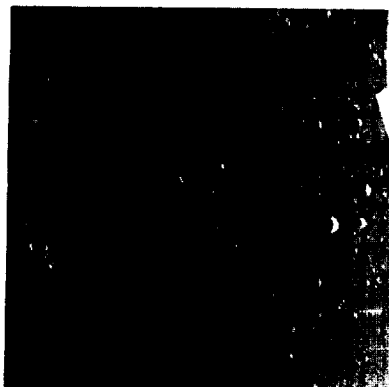
AS8-14-2408



AS8-14-2409



AS8-14-2410

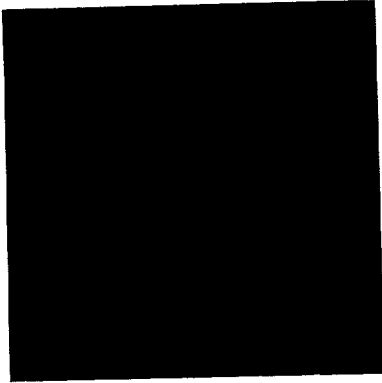


AS8-14-2411

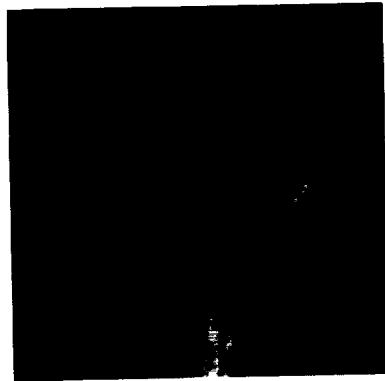


AS8-14-2412

(Available in color.)



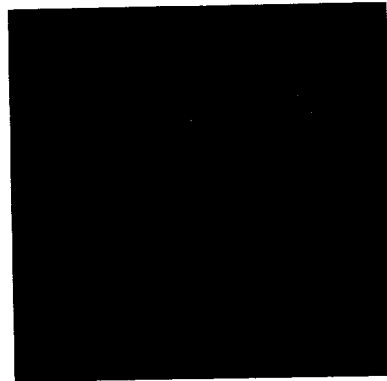
AS8-14-2413



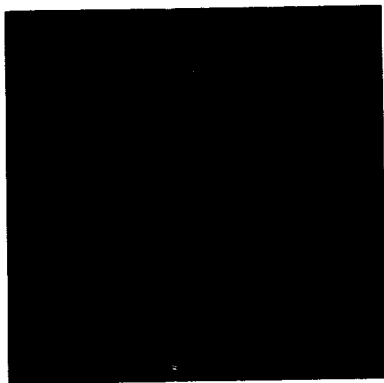
AS8-14-2414



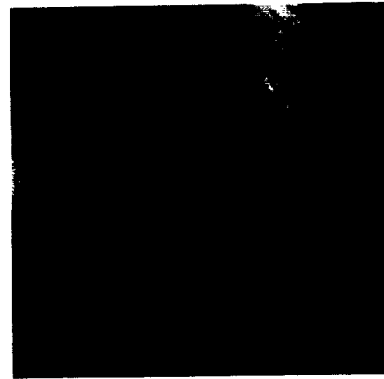
AS8-14-2415



AS8-14-2416

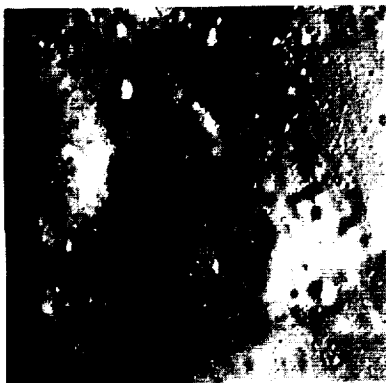


AS8-14-2417



AS8-14-2418

(Available in color.)



AS8-14-2419



AS8-14-2420



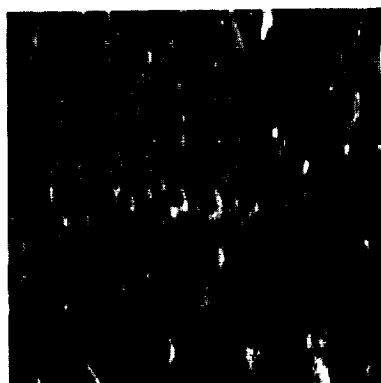
AS8-14-2421



AS8-14-2422

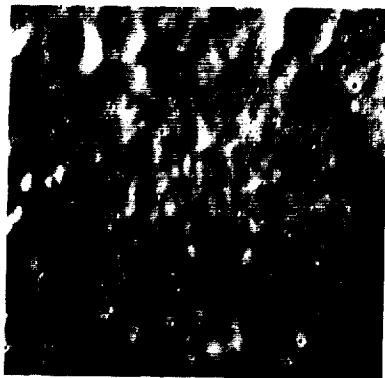


AS8-14-2423



AS8-14-2424

(Available in color.)



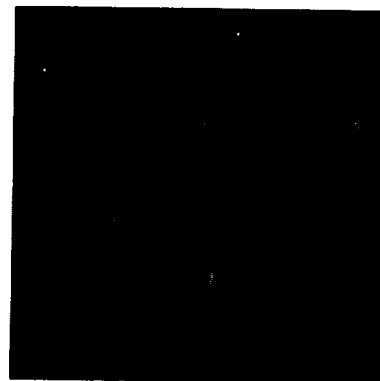
AS8-14-2425



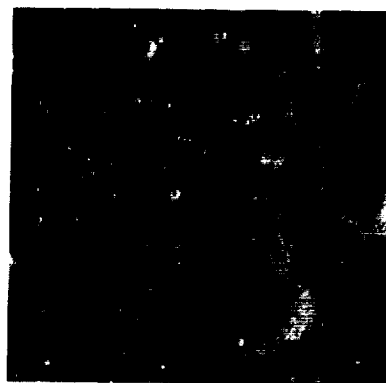
AS8-14-2426



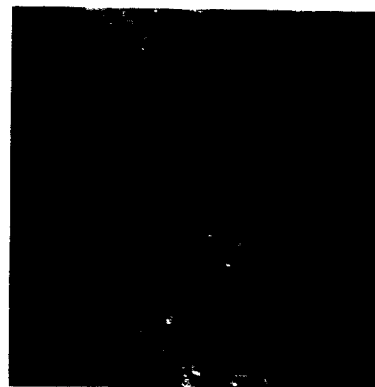
AS8-14-2427



AS8-14-2428



AS8-14-2429

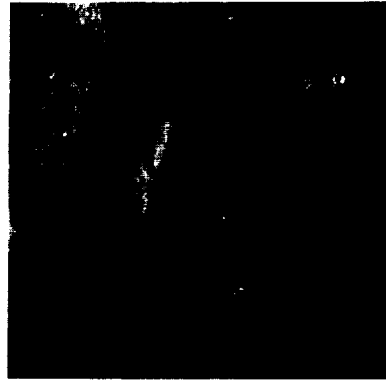


AS8-14-2430

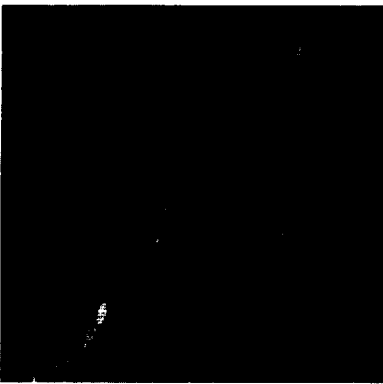
(Available in color.)



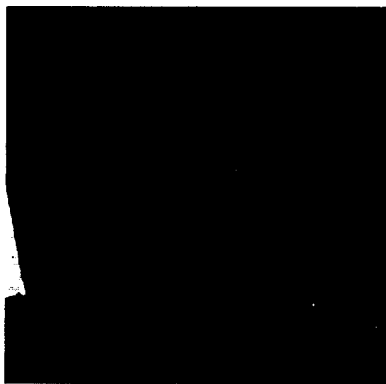
AS8-14-2431



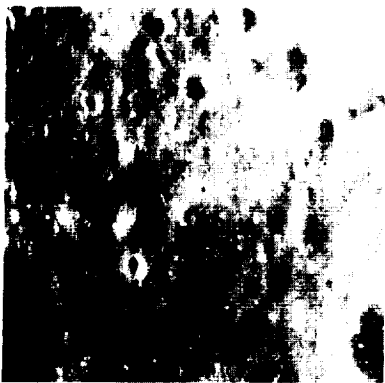
AS8-14-2432



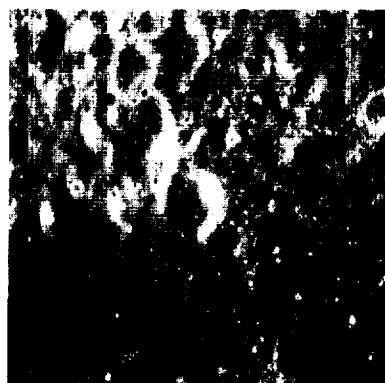
AS8-14-2433



AS8-14-2434



AS8-14-2435



AS8-14-2436

(Available in color.)



AS8-14-2437



AS8-14-2438



AS8-14-2439



AS8-14-2440

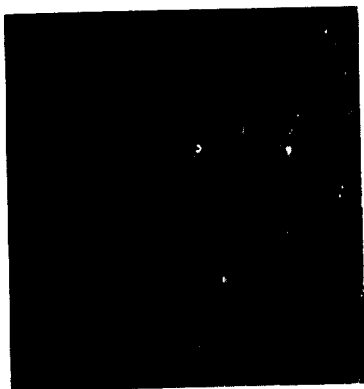


AS8-14-2441

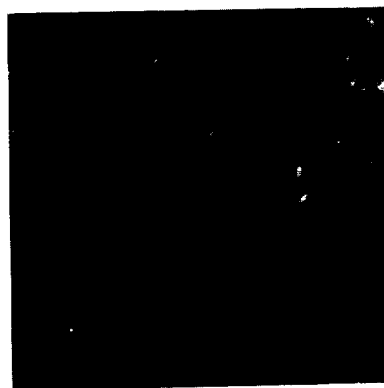


AS8-14-2442

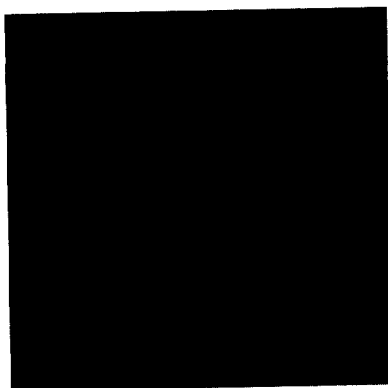
(Available in color.)



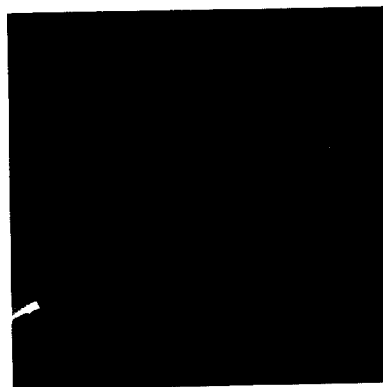
AS8-14-2443



AS8-14-2444



AS8-14-2445



AS8-14-2446



AS8-14-2447

(Available in color.)



AS8-14-2448



AS8-14-2449



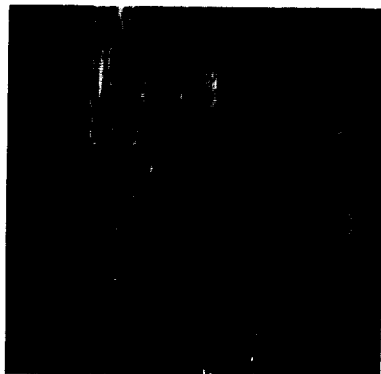
AS8-14-2450



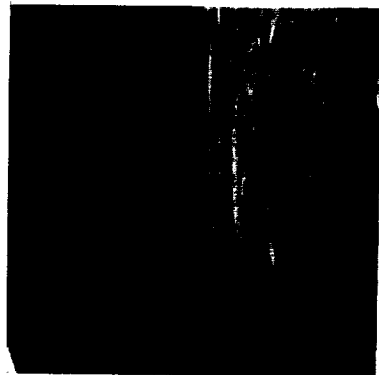
AS8-14-2451



AS8-14-2452

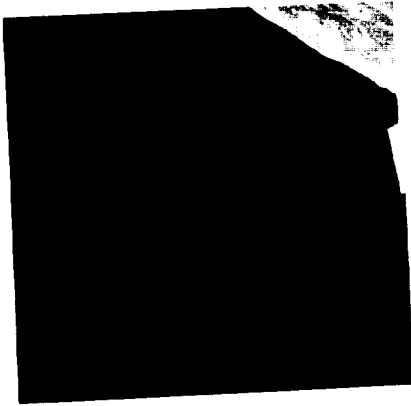


AS8-14-2453

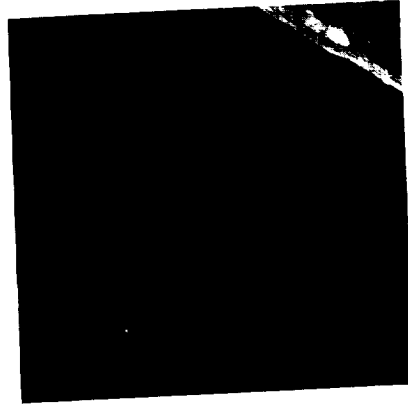


AS8-14-2454

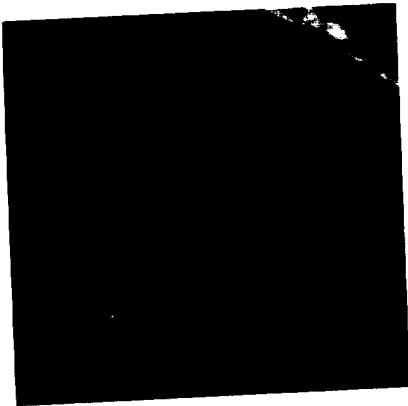
(Available in color.)



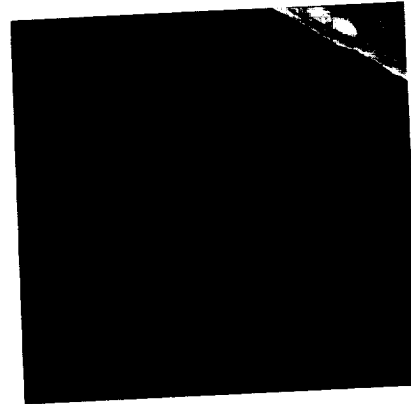
AS8-14-2455



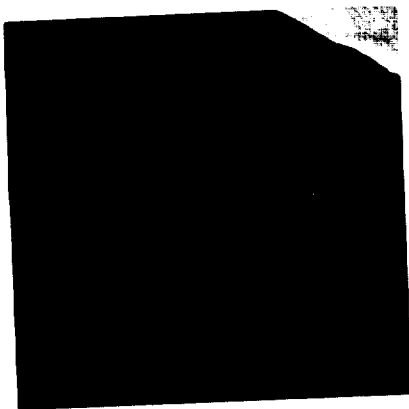
AS8-14-2456



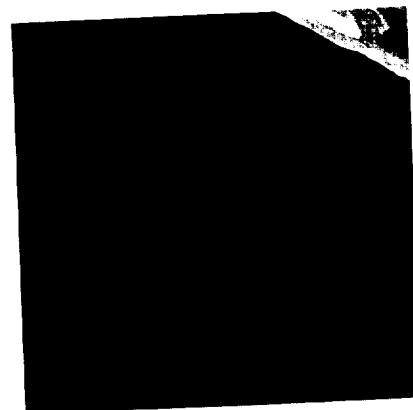
AS8-14-2457



AS8-14-2458



AS8-14-2459

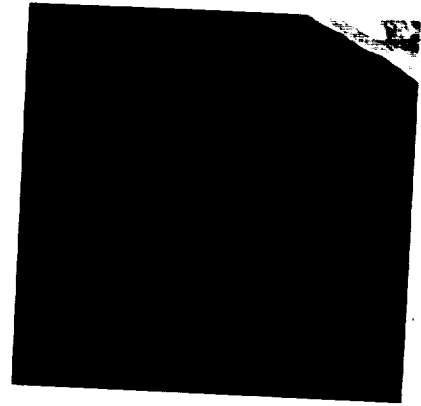


AS8-14-2460

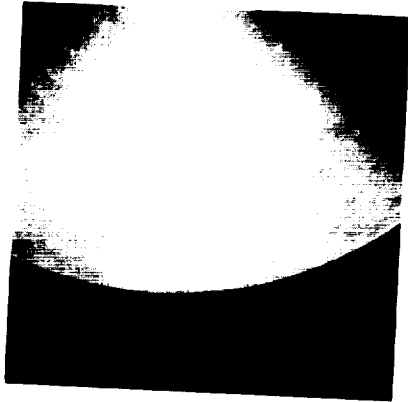
(Available in color.)



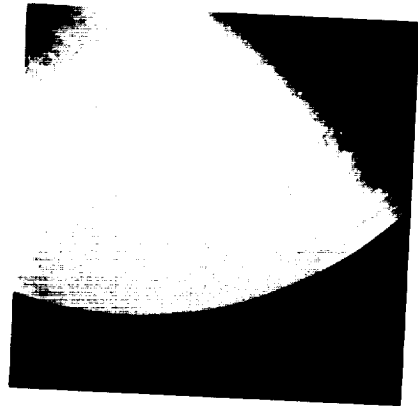
AS8-14-2461



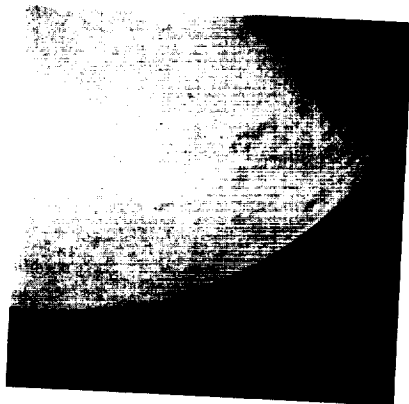
AS8-14-2462



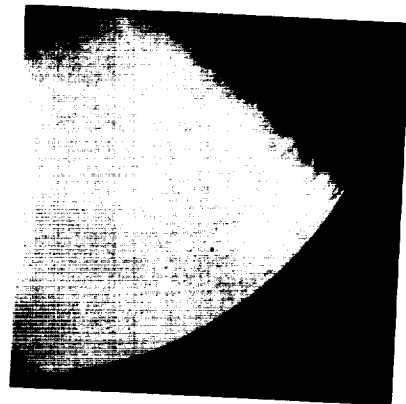
AS8-14-2463



AS8-14-2464

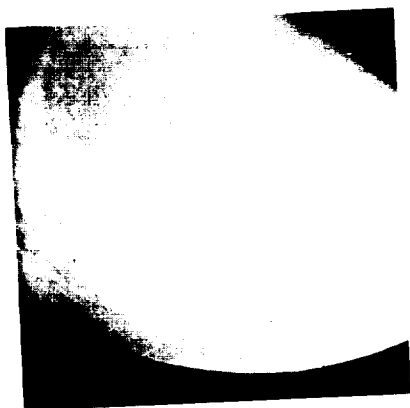


AS8-14-2465

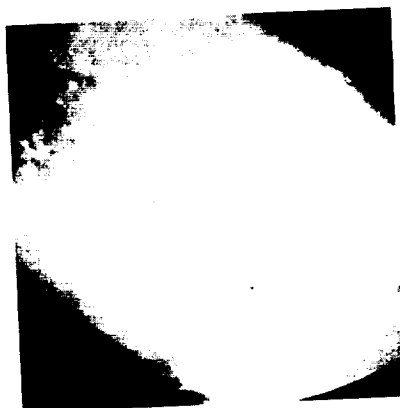


AS8-14-2466

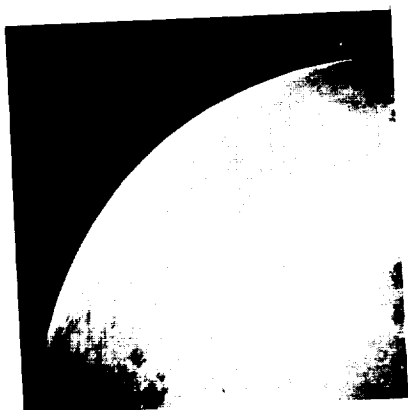
(Available in color.)



AS8-14-2467



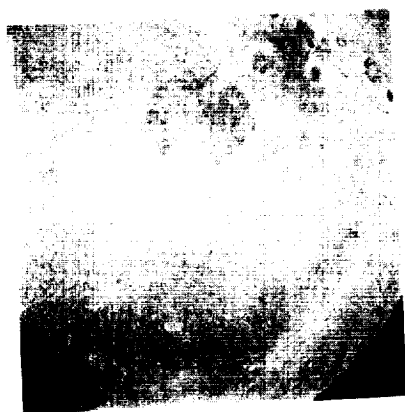
AS8-14-2468



AS8-14-2469

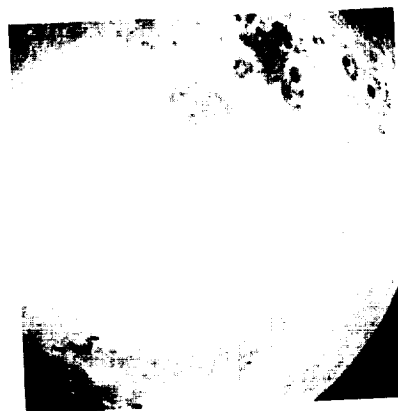


AS8-14-2470



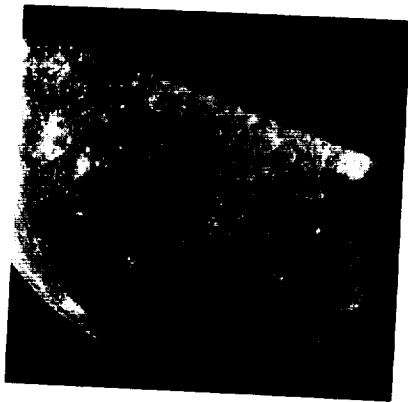
AS8-14-2471

(Available in color.)

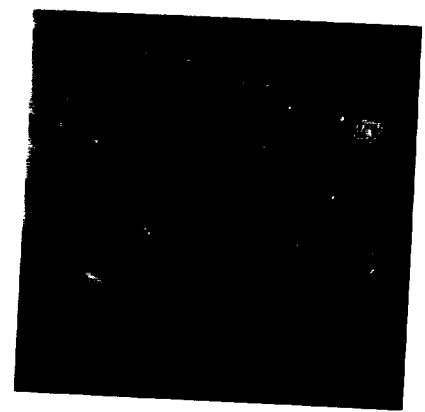


AS8-14-2472

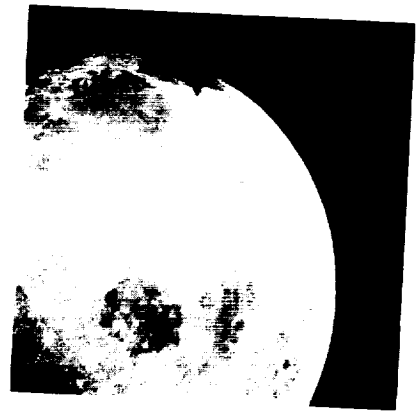
ANALYSIS OF APOLLO 8 PHOTOGRAPHY AND VISUAL OBSERVATIONS



AS8-14-2473



AS8-14-2474



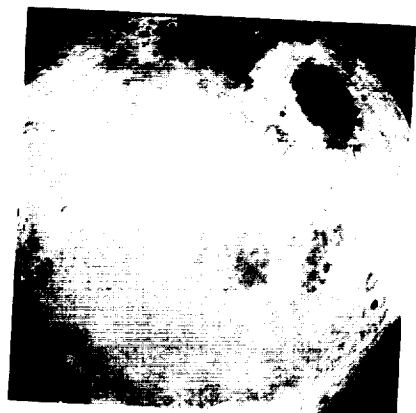
AS8-14-2475



AS8-14-2476

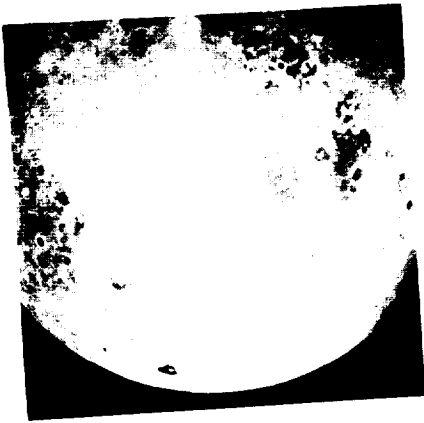


AS8-14-2477



AS8-14-2478

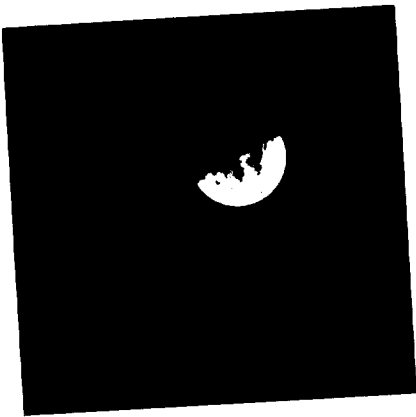
(Available in color.)



AS8-14-2479



AS8-14-2480



AS8-14-2481

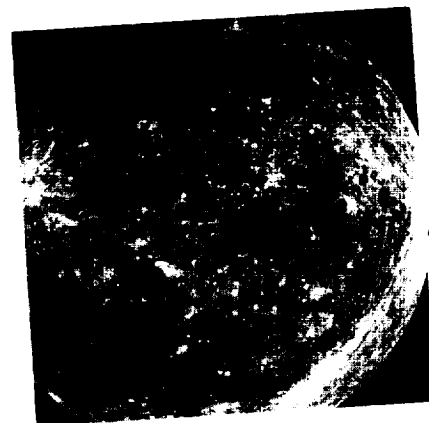


AS8-14-2482

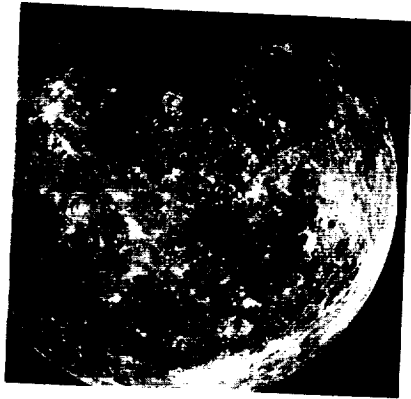


AS8-14-2483

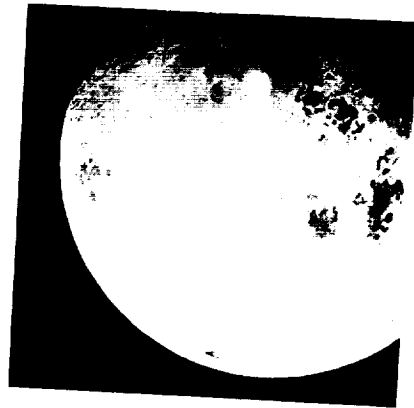
(Available in color.)



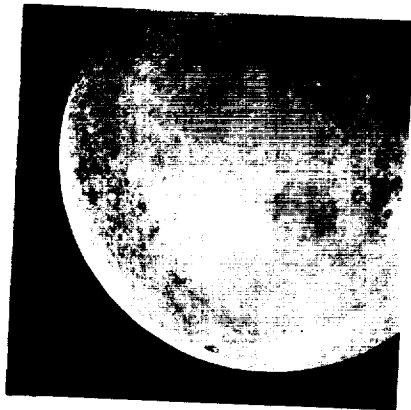
AS8-14-2484



AS8-14-2485



AS8-14-2486



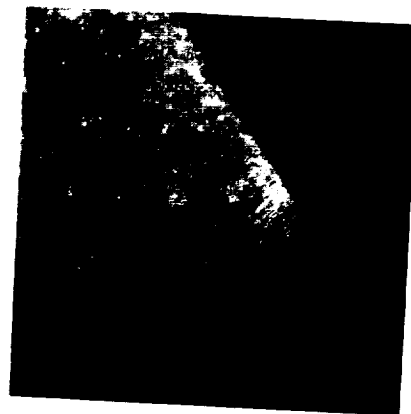
AS8-14-2487



AS8-14-2488



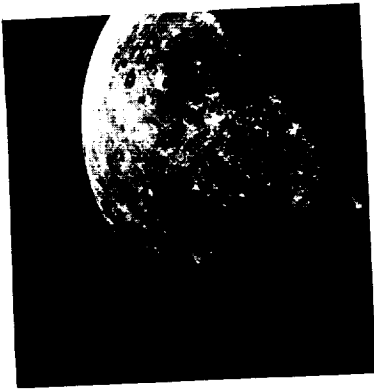
AS8-14-2489



AS8-14-2490

(Available in color.)

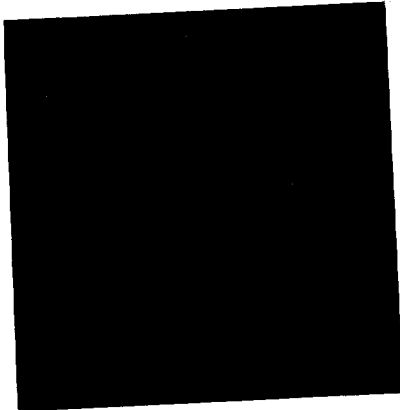
MAGAZINE B



AS8-14-2491



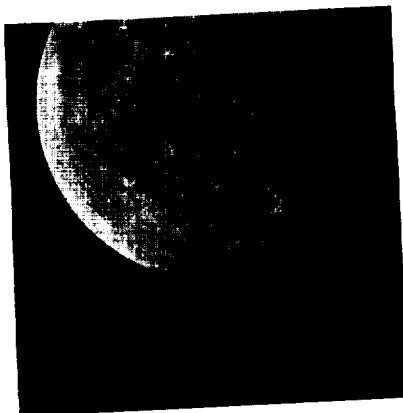
AS8-14-2492



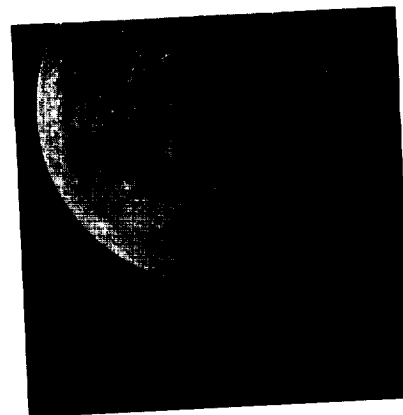
AS8-14-2493



AS8-14-2494

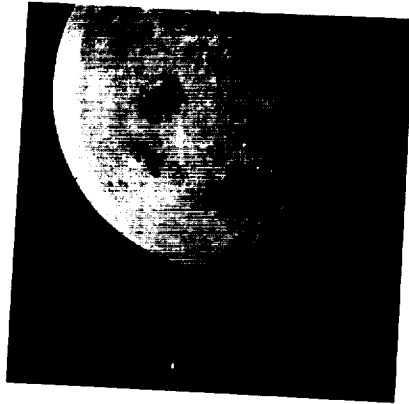


AS8-14-2495

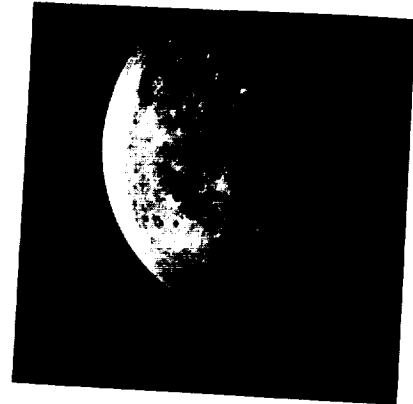


AS8-14-2496

(Available in color.)



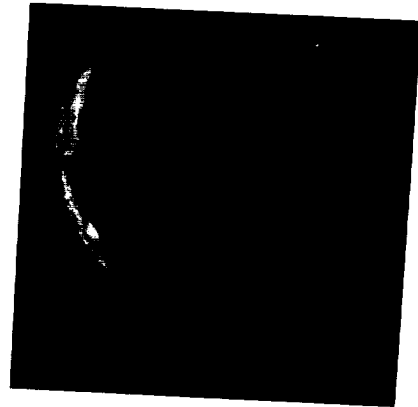
AS8-14-2497



AS8-14-2498



AS8-14-2499



AS8-14-2500



AS8-14-2501



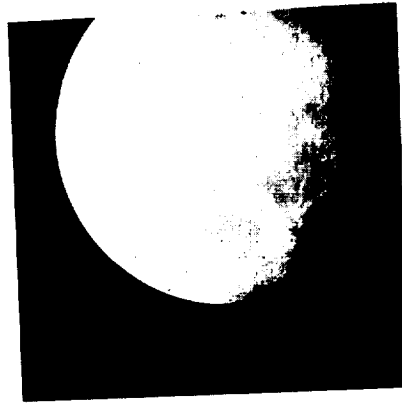
AS8-14-2502

(Available in color.)

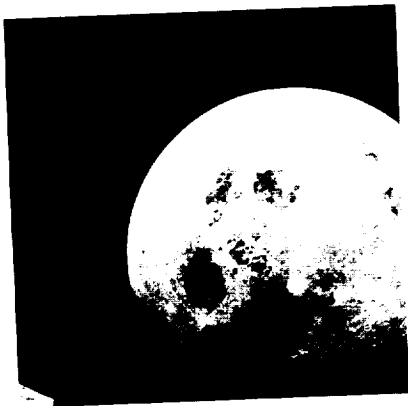
MAGAZINE B



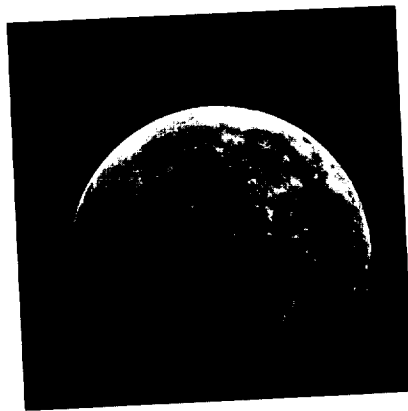
AS8-14-2503



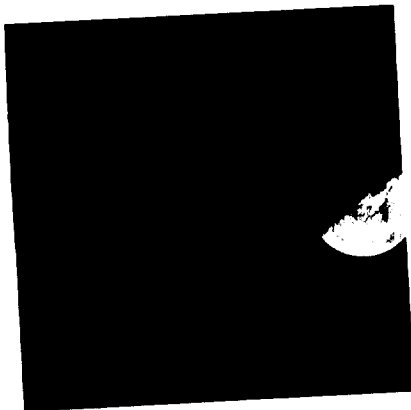
AS8-14-2504



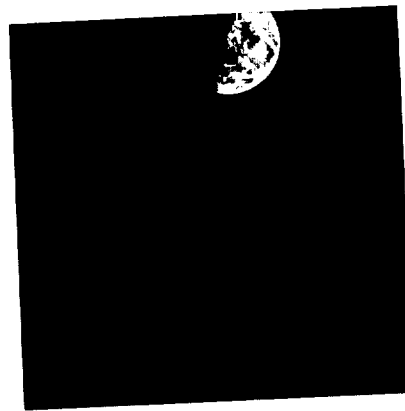
AS8-14-2505



AS8-14-2506

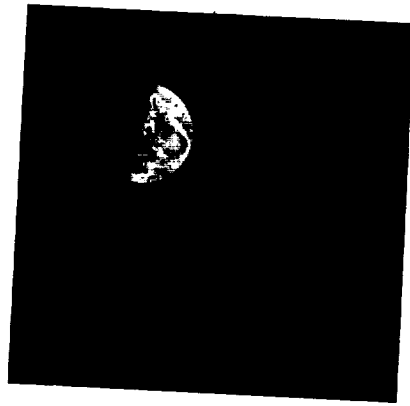


AS8-14-2507

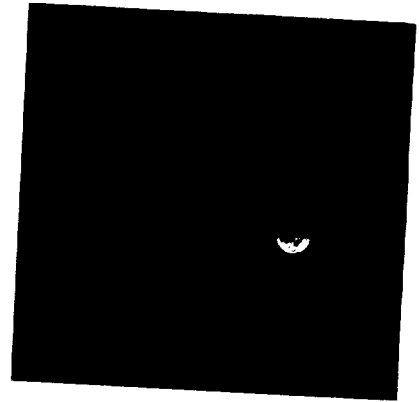


AS8-14-2508

(Available in color.)



AS8-14-2509



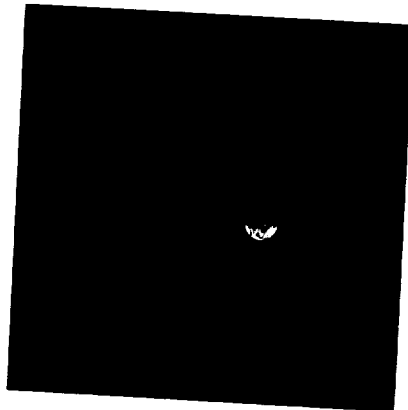
AS8-14-2510



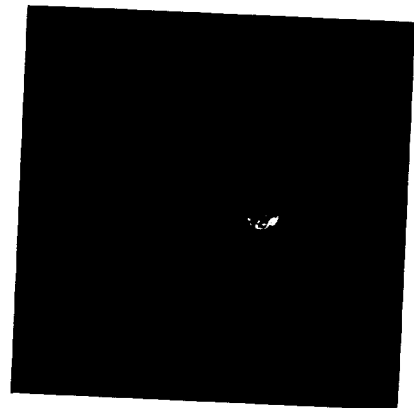
AS8-14-2511



AS8-14-2512



AS8-14-2513

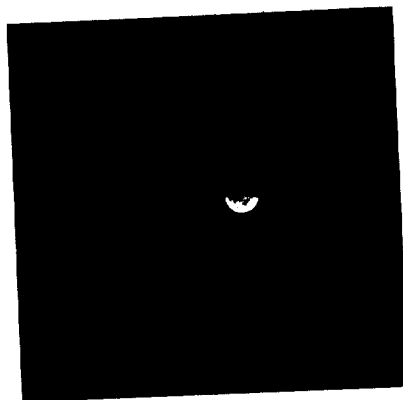


AS8-14-2514

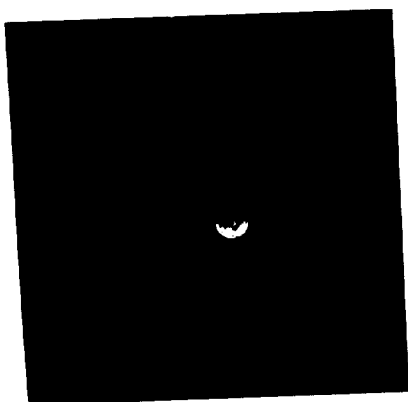
(Available in color.)



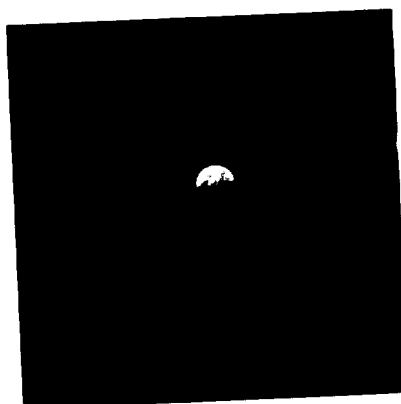
AS8-14-2515



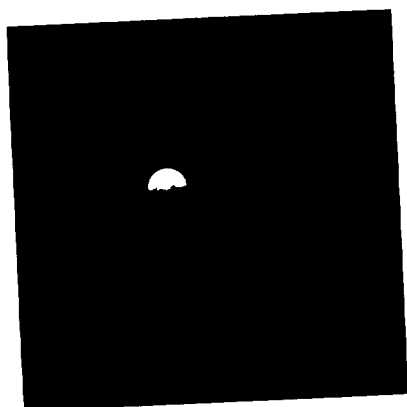
AS8-14-2516



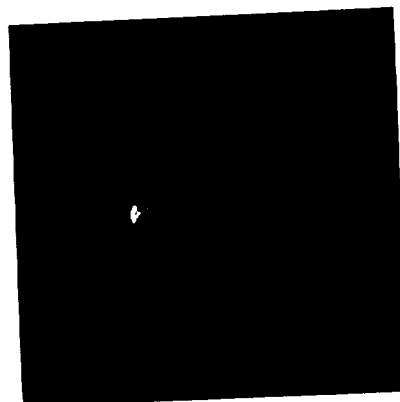
AS8-14-2517



AS8-14-2518

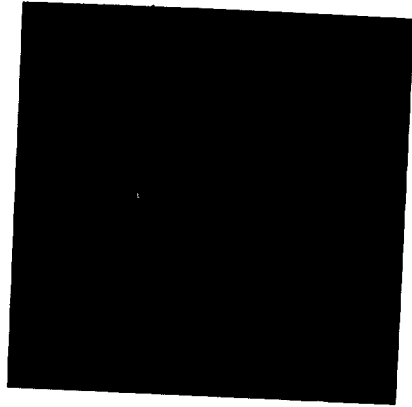


AS8-14-2519

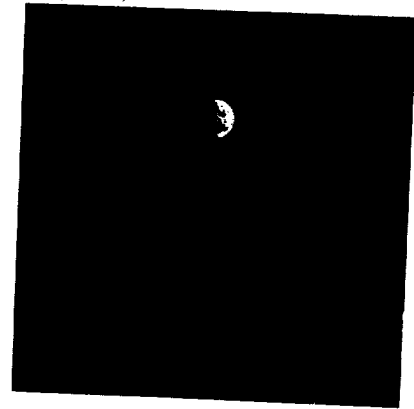


AS8-14-2520

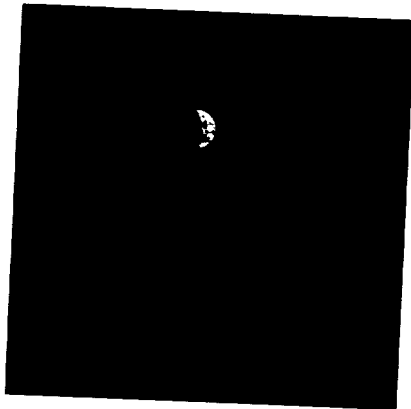
(Available in color.)



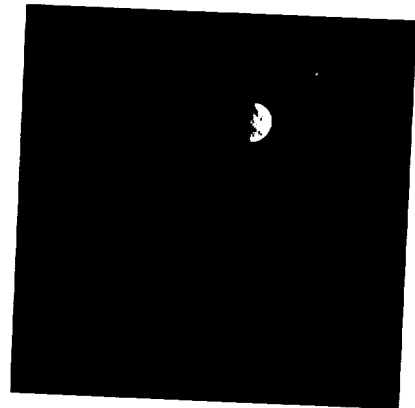
AS8-14-2521



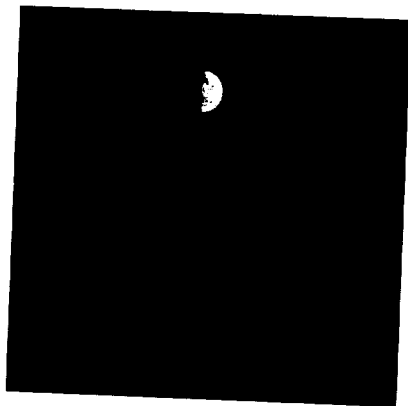
AS8-14-2522



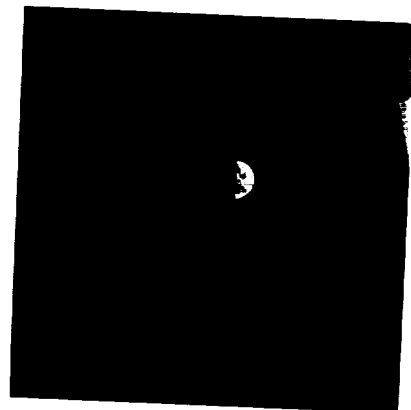
AS8-14-2523



AS8-14-2524

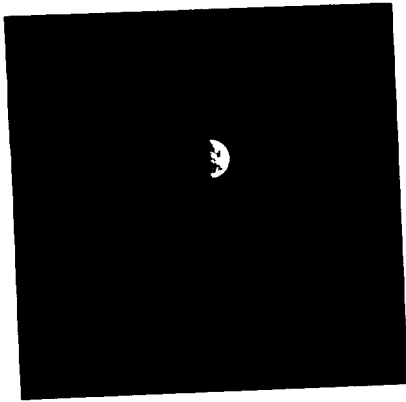


AS8-14-2525

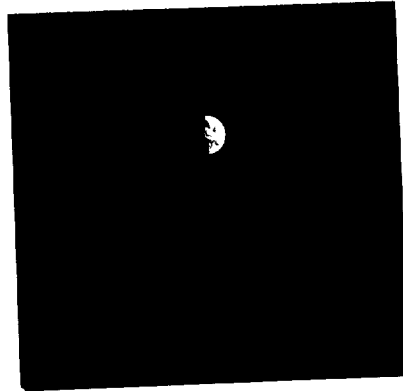


AS8-14-2526

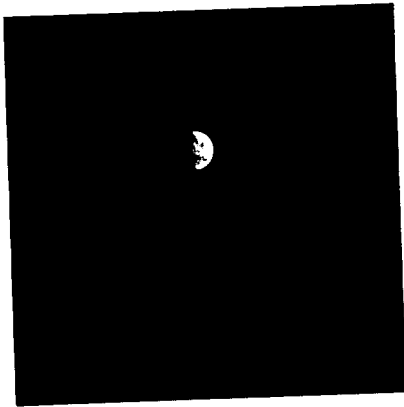
(Available in color.)



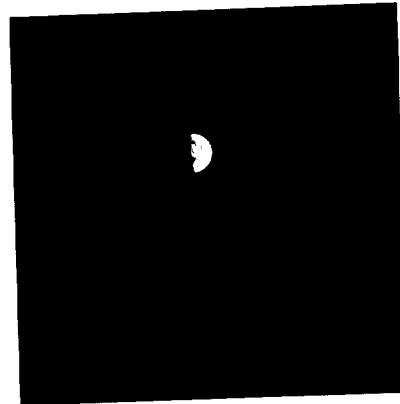
AS8-14-2527



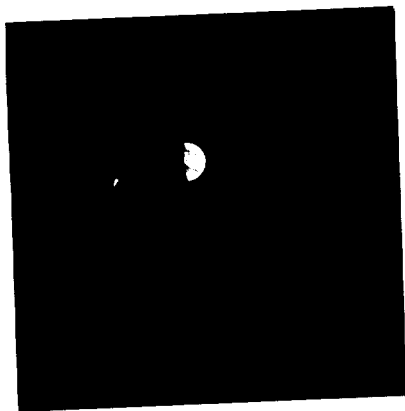
AS8-14-2528



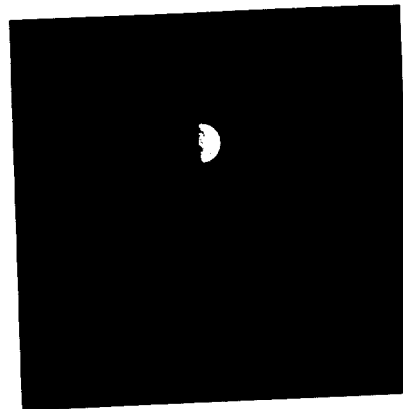
AS8-14-2529



AS8-14-2530

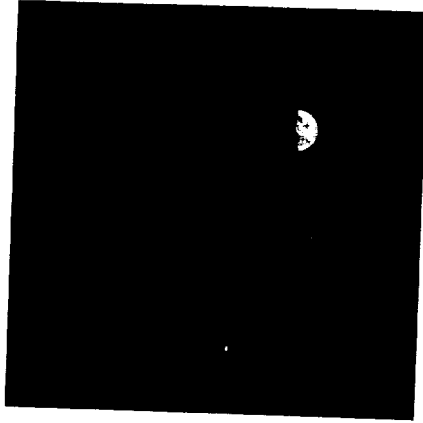


AS8-14-2531

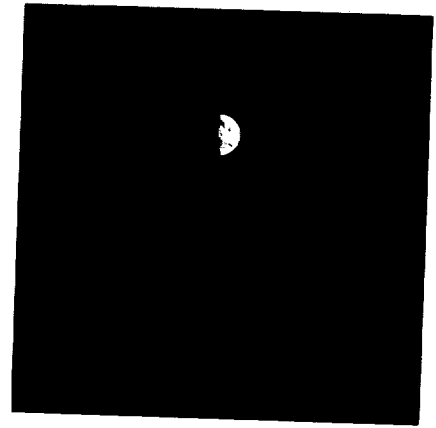


AS8-14-2532

(Available in color.)



AS8-14-2533



AS8-14-2534

(Available in color.)

MAGAZINE

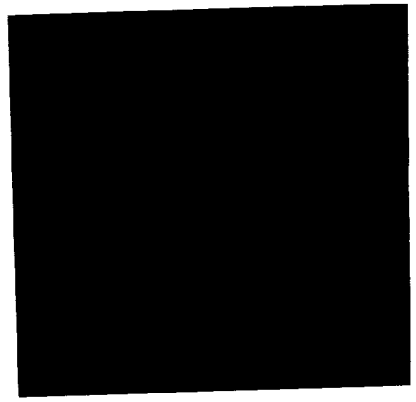
C

AS8-17-2659 to 2827

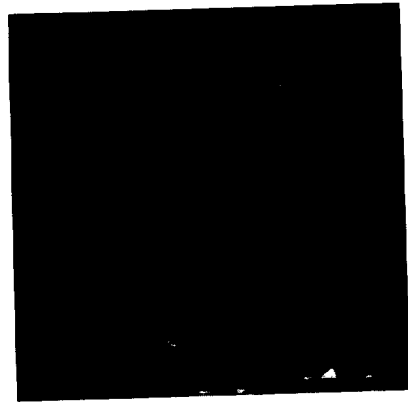
MAGAZINE C
← Z



AS8-17-2659



AS8-17-2660



AS8-17-2661



AS8-17-2662



AS8-17-2663



AS8-17-2664



AS8-17-2665



AS8-17-2666



AS8-17-2667



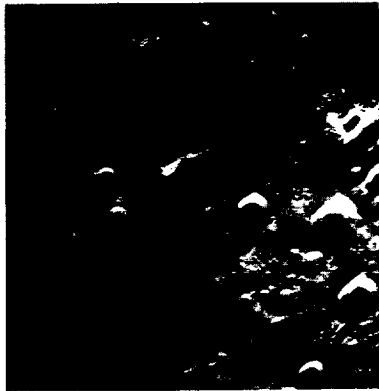
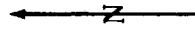
AS8-17-2668



AS8-17-2669



AS8-17-2670



AS8-17-2671



AS8-17-2672



AS8-17-2673



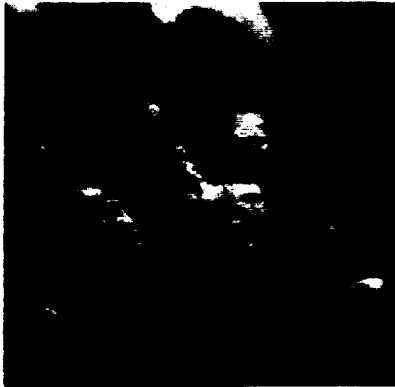
AS8-17-2674



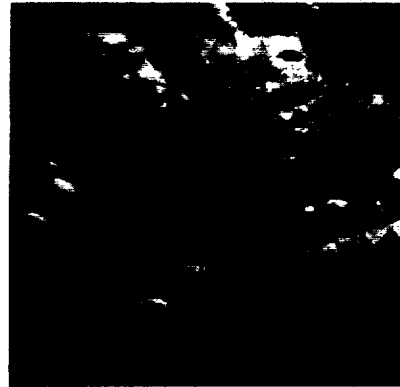
AS8-17-2675



AS8-17-2676



AS8-17-2677



AS8-17-2678



AS8-17-2679



AS8-17-2680

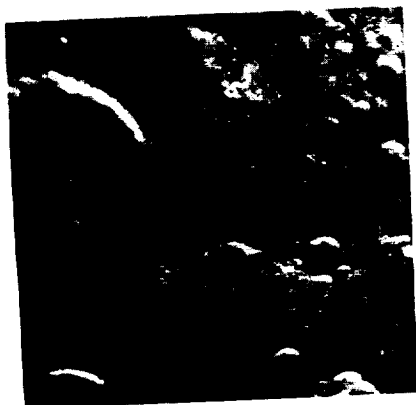
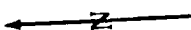


AS8-17-2681

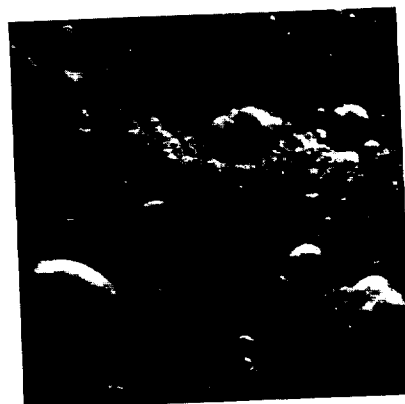


AS8-17-2682

MAGAZINE C



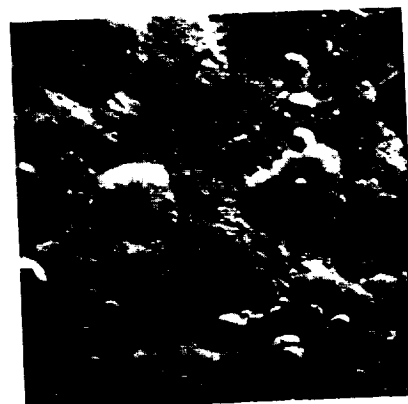
AS8-17-2683



AS8-17-2684



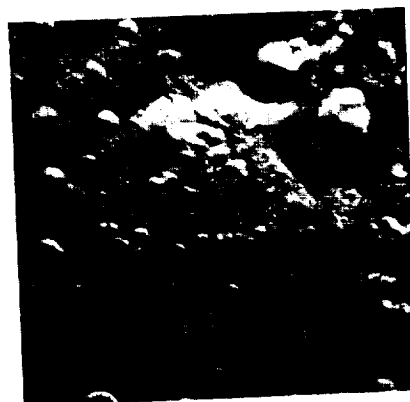
AS8-17-2685



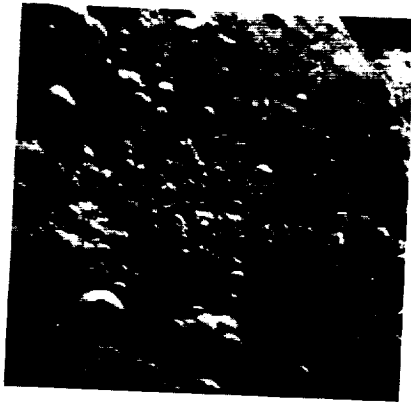
AS8-17-2686



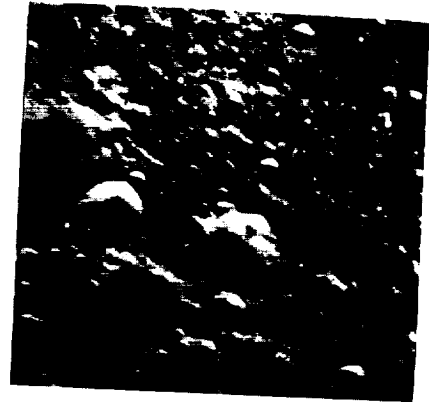
AS8-17-2687



AS8-17-2688



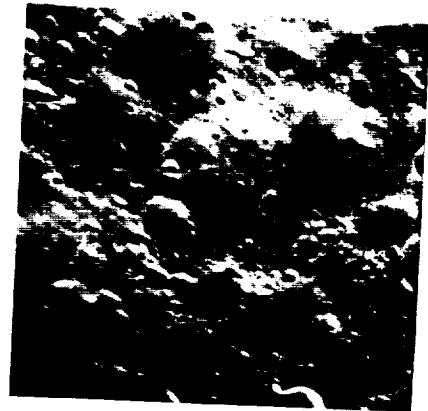
AS8-17-2689



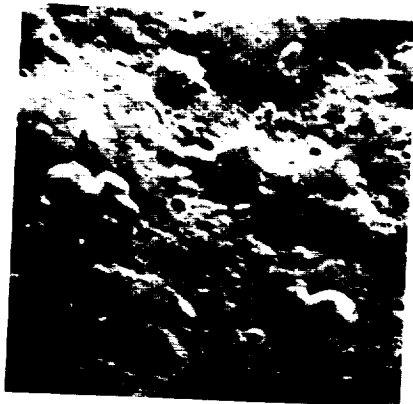
AS8-17-2690



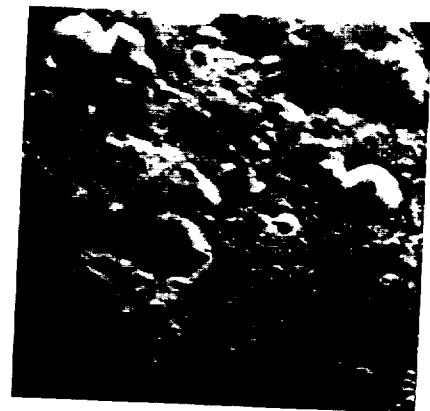
AS8-17-2691



AS8-17-2692



AS8-17-2693

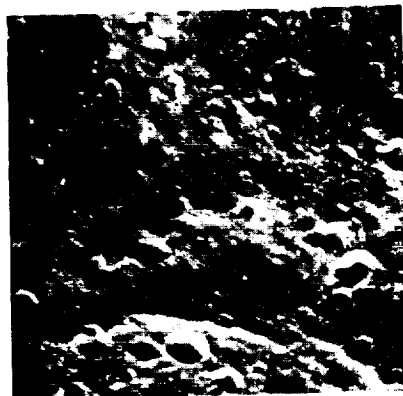


AS8-17-2694

MAGAZINE C



AS8-17-2695



AS8-17-2696



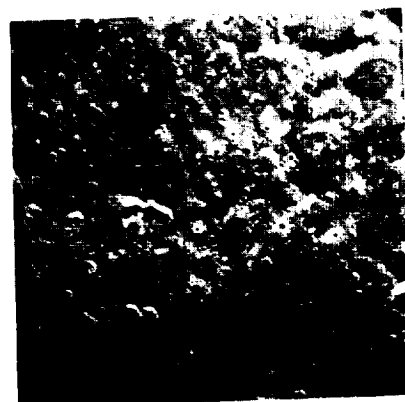
AS8-17-2697



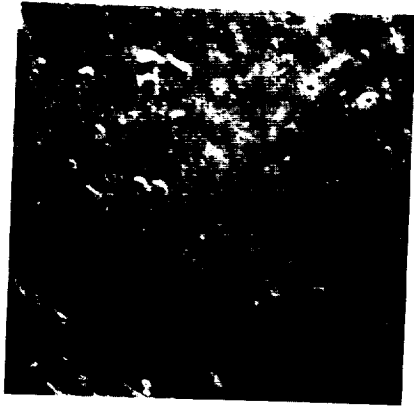
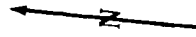
AS8-17-2698



AS8-17-2699



AS8-17-2700



AS8-17-2701



AS8-17-2702



AS8-17-2703



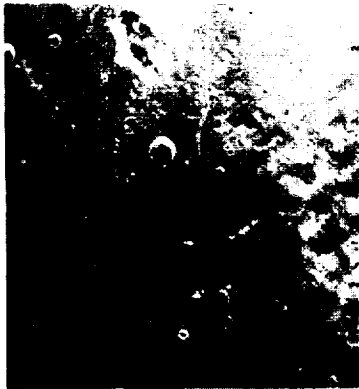
AS8-17-2704



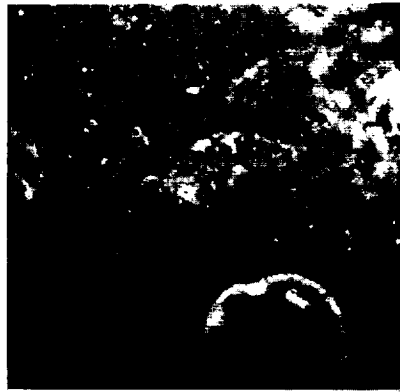
AS8-17-2705



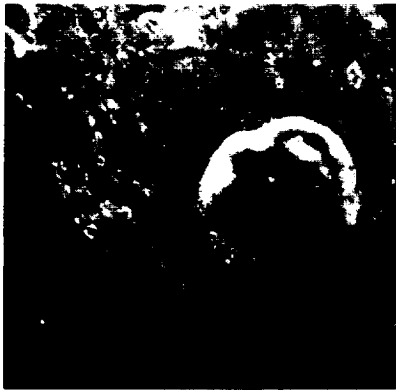
AS8-17-2706



AS8-17-2707



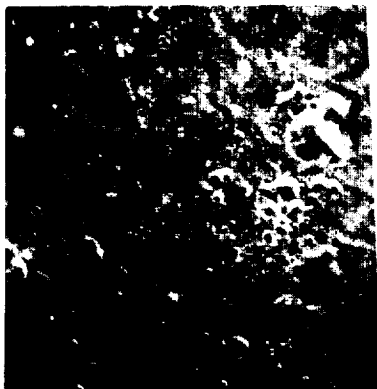
AS8-17-2708



AS8-17-2709



AS8-17-2710



AS8-17-2711



AS8-17-2712



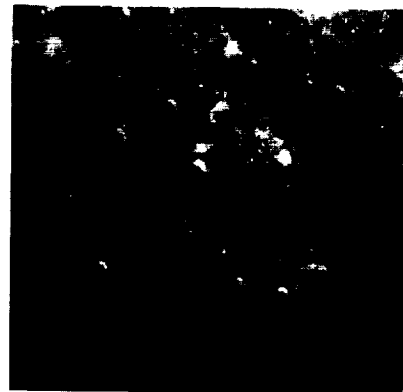
AS8-17-2713



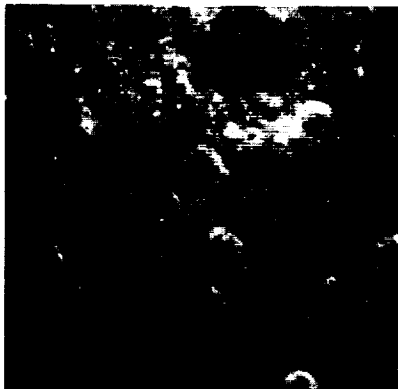
AS8-17-2714



AS8-17-2715



AS8-17-2716

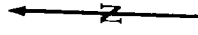


AS8-17-2717

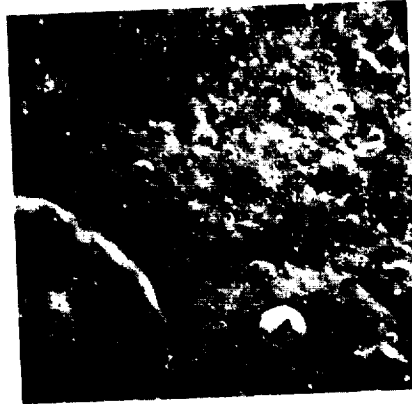


AS8-17-2718

MAGAZINE C



AS8-17-2719



AS8-17-2720



AS8-17-2721



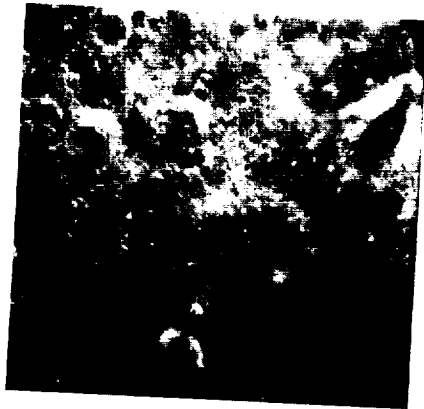
AS8-17-2722



AS8-17-2723



AS8-17-2724



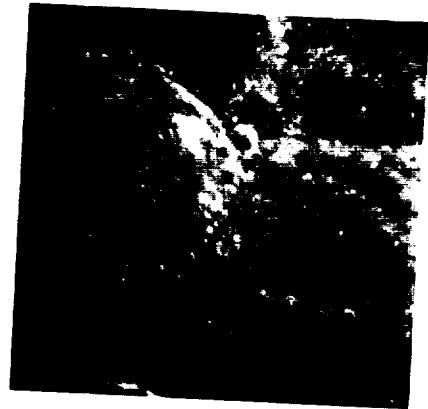
AS8-17-2725



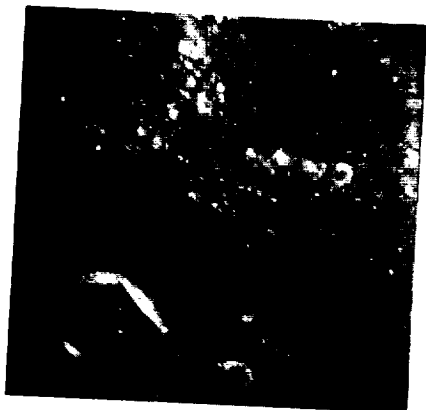
AS8-17-2726



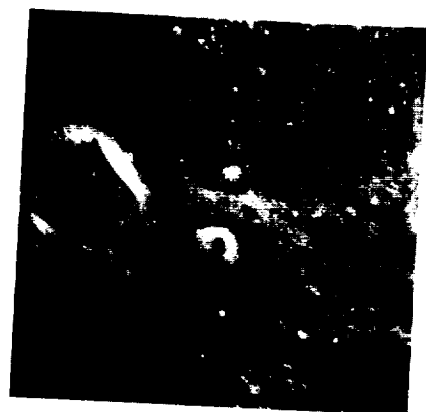
AS8-17-2727



AS8-17-2728

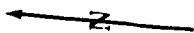


AS8-17-2729



AS8-17-2730

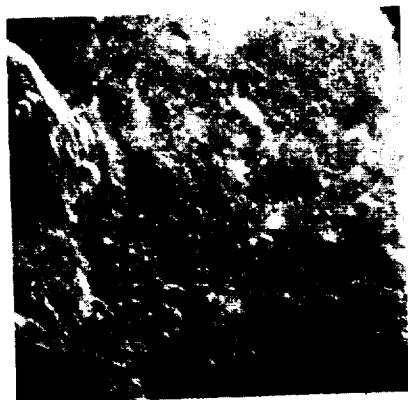
MAGAZINE C



AS8-17-2731



AS8-17-2732



AS8-17-2733



AS8-17-2734



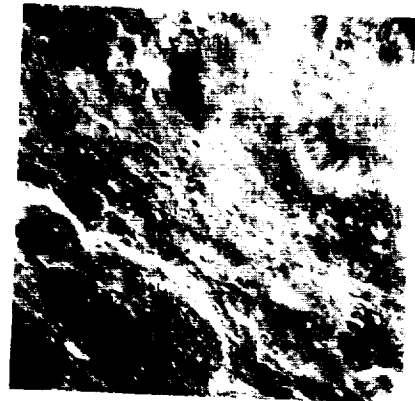
AS8-17-2735



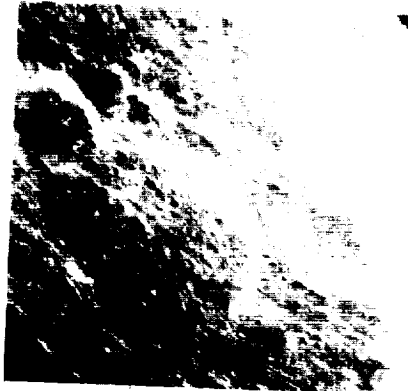
AS8-17-2736



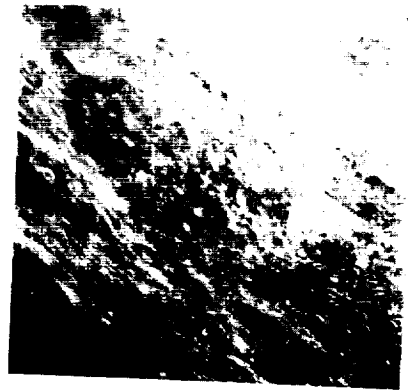
AS8-17-2737



AS8-17-2738



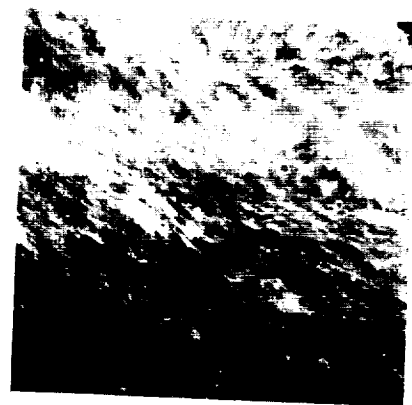
AS8-17-2739



AS8-17-2740

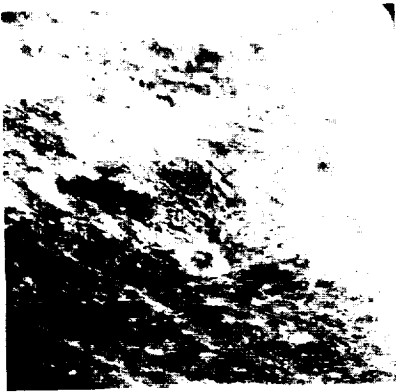


AS8-17-2741



AS8-17-2742

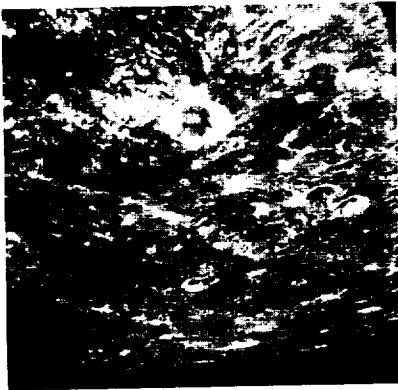
MAGAZINE C



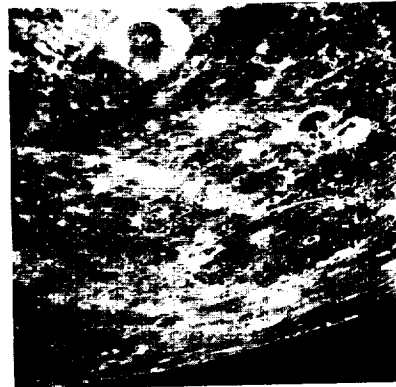
AS8-17-2743



AS8-17-2744



AS8-17-2745



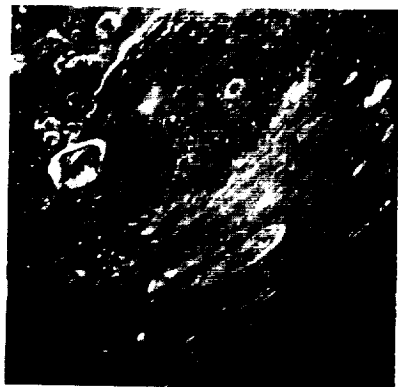
AS8-17-2746



AS8-17-2747



AS8-17-2748



AS8-17-2749



AS8-17-2750



AS8-17-2751



AS8-17-2752



AS8-17-2753



AS8-17-2754



AS8-17-2755



AS8-17-2756



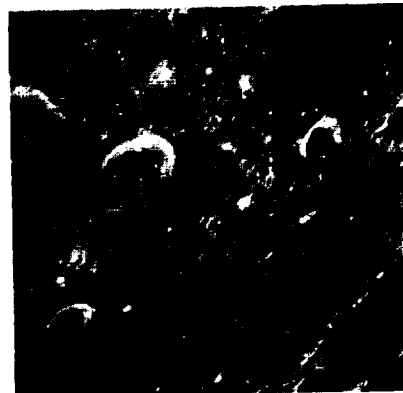
AS8-17-2757



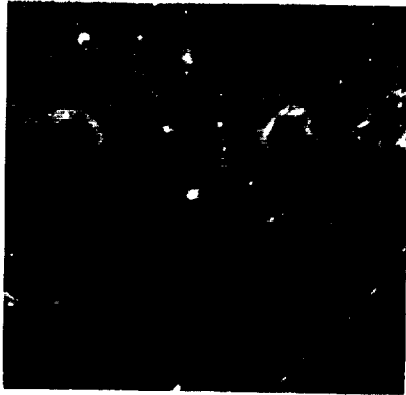
AS8-17-2758



AS8-17-2759



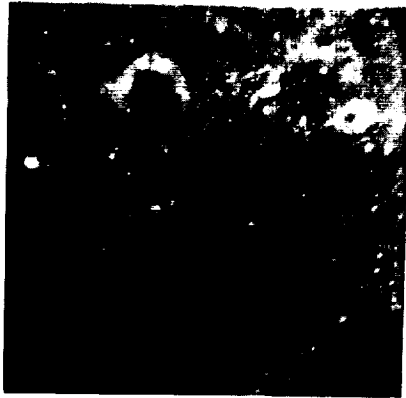
AS8-17-2760



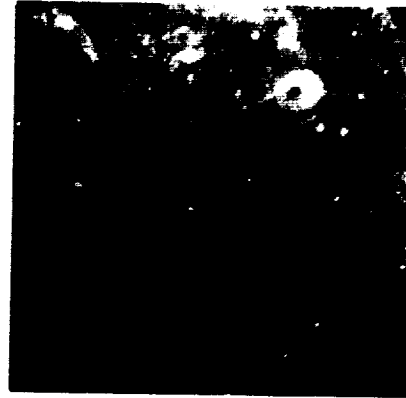
AS8-17-2761



AS8-17-2762



AS8-17-2763



AS8-17-2764



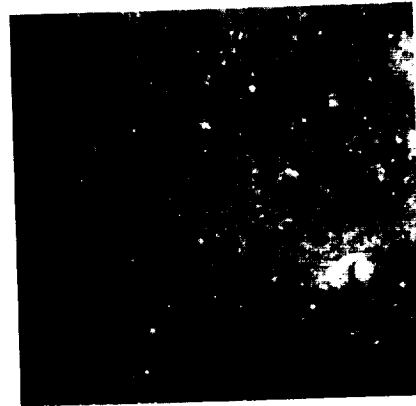
AS8-17-2765



AS8-17-2766



AS8-17-2767



AS8-17-2768



AS8-17-2769



AS8-17-2770



AS8-17-2771



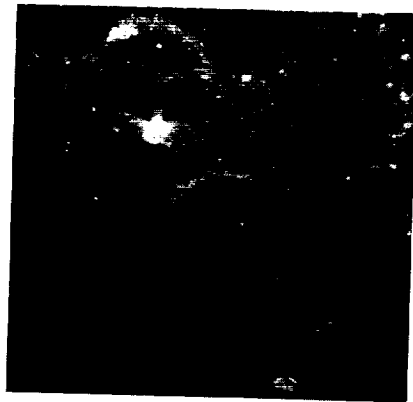
AS8-17-2772



AS8-17-2773



AS8-17-2774



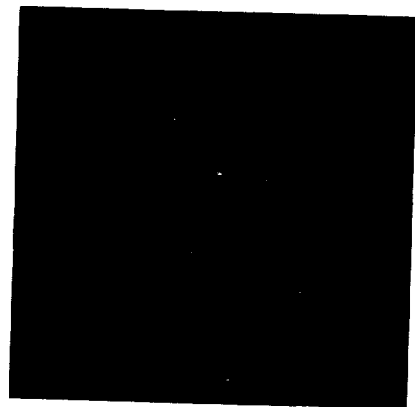
AS8-17-2775



AS8-17-2776



AS8-17-2777

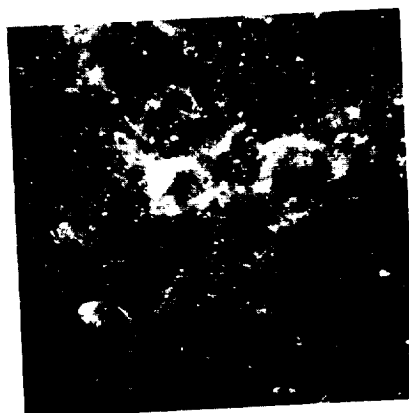


AS8-17-2778

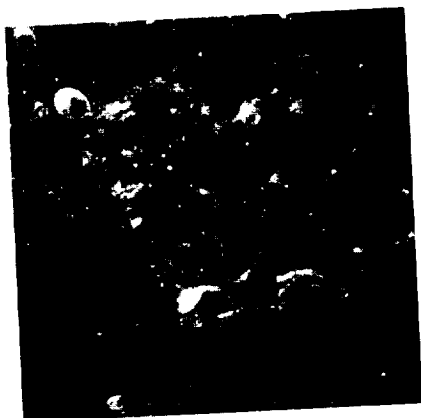
MAGAZINE C



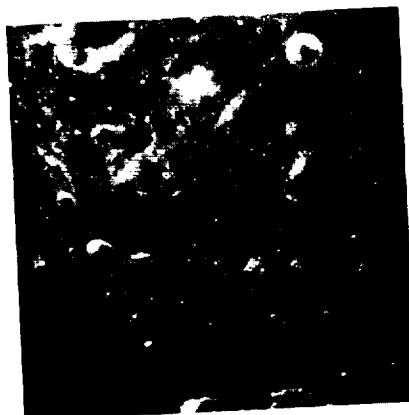
AS8-17-2779



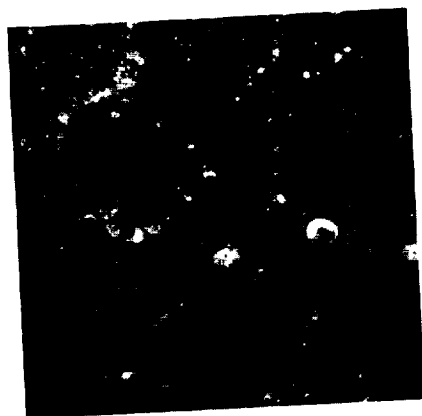
AS8-17-2780



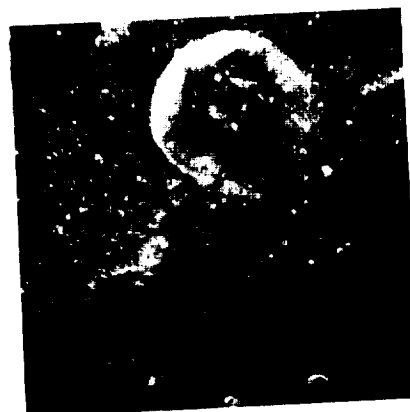
AS8-17-2781



AS8-17-2782



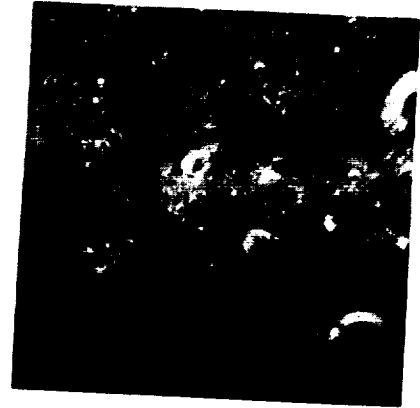
AS8-17-2783



AS8-17-2784



AS8-17-2785



AS8-17-2786



AS8-17-2787



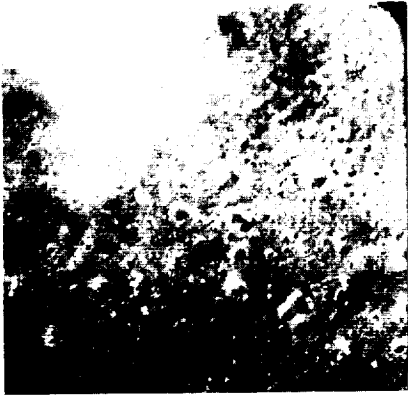
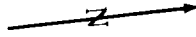
AS8-17-2788



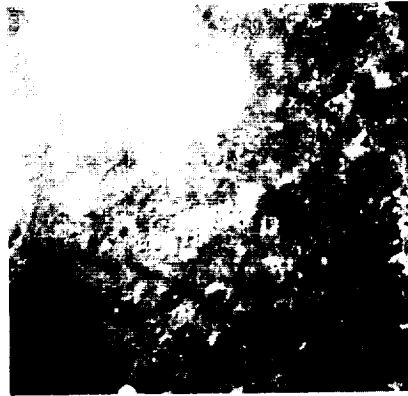
AS8-17-2789



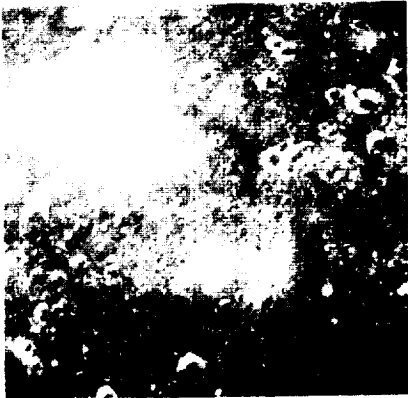
AS8-17-2790



AS8-17-2791



AS8-17-2792



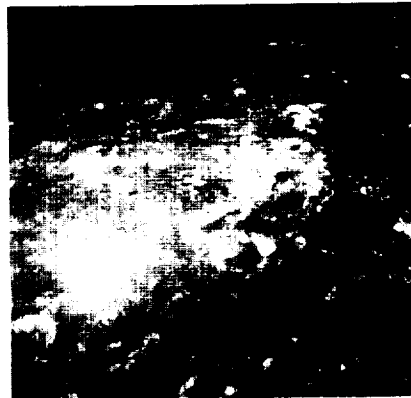
AS8-17-2793



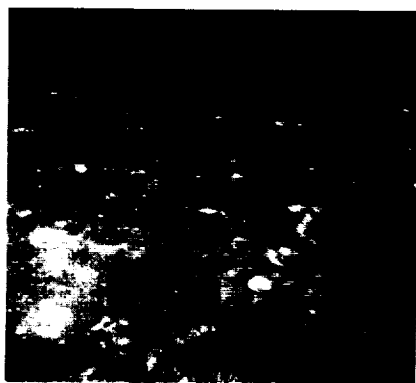
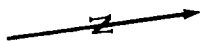
AS8-17-2794



AS8-17-2795



AS8-17-2796



AS8-17-2797



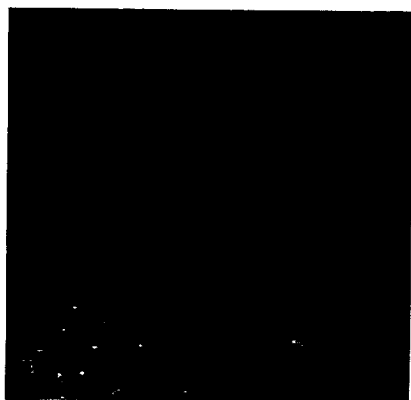
AS8-17-2798



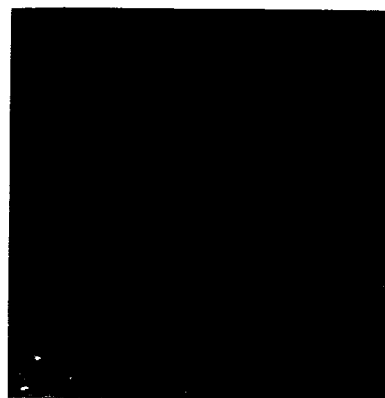
AS8-17-2799



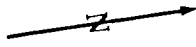
AS8-17-2800



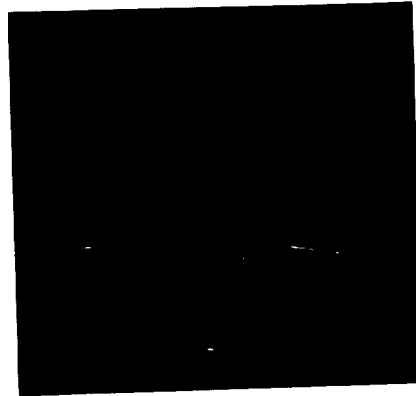
AS8-17-2801



AS8-17-2802



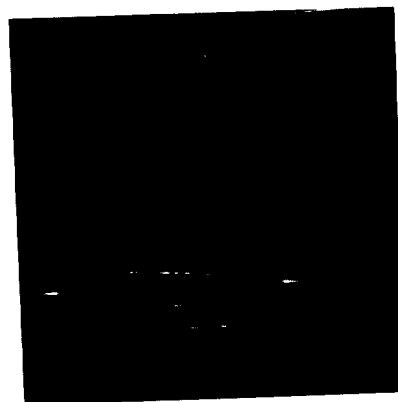
AS8-17-2803



AS8-17-2804



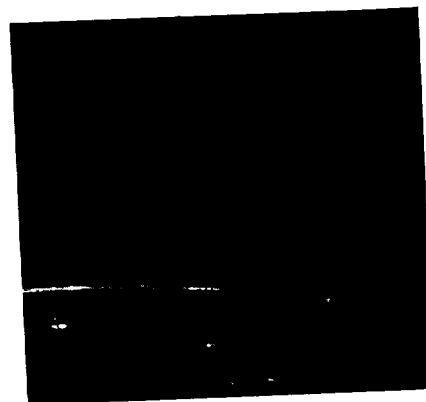
AS8-17-2805



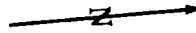
AS8-17-2806



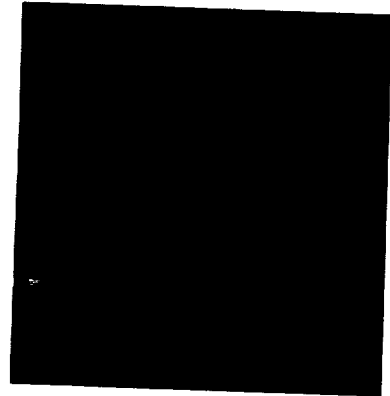
AS8-17-2807



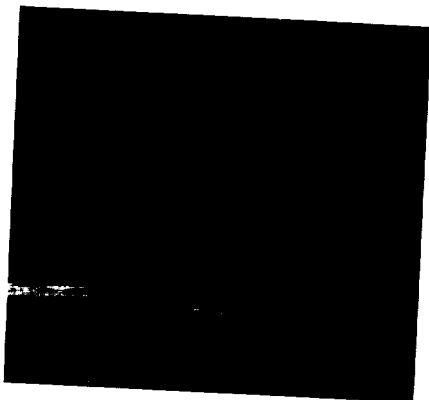
AS8-17-2808



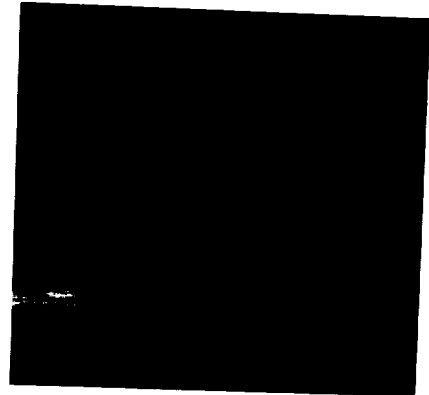
AS8-17-2809



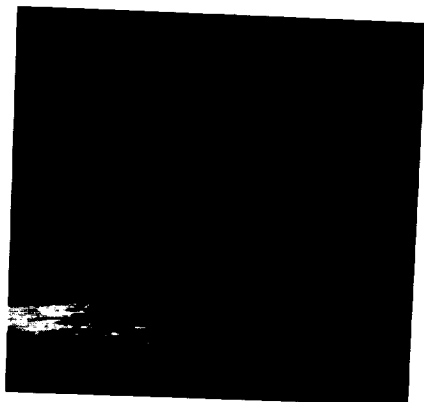
AS8-17-2810



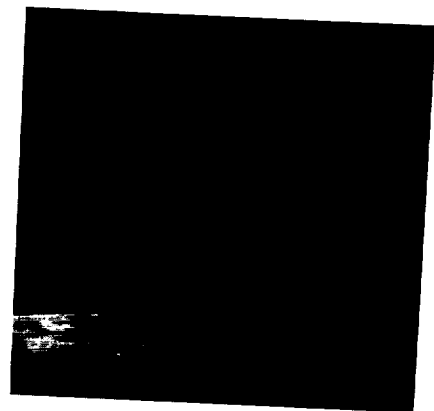
AS8-17-2811



AS8-17-2812



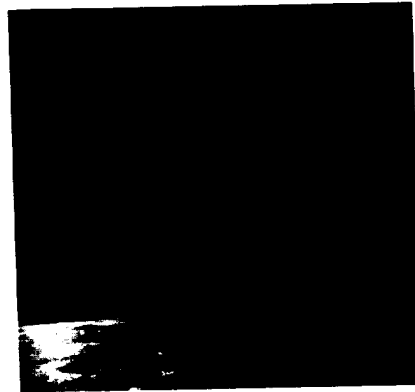
AS8-17-2813



AS8-17-2814



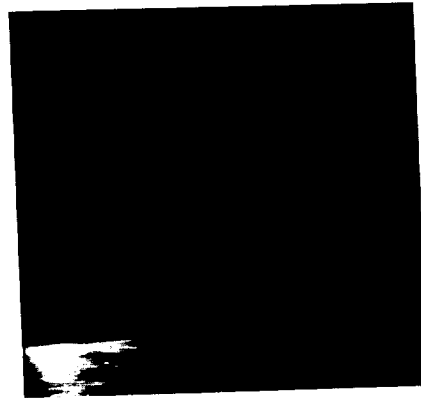
AS8-17-2815



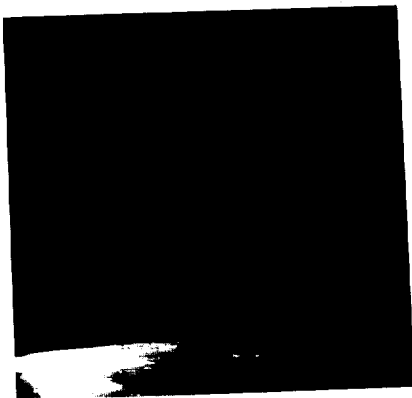
AS8-17-2816



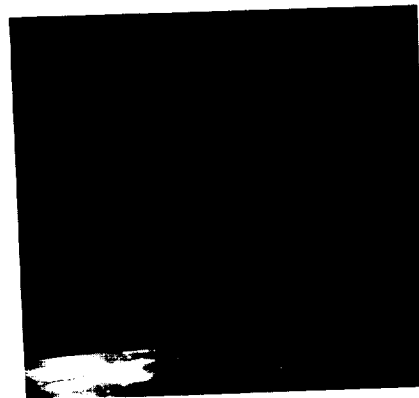
AS8-17-2817



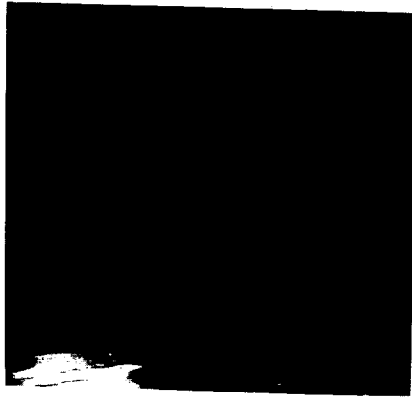
AS8-17-2818



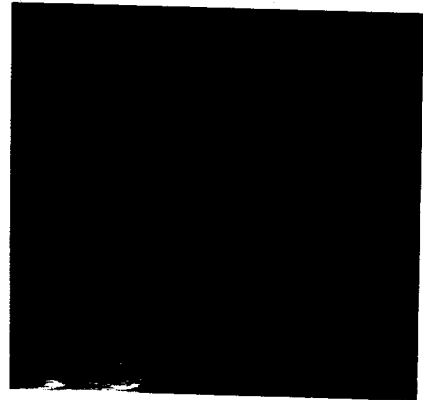
AS8-17-2819



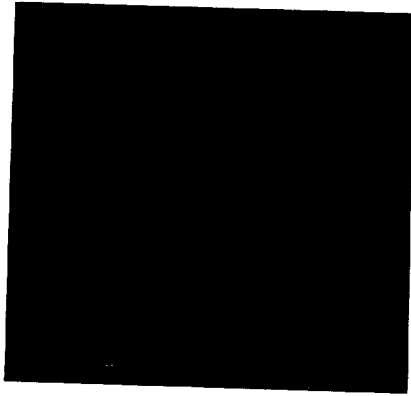
AS8-17-2820



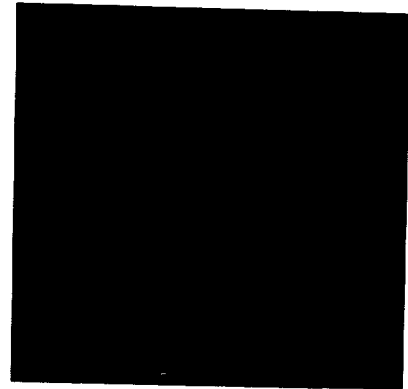
AS8-17-2821



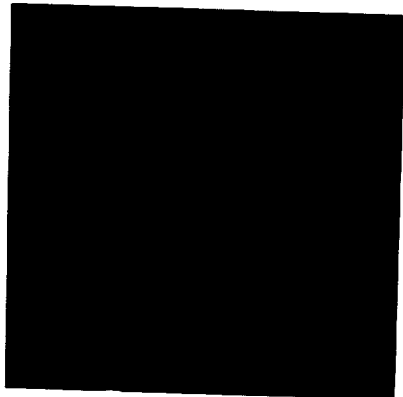
AS8-17-2822



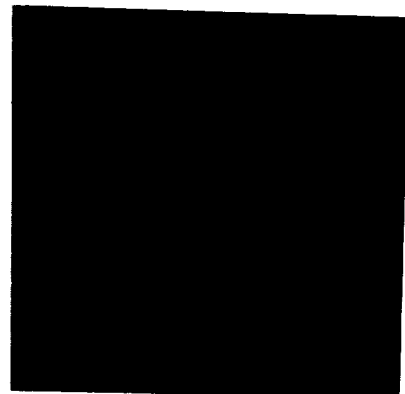
AS8-17-2823



AS8-17-2824



AS8-17-2825



AS8-17-2826



AS8-17-2827



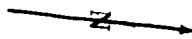
MAGAZINE

D

AS8-12-2044 to 2214



MAGAZINE D



AS8-12-2044



AS8-12-2045



AS8-12-2046



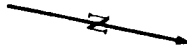
AS8-12-2047



AS8-12-2048



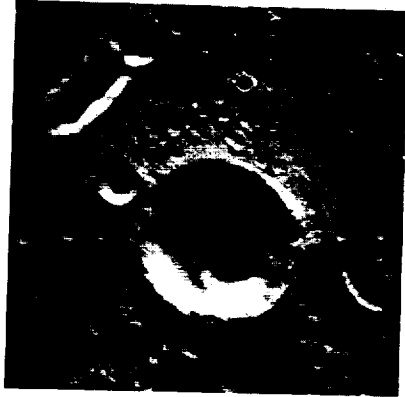
AS8-12-2049



AS8-12-2050



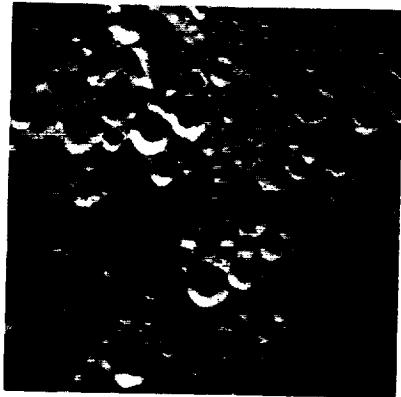
AS8-12-2051



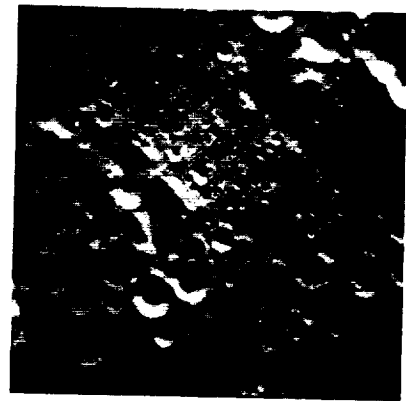
AS8-12-2052



AS8-12-2053

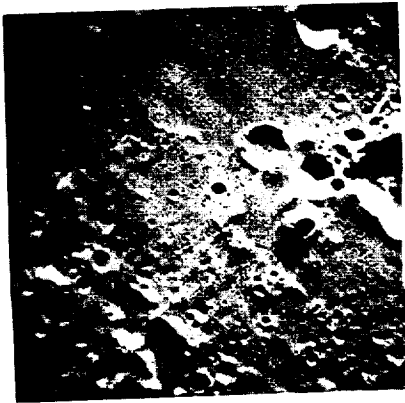


AS8-12-2054



AS8-12-2055

MAGAZINE D



AS8-12-2056



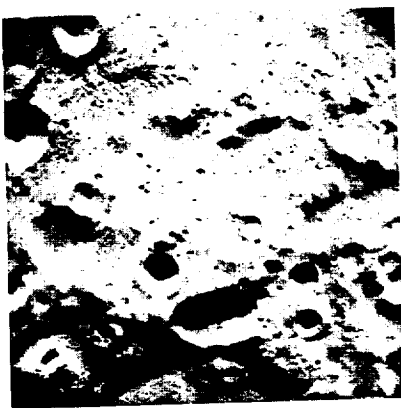
AS8-12-2057



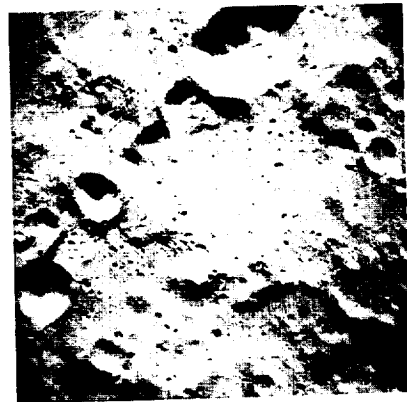
AS8-12-2058



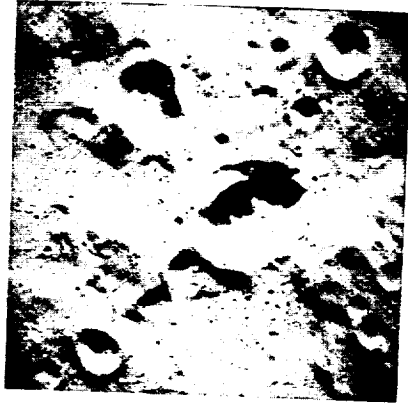
AS8-12-2059



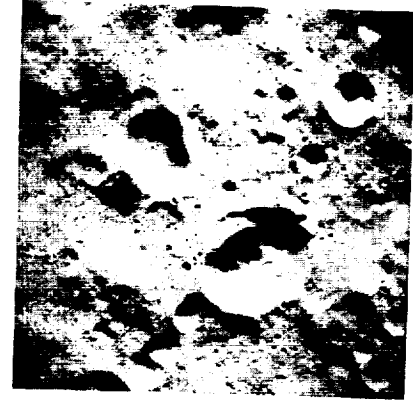
AS8-12-2060



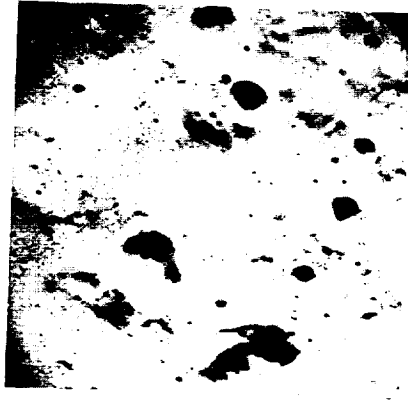
AS8-12-2061



AS8-12-2062



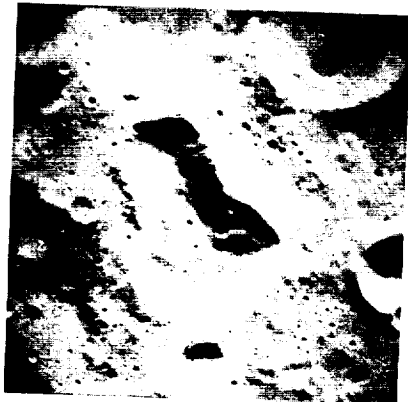
AS8-12-2063



AS8-12-2064



AS8-12-2065

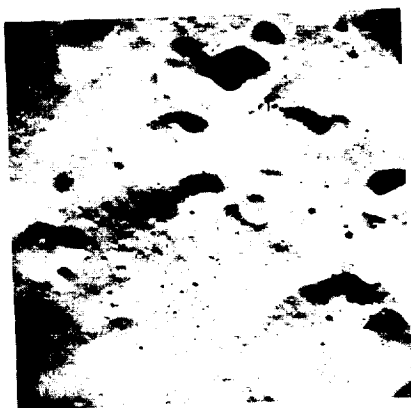


AS8-12-2066



AS8-12-2067

MAGAZINE D



AS8-12-2068



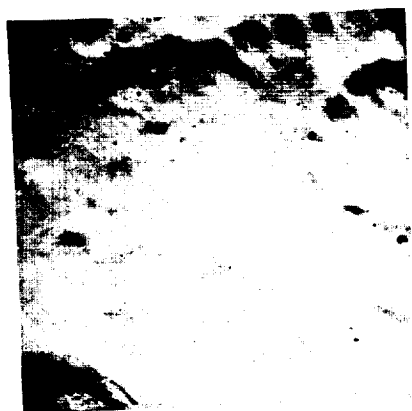
AS8-12-2069



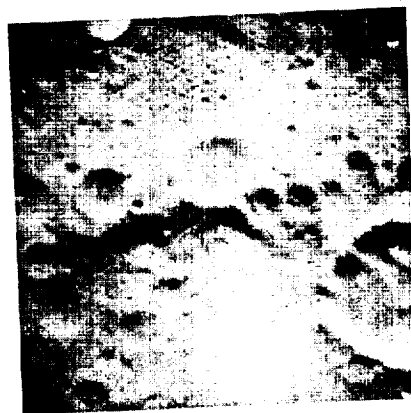
AS8-12-2070



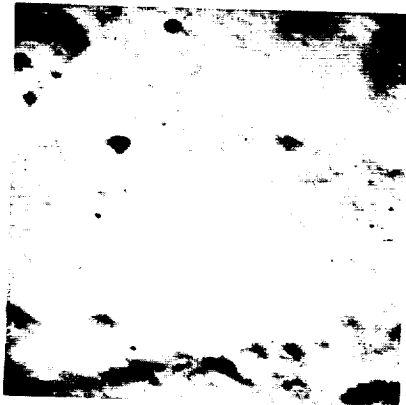
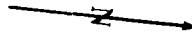
AS8-12-2071



AS8-12-2072



AS8-12-2073



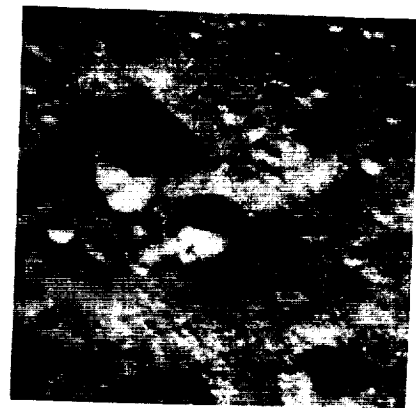
AS8-12-2074



AS8-12-2075



AS8-12-2076



AS8-12-2077



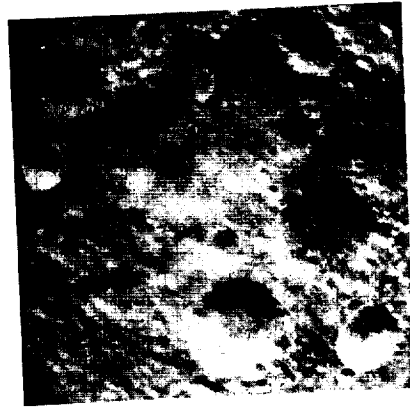
AS8-12-2078



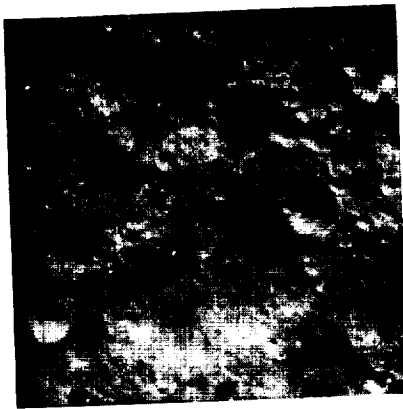
AS8-12-2079



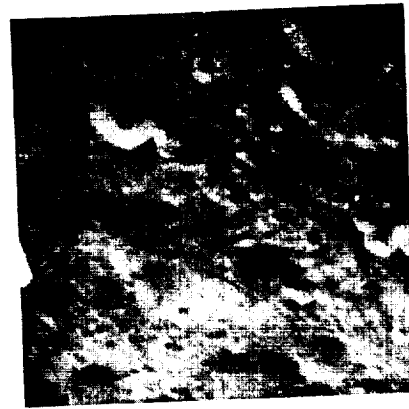
AS8-12-2080



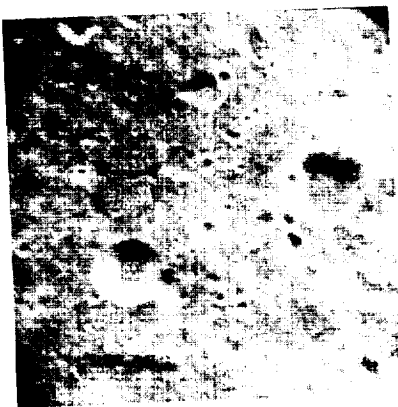
AS8-12-2081



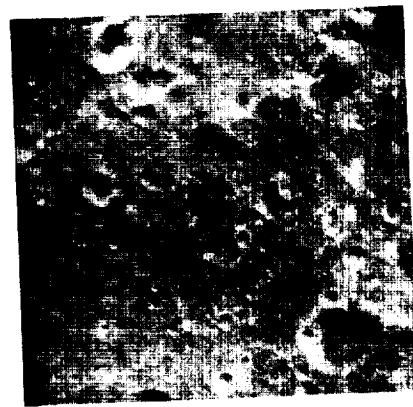
AS8-12-2082



AS8-12-2083



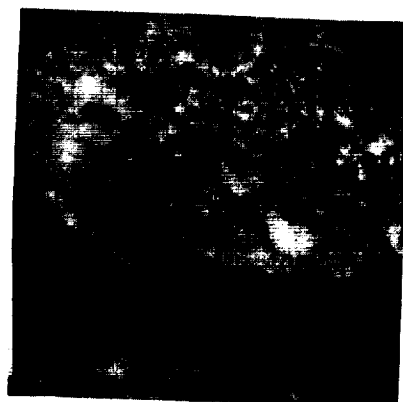
AS8-12-2084



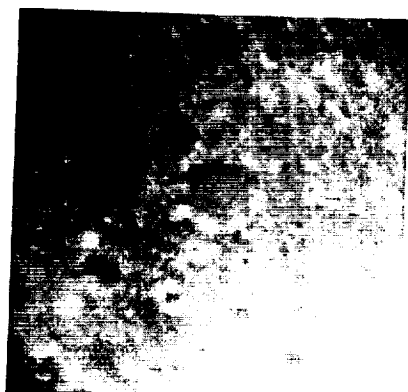
AS8-12-2085



AS8-12-2086



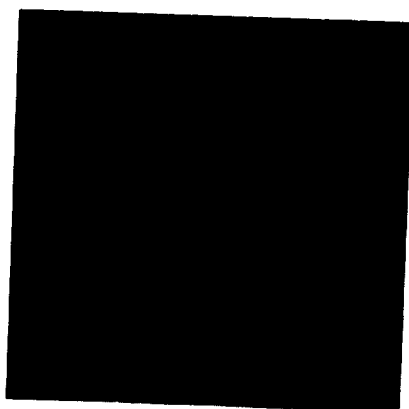
AS8-12-2087



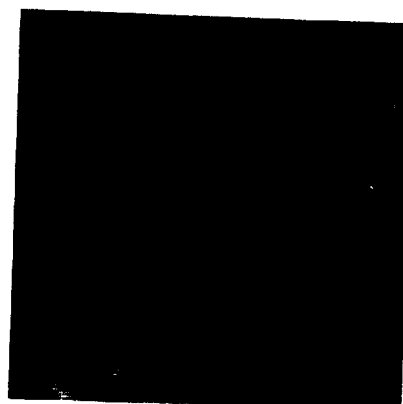
AS8-12-2088



AS8-12-2089

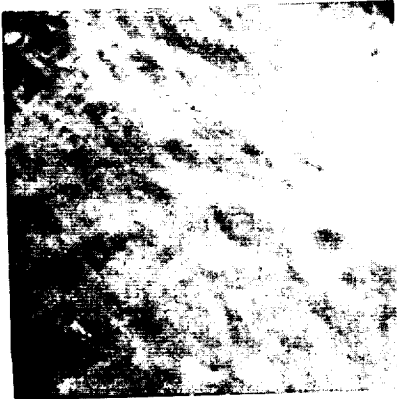


AS8-12-2090



AS8-12-2091

MAGAZINE D



AS8-12-2092



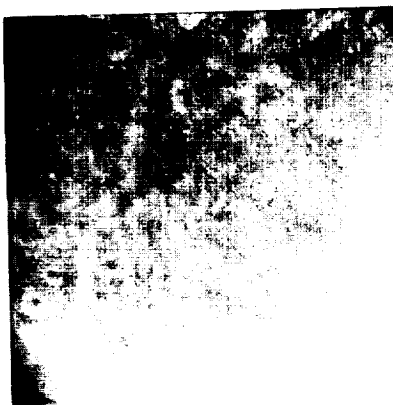
AS8-12-2093



AS8-12-2094



AS8-12-2095



AS8-12-2096



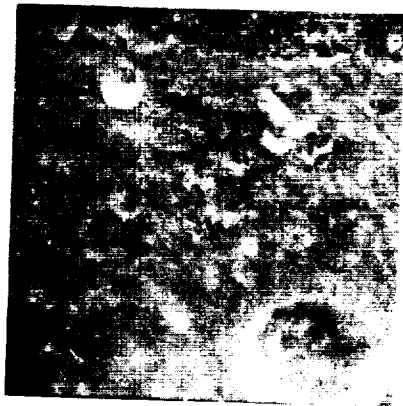
AS8-12-2097



AS8-12-2098



AS8-12-2099



AS8-12-2100



AS8-12-2101



AS8-12-2102

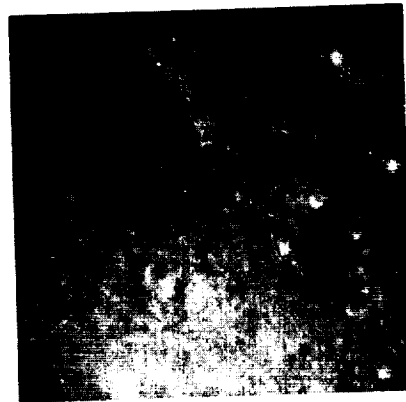


AS8-12-2103

MAGAZINE D



AS8-12-2104



AS8-12-2105



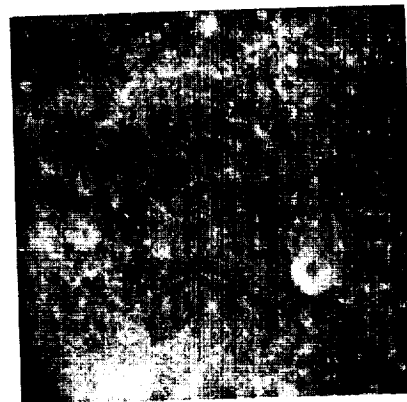
AS8-12-2106



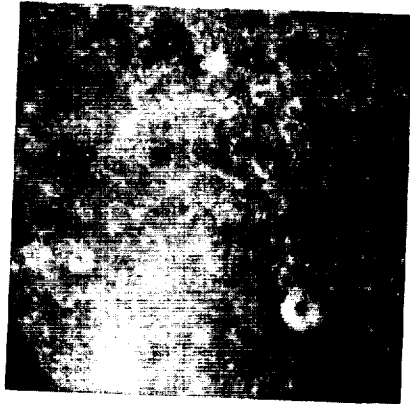
AS8-12-2107



AS8-12-2108



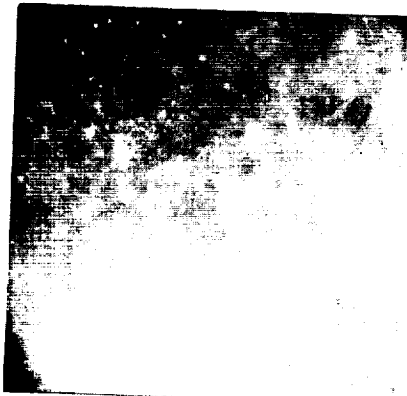
AS8-12-2109



AS8-12-2110



AS8-12-2111



AS8-12-2112



AS8-12-2113



AS8-12-2114

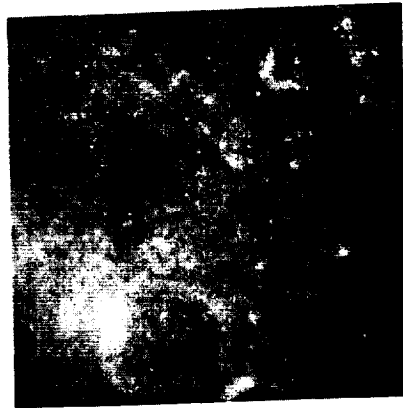


AS8-12-2115

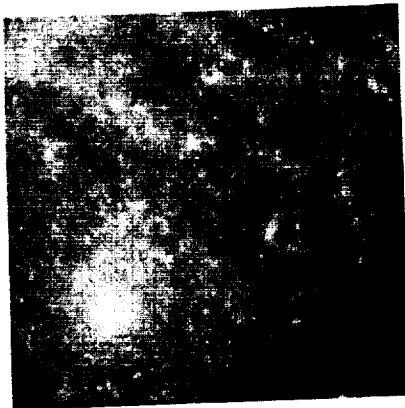
MAGAZINE D



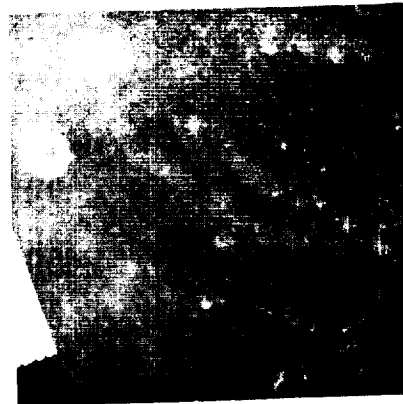
AS8-12-2116



AS8-12-2117



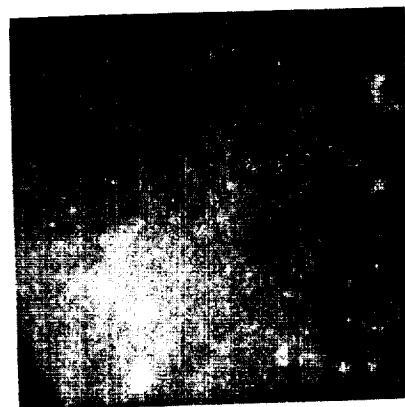
AS8-12-2118



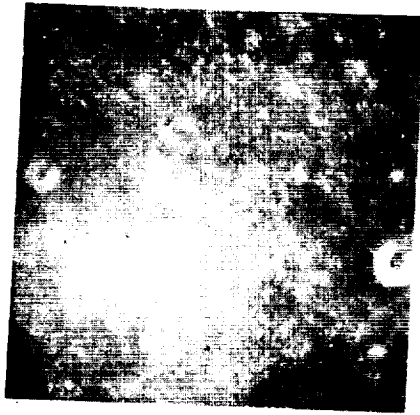
AS8-12-2119



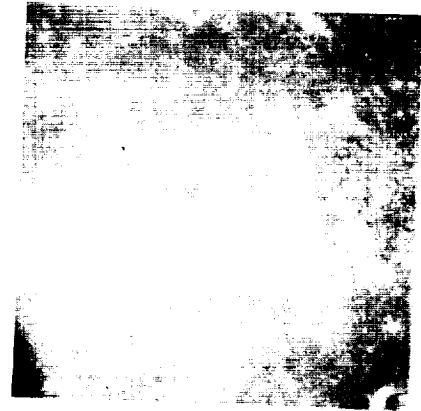
AS8-12-2120



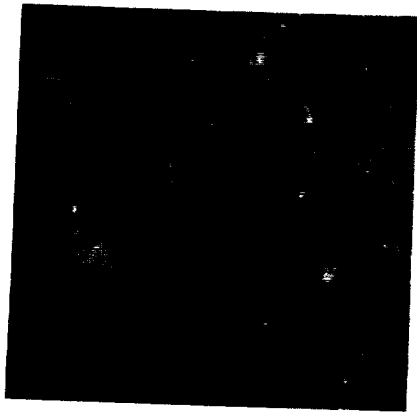
AS8-12-2121



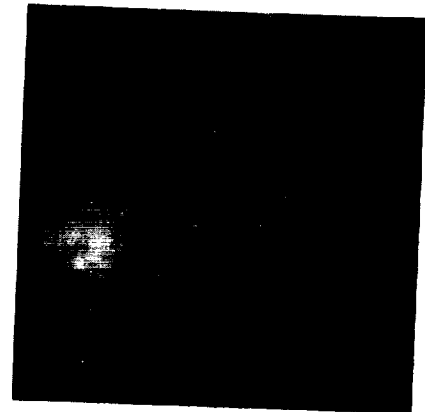
AS8-12-2122



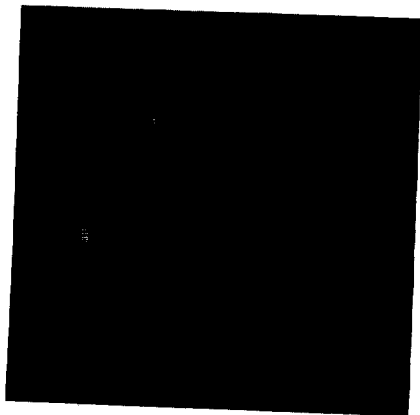
AS8-12-2123



AS8-12-2124



AS8-12-2125



AS8-12-2126



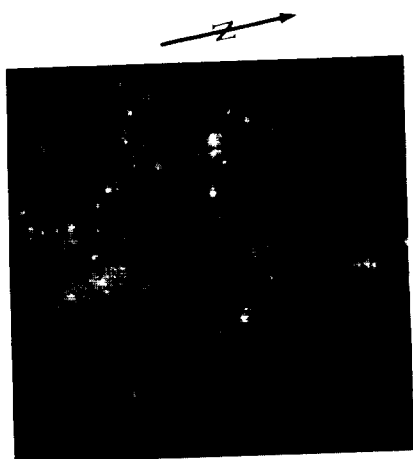
AS8-12-2127



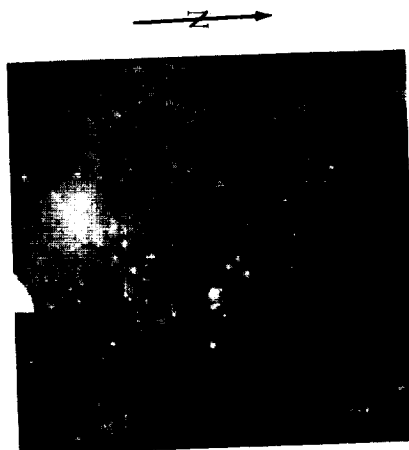
AS8-12-2128



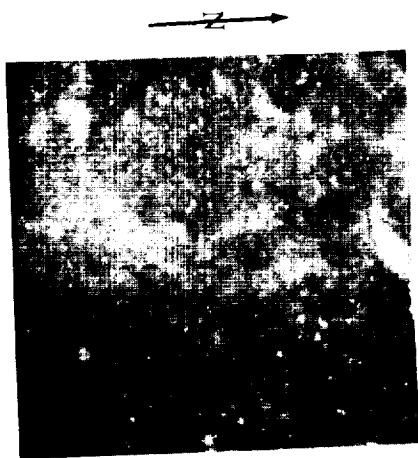
AS8-12-2129



AS8-12-2130



AS8-12-2131

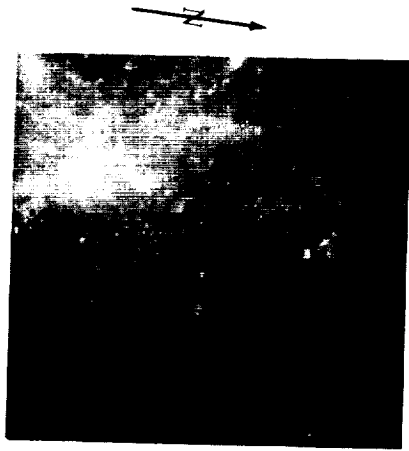


AS8-12-2132

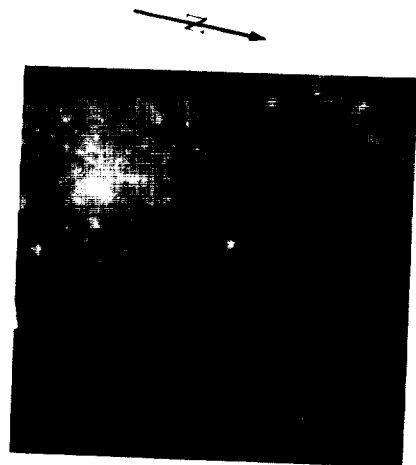


AS8-12-2133

ANALYSIS OF APOLLO 8 PHOTOGRAPHY AND VISUAL OBSERVATIONS



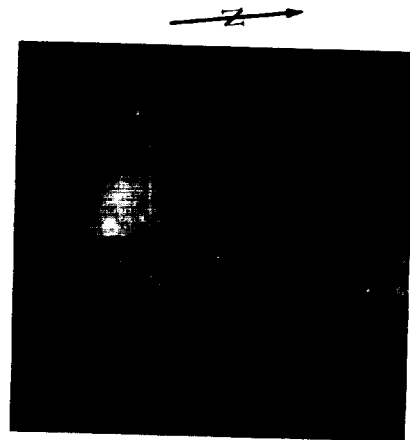
AS8-12-2134



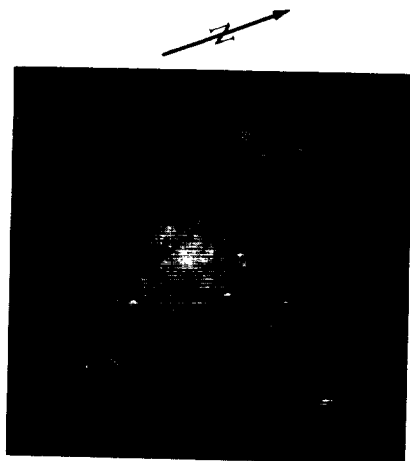
AS8-12-2135



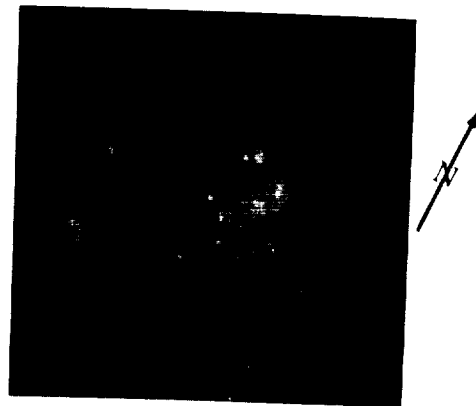
AS8-12-2136



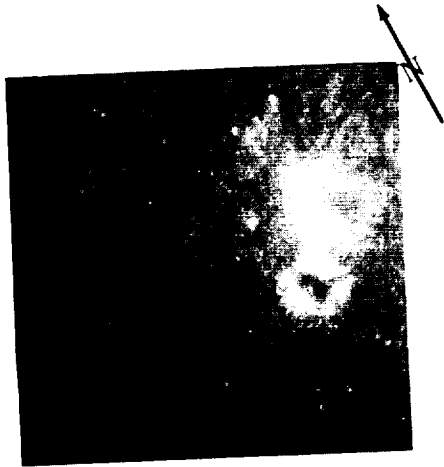
AS8-12-2137



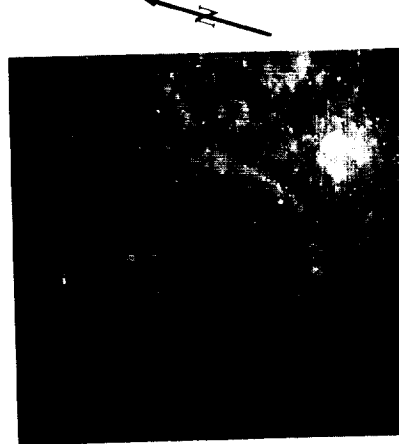
AS8-12-2138



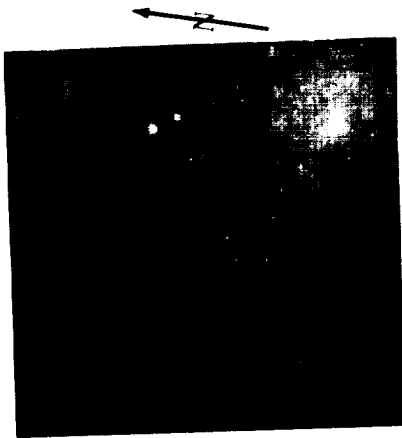
AS8-12-2139



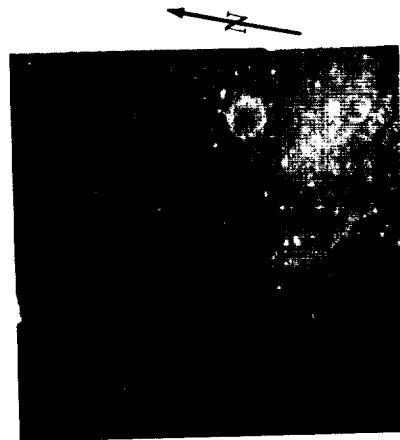
AS8-12-2140



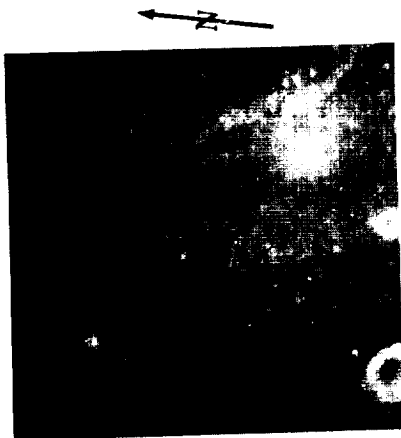
AS8-12-2141



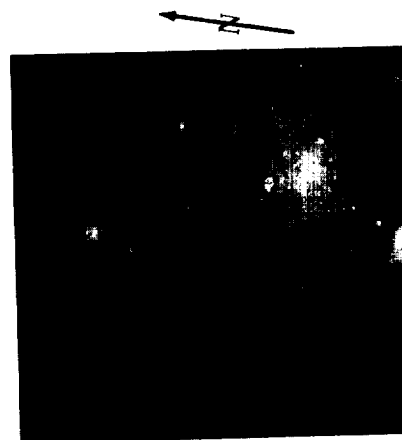
AS8-12-2142



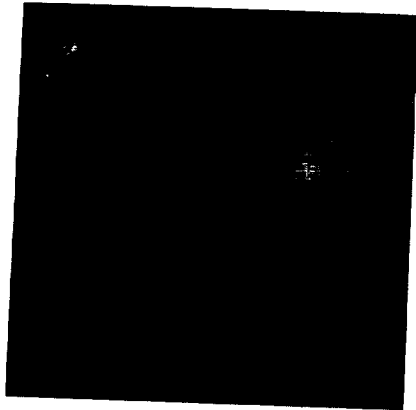
AS8-12-2143



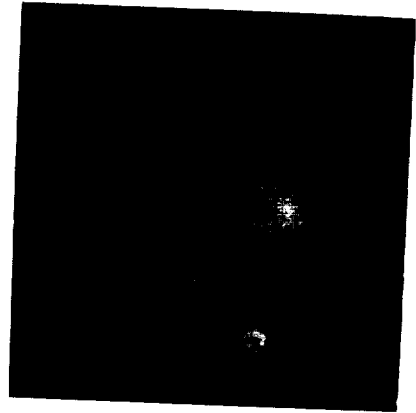
AS8-12-2144



AS8-12-2145



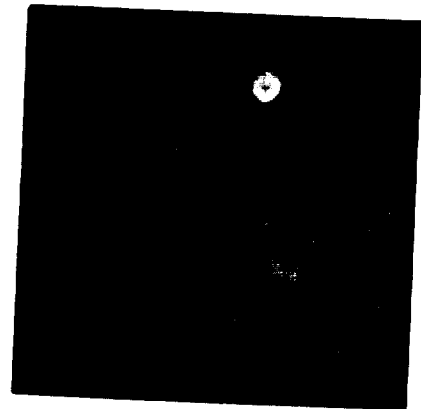
AS8-12-2146



AS8-12-2147



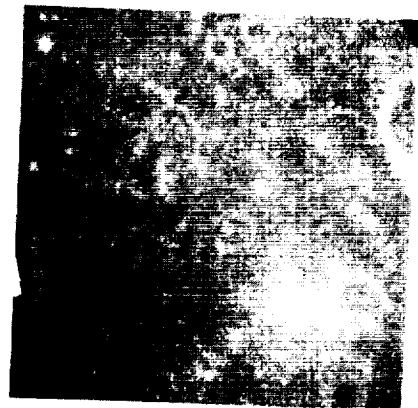
AS8-12-2148



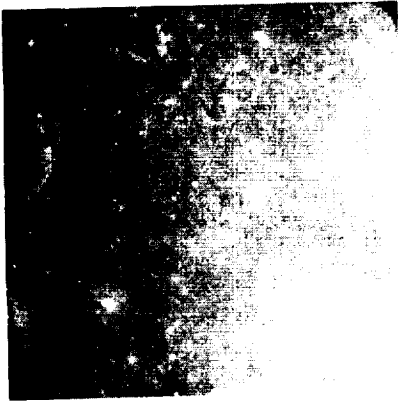
AS8-122149



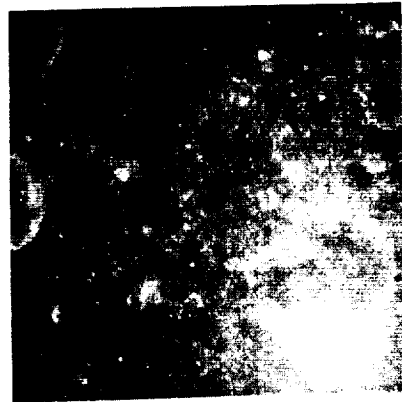
AS8-12-2150



AS8-12-2151



AS8-12-2152



AS8-12-2153



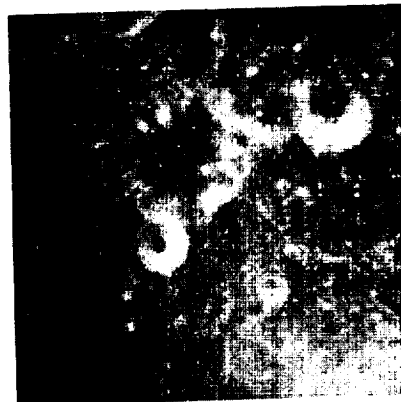
AS8-12-2154



AS8-12-2155



AS8-12-2156



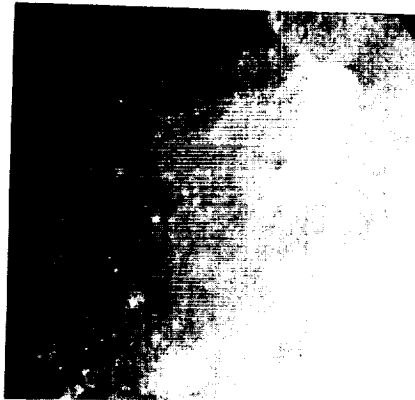
AS8-12-2157



AS8-12-2158



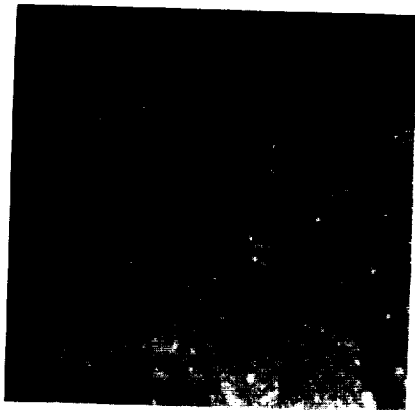
AS8-12-2159



AS8-12-2160



AS8-12-2161

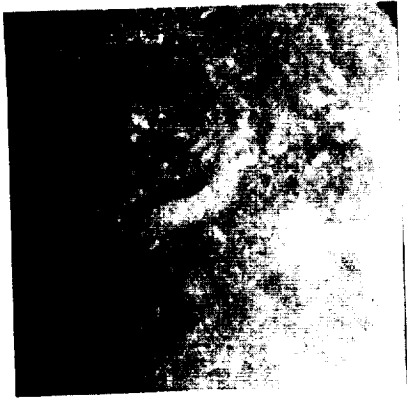


AS8-12-2162



AS8-12-2163

MAGAZINE D



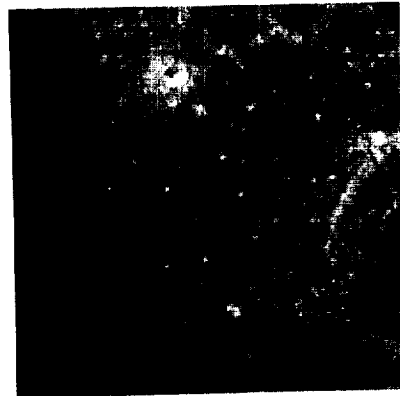
AS8-12-2164



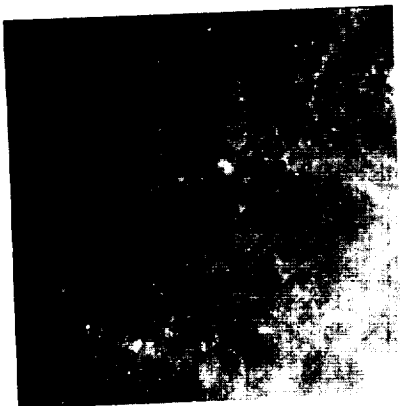
AS8-12-2165



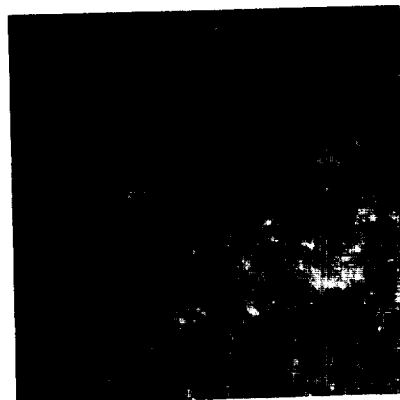
AS8-12-2166



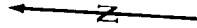
AS8-12-2167



AS8-12-2168



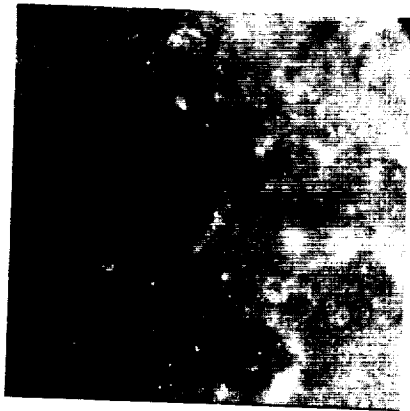
AS8-12-2169



AS8-12-2170



AS8-12-2171



AS8-12-2172



AS8-12-2173

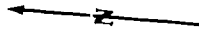


AS8-12-2174



AS8-12-2175

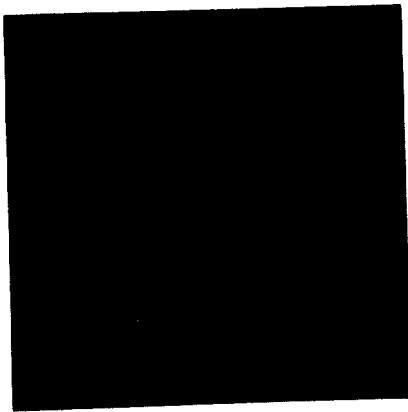
MAGAZINE D



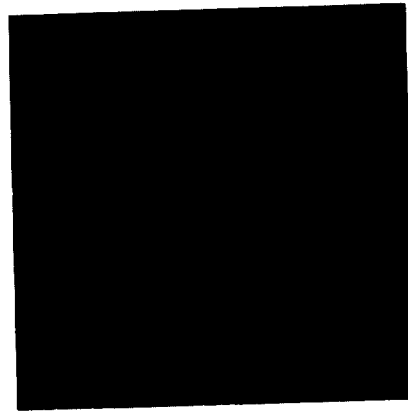
AS8-12-2176



AS8-12-2177



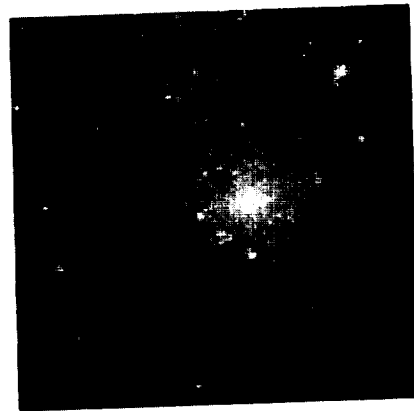
AS8-12-2178



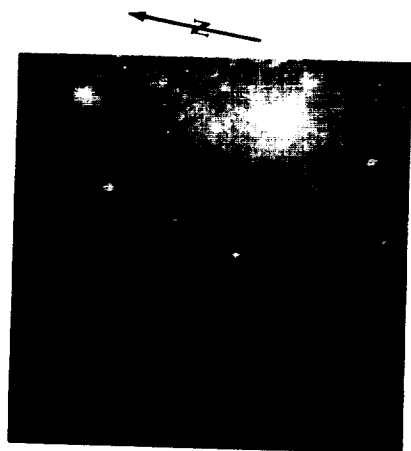
AS8-12-2179



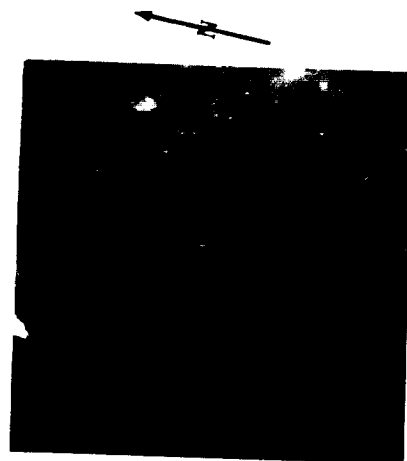
AS8-12-2180



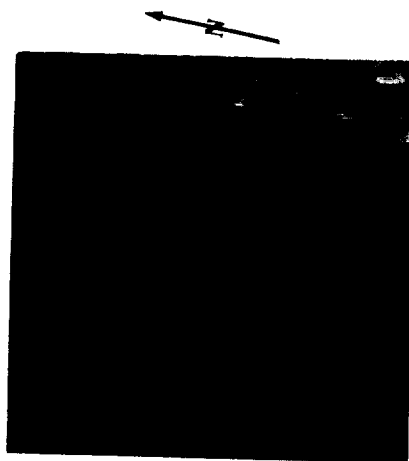
AS8-12-2181



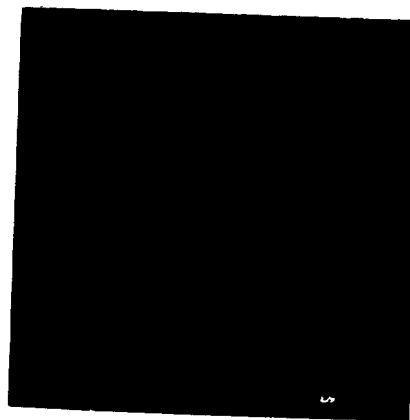
AS8-12-2182



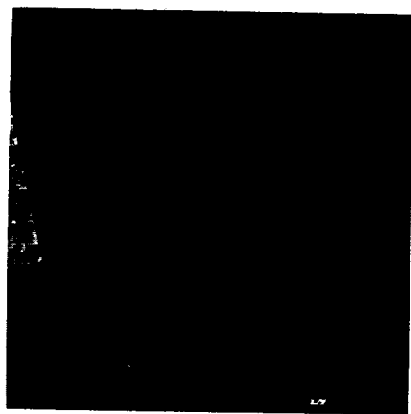
AS8-12-2183



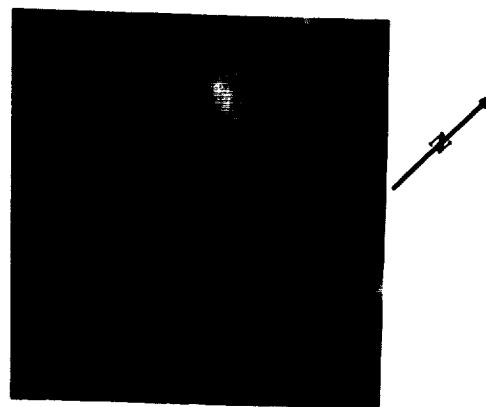
AS8-12-2184



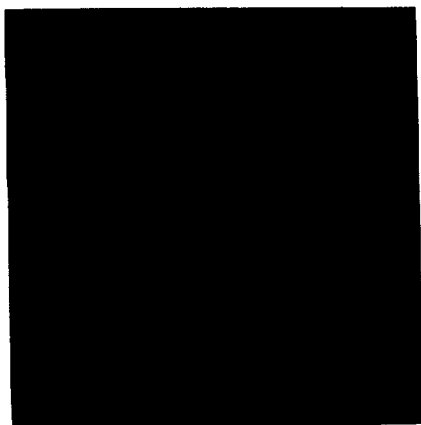
AS8-12-2185



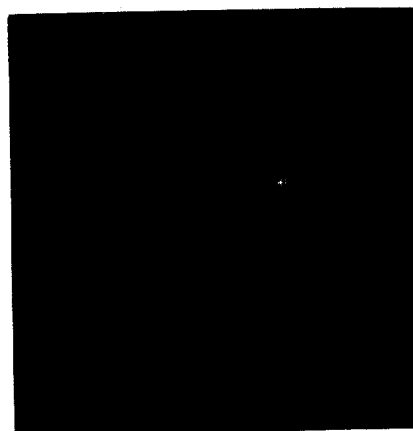
AS8-12-2186



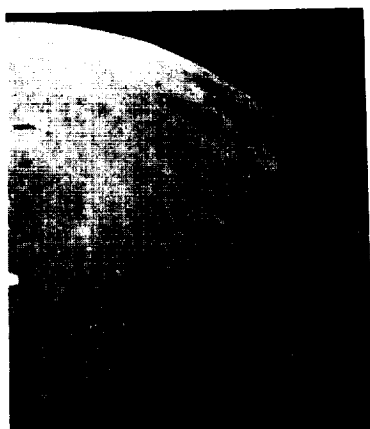
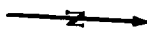
AS8-12-2187



AS8-12-2188



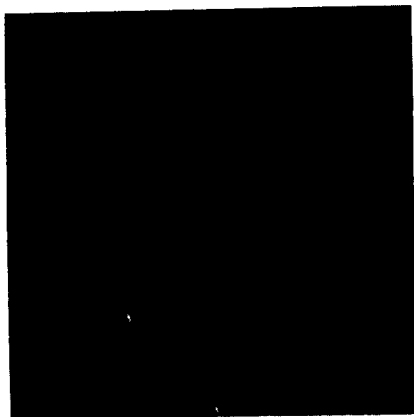
AS8-12-2189



AS8-12-2190



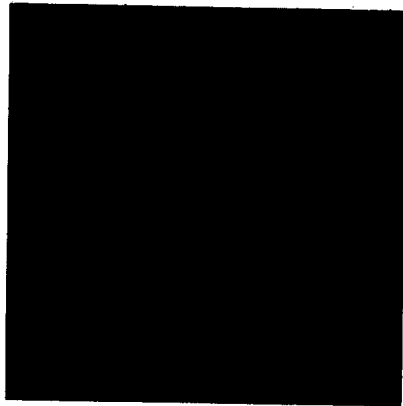
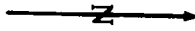
AS8-12-2191



AS8-12-2192



AS8-12-2193



AS8-12-2194



AS8-12-2195



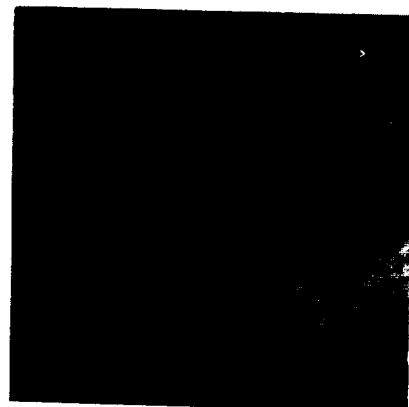
AS8-12-2196



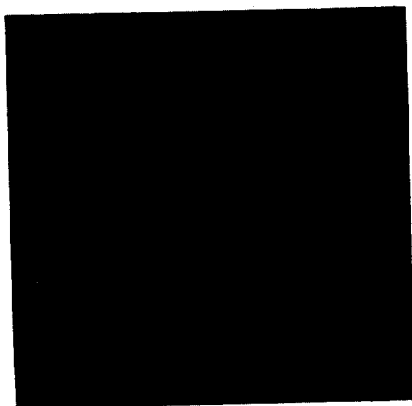
AS8-12-2197



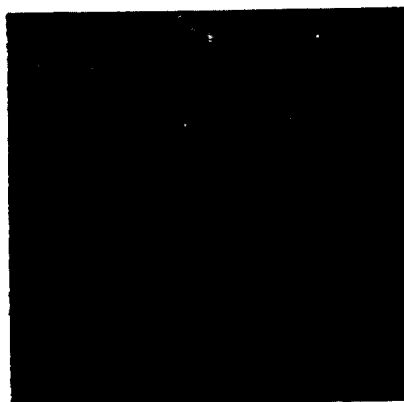
AS8-12-2198



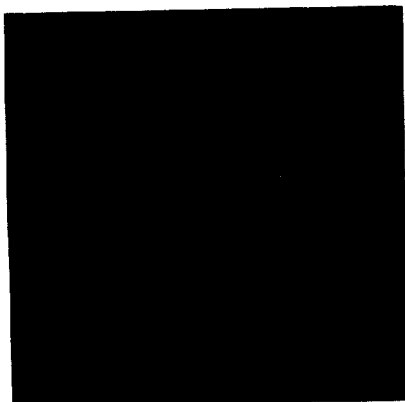
AS8-12-2199



AS8-12-2200



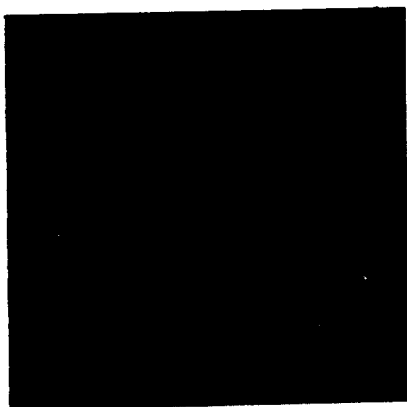
AS8-12-2201



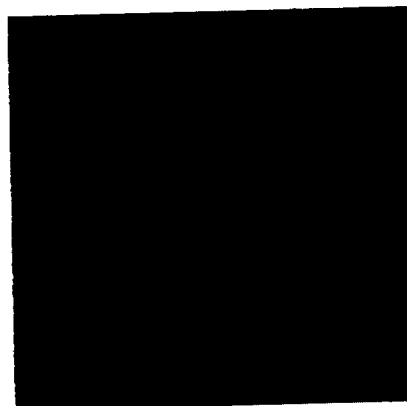
AS8-12-2202



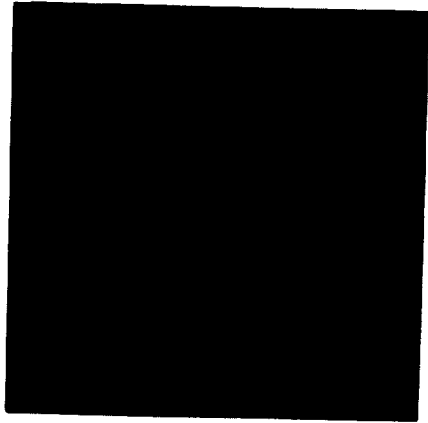
AS8-12-2203



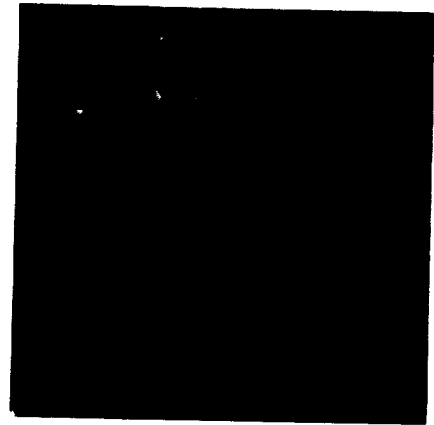
AS8-12-2204



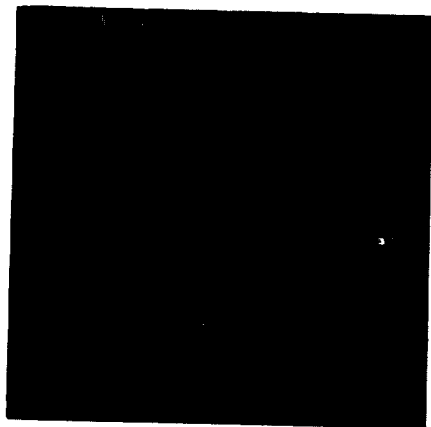
AS8-12-2205



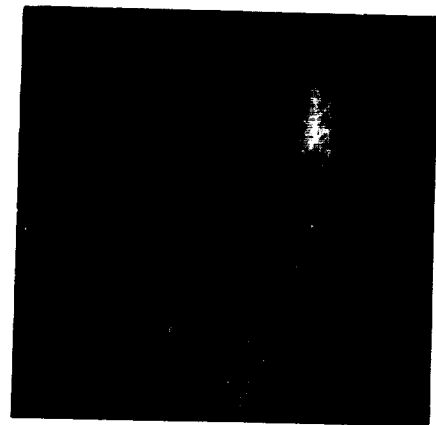
AS8-12-2206



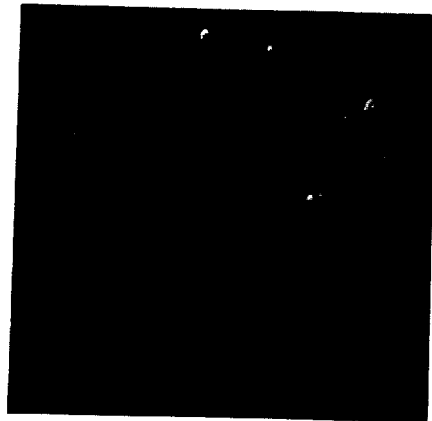
AS8-12-2207



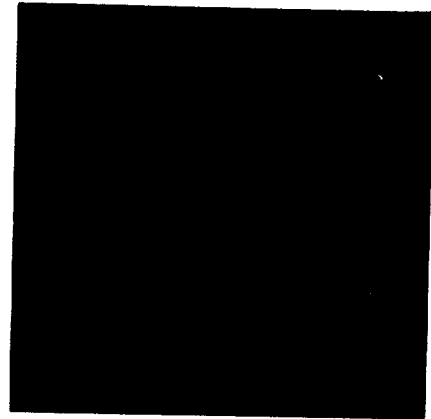
AS8-12-2208



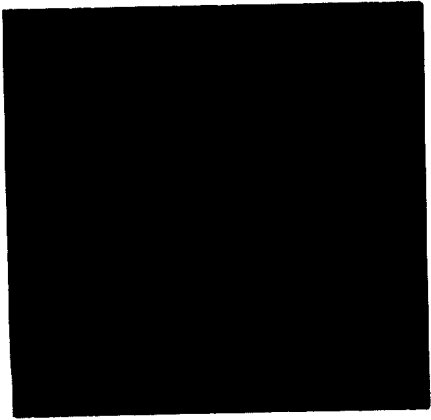
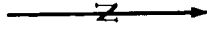
AS8-12-2209



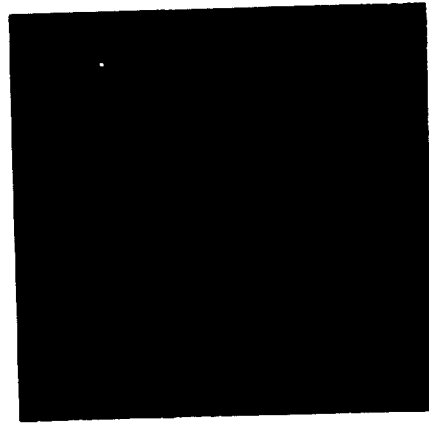
AS8-12-2210



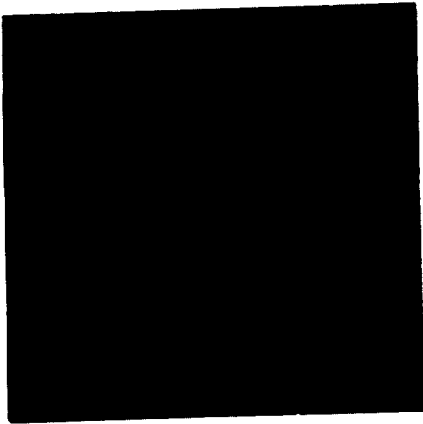
AS8-12-2211



AS8-12-2212



AS8-12-2213



AS8-12-2214



MAGAZINE

E

AS8-13-2215 to 2382



AS8-13-2215



AS8-13-2216



AS8-13-2217



AS8-13-2218



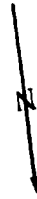
AS8-13-2219



AS8-13-2220



AS8-13-2221



AS8-13-2222



AS8-13-2223



AS8-13-2224



AS8-13-2225



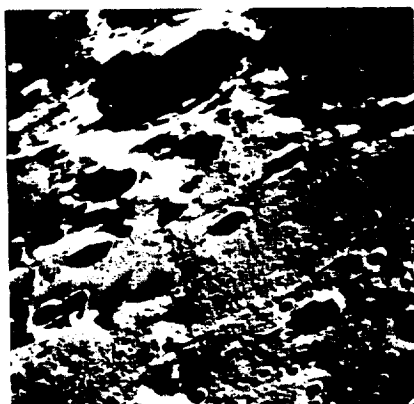
AS8-13-2226



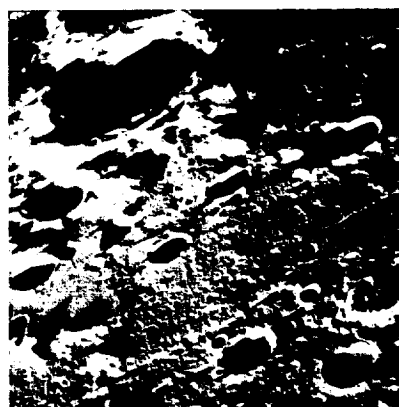
AS8-13-2227



AS8-13-2228



AS8-13-2229



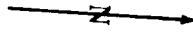
AS8-13-2230



AS8-13-2231



AS8-13-2232



AS8-13-2233



AS8-13-2234



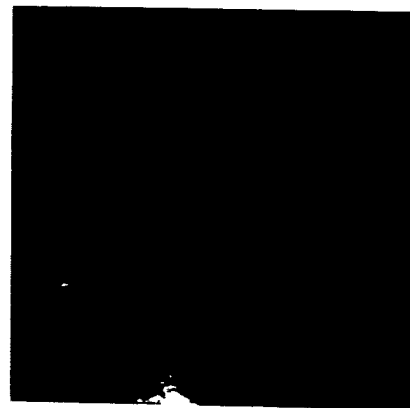
AS8-13-2235



AS8-13-2236



AS8-13-2237



AS8-13-2238



AS8-13-2239



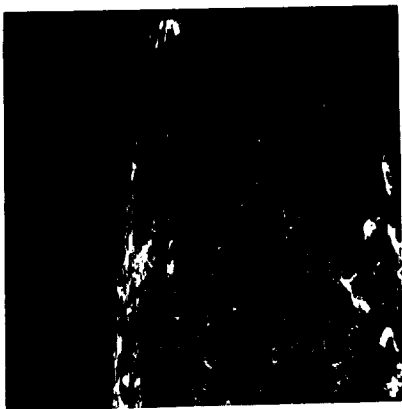
AS8-13-2240



AS8-13-2241



AS8-13-2242



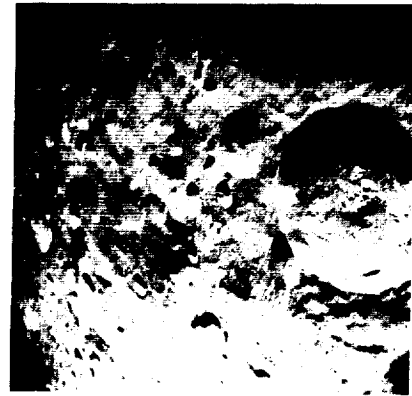
AS8-13-2243



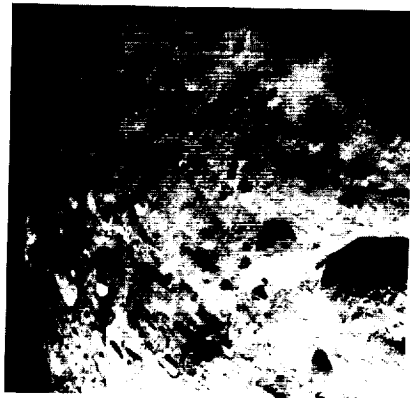
AS8-13-2244



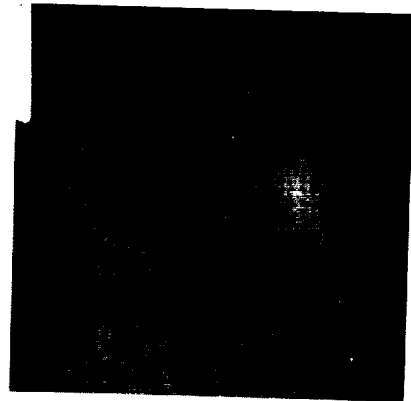
AS8-13-2245



AS8-13-2246



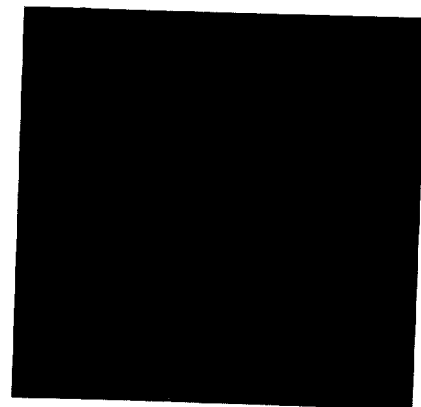
AS8-13-2247



AS8-13-2248



AS8-13-2249



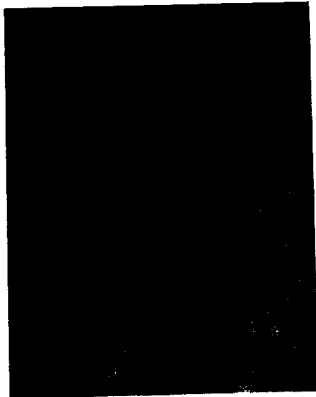
AS8-13-2250



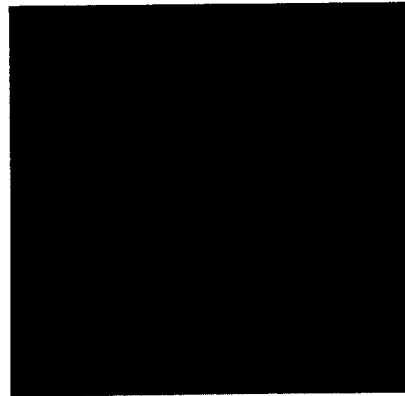
AS8-13-2251



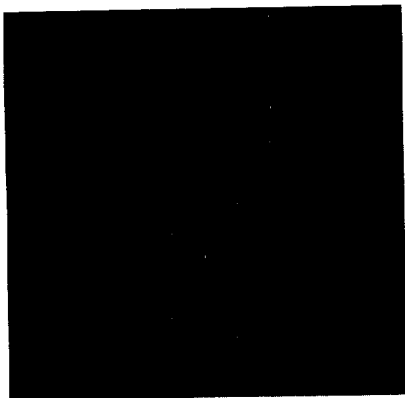
AS8-13-2252



AS8-13-2253



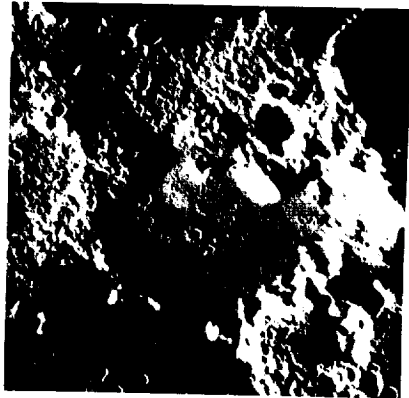
AS8-13-2254



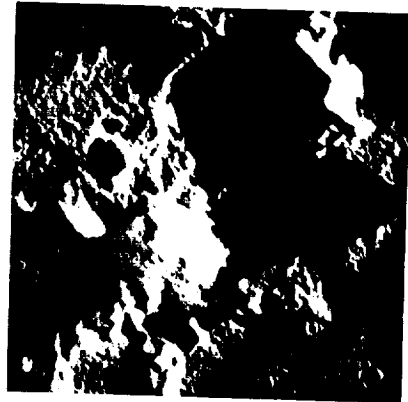
AS8-13-2255



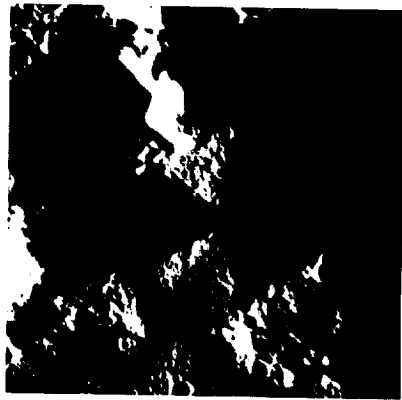
AS8-13-2256



AS8-13-2257



AS8-13-2258



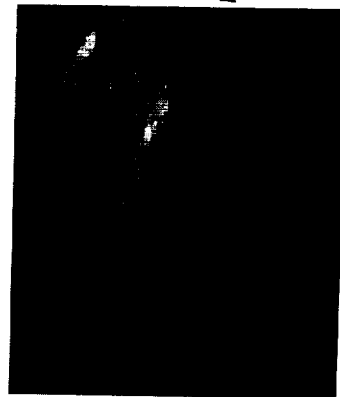
AS8-13-2259



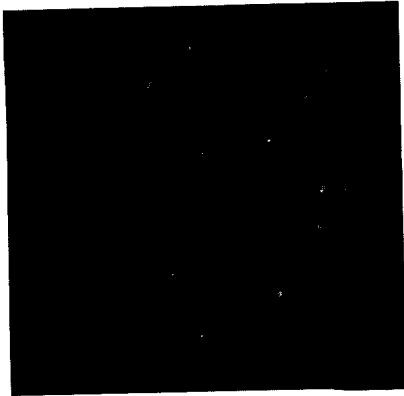
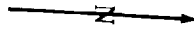
AS8-13-2260



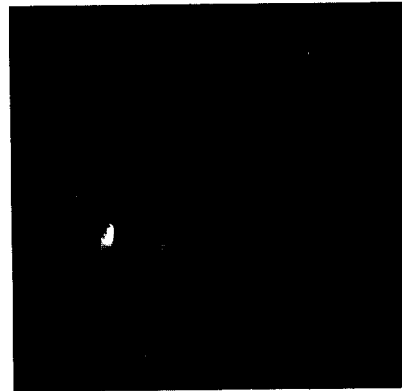
AS8-13-2261



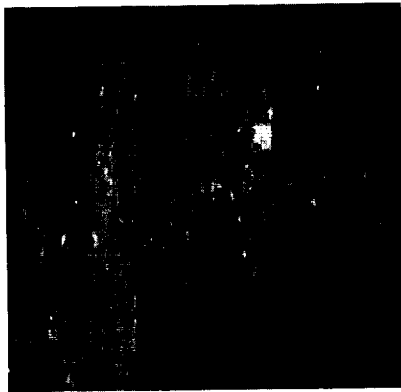
AS8-13-2262



AS8-13-2263



AS8-13-2264



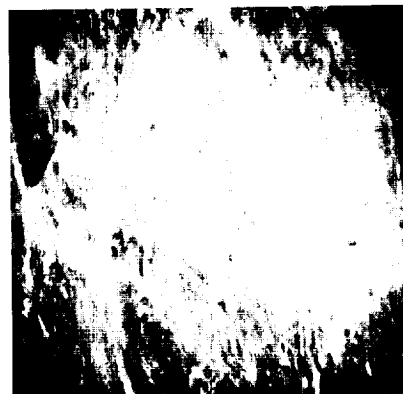
AS8-13-2265



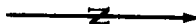
AS8-13-2266



AS8-13-2267



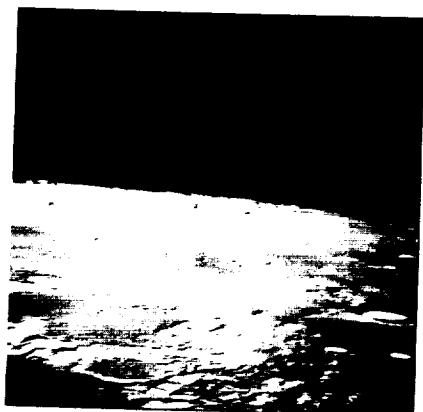
AS8-13-2268



AS8-13-2269



AS8-13-2270



AS8-13-2271



AS8-13-2272



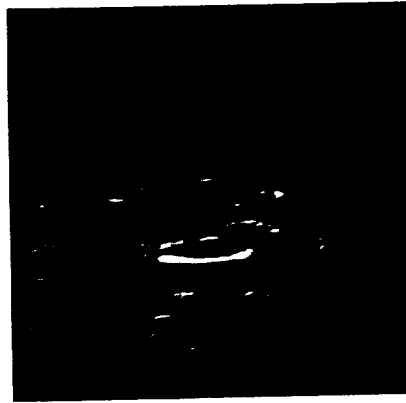
AS8-13-2273



AS8-13-2274



AS8-13-2275



AS8-13-2276



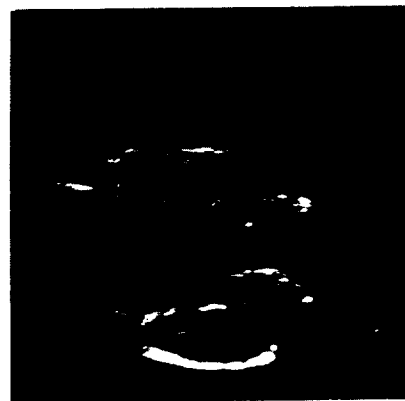
AS8-13-2277



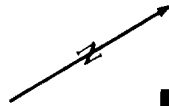
AS 8-13-2278



AS8-13-2279



AS8-13-2280



AS8-13-2281



AS8-13-2282



AS8-13-2283



AS8-13-2284



AS8-13-2285



AS8-13-2286



AS8-13-2287



AS8-13-2288



AS8-13-2289



AS8-13-2290



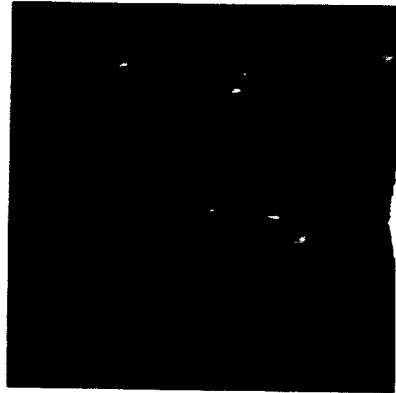
AS8-13-2291



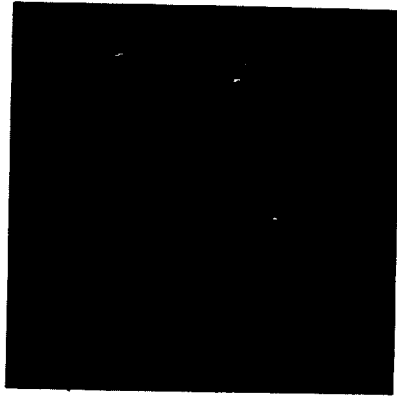
AS8-13-2292



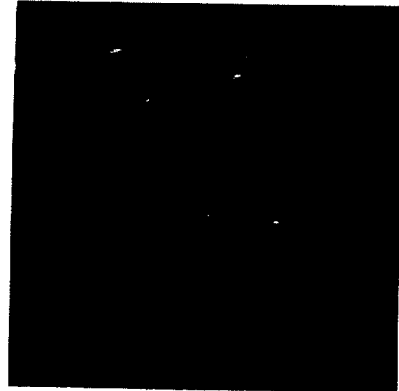
AS8-13-2293



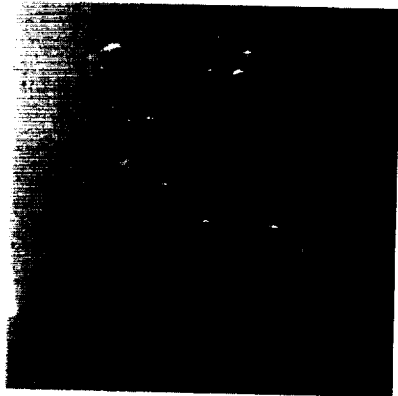
AS8-13-2294



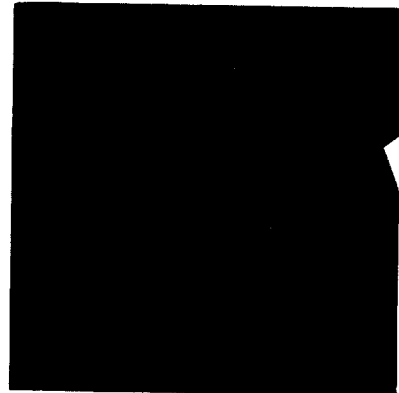
AS8-13-2295



AS8-13-2296



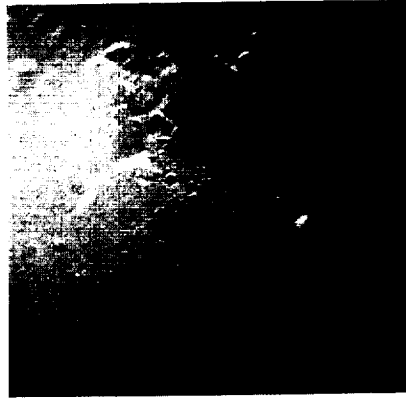
AS8-13-2297



AS8-13-2298



AS8-13-2299



AS8-13-2300



AS8-13-2301



AS8-13-2302



AS8-13-2303



AS8-13-2304



AS8-13-2305



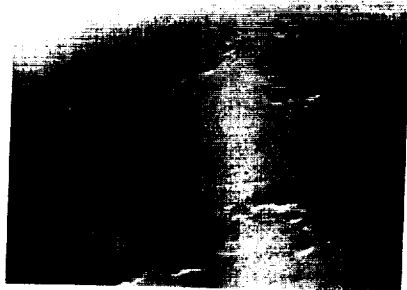
AS8-13-2306



AS8-13-2307



AS8-13-2308



AS8-13-2309



AS8-13-2310





AS8-13-2311



AS8-13-2312



AS8-13-2313



AS8-13-2314



AS8-13-2315



AS8-13-2316

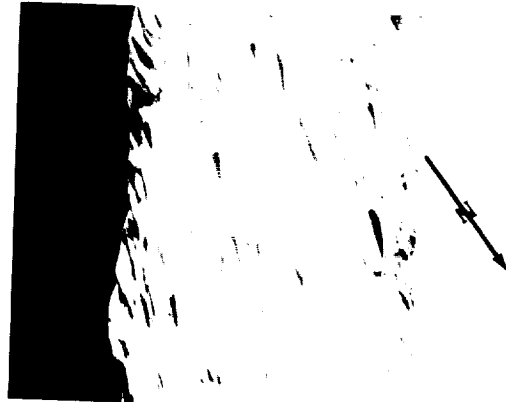
ANALYSIS OF APOLLO 8 PHOTOGRAPHY AND VISUAL OBSERVATIONS



AS8-13-2317



AS8-13-2318



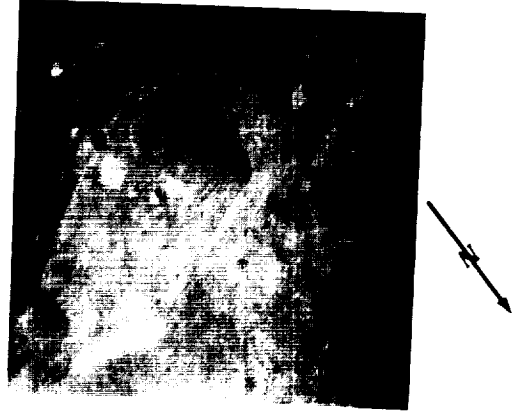
AS8-13-2319



AS8-13-2320



AS8-13-2321



AS8-13-2322



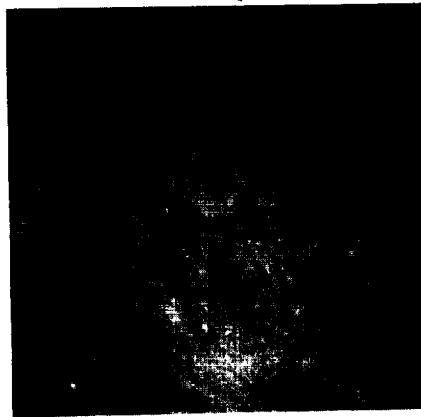
AS8-13-2323



AS8-13-2324



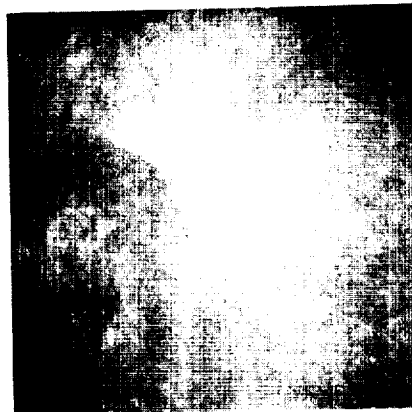
AS8-13-2325



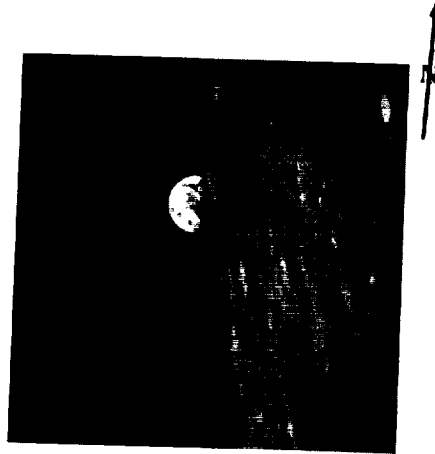
AS8-13-2326



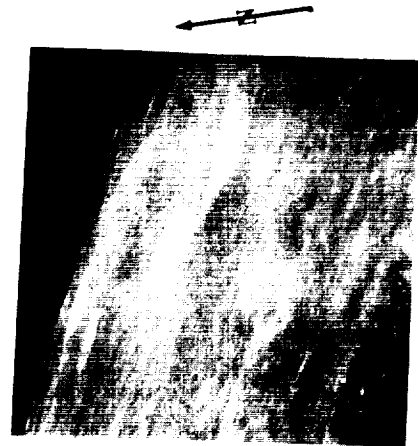
AS8-13-2327



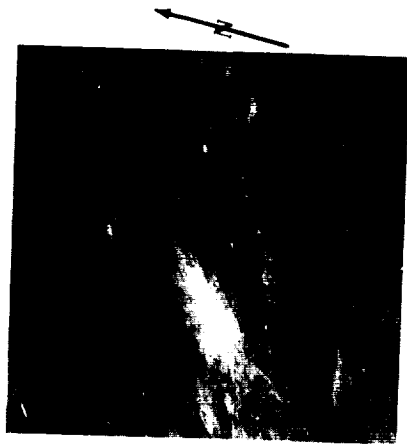
AS8-13-2328



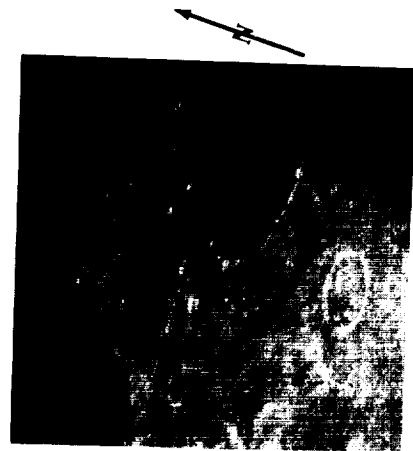
AS8-13-2329



AS8-13-2330



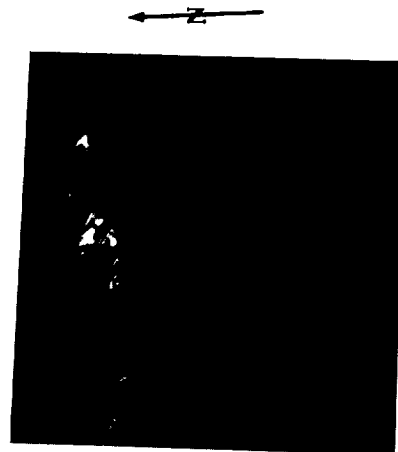
AS8-13-2331



AS8-13-2332



AS8-13-2333



AS8-13-2334



AS8-13-2335



AS8-13-2336



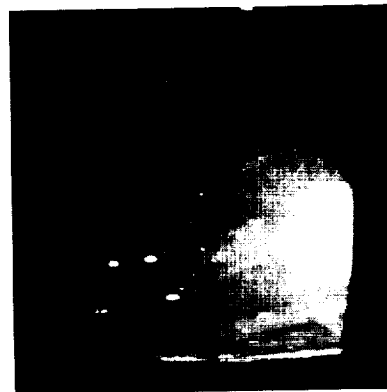
AS8-13-2337



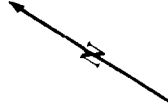
AS8-13-2338



AS8-13-2339



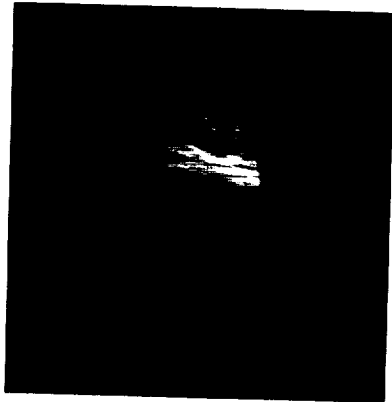
AS8-13-2340



AS8-13-2341



AS8-13-2342



AS8-13-2343



AS8-13-2344



AS8-13-2345



AS8-13-2346



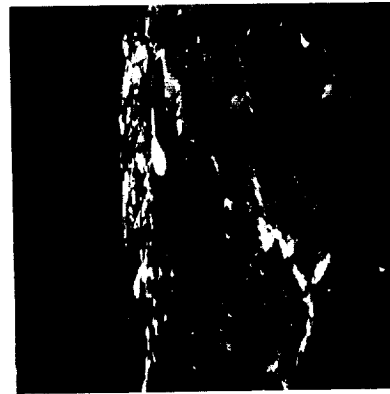
AS8-13-2347



AS8-13-2348



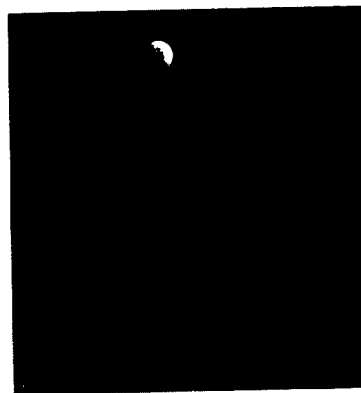
AS8-13-2349



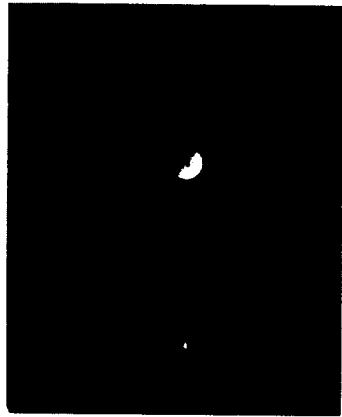
AS8-13-2350



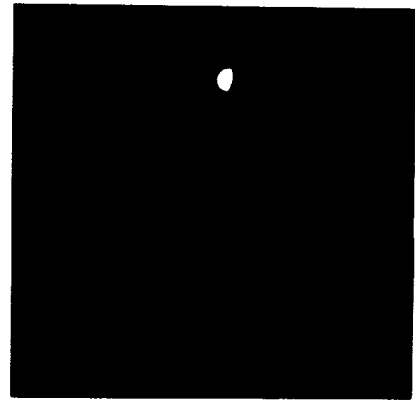
AS8-13-2351



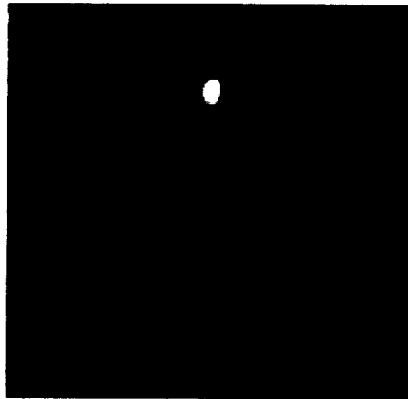
AS8-13-2352



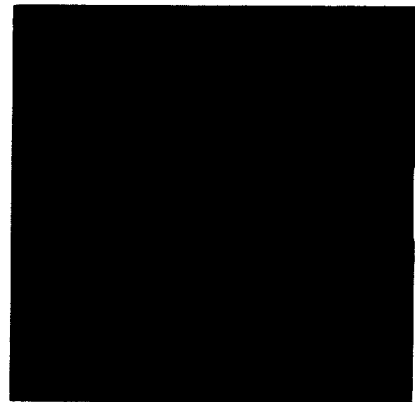
AS8-13-2353



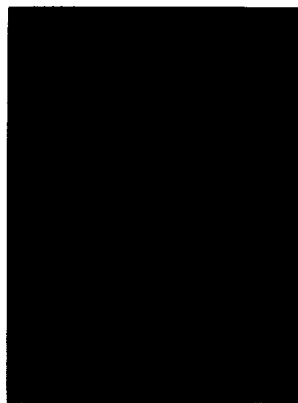
AS8-13-2354



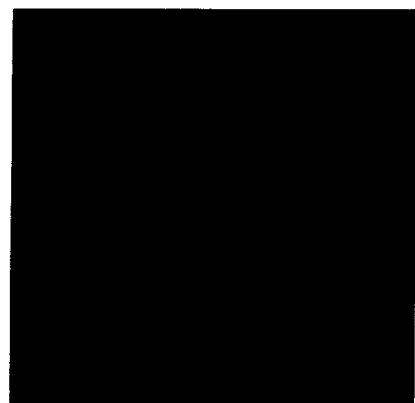
AS8-13-2355



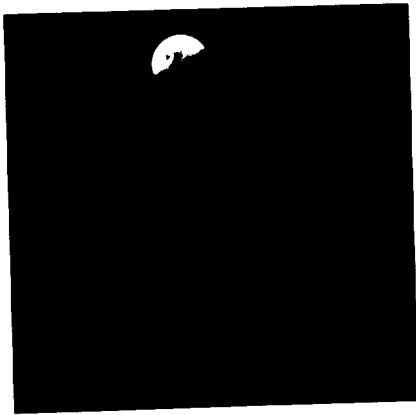
AS8-13-2356



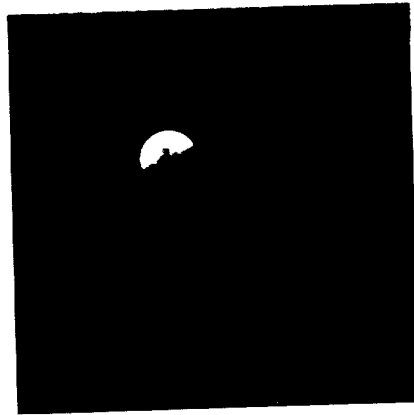
AS8-13-2357



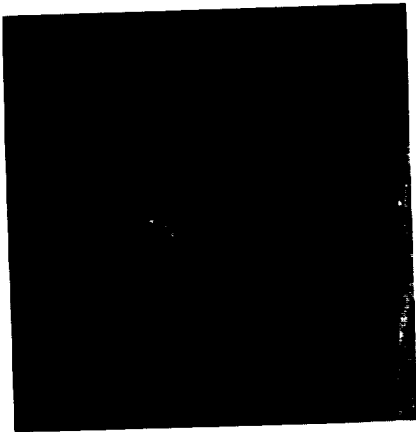
AS8-13-2358



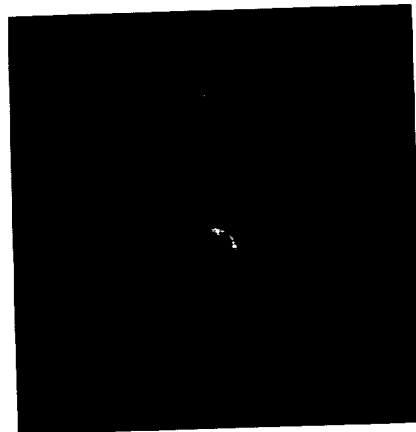
AS8-13-2359



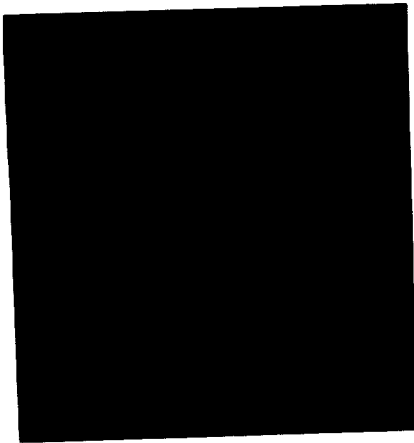
AS8-13-2360



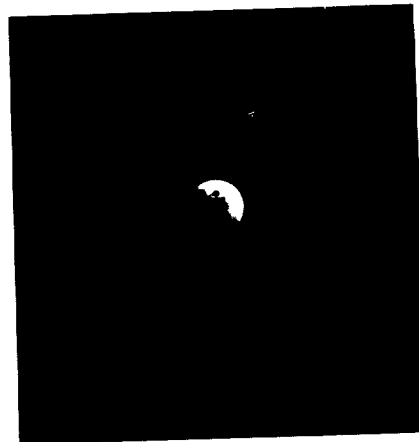
AS8-13-2361



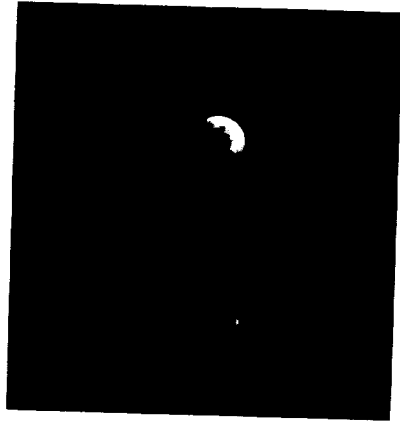
AS 8-13-2362



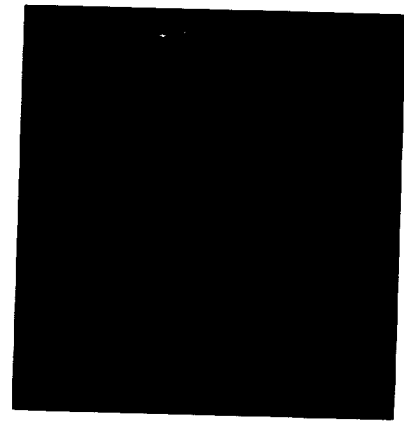
AS8-13-2363



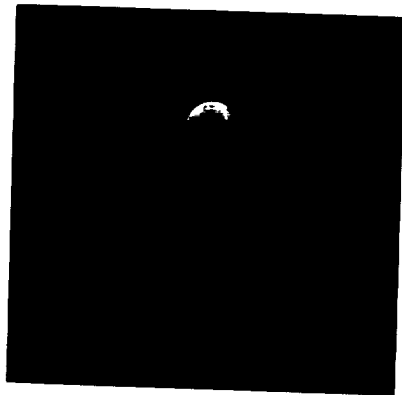
AS8-13-2364



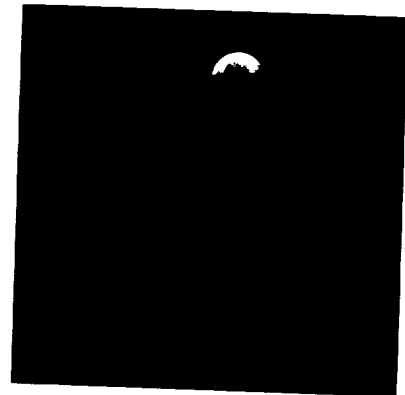
AS8-13-2365



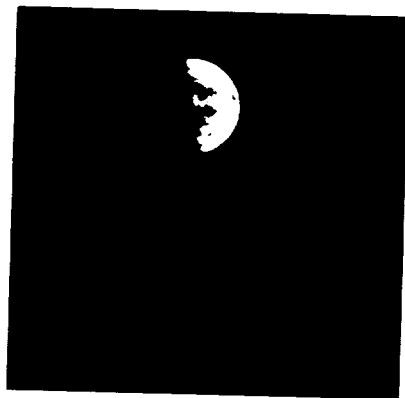
AS8-13-2366



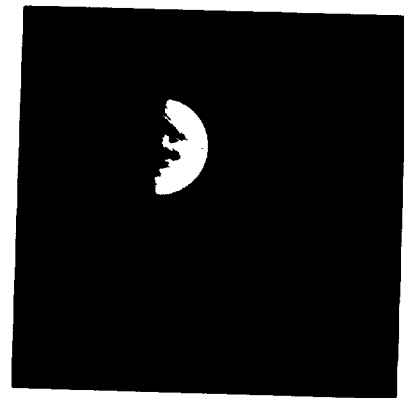
AS8-13-2367



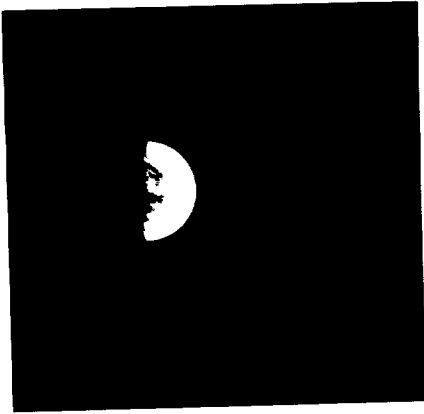
AS8-13-2368



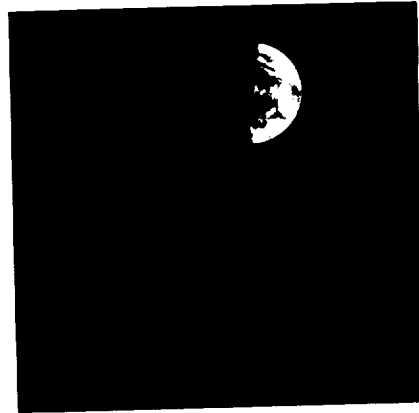
AS8-13-2369



AS8-13-2370



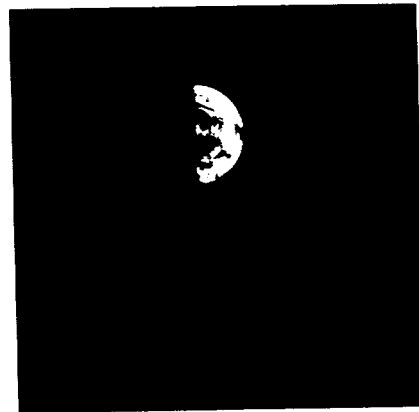
AS8-13-2371



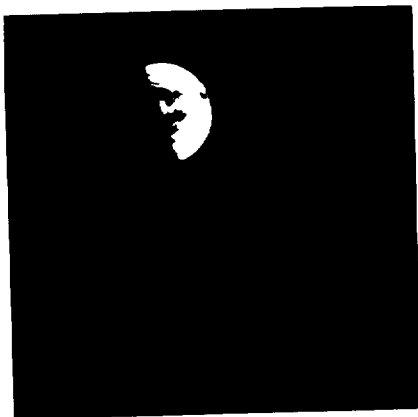
AS8-13-2372



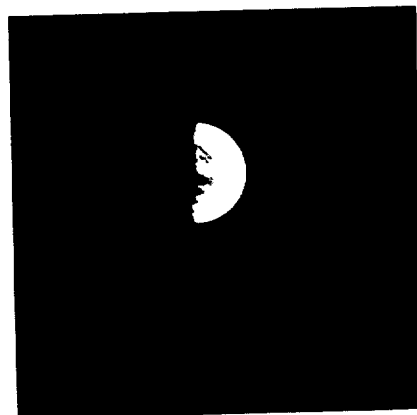
AS8-13-2373



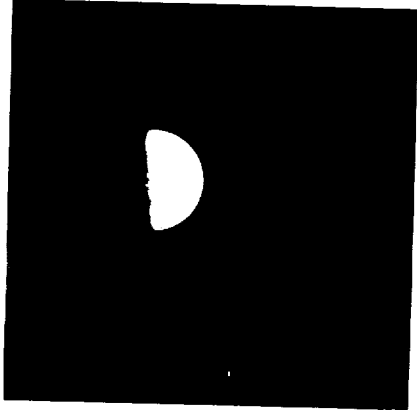
AS8-13-2374



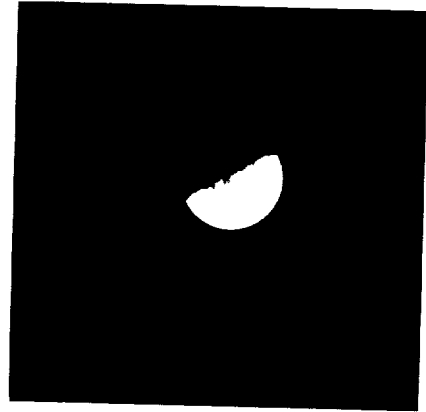
AS8-13-2375



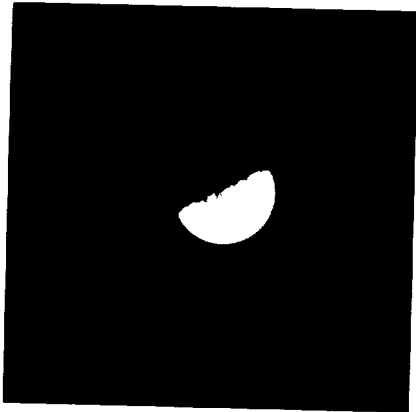
AS8-13-2376



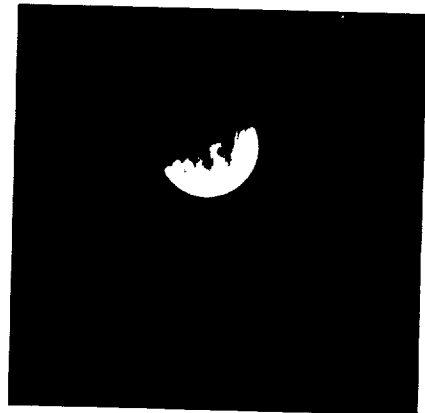
AS8-13-2377



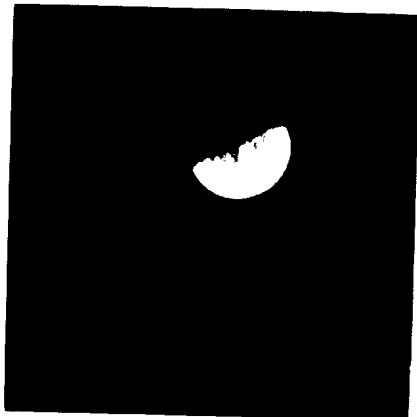
AS8-13-2378



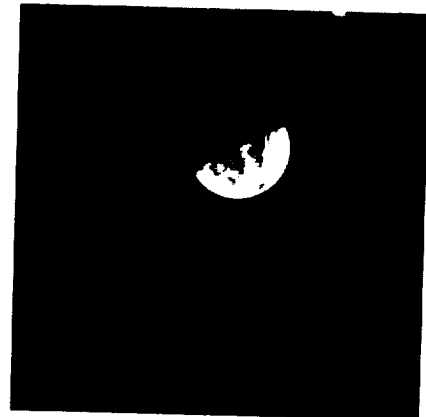
AS8-13-2379



AS8-13-2380



AS8-13-2381

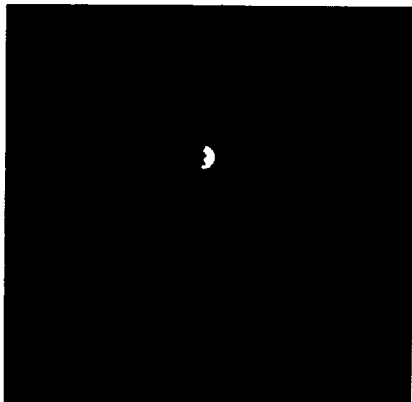


AS8-13-2382

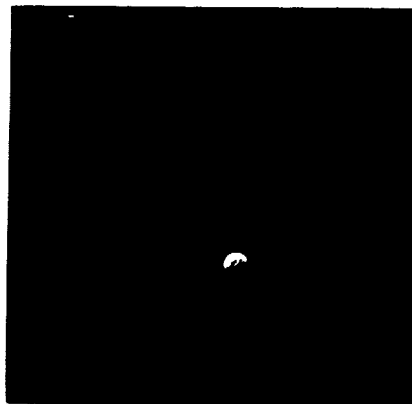
MAGAZINE

F

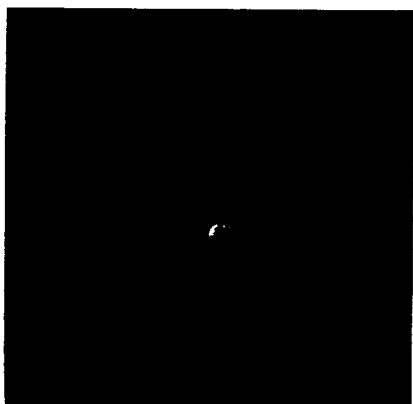
AS8-15-2535 to 2580



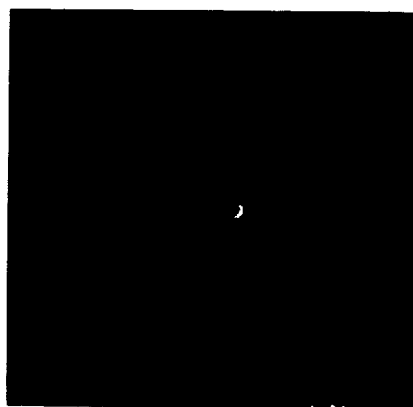
AS8-15-2541



AS8-15-2542



AS8-15-2543



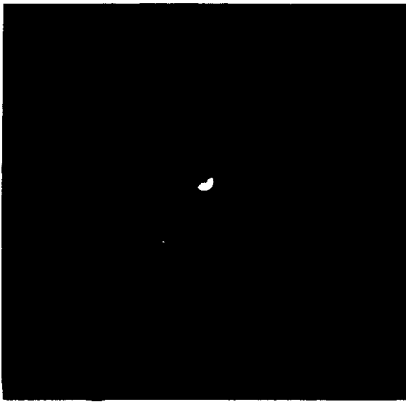
AS8-15-2544



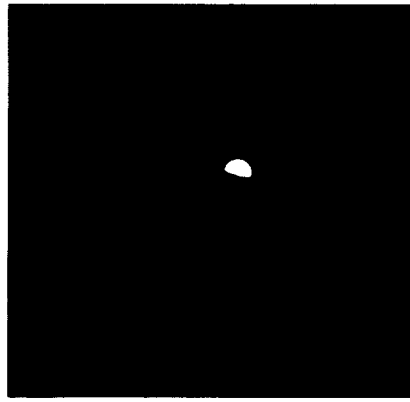
AS8-15-2545



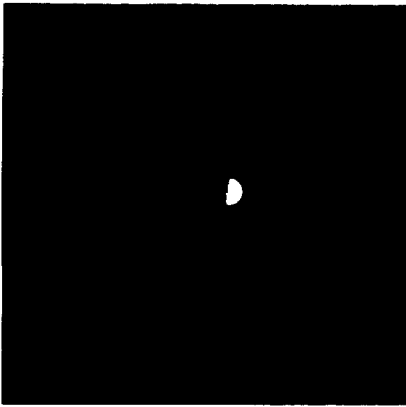
AS8-15-2546



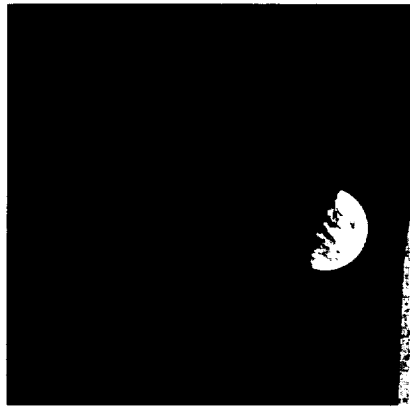
AS8-15-2547



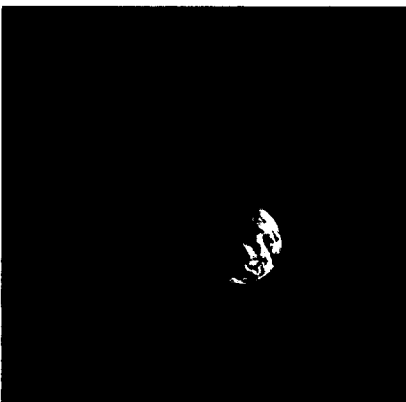
AS8-15-2548



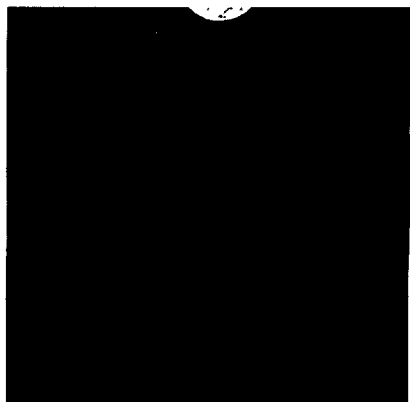
AS8-15-2549



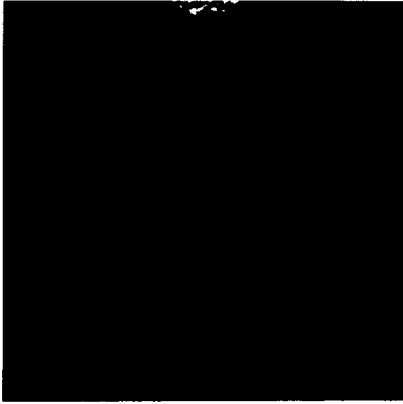
AS8-15-2550



AS8-15-2551



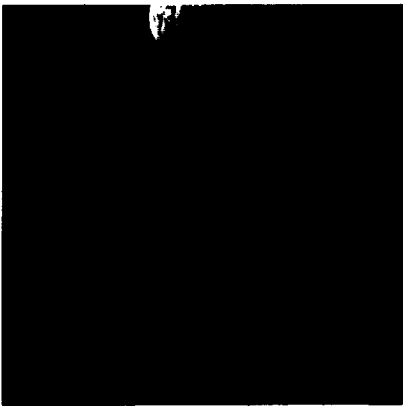
AS8-15-2552



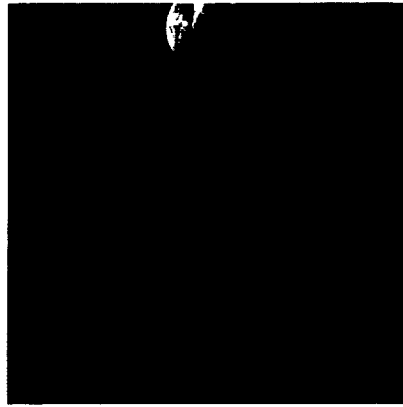
AS8-15-2553



AS8-15-2554



AS8-15-2555



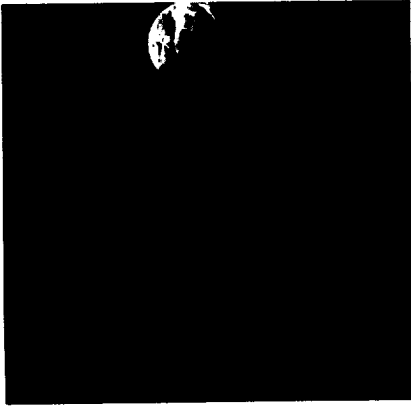
AS8-15-2556



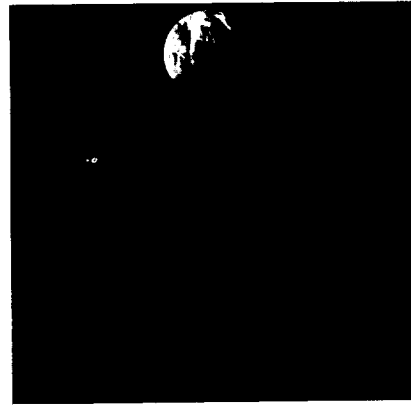
AS8-15-2557



AS8-15-2558



AS8-15-2559



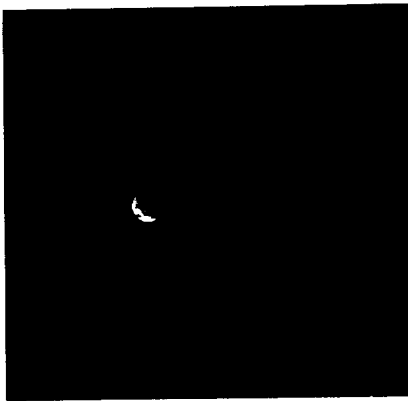
AS8-15-2560



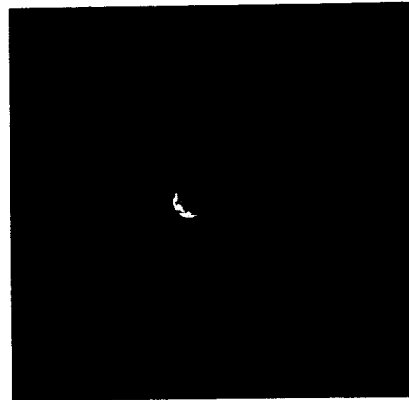
AS8-15-2561



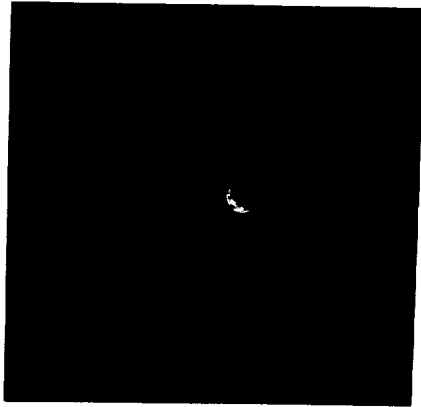
AS8-15-2562



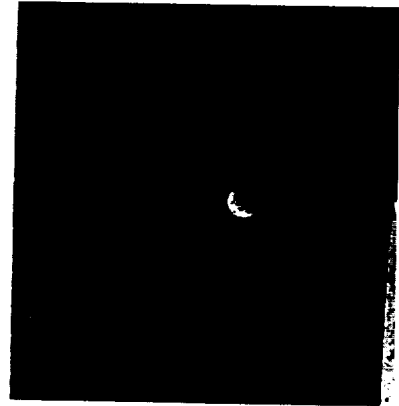
AS8-15-2563



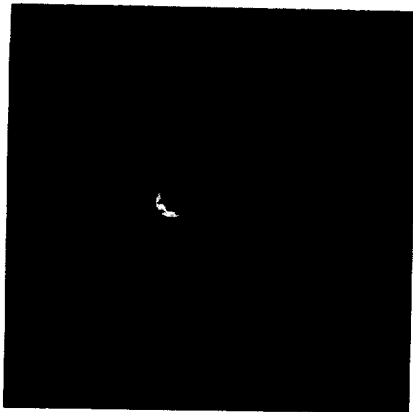
AS8-15-2564



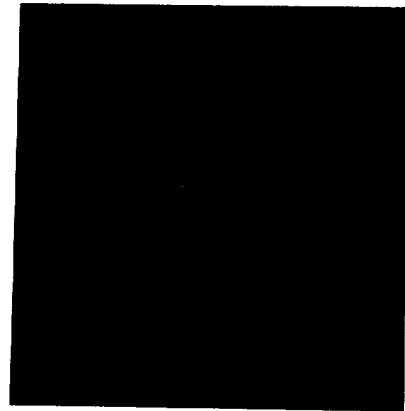
AS8-15-2565



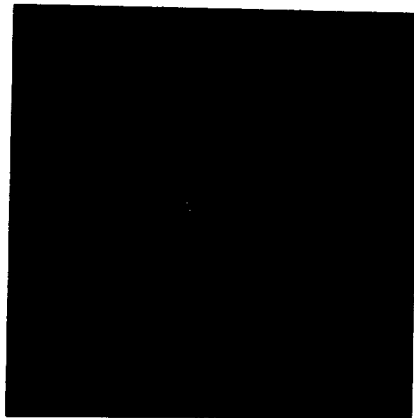
AS8-15-2566



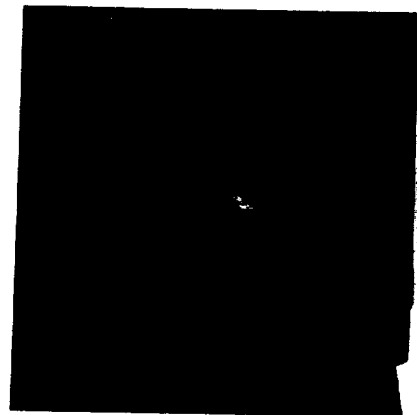
AS8-15-2567



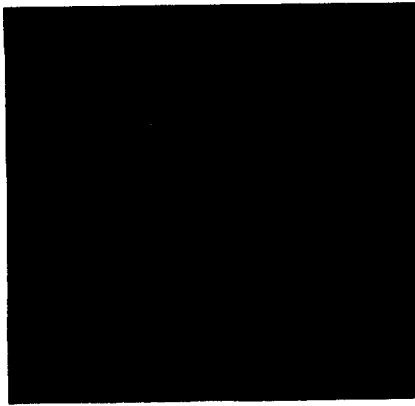
AS8-15-2568



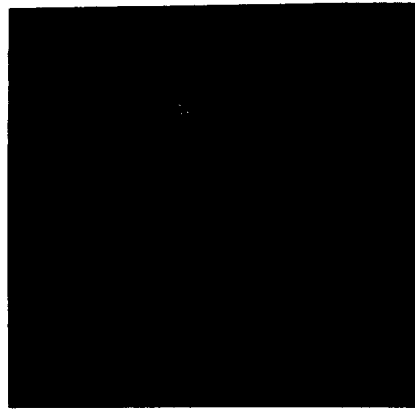
AS8-15-2569



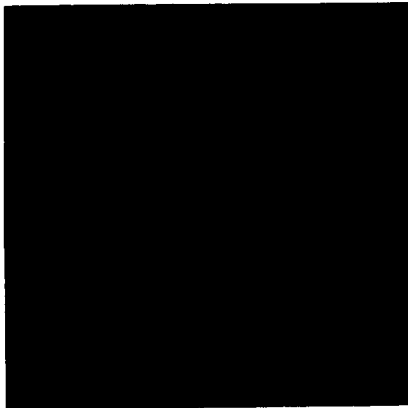
AS8-15-2570



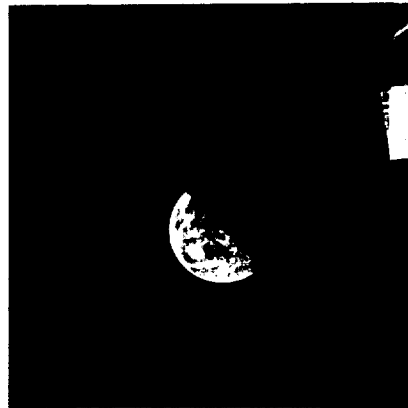
AS8-15-2571



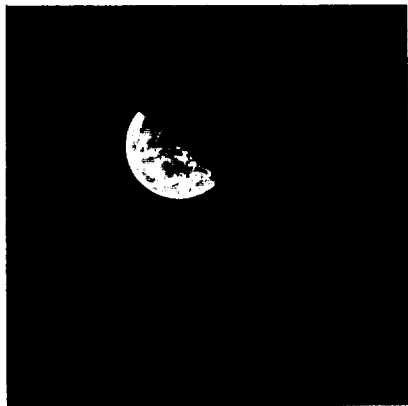
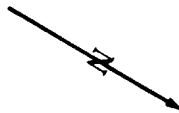
AS8-15-2572



AS8-15-2573



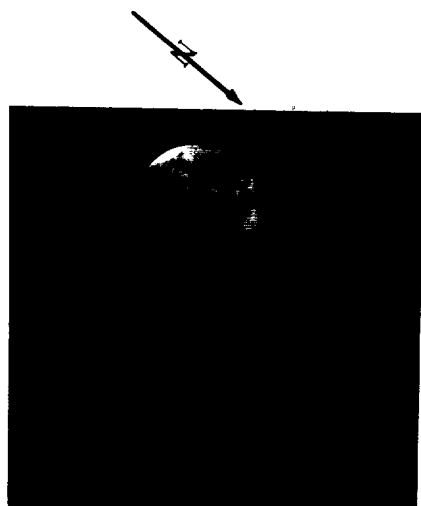
AS8-15-2574



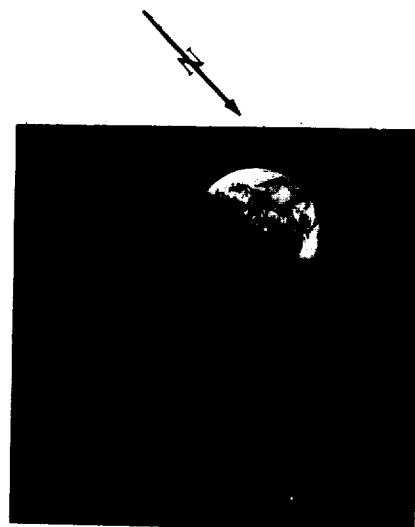
AS8-15-2575



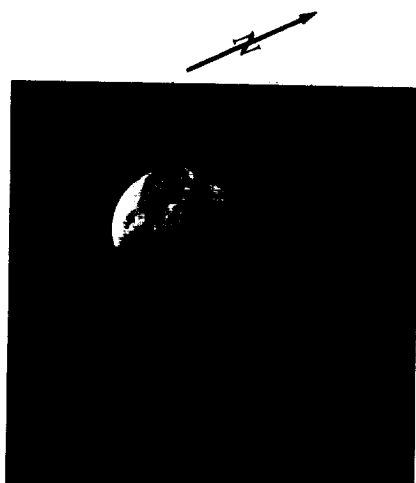
AS8-15-2576



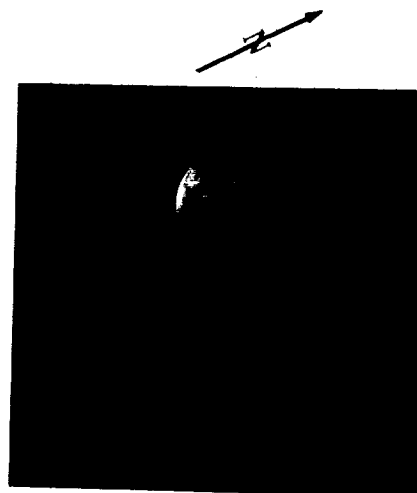
AS8-15-2577



AS8-15-2578



AS8-15-2579

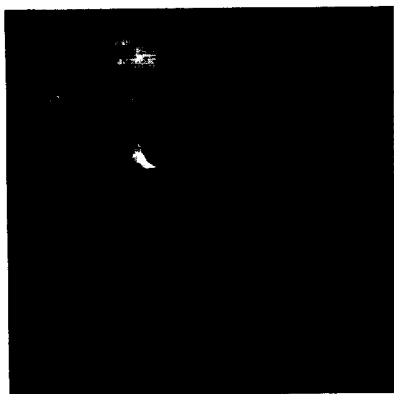


AS8-15-2580

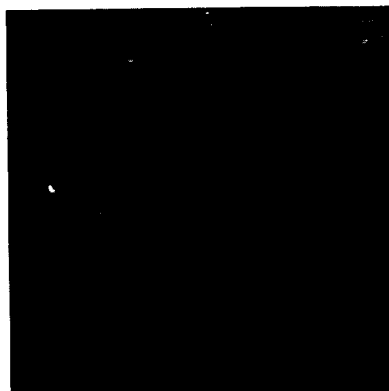
MAGAZINE

G

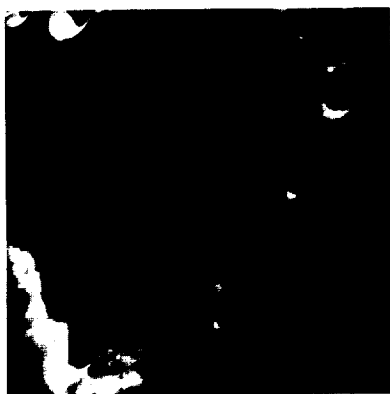
AS8-18-2828 to 2908



AS8-18-2828



AS8-18-2829



AS8-18-2830



AS8-18-2831

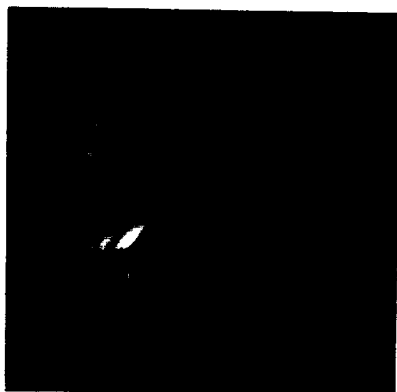


AS8-18-2832



AS8-18-2833

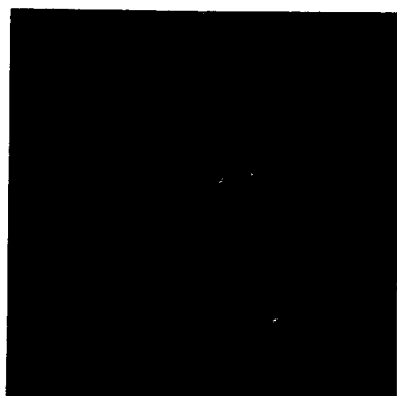
(Available in color.)



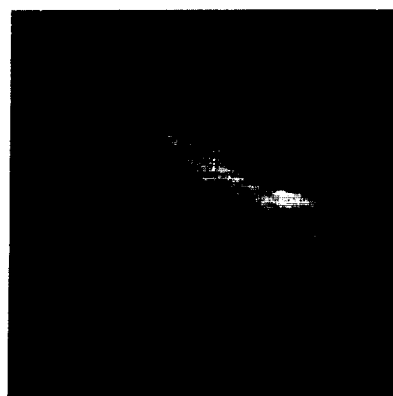
AS8-18-2834



AS8-18-2835



AS8-18-2836



AS8-18-2837



AS8-18-2838

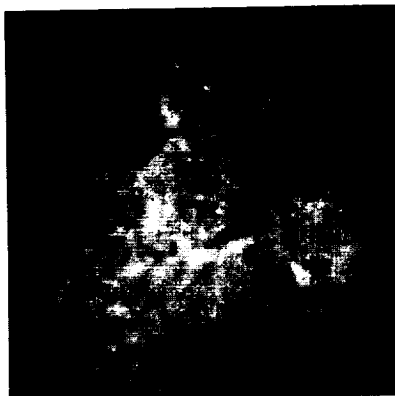


AS8-18-2839

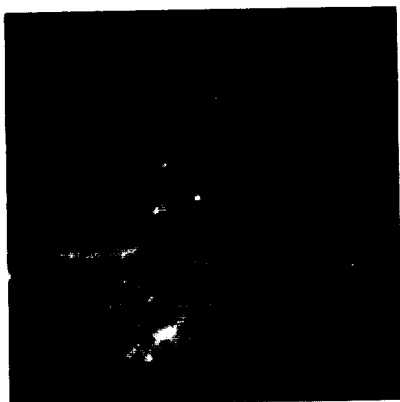
(Available in color.)



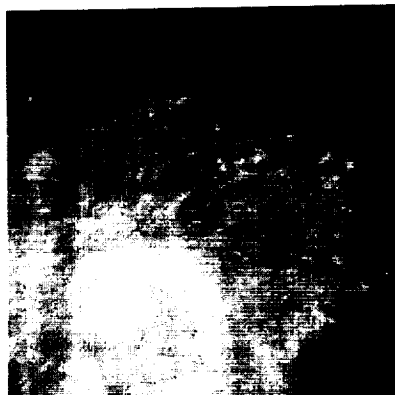
AS8-18-2840



AS8-18-2841



AS8-18-2842



AS8-18-2843

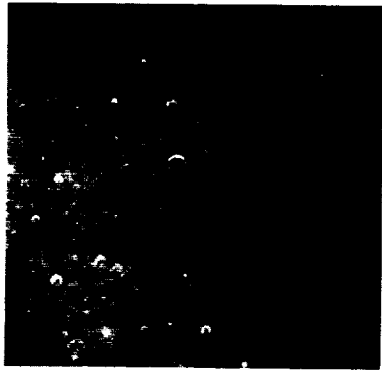


AS8-18-2844

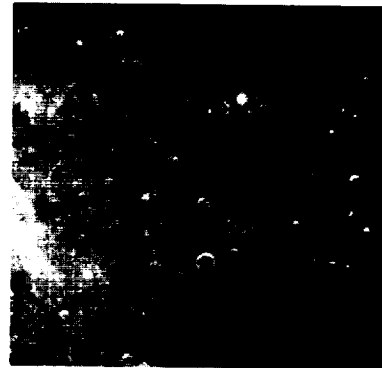


AS8-18-2845

(Available in color.)



AS8-18-2846



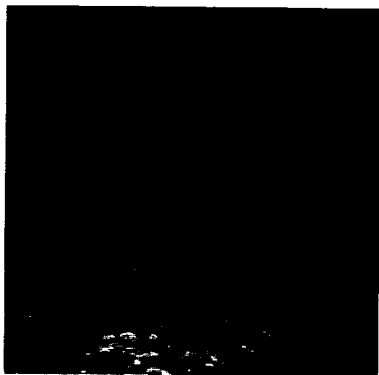
AS8-18-2847



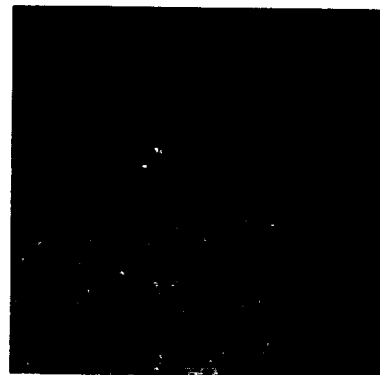
AS8-18-2848



AS8-18-2849

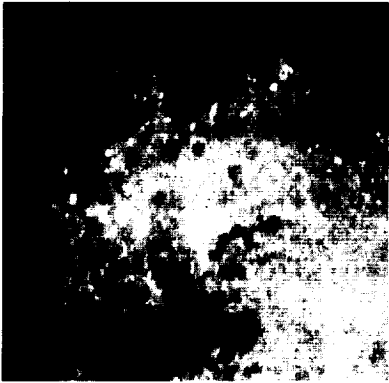


AS8-18-2850

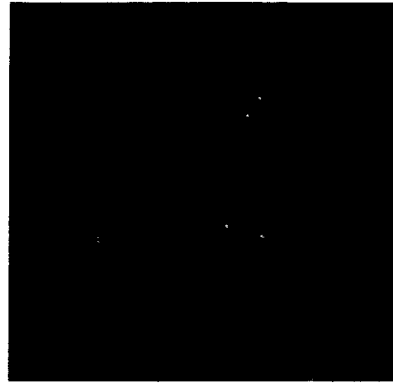


AS8-18-2851

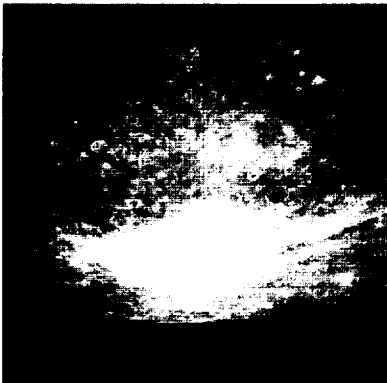
(Available in color.)



AS8-18-2852



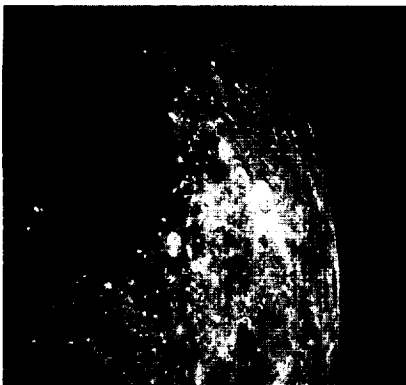
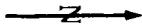
AS8-18-2853



AS8-18-2854



AS8-18-2855

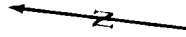


AS8-18-2856

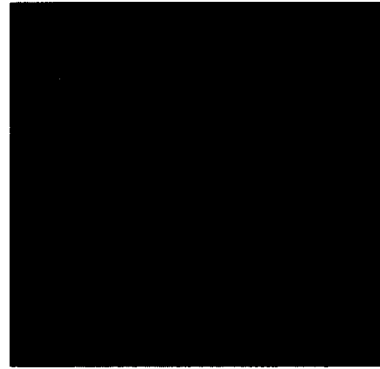


AS8-18-2857

(Available in color.)



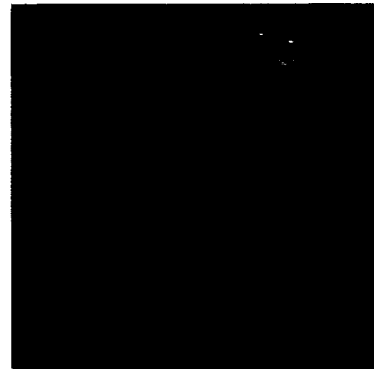
AS8-18-2858



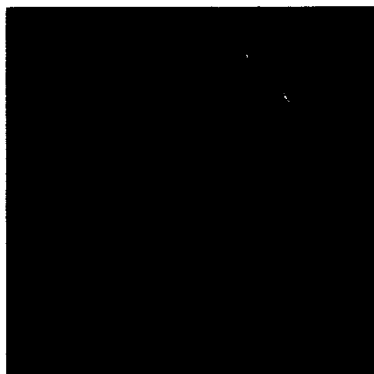
AS8-18-2859



AS8-18-2860



AS8-18-2861

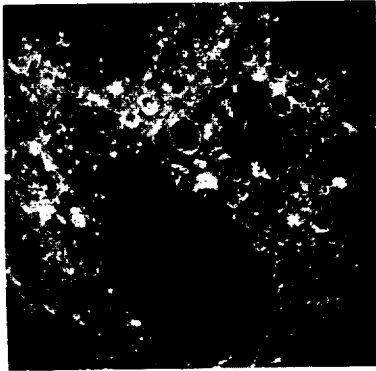


AS8-18-2862

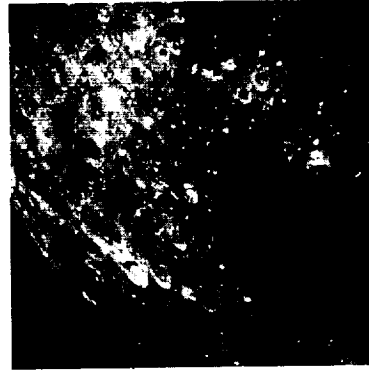


AS8-18-2863

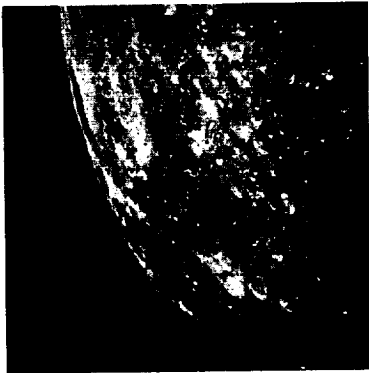
(Available in color.)



AS8-18-2864



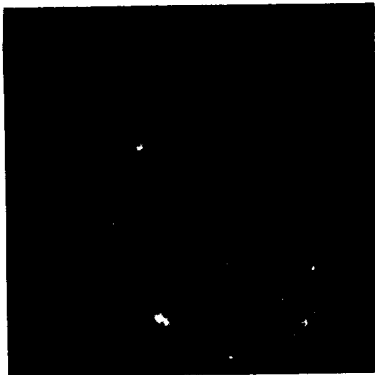
AS8-18-2865



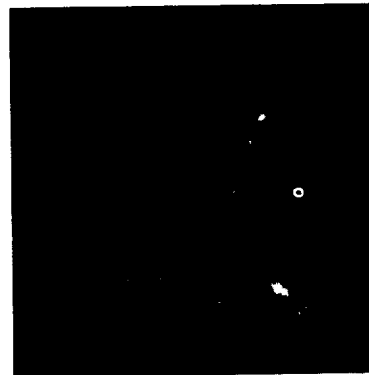
AS8-18-2866



AS8-18-2867

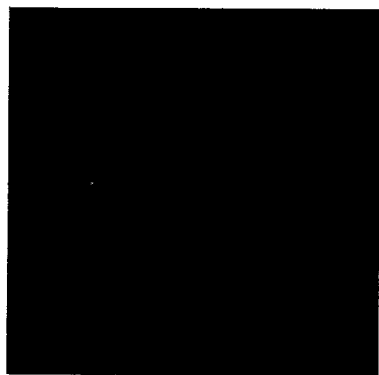


AS8-18-2868

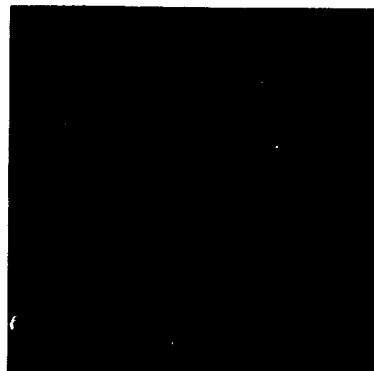


AS8-18-2869

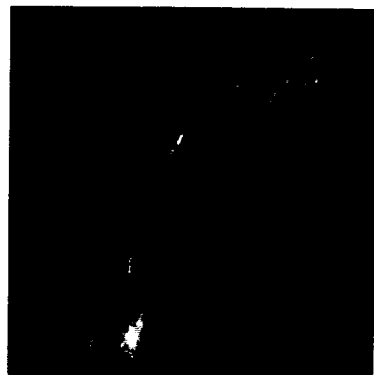
(Available in color.)



AS8-18-2870



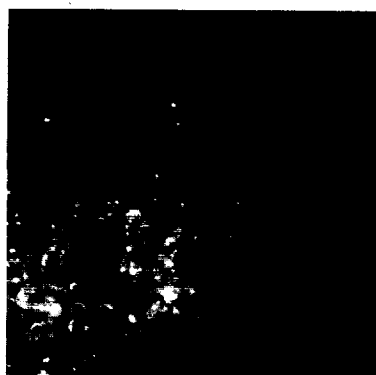
AS8-18-2871



AS8-18-2872



AS8-18-2873



AS8-18-2874



AS8-18-2875

(Available in color.)



AS8-18-2876



AS8-18-2877



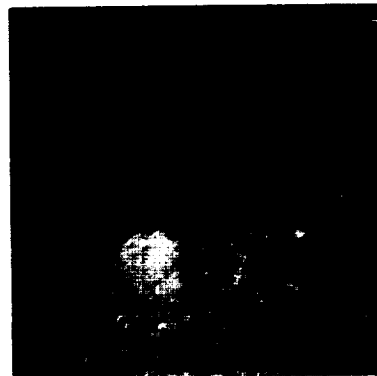
AS8-18-2878



AS8-18-2879

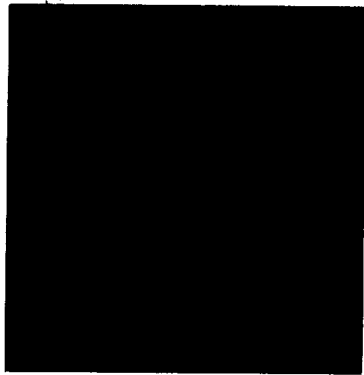


AS8-18-2880

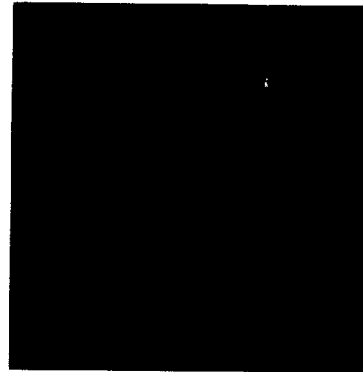


AS8-18-2881

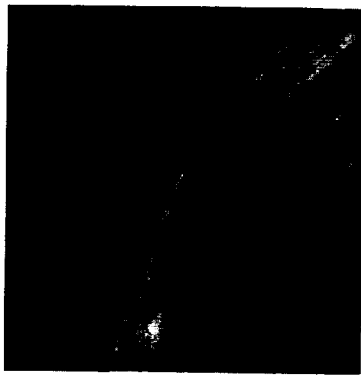
(Available in color.)



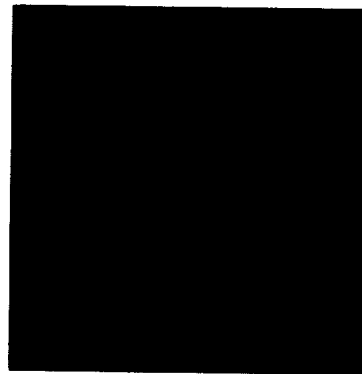
AS8-18-2882



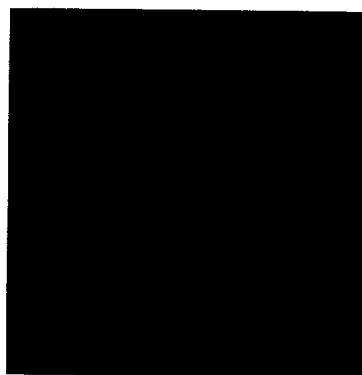
AS8-18-2883



AS8-18-2884



AS8-18-2885



AS8-18-2886



AS8-18-2887

(Available in color.)



AS8-18-2888



AS8-18-2889



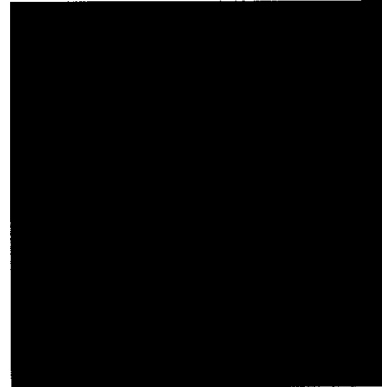
AS8-18-2890



AS8-18-2891

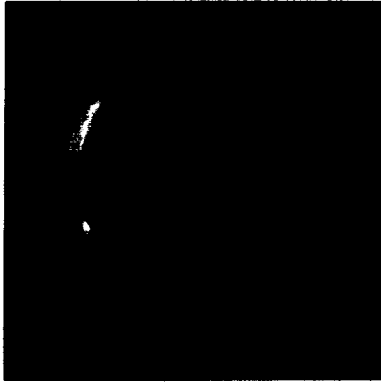


AS8-18-2892

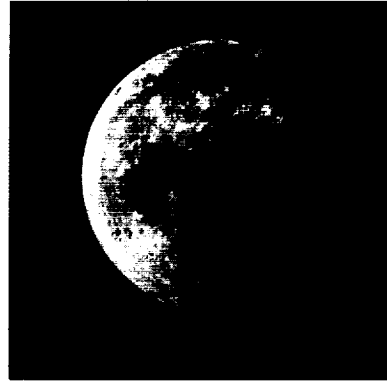


AS8-18-2893

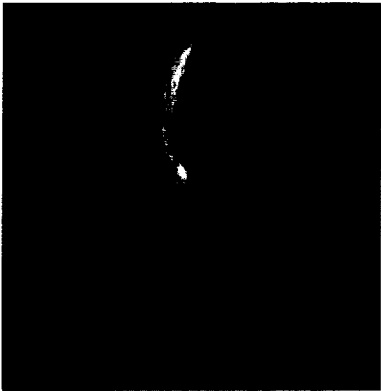
(Available in color.)



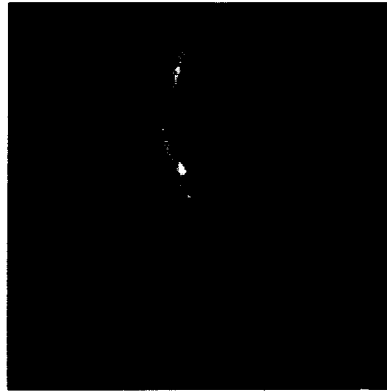
AS8-18-2894



AS8-18-2895



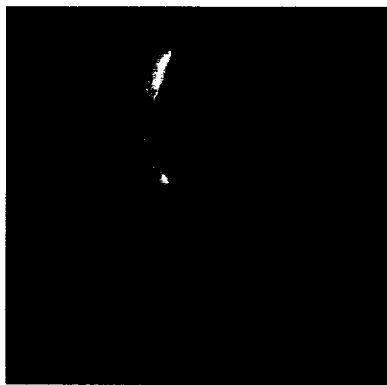
AS8-18-2896



AS8-18-2897

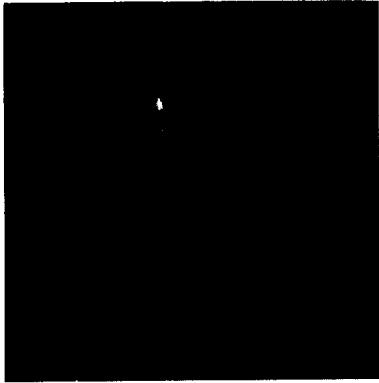


AS8-18-2898

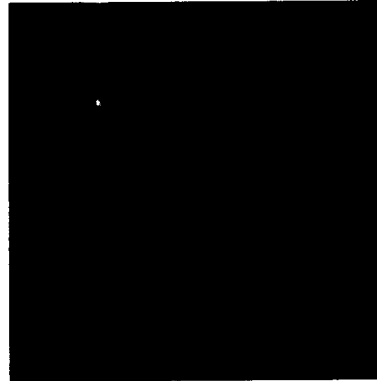


AS8-18-2899

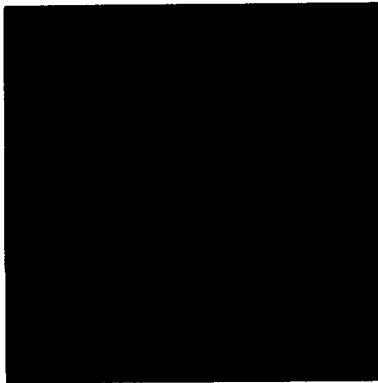
(Available in color.)



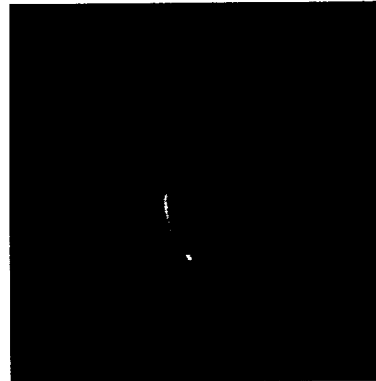
AS8-18-2900



AS8-18-2901



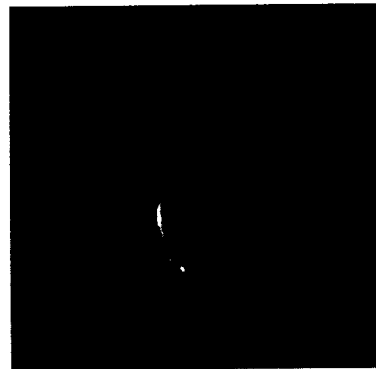
AS8-18-2902



AS8-18-2903

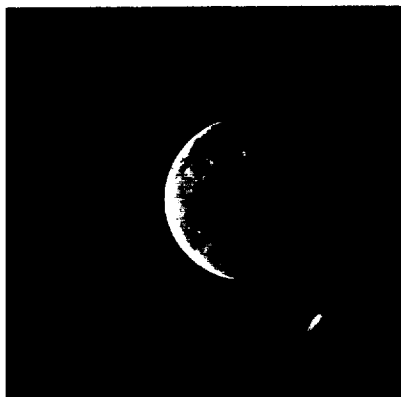


AS8-18-2904



AS8-18-2905

(Available in color.)



AS8-18-2906



AS8-18-2907



AS8-18-2908

(Available in color.)

APPENDIX B

Glossary of Terms

- acutance**—Sharpness—a function of the density difference between two areas.
- albedo**—The ratio of reflected to incident light.
- background**—The region immediately around a point being viewed, usually 5° or less (see **surround**).
- chit area**—An area approximately 200 by 200 meters subjected to computer analysis to determine landing suitability.
- earthshine**—Sunlight reflected from the Earth. Earthshine on the Moon is usually much brighter than moonlight on Earth.
- ejecta**—Material ejected from craters during their formation.
- gamma**—The slope or gradient of the relatively straight-line region of the curve which is the plot of density (ordinate axis) versus the logarithm of exposure (abscissa).
- gegenschein or counterglow**—A brightening of the zodiacal light in the antisolar direction. It is presumably due to the backscattering of sunlight by the interplanetary matter found in the plane of the solar system.
- graben**—A linear depressed block bounded on both sides by normal faults.
- groundtrack**—The vertical projection of the spacecraft trajectory on the lunar surface.
- halo**—A bright ring around a feature on the Moon (nimbus). A bright ring around the spacecraft shadow on the Moon (see **heiligschein**).
- heiligschein**—A bright area around the zero-phase (spacecraft shadow) point.
- image motion compensation**—Movement of a camera, or the film within the camera, to prevent blurred images when photographing moving objects or from a moving vehicle.
- intervalometer**—A device to trip the camera shutter at regular intervals.
- landmark**—Any distinctive lunar feature used for on-board navigational sightings.
- limb**—The edge of the Moon as viewed from Earth.
- lunar orbit insertion**—The propulsive maneuver that reduces the spacecraft velocity to lunar orbital velocity.
- Magellanic clouds**—Two large cloudlike phenomena containing star clusters visible in the Milky Way in the Southern Hemisphere.
- mare, pl maria**—Large area on the lunar surface that is darker in color and of lower elevation and generally smoother than surrounding terra. The maria are generally circular in plan.
- mass wasting**—The slow, downslope movement of debris under the influence of gravity.
- Moulton point or Lagrangian point**—One of the five stability points in the solution of the restricted three-body problem. Particles placed at these points with zero velocity will remain indefinitely. In the Earth-Moon system several of these points possibly contain a small cloud of particles.
- nimbus, pl nimbi**—Patch of lighter material around a crater.
- oblique photography**—Photography taken with the camera axis directed between the horizontal and the vertical. Low-oblique photographs are those that do not contain the horizon. Those photographs in which the horizon appears are called high obliques.
- orbit**—The path of a spacecraft or other satellite around a larger body.
- pass**—A part of revolution when a particular operation is being performed; i.e., a photo pass or landmark tracking pass.
- phase angle**—The angle at the point of intersection formed by the vectors from the source (Sun) and the observer, or camera.
- photoclinometry**—The technique for extracting slope information from an image brightness distribution.
- photometry**—That science dealing with the measure of the intensity and direction of light.
- photometric function**—The relationship of the intensity of reflected light to the angular conditions of viewing and illumination.
- ray, ray system, rayed craters**—A deposit of high albedo material of unknown composition ejected from craters. The ejecta may either intensify cratering or smooth a previously cratered surface. The albedo is believed to decrease with age. The ray system is a group of narrow, linear, sometimes interrupted rays radiating from a crater. A rayed crater is the source of these linear rays.
- regolith**—The layer of fragmental debris that overlies consolidated bedrock.
- rev, revolution**—360° of travel in an orbit.

sensitometry, sensitometric strip—*sensitometry*: The science dealing with the measurement of the sensitivity of the photographic emulsion to processing chemistry, time, and temperature.

sensitometric strip: An exposure of a series of calibrated "gray" levels which allows the determination of the correlation of relative exposure from relative density of the photographic transparency.

sequence camera—A 16-mm camera that can be set to expose 1, 4, 8, 12, or 24 frames per second.

smear—Loss of resolution in a photograph caused by movement of the camera with respect to the object. In the orbital case, smear is most likely to be caused by the movement of the spacecraft along the velocity vector while the shutter is open.

solar corona—The outer atmosphere of the Sun. The temperature is 1 to 2 million degrees Kelvin. The light—having an intensity about one-half the full Moon—is mainly due to sunlight scattered by free electrons.

spotmeter—An automatic reflectance light meter with a 1° angle of acceptance.

stereo, stereoscopic strip—Photography taken so that sufficient forward overlap exists to permit stereoscopic (three-dimensional) viewing and reconstruction of the surface area photographed (see **strip photography**).

strip photography—Photography taken in a systematic manner, with a constant amount of forward overlap, which covers a strip of surface below the spacecraft trajectory (see **stereo strip**).

Sun angle—See **Sun elevation**.

Sun elevation—The angle formed, in a vertical plane, between the incident Sun rays and the local horizontal.

surround—All of the visual field that is outside the background of a point (see **background**).

terminator—The boundary between the illuminated and unilluminated portion of the lunar surface. The Moon's terminator advances approximately 13° per 24 hours.

terra—An area on the lunar surface which is relatively higher in elevation and lighter in color than the maria. The terra is characterized by a rough texture formed by intersecting or overlapping large craters.

transearth—The return portion of the mission between lunar orbit and reentry into the Earth's atmosphere.

transearth injection—The spacecraft propulsive maneuver that increases the velocity to allow return to Earth.

transient event—A transitory change in the appearance of a lunar feature.

translunar—The outbound portion of the lunar mission between Earth orbit and lunar orbit.

translunar injection—The propulsive maneuver that increases spacecraft velocity to allow it to escape the Earth's gravitational field.

vertical photography—Photography taken with the optical axis aligned, as nearly as possible, with the local vertical.

vignetting—The progressive reduction of image illuminance at increasing obliquity.

washout—See **heilighenschein**.

wasting—See **mass wasting**.

zero phase—The condition when the vectors from the source (Sun) and the observer are colinear.

zero-phase photography—Photography which includes the image of zero phase.

zodiacal light—Sunlight scattered by interplanetary matter located in the plane of the solar system. It appears as a faint glow of light in the night sky near the plane of the ecliptic.

APPENDIX C

Author Affiliation

NASA Headquarters

Richard J. Allenby

Manned Spacecraft Center

James H. Sasser

William A. Anders

Frank Borman

James A. Lovell

James L. Dragg

Harold L. Prior

Richard L. Nance

Paul E. Norman

Robert O. Hill

William B. Chapman

Lewis C. Wade

George R. Blackman

Richard W. Underwood

Merritt J. Bender

Goddard Space Flight Center

J. A. O'Keefe

W. S. Cameron

L. Dunkelman

Langley Research Center

W. H. Michael, Jr.

George C. Marshall Space Flight Center

Otha H. Vaughan, Jr.

U.S. Geological Survey

D. E. Wilhelms

D. E. Stuart-Alexander

K. A. Howard

Newell J. Trask

Gordon A. Swann

Harold Masursky

H. G. Wilshire

H. A. Pohn

R. L. Wildey

B. K. Lucchitta

N. A. Gambell

Sherman S. C. Wu

University of Arizona

E. A. Whitaker

Robert G. Strom

D. W. G. Arthur

Bellcomm, Inc.

F. El-Baz

A. F. H. Goetz

H. W. Radin

D. D. Lloyd

Boeing Scientific Research Laboratories

Harold B. Liemohn

Lockheed Electronics Co.

James Davis

Alan Wells

Raytheon Co.

R. O. Esten

TRW Systems Group

K. Ziedman

